Investigating the functional consequences of cardiac ryanodine receptor (RyR2) polymorphisms on arrhythmia-linked Ca^{2+} release dysfunction

By

Aaron Ian Clack

A thesis submitted for the degree of Doctor of Philosophy

September 2010

Department of Cardiology
Wales Heart Research Institute
School of Medicine
Cardiff University

Funding obtained from:

CONTICA

Investigating the functional consequences of cardiac ryanodine receptor (RyR2) polymorphisms on arrhythmia-linked Ca^{2+} release dysfunction

By

Aaron Ian Clack

A thesis submitted for the degree of Doctor of Philosophy

September 2010

Department of Cardiology
Wales Heart Research Institute
School of Medicine
Cardiff University

Funding obtained from:

CONTICA

ProQuest LLC
789 East Eisenhower Parkway
P.O. Box 1346
Ann Arbor, MI 48106-1346

Acknowledgements:

I would like to thank several people for their continued support through the duration of my PhD.

Firstly I would like to thank Professor Tony Lai for allowing me to conduct my work in the Wales Heart Research Institute and for giving me several opportunities to travel and present my work at international meetings. I would like to thank both Dr Chris George and Dr Lowri Thomas for all of their help and support over the course of my PhD, both in and out of the lab.

Thanks to everyone who I worked with at the WHRI. Particularly thanks to Steve Barberini and Nicole Silvester for all of their help with SALVO and thanks to anyone who passaged my cells over the weekends.

The biggest thank you goes to my wife, Gemma, who's constant love, support and patience got me through writing my thesis and I'm fully aware of the thousands of cups of tea I owe her. Thanks also to Mum and Dad and David and Sarah for all of your support whilst writing up and sorry for not seeing you very much over the last 9 months.

Published Abstracts:

The G1885E RyR2 Polymorphism Modulates the Caffeine Sensitivity of an Arrhythmia-linked Mutation. Clack A.I., George, C.H., Thomas, N.L., Lai, F.A. *Biophysical Journal (Annual Meeting Abstracts), 2009, 96 (3); Page 111a*

An L433P Arrhythmia-linked Mutation in RyR2 Uncouples Agonist-evoked Ca^{2+} Release from Homeostatic Ca^{2+} Cycling. *Clack, A.I., Thomas, N.L., Lai, F.A., George, C.H. Biophysical Journal (Annual Meeting Abstracts), 2009, 96 (3); Page 111a*

Abstract:

Mutations in RyR2 alter intracellular Ca^{2+} handling and can result in stress-induced arrhythmias. The phenotype resulting from genetic mutations in other ion channels (channelopathies) are sometimes influenced by the co-inheritance of common single nucleotide polymorphisms (SNPs) in the same gene. Here we provide the first evidence that human RyR2 Ca^{2+} release channel dysfunction associated with an arrhythmogenic right ventricular dysplasia type 2 (ARVD2)-linked mutant (L433P) is affected by a common, co-inherited RyR2 SNP (Gly1885Glu, G1885E).

Confocal laser scanning microscopy and Ca^{2+} imaging of human embryonic kidney cells (HEK) expressing wild-type (WT) and L433P mutant RyR2 showed that L433P-linked Ca^{2+} handling dysfunction was modulated by the incorporation of WT (non-mutant) RyR2 into heterotetramers. RyR2 channels formed exclusively from subunits containing only the G1885E polymorphism appeared functionally normal. However, G1885E profoundly modulated basal and agonist-evoked L433P mutant channel function.

RyR2 homotetramers formed from subunits containing both the G1885E polymorphism and the L433P mutation (i.e. *in cis*) exhibited augmented dysfunction when compared with homotetrameric L433P channels during spontaneous and agonist-evoked Ca^{2+} release events. Conversely, heterotetrameric RyR2 channels composed of subunits that contained *either* the L433P or G1885E substitutions (i.e. *in trans*) displayed a marked attenuation of L433P-linked channel dysfunction.

Analysis of basal and post-activation Ca^{2+} flux levels revealed that complex mechanisms underpinned the observed phenomenon, and highlighted that the predominant changes were associated with the decay phase of the Ca^{2+} transient.

This data provides compelling evidence that mutation-linked RyR2 channel dysfunction is modulated by common sequence polymorphisms and predicts that a more severe clinical phenotype results from the *in cis* inheritance of G1885E / L433P. Our studies also show that co-expression of L433P and G1885E subunits partially restores the functionality of the resultant heterotetrameric channels. The potential therapeutic benefits of positively modulating RyR2 mutant channel dysfunction via such a trans-complementation approach remain to be explored.

Contents

List of Figures

Chapter 1

Chapter 2

Chapter 5

Appendix I

Appendix II

List of Abbreviations

2D	Two-dimensional
3D	Three-dimensional
ADP	Adenosine 5'-diphosphate
AF	Atrial fibrillation
aLQTS	Acquired long QT syndrome
AM	Acetoxymethyl
APS	Ammonium persulphate
ANOVA	Analysis of variance
ARVD	Arrhythmogenic right ventricular dysplasia
ATP	Adenosine 5'-triphosphate
AP	Action potential
β-AR	Beta-adrenergic
BCA	Bicinchoninic acid
BLAST	Basic Local Alignment Search Tool
B-ME	Beta mercaptoethanol
BrS	Brugada syndrome
BSA	Bovine serum albumen
Ca^{2+}	Ionised (free) calcium
$[Ca^{2+}]$	Calcium concentration
$CaCl_2$	Calcium chloride
CaCaM	Ca^{2+}-bound Calmodulin
CaM	Calmodulin
CaMKII	Calcium/Calmodulin-dependent Kinase II
CCD	Central core disease or cardiac conduction defect
cDMEM	Complete / supplemented DMEM
cDNA	Complementary deoxyribonucleic acid
CICR	Calcium-induced calcium release
Cl^-	Chloride ion
CHO	Chinese hamster ovary cell
CoV	Coefficient of variance
CPVT	Catecholaminergic polymorphic ventricular tachycardia
CSQ	Calsequestrin
DAD	Delayed after-depolarisation
dH_20	Distilled water
DHPR	Dihydropyridine receptor OR L-type Ca^{2+} channel
DMEM	Dulbecco's modified eagles medium
DMSO	Dimethylsulfoxide

DNA	Deoxyribonucleic acid
DPSS	Diode-pulsed solid state laser
DR1-3	Divergent Region 1-3
EAD	Early after depolarisation
ECC or EC-Coupling	Excitation-contraction Coupling
ECG	Electrocardiogram
ECL	Enhanced chemiluminescent
EDTA	Ethylenediaminetetraacetic acid
EGTA	Ethyleneglycoltetraacetic acid
E_m	Membrane potential
eGFP	Enhanced green fluorescence protein
ER	Endoplasmic reticulum
F	Fluo3-AM signal intensity
F_0	Basal Fluo3-AM signal intensity
FBS	Foetal bovine serum
FKBP	FK506 binding protein
FRET	Fluorescent resonance energy transfer
GFP	Green fluorescent protein
HCl	Hydrochloric Acid
HEK or HEK-293	Human embryonic kidney 293 cell
HF	Heart failure
hNaV1.5	Cardiac sodium channel (encoded by *SCN5A*)
HPLC	High performance liquid chromatoraphy
HRP	Horse-radish peroxidase
IP_3	Inositol 1,4,5-trisphosphate
IP_3R	Inositol 1,4,5-trisphosphate receptor
K^+	Ionised (free) potassium
kb	Kilobases
KCl	Potassium chloride
kDa	Kilodalton
KH_2PO_4	Potassium dihydrogen phosphate
LB	Luria-Bertani medium
LQTS	Congenital long QT syndrome
LTCC	L-Type calcium channel
mA	Milliamp
mDMEM	Minimal / unsupplemented DMEM
mg	Milligram
ml	Millilitre
Mg^{2+}	Ionised (free) magnesium

MH	Malignant hypothermia
mM	Millimolar
MOPS	Morpholinopropane sulfonic acid
Na^+	Ionised (free) sodium
Na_2HPO_4	Disodium hydrogen phosphate
NaCl	Sodium chloride
mNCX	Mitochondrial sodium-calcium exchanger
NCX	Sodium-calcium exchanger
ng	Nanogram
nm	Nanometre
OD	Optical density
PBS	Phosphate buffered saline
pg	Picogram
PKA	Protein kinase A
PKC	Protein kinase C
PKG	Protein kinase G
PLB	Phospholamban
PM	Plasma membrane
PMCA	Plasma membrane calcium ATPase
PMT	Photomultiplier tube
PVDF	Polyvinylidene difluoride
RCF	Relative centrifugal force
rpm	Revolutions per minute
RSV	Relative signal variability
RT	Room temperature
RyR	Ryanodine receptor
RyR1	Ryanodine receptor - Skeletal Muscle Type I Isoform
RyR2	Ryanodine receptor - Cardiac Muscle Type 2 Isoform
RyR3	Ryanodine receptor - Type 3 Isoform
SALVO	Synchrony-Amplitude-Length-Variability of oscillations
SCN5A	Cardiac sodium channel gene
SDM	Site-directed mutagenesis
SDS	Sodium Dodecyl Sulphate
SDS-PAGE	SDS polyacrylamide gel electrophoresis
SDW	Sterile distilled water
S.E.M.	Standard error of the mean
SERCA	Sarco/endoplasmic reticulum Ca^{2+} ATPase
SNP	Single nucleotide polymorphism
SOC	Super optimal broth supplemented with glucose

SOICR	Store overload-induced calcium release
SR	Sarcoplasmic reticulum
SSS	Sick sinus syndrome
SUDS	Sudden unexplained death syndrome
SV	Signal variability
SVm	Signal variability normalised to the mean
TA	Transmembrane assembly
TAE	Tris-acetate-EDTA
TBS	Tris-buffered saline
TBS-T	Tris-buffered saline with added 0.1% (v/v) Tween-20
TEMED	Tetramethylethylenediamine
T_m	Melting temperature
TM	Transmembrane domain
Torsades de Pointes	TdP
T-tubule	Transverse tubule
v:v or v/v	Volume to volume or volume by volume
µ	Micro or Mean-average
µg	Microgram
µl	Microlitre
UV	Ultraviolet
v:w	Volume to weight or volume by weight
WT	Wild Type
w:v or w/v	Weight to volume or weight by volume

Chapter 1

Introduction

1.1. Calcium signalling

Calcium ions (Ca^{2+}) are a ubiquitous intracellular messenger that regulate a multitude of cellular processes including muscle contraction, gene expression, energy metabolism, cell proliferation and cell death (Laude & Simpson, 2009). The involvement of Ca^{2+} in such a variety of cellular processes stems from the interplay of numerous signalling proteins that regulate the intracellular availability of Ca^{2+} ions (Bootman *et al.*, 2006). Intracellular Ca^{2+} concentration is controlled by a number of processes which increase or decrease the level of cytoplasmic Ca^{2+}, a balance of which determines resting cellular Ca^{2+} levels (see section 4.1.1 - 4.1.2).

Elevation of intracellular Ca^{2+} concentration is achieved by the influx of Ca^{2+} ions through integral plasma membrane (PM) Ca^{2+} channels or through the release of sequestered Ca^{2+} from intracellular stores and acts as a trigger for a number of cellular processes *(Bootman et al., 2001)*. To allow termination of the cellular event initiated by Ca^{2+} to occur, the increased free intracellular Ca^{2+} concentration must decrease in order to reduce cytosolic Ca^{2+} availability. This decrease is achieved through a number of ATP-dependent or independent mechanisms, namely extrusion of Ca^{2+} from the cell through plasma membrane Ca^{2+} ATPases or exchangers, sequestration of Ca^{2+} into intracellular stores through sarcoplasmic/endoplasmic reticulum Ca^{2+} ATPases (SERCA), or by uptake into mitochondria via the mitochondrial uniporter (Berridge *et al.*, 2000; Bootman *et al.*, 2001).

1.1.1. Compartmentalisation of Ca^{2+} signalling

In order for many diverse cellular processes to be regulated by Ca^{2+}, a high level of complexity exists in the nature of the Ca^{2+} signal in terms of localisation, amplitude and duration. The free diffusion of Ca^{2+} throughout the cell is restricted by cytoplasmic buffering and Ca^{2+} extrusion/store uptake, so Ca^{2+} signals must enter the cell in close proximity to its target protein or pass through the cell via a process of signal propagation (Berridge *et al.*, 2000). In the myocyte, Ca^{2+} release from the sarcoplasmic reticulum (SR) stores occurs predominantly through ryanodine receptors (RyRs). Activation of a single Ca^{2+} release channel results in a small, localised, increase in cytoplasmic Ca^{2+} (~30nM), which lasts for ~200 ms, spreads a distance no more than 2μm and is termed

a Ca^{2+} "quark" (Niggli & Shirokova, 2007). The activation of a cluster of several neighbouring RyR's produce elementary Ca^{2+} release events termed Ca^{2+} "sparks". These events result in a greater increase in localised Ca^{2+} of ~200nM, last for ~500ms and spread for no more than 6µm. If several Ca^{2+} sparks occur in close proximity simultaneously, it can result in the propagation of a regenerative Ca^{2+} "wave" which can spread rapidly throughout the cell (see Figure 1.1). The magnitude of Ca^{2+} release is important in determining whether these elementary Ca^{2+} release events can activate neighbouring channels and produce a global Ca^{2+} wave (Cheng *et al.*, 1993). The propagation and degeneration of these elementary Ca^{2+} release events are heavily dependent on the buffering capacity of the proteins and organelles encountered by the Ca^{2+} signal (Bootman *et al.*, 2001).

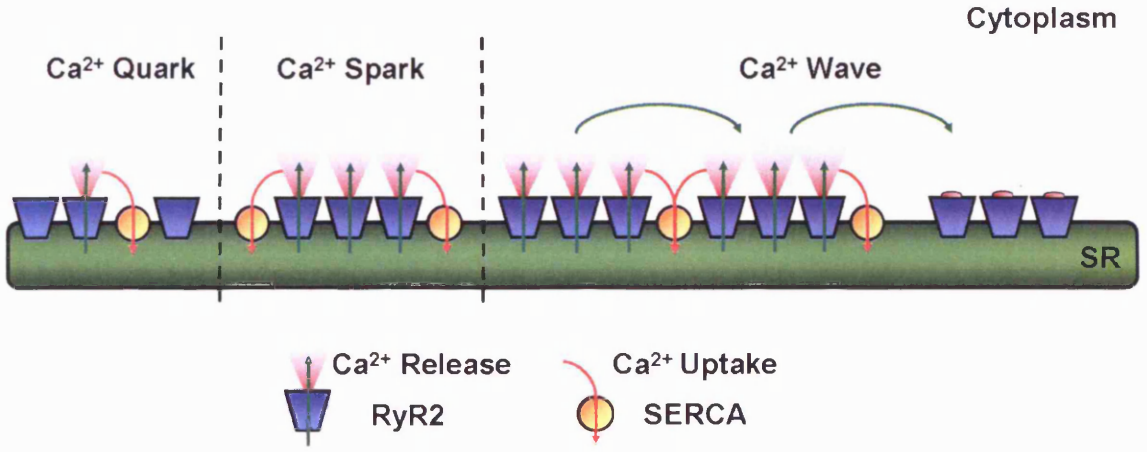

Figure 1.1. Elementary Ca^{2+} release events schematic. *Ca^{2+} release from the SR store through RyR is indicated by green arrows and uptake through SR Ca^{2+} ATPases is indicated by red arrows. Activation of a single Ca^{2+} release channel causes the release of a small amount of Ca^{2+} (quark), which is readily sequestered into the ER/SR. Activation of a cluster of Ca^{2+} release channels produces a greater level of Ca^{2+} release, which can activate channels in close proximity (spark). Sequential activation of neighbouring Ca^{2+} release channels can lead to the propagation of a Ca^{2+} wave that can spread rapidly throughout the cell.*

The duration of the intracellular Ca^{2+} signal is also critical in regulating diverse cellular functions. Sustained elevated cytoplasmic Ca^{2+} can induce cellular apoptosis and as such, the majority of Ca^{2+} signals are presented in a pulsatile or oscillatory manner. (Bootman & Berridge, 1995). Furthermore, increased Ca^{2+} flux between the endoplasmic reticulum (ER) and cytoplasm has also been implicated in cell death (George *et al.*, 2003b). Ca^{2+} signalling is a critical pathway involved in the correct functioning of many different cell types, including amongst others, the cardiac myocyte.

1.1.2. The cardiac myocyte

The myocardium is made up of many different cell types, although cardiac myocytes are the most predominant and fundamental contractile cell in the myocardium. The typical cardiac ventricular myocyte (Figure 1.2) is cylindrical in shape and between 10-20μm in diameter and 50-100μm in length. Individual myocytes are mainly connected in a longitudal direction (end-to-end) and connect at a region termed the intercalated discs, which consist of many adhesion proteins and gap junctions (Shimada *et al.*, 2004).

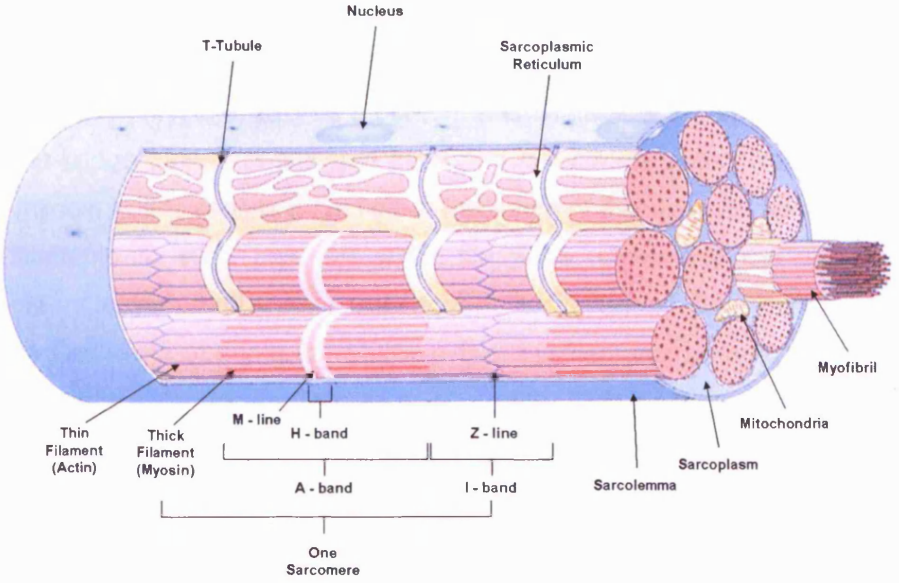

Figure 1.2. Cardiac muscle ultrastructure. *Cardiac muscle comprises of contractile myofibrils, each comprised of several sarcomeres. T-tubules penetrate the cell at regular intervals to allow rapid depolarisation of the myocyte. Mitochondria provide the energy required for dissociation of the myosin head from actin during muscle contraction. Adapted from Davies & Novak (2006).*

The outer-layer of the myocyte is the sarcolemma, which is a lipid bilayer containing a multitude of ion channels allowing the selective ion transport in to and out of the myocyte. Highly ordered invaginations of the sarcolemma form structures termed transverse tubules (t-tubules) that protrude into the myocyte (Walker & Spinale, 1999; Song *et al.*, 2005). T-tubules are between 100-300nm in diameter and occur approximately every 1.8μm along the axis of the cell and result in the sarcolemmal L-type Ca^{2+} channels being in close proximity to the intracellular SR calcium release channel (Figure 1.3, Song *et al.*, 2005).

Each individual myocyte is packed with a highly organised array of myofilament proteins that form the myocyte contractile apparatus, the sarcomere, comprised of 'thin' actin and 'thick' myosin filaments, tropomysin and the troponin complex (troponins T, I and C). Both tropomysin and the troponin complex are located within the thin filament and are involved in actin stabilisation and regulating the extent of myofibril contraction respectively (Walker & Spinale, 1999).

Under resting conditions, when the myocyte is relaxed, tropomysin is wrapped around the actin filament, preventing interaction with the myosin filament. Elevated cytoplasmic Ca^{2+} concentration (systole) causes a conformational change in troponin C which results in the cross-bridge formation between actin and myosin filaments. The release of ADP from the myosin heads causes a change in the angle of the cross-bridge and causes the myosin filaments to slide past the actin filaments, shortening the sarcomere and resulting in myocyte contraction. Subsequent extrusion of Ca^{2+} from the myocyte dissociates Ca^{2+} from troponin C, returning the myofilaments to their original positions and myocyte relaxation occurs (Purves *et al.*, 2003). This process, whereby the cyclical release and re-sequestration of Ca^{2+} in the SR results in the contraction and relaxation of muscle tissue is termed 'excitation-contraction (EC) coupling' (Bers, 2002).

1.1.3. Excitation-contraction coupling

Excitation contraction coupling is the process whereby electrical stimulation of the cardiac myocyte initiates physical contraction of the heart (Bers, 2002). When the heart is relaxed (diastole), intracellular Ca^{2+} is sequestered in the SR. Membrane depolarisation of the myocyte results in an influx of Ca^{2+} into the cell through sarcolemmal voltage-gated L-type Ca^{2+} channels (LTCC). Due to the localisation of the cytoplasmic Ca^{2+} increase to the sarcolemmal-SR junction and the close proximity of RyR2 to the LTCC, this small increase in Ca^{2+} concentration (200-400μM) is sufficient to activate clusters of RyR2 channels (Bers, 2006; Bootman *et al.*, 2006). This produces Ca^{2+} sparks, which subsequently activate neighbouring RyR channels, effectively passing the Ca^{2+} signal through the cell as a propagating Ca^{2+} wave (Figure 1.1) resulting in increased global intracellular Ca^{2+} levels (Keller *et al.*, 2007; Niggli & Shirokova, 2007). The increased availability of intracellular Ca^{2+} causes activation of the cellular contractile machinery and results in

contraction of the myocyte (systole). The amplitude of the Ca^{2+} release transient is proposed to determine the force of the resulting contraction (Bers, 2006; Eisner *et al.*, 2009). Ca^{2+} is then extruded from the cell via the sodium-calcium exchanger (NCX) and plasmalemmal Ca^{2+} ATPase (PMCA) and is returned to the SR and mitochondria by SERCA and the mitochondrial uniporter respectively.

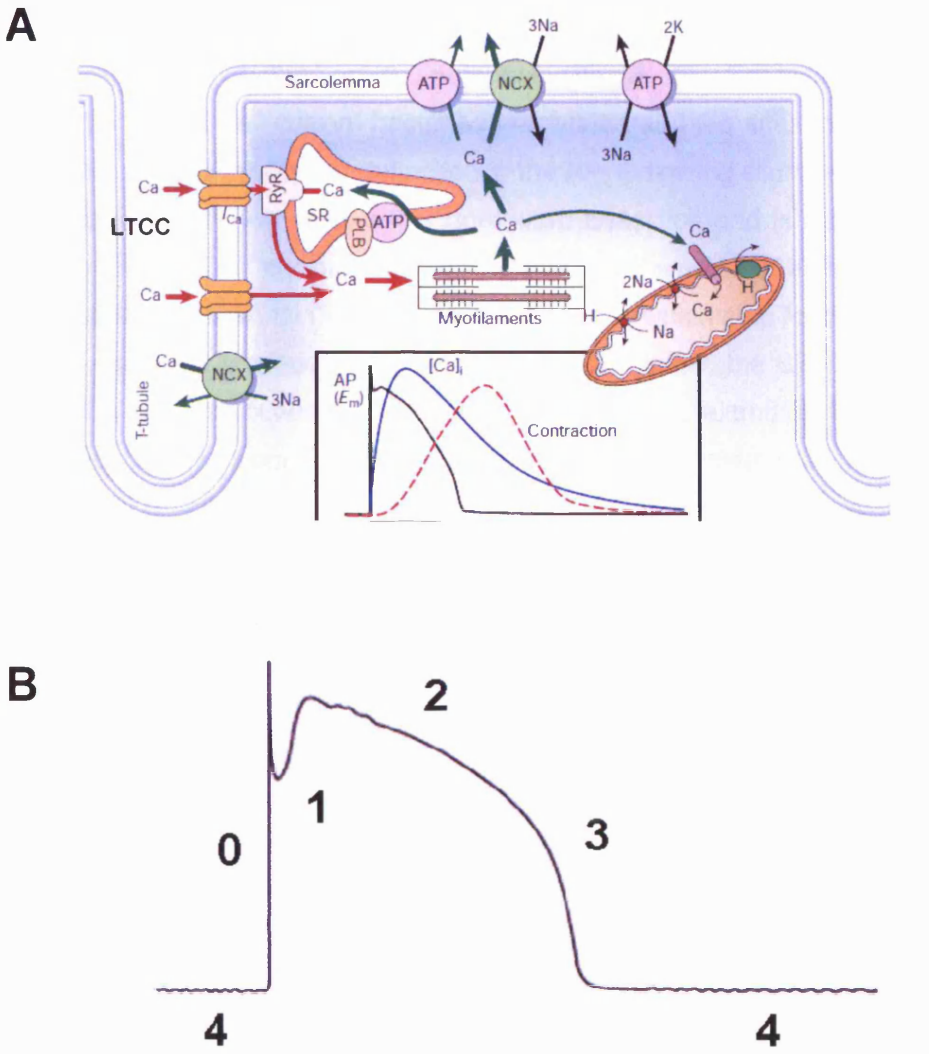

Figure 1.3. Excitation contraction coupling. *Upon membrane depolarisation, an influx of Ca^{2+} (I_{Ca}) through LTCC activates RyR2, causing the release of Ca^{2+} from SR stores. Following contraction, Ca^{2+} dissociates from the myofilaments and is removed from the cytoplasm by sequestration in the SR via SERCA modulated by phospholamban (PLB), extrusion from the cell via NCX and sarcolemmal Ca^{2+} ATPase and taken up by the mitochondria via the uniporter. Insert shows the relative time course of the action potential, intracellular Ca^{2+} transient and contraction of a rabbit ventricular myocyte. From Bers (2002). Distinct phases of the action potential, described in section 1.1.4, are indicated on the representative cardiac action potential shown in panel B, adapted from Marban (2002).*

1.1.4. Cardiac action potential

The electrical origin of EC coupling is the cardiac action potential (AP, Figure 1.3A and B). Myocytes under diastolic conditions exhibit a resting membrane potential (E_m) of approximately -85mV (Phase 4). The voltage-dependent activation of fast inward Na^+ currents results in the rapid depolarisation to approximately +40mV and is represented by the sharp upstroke of the action potential (Phase 0). Following complete depolarisation, the inward Na^+ current becomes inactivated and the efflux of K^+ and Cl^- ions from the cell causes a downward deflection in the AP, indicating slight repolarisation (Phase 1). A plateau of the AP follows this downward deflection and is a result of the balance between inward Ca^{2+} currents through LTCCs and the efflux of K^+ ions through the slow delayed rectifier channel (Phase 2). A rapid repolarisation step follows whereby the inward Ca^{2+} current is stopped by RyR2 mediated Ca^{2+} efflux, the SR Ca^{2+} store is refilled by SERCA and the outward K^+ channels remain open, extruding K^+ ions and therefore positive charge, from the cell (Phase 3). This continues until the resting membrane potential of -85mV is reached, ready for the initiation of the next AP (Phase 4, Marban, 2002; Bers, 2008)

1.1.5. β-adrenergic stimulation of the cardiac myocyte

Physiological sympathetic stimulation of the heart through the activation of β-adrenergic receptors in the myocyte is essential in order to increase cardiac output during periods of high metabolic demand and is often termed the "fight-or-flight" response (Marx & Marks, 2002). β-adrenergic stimulation increases the rate (chronotropy) and force (inotropy) of myocyte contraction and accelerates myocyte relaxation (lusitropy), which culminate in increased cardiac output (Bers, 2008). β-adrenergic stimulation causes an increase in cyclic AMP production which increases protein kinase A (PKA)-mediated phosphorylation of several myocyte Ca^{2+} handling proteins (Figure 1.4, Bers, 2002). Inotropic mechanisms upregulated by PKA phosphorylation include Ca^{2+} influx through LTCC (section 1.2.3.3.1) and the release of Ca^{2+} from the SR through RyR2 (section 1.2.3.2.4). PKA phosphorylation increases lusiotropic activity through increasing SERCA activity (increasing SR Ca^{2+} uptake, see section 1.2.3.3.2) and the dissociation of troponin I from the actin myofilaments (increasing rate of Ca^{2+} liberation from troponin C, section 1.1.2). As such, these processes culminate in an increased level of SR Ca^{2+} and

contribute to a larger Ca^{2+} transient and increased cardiac output (Bers, 2002). The role that PKA phosphorylation on NCX remains highly contentious, with experimental data suggesting that PKA phosphorylation increases (Iwamoto *et al.*, 1998) and decreases (Ginsburg & Bers, 2005) NCX activity.

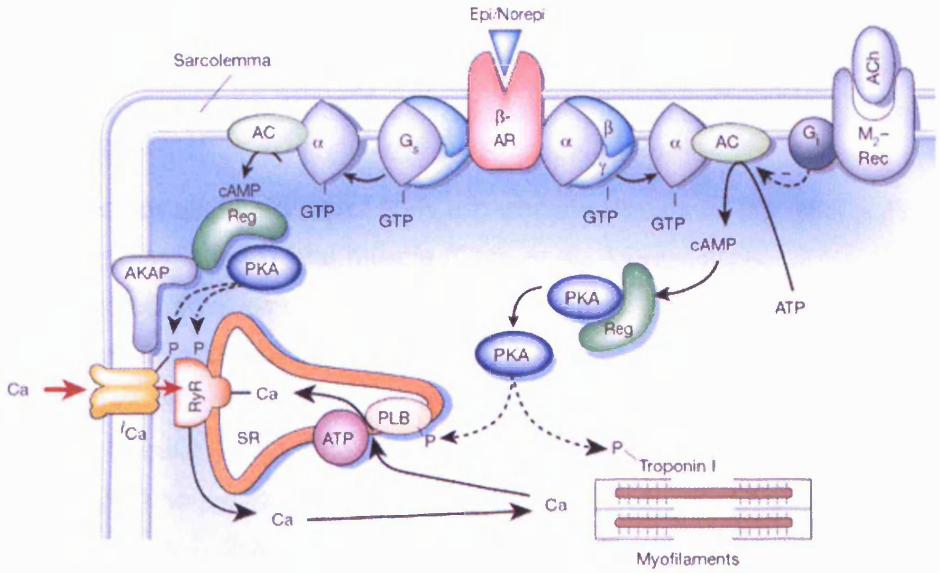

***Figure 1.4. β-adrenergic receptor activation and EC-coupling phosphorylation targets**. The β-adrenergic receptor is activated by circulating epinephrine/norepinephrine. This triggers the activation of a GTP-binding protein (G_s) which stimulates adenylyl-cyclase to produce cAMP, which in turn activates PKA. PKA then phosphorylates phospholamban (PLB), RyR, LTCC (I_{Ca}) and troponin I. CaMKII and the NCX are not shown, as uncertainty remains over whether they are regulated by β-adrenergic stimulation. From Bers, (2002).*

1.2. The ryanodine receptor (RyR)

The ryanodine receptor (RyR) is a large transmembrane SR Ca^{2+} channel that regulates Ca^{2+} release from the SR during Ca^{2+} signalling events, including EC-coupling in contractile tissue. The functional RyR channel is a homotetramer, consisting of four 565kDa subunits with a total molecular mass of ~2.2MDa (Tunwell *et al.*, 1996).

Three tissue-specific isoforms of RyR are encoded by three separate genes. RyR1 is primarily expressed in skeletal muscle (Otsu *et al.*, 1990; Zorzato *et al.*, 1990), RyR2 is primarily expressed in cardiac tissue, as well as the brain (Lai *et al.*, 1988; Otsu *et al.*, 1990; Sorrentino & Volpe, 1993; Tunwell *et al.*, 1996) and RyR3 is expressed in smooth muscle tissue, the brain and the diaphragm (Hakamata *et al.*, 1992; Sorrentino & Volpe, 1993; Fill & Copello, 2002). The three isoforms exhibit 66-70% sequence homology, with the majority of sequence variation occurring in three regions of sequence diversity: divergent regions 1, 2 and 3 (DR1-3), which are thought to be responsible for tissue-specific, physiological differences between isoforms (Sorrentino & Volpe, 1993; Zhang *et al.*, 2003). For example, RyR1 is activated through a mechanism involving physical interaction with the LTCC, whereas RyR2 is activated by CICR in the absence of a physical interaction (Fill & Copello, 2002).

In RyR2, DR1 and DR2 encompass residues 4210-4562 and 1353-1397 respectively and are located towards the top of the cytoplasmic assembly (Figure 1.6, Liu *et al.*, 2002; Liu *et al.*, 2004). This region is proposed to be involved in the interaction of RyR1 with the LTCC, suggesting that sequence variation in this region may be responsible for the physiological difference in activation mechanisms between RyR1 and RyR2 (Fill & Copello, 2002).

There is also heterogeneity between the Ca^{2+}-dependent activation/inactivation profiles of the skeletal muscle and cardiac RyR2 isoforms. RyR2 exhibits a decreased sensitivity to inactivation by high concentrations of Ca^{2+} (>10μM) compared to RyR1, despite similar Ca^{2+}-dependent activation profiles (0.1-10μM, Chen & MacLennan, 1994; Du *et al.*, 1998). Deletion of DR3 (residues 1872-1923 in RyR1, corresponding to residues 1852-1890 in RyR2) from RyR1 was shown to increase channel sensitivity to Ca^{2+}-dependent activation and abolished Mg^{2+} and Ca^{2+}-dependent channel inactivation (Hayek *et al.*, 1999). Given that a proposed low-affinity cytosolic Ca^{2+}-binding site is

located within DR3 of RyR, sequence variation in these regions may contribute to the varying Ca^{2+}-dependent activation/inactivation profiles of the RyR isoforms (Sorrentino & Volpe, 1993).

Knock-out mouse models that were deficient in each of the specific RyR isoforms exhibited extremely detrimental phenotypes. Mice that were deficient in RyR1 exhibited respiratory failure and abnormal skeletal and muscular development, (Takeshima *et al.*, 1994). Those that were deficient in RyR2 exhibited embryonic lethality after 9-10 days coupled with impaired heart development (Takeshima *et al.*, 1998). RyR3-deficient mice exhibited normal development and muscular function, but exhibited increased locomotor activity, suggesting altered neuronal activity in these mice (Takeshima *et al.*, 1996). These RyR-deficient mice illustrate the developmental importance of RyR expression.

The work described in this thesis was carried out exclusively on the cardiac RyR isoform, RyR2, and although there is a great deal of similarity between the three isoforms, RyR2 structure and function will be the focus of the rest of this Introduction.

1.2.1. RyR2 structure

The three-dimensional structure of tetrameric RyR exhibits 4-fold symmetry and appears as a mushroom shaped protein comprising of a small C-terminal transmembrane assembly (TA, 120 x 120 x 60 Å) comprising the channel pore and a larger N-terminal cytoplasmic portion (280 x 280 x 120 Å, Figure 1.5, Orlova *et al.*, 1996; Samso & Wagenknecht, 1998), made up of 10 distinct sub-domains, accounting for approximately 90% of the protein (Figure 1.5, Wang *et al.*, 2007). Clamp-shaped regions at the corners of the RyR tetramer are connected to the centre part of the cytoplasmic assembly by part of the protein termed "handle" domains (Figure, 1.5) and are proposed to be involved in inter-RyR2 interactions (section 1.2.2).

The cytoplasmic assembly plays a major role in the regulation of RyR channel activity. The targeted insertion of the GFP epitope into various locations of RyR2 has revealed the location of several primary sequence motifs in the RyR2 three-dimensional structure, which are important in channel regulation, the approximate locations of which are indicated in Figure 1.6 and summarised in Table 1.1.

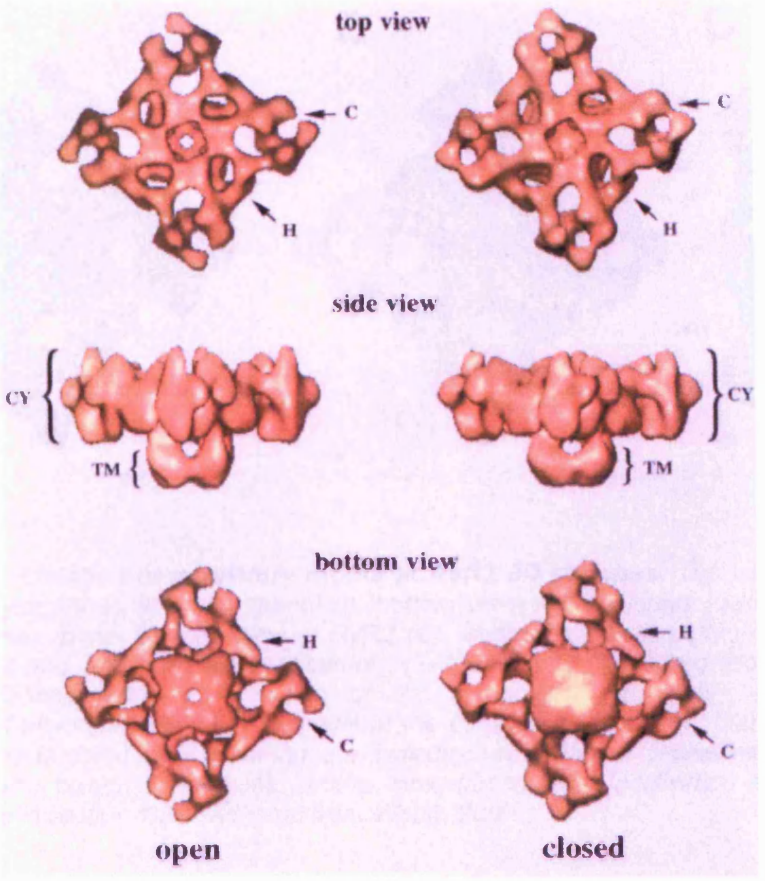

***Figure 1.5. Three-dimensional representation of the RyR channel in the open and closed conformation (30 Å resolution)**. Channels are represented in the open (left images) and closed (right images) confirmation when viewed from the cytoplasmic face (top panels), the side (middle panels) and from the luminal side of the channel (bottom panels). The open confirmation of the channel was induced by incubation of the purified channels with 100μM Ca^{2+} and 100nM ryanodine. The clamp-shaped structures (C) and the handle structure (H) are indicated. The clamp-shaped structures appear to open when the channel is in the open state, however this is an artifact of the resolution at which the structure was determined. From Orlova (1996)*

The divergent regions are all located on the periphery of the RyR2 cytoplasmic assembly. DR1 is located on the "handle" domain encompassing subdomain 3 (Liu *et al.*, 2002). DR2 is located in the subdomain 6, which forms part of the clamp structures (Liu *et al.*, 2004), which are proposed to undergo a conformational change during transition between the open and closed state of the channel (Orlova *et al.*, 1996), leading to a proposed role of DR2 in RyR:RyR interactions (section 1.2.2). DR3 is located in subdomain 9, also within the clamp structures (Zhang *et al.*, 2003) and is proposed to be critical for correct channel regulation by Ca^{2+} and Mg^{2+} (Hayek *et al.*, 1999).

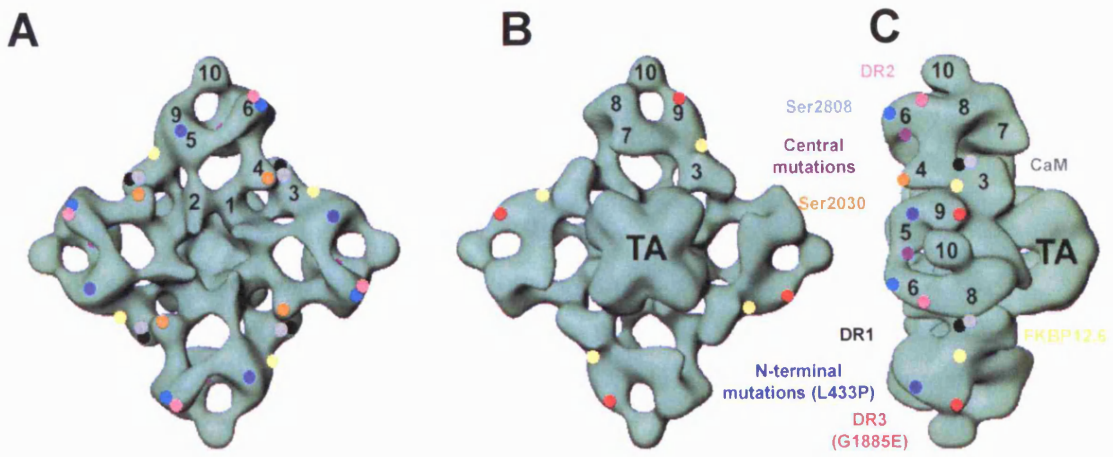

Figure 1.6. Location of regulatory motifs in RyR2 3D structure. *Top view of RyR2 from the cytoplasmic assembly (panel A), bottom view of the channel looking towards the SR lumen (panel B), side view of RyR2 (C), illustrates the disparity in size of the cytoplasmic and transmembrane assembly (TA) domains. Numbered regions (1-10) indicate distinguishable sub-domains of the cytoplasmic assembly. Approximate locations of important regulatory domains in the cytoplasmic assembly that have been identified by targeted GFP insertion are indicated by coloured circles and labels of corresponding colour. References for the three-dimensional localisation experiments are detailed in section 1.2.1. Adapted from Wang, 2007.*

DR3 is located adjacent to the proposed binding site of an important RyR2 regulatory protein, FKBP12.6 (section 1.2.3.2.1), which is located in subdomain 3 of the cytoplasmic assembly (Sharma *et al.*, 2006) which has recently been corroborated in fluorescent energy transfer (FRET) based experiments (Cornea *et al.*, 2010). The proposed interaction site of another RyR2 regulatory protein, calmodulin (CaM, section 1.2.3.2.3) has also been mapped to the cytoplasmic assembly. When in its Ca^{2+}-free form (apoCaM), difference mapping localises CaM to subdomain 3, although upon Ca^{2+}-binding the centre of the mapped difference is shifted by 33 Å, although these two areas of mapped difference overlap (Samso & Wagenknecht, 2002).

Genetic mutations identified in RyR have been shown to cluster into 3 distinct regions of the RyR sequence (section 1.3.2), two of which have subsequently been mapped on the 3D RyR2 structure. The N-terminal mutation domain has been localised to the clamp structure of the cytoplasmic assembly and is located between sub-domains 5 and 9 (Wang *et al.*, 2007), placing it in relatively close physical proximity to DR3. A second mutation domain is located in the centre of the protein sequence and has been mapped

to the bridge structure between sub-domains 5 and 6 in the cytoplasmic assembly (Liu *et al.*, 2005), adjacent to the N-terminal mutational domain, the potential implications of which are discussed in section 1.3.4.2.

Two phosphorylation sites involved in the regulation of RyR2 (section 1.2.3.2.4) have been mapped to the cytosolic face of the cytoplasmic assembly. A serine residue at position 2808 in the RyR2 sequence (Ser2808) is located in subdomain 6 of the cytoplasmic clamp region, placing it in close proximity to the central mutation domain (Meng *et al.*, 2007). Phosphorylation of S2808 is proposed by some groups to cause the dissociation of the RyR stabilising protein FKBP12.6, although this phenomenon remains highly disputed (section 1.2.3.2.4). However, the S2808 phosphorylation site is between 105 and 120 Å from the mapped FKBP12.6 binding site, making a direct involvement of S2808 phosphorylation in FKBP12.6 binding unlikely (Meng *et al.*, 2007). Similarly, a serine residue at position 2030 (S2030) has been proposed as a second phosphorylation site (Xiao *et al.*, 2005) and has been mapped to subdomain 4 at the top of the cytoplasmic assembly (Jones *et al.*, 2008b), which is also distant from the FKBP12.6 binding site. The controversial role of RyR2 phosphorylation in channel regulation will be discussed in section 1.2.3.2.4.

Although difference mapping of RyR2 following targeted GFP insertion has been extensively used in the localisation of particular motifs in the RyR2 3D-structure, the reliability of this procedure is somewhat questionable. Most RyR2 regulatory motifs have been mapped to the periphery of the cytoplasmic assembly, particularly to the clamp-shaped regions (see Figure 1.6). Whether the mapped differences actually constitute the inserted GFP epitope, or are a result of GFP insertion within the centre of the molecule displacing the flexible clamp regions, remains unknown. However, there is an element of reconciliation between difference mapping studies, which place the N and C-terminal mutation domains in close proximity in the 3D structure (Liu *et al.*, 2006; Wang *et al.*, 2007) with FRET-based (Liu *et al.*, 2010) and peptide-competition binding studies (Yamamoto *et al.*, 2002), which demonstrate an interaction between these two domains. Recent evidence from another FRET based study reconciles the location of the FKBP12.6 binding site as determined in these difference mapping studies (Sharma *et al.*, 2006; Cornea *et al.*, 2010).

Regulatory Motif	GFP insertion location (Residue)	Cytoplasmic Sub-domain	Notes	References
N-terminal mutation domain	S437	Between domains 5 and 9	Domain contains residues 77 - 466 (Medeiros-Domingo, 2009). In close proximity (30Å) to central mutation domain.	*Wang, 2007*
Divergent Region 2	T1366	6	Localised to "clamp" structure.	*Liu, 2004.*
Divergent Region 3	T1874	9	Localised to "clamp" structure, adjacent to FKBP12.6 binding site. Region proposed to contain Ca^{2+}/Mg^{2+} binding site (Hayek, 1999). Adjacent to FKBP12.6 binding site.	*Zhang, 2003.*
Ser2030	T2023	4	Distant from FKBP12.6 binding site.	*Jones, 2008.*
Central mutation domain	S2367	Bridge between domains 5 and 6	Domain contains residues 2246 to 2534 (Medeiros-Domingo, 2009). In close proximity (30Å) to N-terminal mutation domain.	*Liu, 2006.*
Ser2808	Y2801	6	Localised to clamp structure, 105 - 120Å from FKBP12.6 binding site. Adjacent to central mutation domain.	*Meng, 2007.*
Divergent Region 1	D4365	3	Localised to "handle" domain.	*Liu, 2002.*
FKBP12.6 binding site	Difference mapping carried out in the presence and absence of FKBP12.6 (Proposed T1874 residue)	3, adjacent to domain 9.	Adjacent to clamp structures. Displaced 1-2nm upon channel opening.	*Wagenknecht, 1996.* *Sharma, 2006.*
Calmodulin binding site	Difference mapping carried out in the presence and absence of CaCaM and apoCaM (Proposed 3630-3638 residues in RyR1)	3	Shifts ~33 ± 5Å upon Ca^{2+} binding.	*Samso & Wagenknecht, 2002.*

Table 1.1. Summary of motifs mapped in the 3D RyR2 structure. *Domain numbers correspond to the sub-domains illustrated in Figure 1.6. Unless stated, motif localisation was determined through the targeted insertion of the GFP coding sequence into RyR2 cDNA.*

The open conformation of RyR contains a C-terminal pore, through which Ca^{2+} ions are released from the SR during CICR (Figure 1.5, Orlova *et al.*, 1996). Although there is consensus that the pore region contains several membrane-spanning domains, there remains contention over the precise number of transmembrane domains. Models containing between 4 and 12 transmembrane domains have been proposed (Takeshima *et al.*, 1989; Zorzato *et al.*, 1990; Tunwell *et al.*, 1996; Du *et al.*, 2002). All of these models agree that both N and C termini are found on the cytoplasmic side of the SR membrane, indicating that the RyR spans the membrane an equal number of times. The position of the final pair of transmembrane domains (M8 and M10) and the intervening ion-selectivity filter (p-loop, M9) have been confirmed, but ambiguity remains over the number of proceeding domains (Du *et al.*, 2002; Meur *et al.*, 2007) with a 6-8 transmembrane domain being in particular favour (Du *et al.*, 2002; Hamilton & Serysheva, 2009).

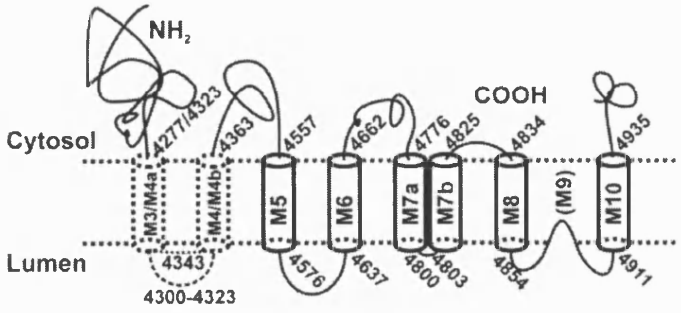

Figure 1.7. Proposed RyR membrane topology. *The proposed 6 transmembrane segment topological model of RyR1. Segments indicated by dashed lines indicate the tentative nature of the first predicted helical hairpin loop. The numbers inside each transmembrane sequence (M3-M10) are those proposed by Zorzato et al (1990). M9 represents the selectivity filter, although it is not a transmembrane segment. from Du et al 2002.*

The C-terminus was proposed to contain a conserved peptide sequence located in TM4 (of the four TM model, corresponding to TM6 of the 6TM model and M10 in Figure 1.7) that retains RyR1 within the ER membrane (Bhat & Ma, 2002), although a subsequent study showed that a TM1 RyR fragment exhibited a significantly higher degree of ER retention, suggesting that the primary retention signal lies within the first TM domain (M5 in Figure 1.7, Meur *et al.*, 2007). Furthermore, the extreme C-terminal 15 amino acid residues of RyR2 have been proposed to be essential for RyR2 tetramerisation (Stewart *et al.*, 2003).

1.2.2. RyR:RyR interaction & coupled gating

As detailed in section 1.1.1, the propagation of an intracellular Ca^{2+} signal requires the coordinated activation of several neighbouring RyR2 channels. As such, RyR2 exists in a highly organised lattice-like arrangement with each RyR tetramer interacting with 4 neighbouring RyR tetramers (Yin & Lai, 2000; Yin *et al.*, 2005b) as depicted in Figure 1.8.

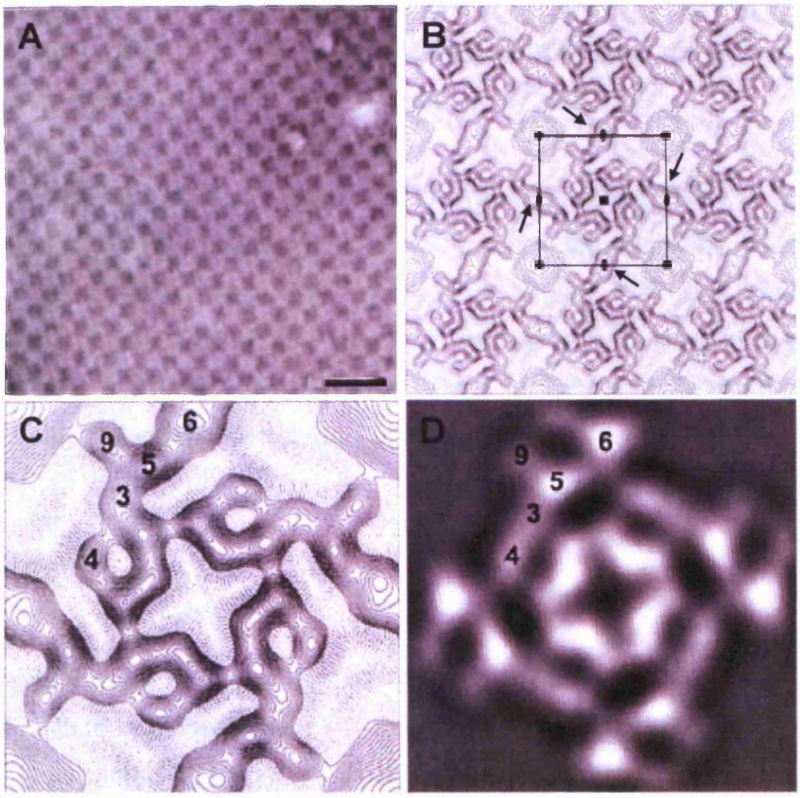

***Figure 1.8. Physical interaction of RyR tetramers**. Two-dimensional crystallisation of RyR on a lipid membrane exhibits a lattice-like appearance as shown in the electron micrograph in panel A (Scale bar represents 100μM). A projection map of an RyR 2D array is indicated in panel B. The point within the square indicates the RyR pore and the arrows indicate the interacting cytoplasmic sub-domain 6 of neighbouring RyRs. Resolution is ~20 Å. Adapted from Yin (2005b). The "clamp" structure containing sub-domains 3,4,5,6 and 9 are clearly visible in the projection structure in panel C and corroborate single channel structure obtained from previous cryo EM-studies (Radermacher et al., 1994).*

This organisation of RyR channels in a "chequerboard" arrangement has functional implications, in that interacting channels tend to open and close in unison in response to agonist-induced activation. This phenomenon has been termed "coupled gating" and has been observed in both RyR1 and RyR2 (Marx *et al.*, 1998; Marx *et al.*, 2001). *Marx et al* have proposed that this interaction is mediated by FKBP12.6 and that dissociation of

FKBP12.6 from RyR2 disrupts this coupled gating, without causing physical uncoupling of RyR tetramers (Marx *et al.*, 2001). However, this has been contested by another group who observed no functional consequences of FKBP12.6-dissociation on RyR2 coupled gating (Hu *et al.*, 2005). Furthermore, modelling of RyR arrays heavily suggests that domains 6 and 10 are the regions of the cytoplasmic assembly that interact with neighbouring RyR2s (Yin *et al.*, 2005a), making the role of FKBP12.6 in RyR:RyR interaction unlikely, given that the proposed FKBP12.6 binding site is located near the junction between sub-domains 3 and 9 (Sharma *et al.*, 2006).

Recently, it was demonstrated that luminal Ca^{2+} regulates the stability of the interaction between coupled RyR2 channels in lipid bilayer experiments (Gaburjakova & Gaburjakova, 2008). Additionally, the depletion of luminal Ca^{2+} was shown to cause greater instability in the RyR2:RyR2 coupling when channels were in the open state, which according to the model of *Liang et al*, leads to the decrease in channel opening required for fast RyR2 inactivation (Liang *et al.*, 2007).

1.2.3. Modulation of RyR2

Although RyR2 has a central role in cardiac myocyte Ca^{2+} signalling, many other proteins and cellular processes are involved in the regulation of RyR2 channel function. The channel is regulated by many physiological ligands including Ca^{2+} itself, magnesium (Mg^{2+}) and ATP (section 1.2.3.1). Some of these modulators are accessory proteins which interact directly with RyR2 and constitute the macromolecular complex (section 1.2.3.2), whereas others indirectly regulate RyR2 activity by altering the intracellular ionic environment (section 1.2.3.3). The functional effects of each of these RyR2 modulators on RyR2 activity will be discussed here. Furthermore, several non-physiological compounds, including ryanodine, caffeine and ruthenium red have also been shown to alter RyR2 activity and have proved useful tools in investigating RyR2 function and will be discussed in section 3.1.1.2 and 3.1.5.

1.2.3.1. Physiological ligands

Ca^{2+} itself is the main effecting ligand of RyR2, responsible for both channel activation and inactivation, with Ca^{2+} binding sites present on both the luminal and cytosolic sides

of the channel (Figure 1.9, Laver, 2007). RyR2 is activated by low micromolar concentrations of cytoplasmic Ca^{2+} (1-10μM, Rousseau *et al.*, 1986; Rousseau & Meissner, 1989; Chen *et al.*, 1998) and in the absence of other regulatory factors i.e. Mg^{2+}, ATP (discussed below), RyR2 exhibits a biphasic, bell-shaped activation/inactivation curve (Meissner & Henderson, 1987; Li & Chen, 2001) with the channel being inactivated by millimolar cytoplasmic Ca^{2+} concentrations (1-10mM). This could correspond to the interaction of Ca^{2+} with the A-site and I_1-sites described in Figure 1.9 (Laver, 2007).

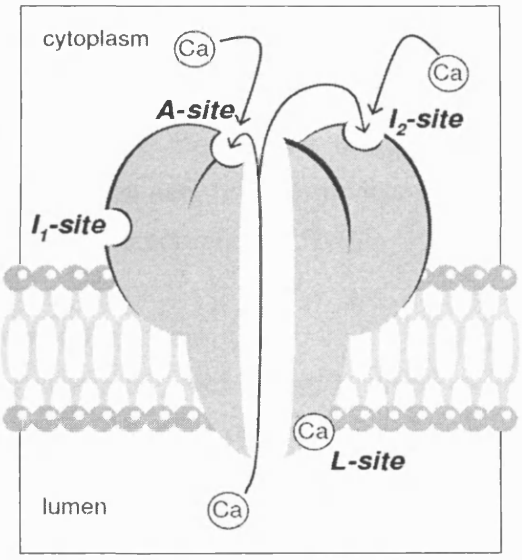

Site	Regulatory Role	Ligand	K_a
L-site	Luminal Activation	Ca^{2+}	60μM
A-site	Cytoplasmic Activation	Ca^{2+}	1-10μM
I_1-site	Cytoplasmic Inhibition	Ca^{2+} and Mg^{2+}	~10mM
I_2-site	Cytoplasmic Inactivation	Ca^{2+}	1μM

Figure 1.9. Schematic representation of RyR2 Ca^{2+} binding sites. *RyR2 is regulated by the binding of Ca^{2+} to three binding sites. The L-site is the luminal Ca^{2+} activation site, the A-site is the cytoplasmic Ca^{2+} activation site, the I_2-site is the cytoplasmic inactivation site and the I_1 site is the non-specific Ca^{2+}/Mg^{2+} inhibition site. From Laver, (2007).*

Single channel analysis of human RyR2 channels demonstrated that raising the cytosolic Ca^{2+} concentration from 1 to 100μM (with 67mM luminal Ca^{2+}) resulted in a significant increase in channel opening events (Holmberg & Williams, 1989). In the absence of luminal Ca^{2+} and any RyR2 activating cofactors, increasing cytoplasmic Ca^{2+}

concentration was shown to increase channel open probability (P_o) from 0 to 0.6 with a half maximal activating cytoplasmic Ca^{2+} concentration of 5μM (Sitsapesan & Williams, 1994).

The I_1 site is non-specific for divalent cations (Ca^{2+} and Mg^{2+}) with relatively low affinity (~10mM). A C-terminal fragment of RyR1 (residues 4007 to 5037) does not exhibit Ca^{2+}/Mg^{2+} inhibition, suggesting the I_2-site is in the N-terminal 4007 amino acids, and further studies have implicated amino acid residues 1873-1903, 1641-2437 and 615 with the I_2-site (Laver, 2006, 2007)

Luminal Ca^{2+} also plays a major part in regulating RyR2 activity and several models have been proposed by which luminal Ca^{2+} regulates RyR2 channel activation and inactivation. Although the precise mechanism of luminal Ca^{2+} regulation of RyR2 remains unknown, it is likely that each of the models described below contributes to luminal Ca^{2+}-depedent activation/inactivation of RyR2.

Ca^{2+} feed through hypothesis

Single-channel analysis of RyR2 in lipid bilayers, demonstrated that in the absence of cytoplasmic Ca^{2+} or other activating factors, increasing luminal Ca^{2+} up 10mM did not cause significant channel activation. (Xu & Meissner, 1998). It was subsequently proposed that luminal-to-cytoplasmic Ca^{2+} flux was required for activation by way of luminal Ca^{2+} binding to the cytoplasmic activation site, leading them to term this the Ca^{2+} feed-through hypothesis (Tripathy & Meissner, 1996).

Direct Luminal Ca^{2+} activation hypothesis

Another group showed that under conditions which prevented luminal-to-cytoplasmic Ca^{2+} flux, increasing luminal Ca^{2+} concentration significantly increased channel RyR2 activation (Ching *et al.*, 2000). Furthermore, trypsin digestion of the luminal face of RyR2 abolished luminal Ca^{2+} activation but did not alter Ca^{2} luminal-to-cytosolic Ca^{2+} flux, questioning the feed-through hypothesis and suggesting the presence of a luminal Ca^{2+} activation site (L-site).

Luminal-triggered Ca^{2+} feed-through hypothesis

The most recently proposed model incorporates both of the other activation mechanisms and proposes that RyR2 is activated by Ca^{2+} binding to either a luminal (L-site) or cytoplasmic Ca^{2+} binding site (A site) and is inactivated by Ca^{2+} binding to an inhibitory cytoplasmic Ca^{2+} binding site (I2-site, Laver, 2007). This group propose that Ca^{2+}-binding to the L-site causes brief channel openings, allowing small amounts of luminal-to-cytoplasmic Ca^{2+} flux causing a localised increase in the vicinity of the cytoplasmic A-site. Activation of the A-site was proposed to prolong channel openings and further SR Ca^{2+} release, which providing that this Ca^{2+} flux is of sufficient magnitude, caused channel inactivation by binding to the I_2-site.

Luminal Ca^{2+} sensitised cytosolic Ca^{2+} activation

This model proposes that luminal Ca^{2+} regulates RyR2 by altering the sensitivity of channels to activation by cytoplasmic Ca^{2+} (Qin *et al.*, 2008). It is proposed that an increase in luminal Ca^{2+} concentration leads to an increase in the maximal channel P_o at a given cytoplasmic Ca^{2+} concentration, as demonstrated in single channel studies (Qin, 2008, J Gen Physiol).

Calsequestrin-dependent luminal Ca^{2+} activation

This model proposes that the Ca^{2+}-binding protein, calsequestrin (CSQ, see section 1.2.3.2.2) acts as a putative luminal Ca^{2+} sensor. When SR Ca^{2+} is low, CSQ is proposed to exert an inhibitory effect on RyR2, preventing channel opening and contributing to channel inactivation (Gyorke & Terentyev, 2008). As SR Ca^{2+} content increases during SR refilling, CSQ is proposed to undergo a conformational change, dissociating it from the RyR2 quaternary complex and relieving RyR2 inhibition.

Magnesium inhibits human RyR2 activity in the millimolar concentration range (Holmberg & Williams, 1989; Rousseau & Meissner, 1989; Du *et al.*, 1998; Li & Chen, 2001), most likely through interaction with the I_i-site described above. This inhibitory effect was most prominent in low cytoplasmic Ca^{2+} concentrations, suggesting that Mg^{2+} exhibits its main physiological effects during diastole (Holmberg & Williams, 1989).

However, Mg^{2+} has recently been shown to increase RyR2 activation at intermediate Ca^{2+} concentrations (10-100μM), although this was only observed in rabbit RyR2, which does not exhibit the typical biphasic Ca^{2+}-dependence of activation/inactivation (Chugun *et al.*, 2007). Mg^{2+} is thought to result in channel inactivation through competitive binding to the non-specific divalent cation I_1-binding site and has also recently been proposed to compete with luminal Ca^{2+} to bind the L-site (Laver, 2007).

ATP is a potent RyR2 agonist and has been shown to increase RyR2 P_o, but only in the presence of cytoplasmic Ca^{2+} (Witcher *et al.*, 1991; Li & Chen, 2001; Laver, 2007), suggesting that ATP sensitises RyR2 to activation by this ligand, rather than directly activating the channel.

1.2.3.2. The RyR2 macromolecular complex

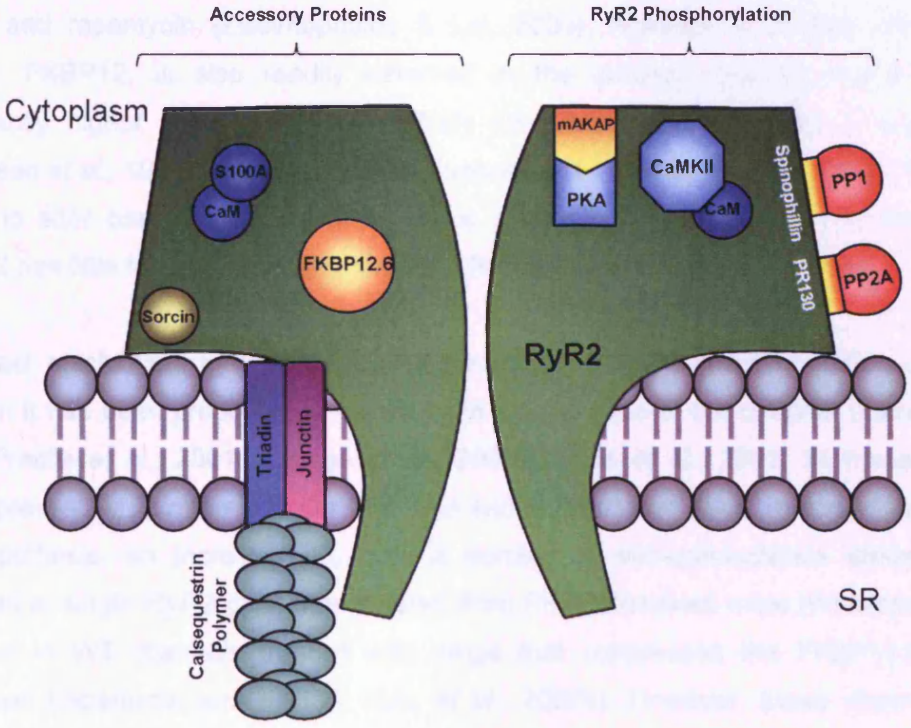

Figure 1.10. RyR2 macromolecular complex. *A schematic representation of the known components of the RyR2 macromolecular complex. Each tetramer may contain more than one interaction site for each accessory protein, as detailed in the text. The right hand side of the figure details anchoring proteins and kinases involved in the phosphorylation of RyR2. Proteins may not be constitutively bound to RyR2, as their interaction may depend on physiological conditions, e.g. phosphorylation status.*

As well as being activated and inactivated by free intracellular ions, RyR2 channel activity is also regulated by a number of accessory proteins. The cytoplasmic assembly of RyR2 acts as a scaffold to which many of these regulatory proteins bind, some of which co-precipitate with RyR2 (Marks *et al.*, 2002; Bers, 2004). The RyR2 channel and its associated proteins are commonly referred to as the RyR2 macromolecular complex and the proteins that compose this assembly are detailed here.

1.2.3.2.1. FK506-binding protein

The FK506 binding protein (FKBP12.6) is a 12.6kDa accessory protein that directly interacts with the cytoplasmic assembly, with a single FKBP12.6 binding site present on each RyR2 monomer (Timerman *et al.*, 1996; Sharma *et al.*, 2006). FKBP12.6 is described as an immunophillin due to its interaction with the immunosuppressant drugs FK506 and rapamycin (Zissimopoulos & Lai, 2005). Although a smaller FKBP12.6 isoform, FKBP12, is also readily detected in the cardiac myocyte, RyR2 has a significantly higher (~600-1000 fold) affinity for FKBP12.6 with which it co-purifies (Timerman *et al.*, 1996; Guo *et al.*, 2010). Furthermore, FKBP12.6, but not FKBP12, was shown to alter basal RyR2 activity in terms of Ca^{2+} spark frequency indicating that FKBP12 has little functional consequence on RyR2 function (Guo *et al.*, 2010).

The exact mechanism by which FKBP12.6 modulates RyR2 activity remains unclear, although it has been proposed to stabilise the closed state of the channel (Marx *et al.*, 2000; Prestle *et al.*, 2001; George *et al.*, 2003a; Yano *et al.*, 2003; Wehrens *et al.*, 2005), preventing spontaneous Ca^{2+} release and diastolic Ca^{2+} leak. In accordance with this hypothesis, an increased P_o and a number of sub-conductance states were observed in single RyR2 channels isolated from FKBP-knockout mice (Wehrens *et al.*, 2003) or in WT channels treated with drugs that suppressed the FKBP12.6:RyR2 interaction (rapamycin and FK506, Xiao *et al.*, 2007b). However, these observations were contested by results from another FKBP12.6 deficient mouse model, in which the absence of FKBP12.6 did not alter single RyR2 channel biophysical properties, agonist-sensitivity or the incidence of spontaneous Ca^{2+} release compared to WT mice (Xiao *et al.*, 2007b). Other studies have also demonstrated that FKBP12.6 does not have a significant effect on RyR2 channel function (Timerman *et al.*, 1996; Barg *et al.*, 1997).

It has also been proposed that the association of FKBP12.6 with RyR2 is highly dependent on RyR2 phosphorylation status and that 'hyper-phosphorylation' of RyR2 can lead to FKBP12.6 dissociation and channel destabilisation (Marx *et al.*, 2000; Wehrens *et al.*, 2003). However, this is also a highly contentious observation (Stange *et al.*, 2003; Meng *et al.*, 2007; Xiao *et al.*, 2007a; Guo *et al.*, 2010), which will be discussed further in section 1.2.3.2.4. Another area of continuing debate is the role of FKBP12.6 in arrhythmia caused by mutations in RyR2, which will be discussed in section 1.3.4.3.

1.2.3.2.2. Calsequestrin, Junctin and Triadin

It is well established that RyR2 channel activity is regulated by the SR free Ca^{2+} concentration, although the precise mechanism by which this occurs remains unknown (section 1.2.3.1). Calsequestrin (CSQ, encoded by *CASQ1 in skeletal muscle and CASQ2* in cardiac muscle) is a 42kDa high-capacity, low-affinity luminal SR Ca^{2+} binding protein (MacLennan, 1971) and has been proposed as the RyR luminal Ca^{2+} sensor in skeletal and cardiac muscle (section 1.2.3.1, Kim *et al.*, 2007; Gyorke *et al.*, 2009), although this role is disputed by other groups (Knollmann *et al.*, 2006). During Ca^{2+} uptake and release, CSQ forms a quaternary complex with RyR2 and two "anchoring" proteins; junctin and triadin which are 26kDa and 35kDa respectively (Figure 1.10, Zhang *et al.*, 1997)

Depending on the ionic environment, CSQ can exist in a range of highly organised aggregates ranging from monomers and dimers in the presence of low luminal [Ca^{2+}] to long CSQ polymers at high luminal [Ca^{2+}] (Beard *et al.*, 2005; Kim *et al.*, 2007). The C-terminal of CSQ is highly negatively charged and allows high capacity binding of Ca^{2+} ions (~50 per monomer) and interacts with junctin and triadin bound to the lumenal face of RyR (Kim *et al.*, 2007). This effectively ensures that high amounts of Ca^{2+} are stored at the RyR pore mouth, ready for Ca^{2+} release during EC-coupling.

Junctin and triadin have been shown to be constitutively bound to RyR2 during EC coupling, yet CSQ only interacts with junctin/triadin when free SR Ca^{2+} is low (Zhang *et al.*, 1997). Under these conditions, CSQ exerts an inhibitory effect on RyR2, which is proposed to allow more efficient SR Ca^{2+} refilling. At high luminal Ca^{2+}, the CSQ Ca^{2+}

binding sites become occupied causing a conformational change in CSQ and its subsequent dissociation from the quaternary complex, abolishing the inhibitory effect of CSQ and allowing channel opening and subsequent SR Ca^{2+} release (Kim *et al.*, 2007). The presence of all three accessory proteins is required for CSQ to regulate RyR2 activity in response to changes in luminal [Ca^{2+}] (Gyorke *et al.*, 2004; Gyorke *et al.*, 2009).

CSQ knockout mice were arrhythmogenic following exercise and exhibited an increase in spontaneous SR Ca^{2+} release from the SR coupled with an increased SR volume, despite exhibiting a normal systolic Ca^{2+} transient (Knollmann *et al.*, 2006), presenting a similar phenotype to that of CPVT patients (sections 1.3.1 and 1.3.4). Furthermore, mutations in CSQ, most of which are autosomal recessive, have been identified in patients exhibiting a CPVT-phenotype, implicating altered CSQ regulation of RyR2 in arrhythmia (section 1.3.4, Lahat *et al.*, 2001a; 2001b; Dirksen *et al.*, 2007).

1.2.3.2.3. Calmodulin

Calmodulin (CaM) is a 16.7kDa, ubiquitously expressed Ca^{2+} binding protein that regulates RyR2 channel activity through interaction with sub-domain 3 of the RyR2 cytoplasmic assembly (Samso & Wagenknecht, 2002; Bers, 2004). CaM consists of two pairs of Ca^{2+} binding EF hand domains separated by a flexible peptide linker sequence. In its Ca^{2+} free from, CaM appears as a dumbbell-shaped protein and is referred to as apoCaM and upon binding Ca^{2+} it undergoes a conformational change and is referred to as Ca^{2+}-calmodulin (CaCaM, Chin & Means, 2000). CaCaM has been shown to inhibit RyR2 activity at all cytoplasmic Ca^{2+} concentrations (Witcher *et al.*, 1991; Balshaw *et al.*, 2002; Yamaguchi *et al.*, 2003), and is proposed to do so by desensitising RyR2 to Ca^{2+}-dependent activation (Yamaguchi *et al.*, 2003). CaM has been proposed to inhibit diastolic RyR2 opening and recently the abolition of CaM binding to RyR2 in a knock-in mouse model harbouring a central domain CPVT mutation resulted in an arrhythmogenic phenotype (Xu *et al.*, 2010), suggesting CaM has a critical role in regulating RyR2 function. CaCaM also regulates the activity of Ca^{2+}/Calmodulin-dependent kinase II (CaMKII), a serine/threonine kinase involved in RyR2 phosphorylation (section 1.2.3.2.4).

1.2.3.2.4. Regulation of RyR2 by protein kinases

Although there is consensus that phosphorylation plays a major role in the regulation of RyR2 activity, there remains a great deal of contention as to the precise mechanism and functional consequences of channel phosphorylation. To date, three phosphorylation sites have been identified in RyR2, which are serine residues located at amino acid positions 2808, 2814 and 2031 in the human RyR2 sequence (Witcher *et al.*, 1991; Wehrens *et al.*, 2004; Xiao *et al.*, 2005; Huke & Bers, 2008). RyR2 is phosphorylated by a number of protein kinases, but the most-well documented are protein kinase A (PKA) and Ca^{2+}/calmodulin-dependent kinase II (CaMKII).

The serine at residue 2808 (S2808, S2809 in mice) was the first RyR2 phosphorylation site to be indentified (Witcher *et al.*, 1991) and has been proposed to be phosphorylated by CaMKII (Witcher *et al.*, 1991; Rodriguez *et al.*, 2003) and by PKA (Marx *et al.*, 2000; Rodriguez *et al.*, 2003; Wehrens *et al.*, 2003). However, a subsequent study demonstrated that CaMKII was unable to phosphorylate this residue, but phosphorylated a nearby serine residue, S2814 (S2815 in mice) which was not subject to PKA phosphorylation, suggesting that S2814 is an exclusive CaMKII phosphorylation site (Wehrens *et al.*, 2004).

The most recently identified phosphorylation site in RyR2 is a serine residue located at amino acid position 2030 in mice (S2030, S2031 in humans), which was shown to be subject to phosphorylation by PKA (Xiao *et al.*, 2005), but not by CaMKII, leading to the proposal that this was a PKA-specific phosphorylation site.

A recent study comparing the residue-specific phospho-antibodies used by different research groups in the investigation of RyR2 phosphorylation, has demonstrated that the sensitivities of each groups antibodies varied significantly (Huke & Bers, 2008). This suggests that these phospho-specific antibodies are not the most reliable indicators of RyR2 phosphorylation at specific residues and could explain some of the discrepancies in results obtained from different groups.

PKA-mediated phosphorylation of RyR2 has been shown to increase RyR2 P_o and cause the channel to exhibit several sub-conductance states (Marx *et al.*, 2000), although the observation of sub-conductance states has not been repeated to date.

Increased P_o following PKA phosphorylation was proposed to be the result of FKBP12.6 dissociation mediated by PKA phosphorylation of RyR2 (Marx *et al.*, 2000; Wehrens *et al.*, 2003). Similarly, CaMKII phosphorylation of RyR2 has also been shown to increase channel P_o (Witcher *et al.*, 1991; Wehrens *et al.*, 2004) but did not result in the dissociation of FKBP12.6 or in the observation of channel sub-conductance states (Wehrens *et al.*, 2004), suggesting that PKA and CaMKII alter RyR2 gating parameters through distinct mechanisms.

However, the functional consequences of RyR2 phosphorylation remain highly controversial, with several groups reporting that PKA and CaMKII-mediated phosphorylation does not cause the dissociation of FKBP12.6 from RyR2 (Jiang *et al.*, 2002; Stange *et al.*, 2003; Xiao *et al.*, 2005) or alter the biophysical properties of the channel (Stange *et al.*, 2003). Additionally, RyR2 has been shown to be phosphorylated at S2808 by PKA to approximately 75% of maximal levels under resting conditions, yet exhibits low channel activity (Carter *et al.*, 2006). As such, the precise role of phosphorylation and FKBP12.6 dissociation remains highly controversial.

The effects of PKA phosphorylation on RyR2 activity are further confounded by the fact that PKA phosphorylates a number of other Ca^{2+} handling proteins e.g. the SR Ca^{2+} ATPase, LTCC, whose effects, such as altered SR Ca^{2+} load, may alter RyR2 activity (Bers, 2002).

1.2.3.2.5. Protein Phosphatases – PP1 and PP2A

As phosphorylation is generally thought to increase RyR2 activity during periods of β-adrenergic stimulation (Marx *et al.*, 2000), there must also be a mechanism to reverse the action of RyR2 phosphorylation when β-adrenergic stimulation ceases. Several protein phosphatases (PP) reside in the RyR2 macromolecular complex and interact with RyR2 indirectly through adaptor proteins e.g. spinophillin, mAKAP (Marx *et al.*, 2000). Each of these proteins interacts with each other through substrate-specific isoleucine/leucine zipper (ILZ) sequences.

Much, like the role of phosphorylation in RyR2 regulation, the involvement of PP1 and PP2A in channel regulation remains controversial. PP1 and PP2A have been shown to

cause a depletion of SR Ca^{2+} stores and an increase in channel activity (Terentyev *et al.*, 2003; Carter *et al.*, 2006). This is a rather surprising observation as phosphorylation and dephosphorylation of RyR2 are opposing processes and would be expected to result in opposite effects on channel activity. A potential explanation could be that deviation from 75% of maximal S2809 phosphorylation levels increases RyR2 activity and protein kinases and phosphatases act in unison to regulate RyR2 activity (Carter *et al.*, 2006).

1.2.3.2.6. Other macromolecular proteins

S100A is 21kDa accessory protein that to date has received little attention in terms of its modulatory effect on RyR2 function. However, S100A competitively binds at the CaM binding site on RyR2 (Prosser *et al.*, 2008) and ablation of S100A results in a decrease in agonist-evoked SR Ca^{2+} release (Wright *et al.*, 2008), which is proposed to result from increased CaM binding in the absence of S100A.

Sorcin is a relatively novel 22kDa Ca^{2+} binding protein that localises to the RyR2 and LTCC junction (Farrell *et al.*, 2003). Upon binding Ca^{2+}, sorcin adopts a membrane bound form in which it is proposed to inhibit RyR2 over a wide range of Ca^{2+} concentrations (Valdivia, 1998). Sorcin has also been shown to directly interact with CaMKII and inhibit CaMKII activity, while CaMKII has been shown to phosphorylate sorcin (Anthony *et al.*, 2007), suggesting a collaborative regulatory effect on RyR2 activity.

1.2.3.3. Other myocyte Ca^{2+} handling proteins

Together with proteins in the RyR2 macromolecular complex, several other myocyte Ca^{2+} handling proteins are involved in regulating the availability of intracellular Ca^{2+} in the myocyte, and as such can indirectly influence RyR2 function.

1.2.3.3.1. L-Type Ca^{2+} channel

Although LTCC is not part of the RyR2 macromolecular complex *per se*, and there is no physical interaction between LTCC and RyR2 (unlike in RyR1, Lu *et al.*, 1994), these

two proteins exhibit an apparent functional coupling (see section 1.1.3). In order for resting Ca^{2+} homeostasis to be achieved, the LTCC current must be periodically stopped to allow cytoplasmic Ca^{2+} sequestration in intracellular stores, prior to the initiation of the subsequent action potential. LTCC is subject to two inactivation mechanisms; voltage-dependent inactivation and Ca^{2+}-dependent inactivation. Following SR Ca^{2+} release, the cytoplasmic Ca^{2+} concentration in the vicinity of the LTCC is dramatically increased and results in channel inactivation (Benitah *et al.*, 2010).

The functional LTCC is heterotetrameric and consists of a number of subunits (α_1, β, α_2, δ). Several isoforms of each subunit have been identified and the subunit composition of the LTCC varies between tissues (Treinys & Jurevicius, 2008), possibly accounting for the functional differences observed between activation mechanisms. Like RyR2, LTCC activity is modulated by phosphorylation by a number of kinases (PKA, PKC, PKG), which in the case of PKA, is consistent with the observation of altered Ca^{2+} current following β-adrenergic stimulation (Bodi *et al.*, 2005; Benitah *et al.*, 2010).

1.2.3.3.2. Sarco-endoplasmic Ca^{2+} ATPase and phospholamban

The human cardiac sarco-endoplasmic reticulum Ca^{2+} ATPase (SERCA), a 110kDa protein encoded for by the *SERCA2a* gene, is located in the SR membrane of the myocyte and is responsible for the sequestration of cytoplasmic Ca^{2+} in to the SR following myocyte contraction (Verboomen *et al.*, 1992). Each SERCA molecule contains two Ca^{2+} binding domains in the transmembrane region, a phospholamban (PLB) binding site in the cytoplasmic "head" and a thapsigargin binding site at the cytoplasmic face of the SR membrane (Toyoshima *et al.*, 2000).

SERCA activity is modulated by an SR membrane bound protein; phospholamban (PLB), which is a 22kDa protein comprising of a single transmembrane domain and a cytoplasmic "head" domain connected by a flexible linker sequence (Smith *et al.*, 2001). In its unphosphorylated state, PLB binds and inhibits SERCA, reducing the rate of Ca^{2+} uptake into the SR. PLB is readily phosphorylated by PKA and CaMKII and becomes dissociated from SERCA upon phosphorylation, increasing the rate of Ca^{2+} uptake into the SR and explaining the observed increase in Ca^{2+} transient amplitude following β-AR stimulation (Bers, 2008). The interaction between PLB and SERCA can also be

interrupted in the absence of PLB phosphorylation by increasing cytosolic Ca^{2+} above a certain threshold level, causing the loss of SERCA inhibition and an increase in the rate of Ca^{2+} uptake into the SR (Periasamy & Huke, 2001). Furthermore, PLB knockout mice displayed significantly increased SR Ca^{2+} load and rate of SR Ca^{2+} uptake and a decreased relaxation time (Chu *et al.*, 1998), indicative of increased SERCA activity in the absence of PLB.

SERCA Ca^{2+} uptake activity is Ca^{2+}-dependent, as demonstrated by the increase in rate of radio-labelled ^{45}Ca ion uptake by microsomes over-expressing SERCA2a in the presence of increasing Ca^{2+} concentrations, with a half maximal rate of Ca^{2+} uptake ($K_{0.5}$) at 0.34μM (Verboomen *et al.*, 1992). This infers that the rate of Ca^{2+} uptake into the SR is fastest during periods of elevated cytoplasmic Ca^{2+}, such as immediately following transient Ca^{2+} release during EC-coupling. There is evidence that SERCA expression and Ca^{2+} transfer activity is down-regulated in several experimental models of HF (reviewed by Bers, 2006).

1.2.3.3.3. Sodium-calcium exchanger (NCX)

Following CICR, the majority of cytoplasmic Ca^{2+} is resequestered in to the SR by SERCA (~75% in humans, Figure 4.1, Piacentino *et al.*, 2003), however, Ca^{2+} is also extruded from the cell, predominantly through a plasma membrane sodium-calcium exchanger (NCX, Bers, 2002; Piacentino *et al.*, 2003). NCX activity is electrogenic, in that a single Ca^{2+} ion is extruded from the cell in exchange for 3 Na^{+} ions, resulting in a net decrease in membrane potential. As such the outward Ca^{2+} current through NCX is evident throughout the majority of the action potential and is critical for myocyte repolarisation.

The role of phosphorylation in the regulation of NCX activity remains controversial with several groups reporting that PKA phosphorylation increases NCX activity, whereas others report that PKA-mediated phosphorylation has no effect on NCX (reviewed by Reppel *et al.*, 2007). However, given that a macromolecular complex containing protein kinase and phosphatase anchoring proteins (e.g. mAKAP) and the protein phosphatases PP1 and PP2 is present on the cytoplasmic face of NCX, a potential role of phosphorylation on NCX regulation is likely.

Over-expression of NCX in knock-in mouse models resulted in increased LTCC current amplitude, suggesting an element of compensation by LTCC following increased cytoplasmic Ca^{2+} extrusion (Reuter *et al.*, 2004). In contrast, knock-out mice deficient in NCX exhibited embryonic lethality, with myocytes isolated from 9.5 day post-coitum embryos displaying normal Ca^{2+} transients under resting conditions (Reuter *et al.*, 2003). However, following β-adrenergic or agonist stimulation when SR Ca^{2+} transient magnitude was increased, normal Ca^{2+} homeostasis was unable to be achieved, indicating a critical role of NCX in intracellular Ca^{2+} handling.

1.2.3.3.4. Slow Ca^{2+} extrusion mechanisms

Together with SERCA and NCX-mediated cytoplasmic Ca^{2+} removal, relatively small amounts of Ca^{2+} are extruded from the cell by a plasmalemmal Ca^{2+} ATPase (PMCA) or sequestered in the mitochondria via a uniporter. These two mechanisms of Ca^{2+} removal are collectively termed "slow mechanisms" and are proposed to account for approximately 1-2% of cytoplasmic Ca^{2+} removal following Ca^{2+} induced Ca^{2+} release (Bers, 2002), meaning that their functional impact on myocyte Ca^{2+} cycling and CICR is negligible compared to the other Ca^{2+} extrusion mechanisms.

Like SERCA, PMCA-mediated Ca^{2+} extrusion is an energy-driven process, with a single Ca^{2+} ion being removed from the cell for each molecule of ATP that is hydrolysed. PMCA activity is regulated by CaM which upon binding the ATPase causes a slight increase in PMCA Ca^{2+} affinity (Di Leva *et al.*, 2008). The uptake of Ca^{2+} into the mitochondrial uniporter is a passive process, in that Ca^{2+} moves down the electrochemical gradient from the cytoplasm during systole when cytoplasmic Ca^{2+} concentration is high. The uptake of Ca^{2+} into the mitochondria is believed to be involved in determining the rate of energy production, the spatio-temporal nature of intracellular Ca^{2+} signals and the regulation of cell death (Kirichok *et al.*, 2004).

1.3. Dysfunctional Ca^{2+} signalling and disease

Given the highly orchestrated nature of myocyte Ca^{2+} signalling and the integral role that RyR2 plays in this pathway, it is unsurprising that dysfunctional SR Ca^{2+} release through RyR2 is implicated in cardiac pathology.

Alterations in SR Ca^{2+} store load have been associated with many aspects of myocyte Ca^{2+} handling dysfunction and SR Ca^{2+} load can be altered through perturbed activity of many of the Ca^{2+} handling proteins discussed in sections 1.1.3. An increase in SR Ca^{2+} content can increase the sensitivity of RyR2 to activation and can result in increased spontaneous Ca^{2+} release i.e. Ca^{2+} sparks (Bers, 2006; Gyorke & Carnes, 2008). If such Ca^{2+} release is of sufficient amplitude, it can activate inward Na^{+} currents through NCX, which can lead to early and delayed after depolarisations (EADs and DADs, see section 5.1.1) which can cause the initiation of premature action potentials and lead to arrhythmia (Bers, 2006). Contrarily, downregulation of SERCA or upregulation of NCX causes a decrease in Ca^{2+} transient amplitude and can result in impaired cardiac contractility, as observed during HF (Bers, 2006, Phsyiol). Decreased SR Ca^{2+} load can also occur as a result of Ca^{2+} leak from the SR resulting from destabilised or "leaky" RyR2 channels (Marx *et al.*, 2000). Not only can this Ca^{2+} leak result in decreased transient amplitude, but if the leak is sufficient it could potentially activate inward Na^{+} currents through NCX and cause premature APs as described above.

Over the last decade, a great deal of evidence has demonstrated that mutations in the gene encoding RyR2 alter many parameters of SR Ca^{2+} release and have been associated with two arrhythmia-linked conditions, which are described in section 1.3.1.

1.3.1. CPVT and ARVD2

Catecholaminergic polymorphic ventricular tachycardia (CPVT) is an arrhythmogenic condition characterised by the occurrence of syncopal episodes and sudden cardiac death under conditions of physical or emotional stress. CPVT does not cause structural aberrations of the heart and the patients present a normal ECG pattern under resting conditions, making the disorder relatively difficult to diagnose (Leenhardt *et al.*, 1995; Priori *et al.*, 2002). Only after increased β-adrenergic stimulation do patients exhibit

bidirectional ventricular tachycardia, which if persistent can result in arrhythmia. Males who have inherited a mutation in RyR2 have been reported to be at slightly higher risk of exhibiting CPVT than females (Priori *et al.*, 2002; Medeiros-Domingo *et al.*, 2009), although this difference is only observed in some earlier cohorts (George *et al.*, 2007).

CPVT has been linked to chromosome 1q42-q43 (Swan *et al.*, 1999), a region which encompasses the locus for *RyR2*. Mutations in this gene have since been associated with CPVT (Priori *et al.*, 2001). These mutations are inherited in an autosomal dominant fashion, meaning that inheritance of a single disease-linked allele is sufficient to result in a CPVT phenotype and exhibits a high mortality rate (30-50% by the age of 30 years old, Fisher *et al.*, 1999). Arrhythmogenic right ventricular dysplasia type 2 (ARVD2) is a similar condition to CPVT, in that it presents as stress-induced arrhythmias on a background of a normal resting ECG (Rampazzo *et al.*, 1995) and is an autosomal dominant disease caused by genetic mutations in RyR2 (Tiso *et al.*, 2001). However, ARVD2 is distinguishable from CPVT due to the observation of partial replacement of the sub-epicardial right-ventricular myocardium with fatty-fibrous tissue in affected patients (Rampazzo *et al.*, 1995).

CPVT has also been linked to a distinct second chromosomal location, 1p13-21 (Lahat *et al.*, 2001a; Lahat *et al.*, 2001b) and was subsequently shown to result from mutations in the *CASQ2* gene (Lahat *et al.*, 2002). Unlike the autosomal dominant form of CPVT caused by mutations in RyR2, mutations in *CASQ2* are autosomal recessive in nature (Lahat *et al.*, 2002), meaning that inheritance of a *CASQ2* disease-linked mutation on both alleles is required to result in a CPVT phenotype.

1.3.2. Identification of disease-linked RyR2 mutations

The onset of CPVT was first attributed to mutations in RyR2 through the genotyping of a number of patients who exhibited bidirectional ventricular tachycardia on a background of a normal resting ECG and a structurally normal heart (Leenhardt *et al.*, 1995; Priori *et al.*, 2001; Postma *et al.*, 2005).

The majority of CPVT patients demonstrate a family history of CPVT symptoms, such as syncope or sudden cardiac death, suggesting the inheritability of the condition. However

in some cases the patient was the only symptomatic family member and neither parent carried the mutant allele, suggesting that CPVT mutations can also arise in a *de novo* manner (Priori *et al.*, 2001; Laitinen *et al.*, 2003; Postma *et al.*, 2005; Marjamaa *et al.*, 2009). CPVT-associated mutations tend to be located in regions of the gene that are highly conserved between species and isoforms, suggesting that they are of particular functional importance (Laitinen *et al.*, 2001; Priori *et al.*, 2001; Postma *et al.*, 2005; Marjamaa *et al.*, 2009). RyR2 mutations also appear to cluster in three distinct regions of the protein, that correspond to regions of RyR1 in which mutations have been shown to be associated with malignant hypothermia (MH) and central core disease (CCD, Priori & Napolitano, 2005). These domains are located towards the cytoplasmic N-terminus (residues 77-466, CPVT I), the central domain (residues, 2246-2534, CPVT II) and the C-terminal channel region (residues 3778-4959), which is sometimes split into two domains, CPVT III and IV, Figure 1.11, (George et al., 2007; Medeiros-Domingo et al., 2009).

Genotyping studies are often targeted to these regions of RyR2, resulting in screening of only a portion of the coding exons (Priori *et al.*, 2001; Laitinen *et al.*, 2003; Choi *et al.*, 2004; Postma *et al.*, 2005; Nishio *et al.*, 2008). This infers that substitutions that reside outside of these mutational "hot-spots" may sometimes be overlooked and can result in a CPVT patient being described as genotype-negative, despite the possibility that a mutation may be present outside of these mutation clusters (Creighton *et al.*, 2006). Although the majority of studies in which sequencing of the entire RyR2 coding sequence has been carried out tend not to report disease-linked mutations outside of these mutational "hot-spots" (Laitinen *et al.*, 2001; Tiso *et al.*, 2001; Bagattin *et al.*, 2004; Marjamaa *et al.*, 2009b), there are exceptions to this in which mutations have been identified at the peripheries of these clusters (Marjamaa *et al.*, 2009a; Medeiros-Domingo *et al.*, 2009). Furthermore, common polymorphisms have been identified in the regions between these mutational clusters which may or may not have functional significance (section 1.4.4.2.2 and 1.4.4.2.3, Laitinen *et al.*, 2001; Tiso *et al.*, 2001).

Cases of ARVD2 have been reported, in which symptomatic individuals have inherited two RyR2 disease-linked mutations on the same allele i.e. R176Q/T2504M (Tiso *et al.*, 2001), with subsequent functional characterisation in a heterologous system revealing that either mutation alone was sufficient to perturb intracellular Ca^{2+} handling (Thomas *et al.*, 2004). However, the homotetrameric co-expression of R176QM/T2504M exhibited

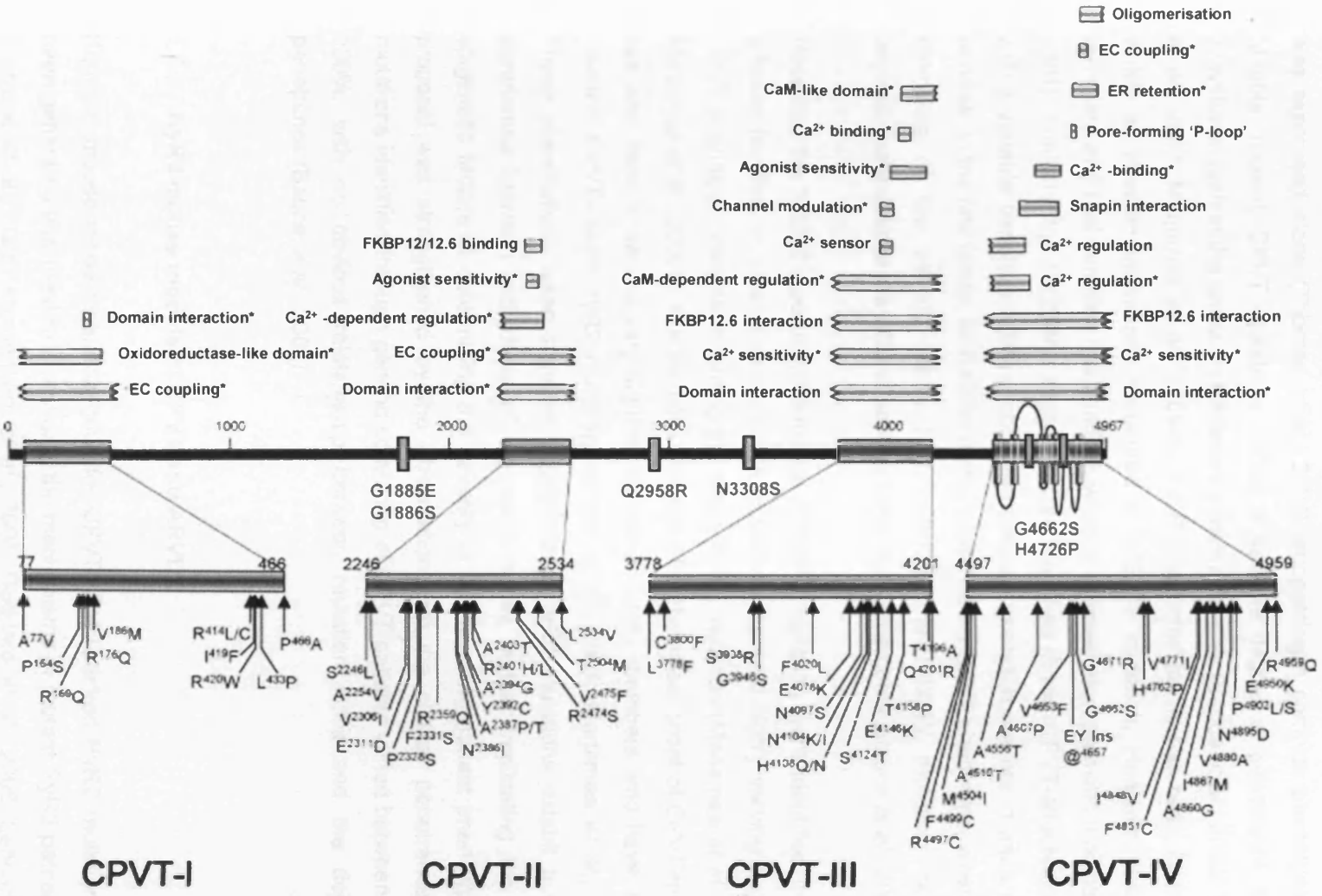

Figure 1.11. CPVT/ARVD2 mutations cluster in distinct regions of RyR2. *Disease-linked RyR2 mutations cluster into an N-terminal (CPVT I), central (CPVT II) and a C-terminal and transmembrane domain (CPVT III and IV). CPVT III and IV are often classed as a single mutational domain. These regions contain functionally important regulatory motifs. Asterisked fragments indicate the functional role was ascertained in RyR1. Adapted from (George et al., 2007a). Recent genetic screening of RyR2 has identified further mutations, extending the peripheries of these mutational domains (Medeiros-Domingo et al., 2009; Thomas et al., 2010). Polymorphisms that have been identified in RyR2 are indicated in blue and will be discussed further in section (Tiso et al., 2001; Postma et al., 2005; Marjamaa et al., 2009a).*

different intracellular Ca^{2+} handling characteristics compared to when either mutation was expressed alone (Thomas *et al.*, 2004), suggesting a complex phenotype of the "double" mutant. CPVT mutations exhibit a variable degree of penetrance between individuals, both in the same and different affected families (Bauce *et al.*, 2002; Thomas *et al.*, 2007; Marjamaa *et al.*, 2009b). A CPVT-affected family has been identified in which all affected individuals harboured a P2328S mutation. However, two family members who had inherited this mutation were completely asymptomatic (Laitinen *et al.*, 2001). Similarly, the R420W substitution was identified in two CPVT-affected families, with a variable penetrance being observed between mutation carriers in each of these families. In the first family, all R420W carriers exhibited a CPVT phenotype, whereas two members of the second family had inherited the R420W mutation, but were asymptomatic despite the SCD of several other family members (Bauce *et al.*, 2002).

Recently, the N3308S polymorphism and R3570W mutation were identified in CPVT-affected families, in which carriers of the mutation displayed highly varying degrees of CPVT phenotype, despite inheriting the same RyR2 mutation (Marjamaa *et al.*, 2009a; Marjamaa *et al.*, 2009b). Furthermore, the age of pathological onset of CPVT-mutations has also been shown to vary significantly within family members who have inherited identical CPVT-linked RyR2 mutations (Priori *et al.*, 2001; Marjamaa *et al.*, 2009a). These observations taken together suggest that RyR2 mutations exhibit a variable penetrance between individuals of the same family, further implicating the role of epigenetic factors in determining the severity of the resulting mutant phenotype. This proposal was strengthened by the observation that the clinical penetrance of six mutations identified through genetic screening of CPVT patients varied between 25 and 100%, with no obvious relationship between mutation locus and the degree of penetrance (Bauce *et al.*, 2002).

1.3.3. RyR2 mouse models of CPVT and ARVD2

Knock-in mouse models heterozygous for CPVT/ARVD2-linked RyR2 mutations have been generated and used to investigate the mechanisms of mutant RyR2 pathogenesis (Cerrone *et al.*, 2005; Kannankeril *et al.*, 2006; Goddard *et al.*, 2008; Lehnart *et al.*, 2008; Fernandez-Velasco *et al.*, 2009; Uchinoumi *et al.*, 2010). These models allow investigation into the effects of RyR2 mutations in the intact heart of a mammalian

organism, although considerations must be made for differences in cardiac physiology between species e.g. heart rate, relative contributions of Ca^{2+} extrusion mechanisms, cardiac output etc.

A knock-in mouse, heterozygous for the C-terminal R4496C mutation ($R4496C^{+/-}$), the mouse equivalent to the human R4497C CPVT-linked mutation (Priori, 2001), displayed no structural aberrations of the heart and exhibited a normal ECG under resting conditions (Cerrone *et al.*, 2005), in agreement with the CPVT phenotype observed in humans. However, $R4496C^{+/-}$ mice displayed a significantly increased susceptibility to bidirectional and polymorphic VT in response to exercise stress-testing or β-adrenergic stimulation and caffeine administration, a phenomenon characteristic of CPVT (Priori *et al.*, 2002). The treatment of $R4497C^{+/-}$ mice with β-blockers did not prevent the onset of arrhythmia in these mice (Cerrone *et al.*, 2005), which is reflective of only the partial success of β-blocker administration in preventing arrhythmia in CPVT patients carrying this mutation. A phenomenon that was first described in $R4496C^{+/-}$ mice, was the observation that myocytes isolated from these mice exhibited increased spontaneous SR Ca^{2+} release under basal, non-stimulated conditions, which was exacerbated following β-adrenergic stimulation (Liu *et al.*, 2006; Fernandez-Velasco *et al.*, 2009). This provides the first evidence that CPVT-linked RyR2 mutations cause an underlying defect in intracellular Ca^{2+} handling at rest, which is worsened following β-adrenergic stimulation, corroborating observations made through heterologous expression and subsequent functional characterisation of R4496C (section 3.1.1.6, Jiang *et al.*, 2002).

Another mouse model has been generated, which is heterozygous for the R2474S central domain CPVT-linked RyR2 mutation (Lehnart *et al.*, 2008). As in other mouse models, $R2474S^{+/-}$ mice displayed a normal heart rate and rhythm at rest, but exhibited bidirectional and polymorphic VT following exercise stress-testing and epinephrine administration. Myocytes isolated from these mice also exhibited an increased spontaneous Ca^{2+} release event frequency following β-adrenergic stimulation, an observation that was not evident at rest or in WT myocytes. Interestingly, these mice also exhibited spontaneous brain seizures, independently of cardiac arrhythmias (Lehnart *et al.*, 2008), providing evidence that mutant RyR2 dysfunction is not limited to cardiac disorders, although this has not been observed in humans suggesting this phenotypic manifestation may be species-specific. Unlike the other mouse models, these mice displayed a reduced RyR2-FKBP12.6 interaction under resting conditions,

which was exacerbated following PKA-mediated RyR2 phosphorylation, which is consistent with the model proposed by *Marx* (2000, section 1.3.4.3) and *Wehrens* (2003). Conversely, a second mouse model harbouring the same R2474S mutation has been generated and characterized by another group (Uchinoumi *et al.*, 2010) who observed a slightly different phenotype. Although these mice presented bidirectional or polymorphic VT in response to exercise or caffeine/epinephrine administration, they also exhibited increased spontaneous polymorphic ventricular contractions under resting conditions. The increase in the occurrence of VT was attributable to an observed increase in spontaneous SR Ca^{2+} release events in myocytes isolated from the $R2474S^{+/-}$mouse, both at rest and following β-adrenergic stimulation. However in contrast to *Lehnart's* R2474S heterozygous mouse, *Uchinoumi et al* did not observe spontaneous seizures in their R2474S mouse model, nor did they observe the increase in PKA-mediated hyper-phosphorylation of RyR2 and subsequent FKBP12.6 dissociation (Uchinoumi *et al.*, 2010), illustrating phenotypic differences between the two heterozygous mouse models harbouring the same R2474S mutation (Lehnart *et al.*, 2008; Uchinoumi *et al.*, 2010), which could be attributable to differences in the genetic background of the mice (Cook *et al.*, 2009).

Similarly, a knock-in mouse heterozygous for the N-terminal R176Q ARVD2/CPVT-linked RyR2 mutation ($R176Q^{+/-}$) has been produced (Kannankeril *et al.*, 2006). These mice exhibited a normal resting ECG and exhibited premature ventricular beats following β-adrenergic stimulation, which developed into bidirectional VT under pacing conditions (Kannankeril *et al.*, 2006), similar to the phenotype observed in ARVD2 and CPVT patients. However, there was no evidence of the ARVD2-characteristic fibro-fatty infiltration of the right ventricle (Rampazzo *et al.*, 1995) in hearts isolated from $R176Q^{+/-}$ mice, although a decrease in systolic function was observed. This suggests this mouse model is a more representative of the CPVT phenotype and suggests the co-inherited T2504M mutation may be responsible for the ARVD2 phenotype observed in some patients (Tiso *et al.*, 2001).

Recently, a central domain CPVT-linked RyR2 mutation, P2328S, was investigated in mice that were both homozygous ($P2328S^{+/+}$) or heterozygous ($P2328S^{+/-}$) for the mutation (Goddard *et al.*, 2008). Compared to either WT or $P2328S^{+/-}$ mice, $P2328S^{+/+}$ mice exhibited a much more severe arrhythmogenic phenotype, displaying increased VT

Mutation	Disease	Location	Knock-in Mouse Phenotype	Isolated Myocyte Phenotype	References
R176Q	ARVD2	N-terminus	Developed arrhythmia upon caffeine/epinephrine administration	Increased Spontaneous Ca^{2+} release at rest and upon catecholamine treatment.	*Kannankeril, 2006*
P2328S (homozygote)	CPVT	Central Domain	Higher VT incidence than heterozygote. EADs and arrhythmia at rest (6/11 hearts) Developed arrhythmia upon catecholamine treatment (11/11 mice).	Increased spontaneous Ca^{2+} release at rest, enhanced by catecholamine treatment. Decreased SR Ca^{2+} upon catecholamine treatment.	*Goddard, 2008*
P2328S (heterozygote)	CPVT	Central Domain	Developed arrhythmia upon catecholamine treatment (5/7 mice).	Normal phenotype at rest and upon catecholamine treatment	*Goddard, 2008*
R2474S (i) (homozygote)	CPVT	Central Domain	Lethal developmental phenotype - S107 treatment prevented embryonic lethality.	n/a	*Lehnart, 2008*
R2474S (i) (heterozygote)	CPVT	Central Domain	Exhibited tonic-clonic seizures spontaneously and in response to weak stimuli i.e. arousal from sleep. Developed arrhythmia upon exercise / catecholamine treatment (8/9 mice) - S107 treatment prevented arrhythmia and decreased seizure propensity.	Increased spontaneous Ca^{2+} release at rest, enhanced by catecholamine treatment. Decreased RYR2-FKBP12.6 interaction - S107 restored FKBP12.6 binding and stabilized channel.	*Lehnart, 2008*
R2474S (ii)	CPVT	Central Domain	No observed tonic-clonic seizures. Developed arrhythmia in response to weak stimuli i.e. light and sound as well as caffeine/catecholamine treatment.	Prolonged SR Ca^{2+} transient and lower SR Ca^{2+} load. Increased spontaneous Ca^{2+} release at rest, enhanced by catecholamine treatment.	*Uchinoumi, 2010* *Xu, 2010*
R4496C	CPVT	C-terminus	Developed arrhythmia upon exercise/catecholamine treatment (5/14 mice) - β-blockers did not prevent arrhythmia (4/5 mice) - K201 did not prevent DAD's or VT (5/5 mice)	Increased spontaneous Ca^{2+} release at rest, enhanced by catecholamine treatment. Increased DADs at rest (21/33 myocytes) and upon catecholamine treatment (29/33) - not prevented by K201 treatment. - Increased Ca^{2+} sparks and waves following ouabain-induced SR Ca^{2+} overload.	*Cerrone, 2005, Liu, 2006, Fernandez-Verlasco, 2009* *Sedej, 2010*

Table 1.2. CPVT/ARVD2-linked RyR2 mutant knock-in mouse models. *Summary of the currently available RyR2-mouse models carrying CPVT/ARVD2-associated mutations. Mice containing the same mutation which were generated by different groups are denoted by (i) and (ii).*

under resting conditions (6/11, 55%) or following β-adrenergic stimulation (11/11, 100%, (Goddard *et al.*, 2008). This is the first instance in which an RyR2 mutation has been characterised both homozygously and heterozygously in a mouse model and suggests that the relative prevalence of the mutant allele is imperative in determining the severity of the disease phenotype, although homozygous CPVT mutation inheritance is not observed *in vivo.* Interestingly, cross-breeding of R2474S$^{+/-}$ mice did not produce offspring in accordance with Mendelian inheritance patterns with only 3.5% of offspring exhibiting an R2474S$^{+/+}$ genotype after 16.5 days of embryonic development (Lehnart *et al.*, 2008). This suggests that homozygous inheritance of R2474S results in a more severe or lethal developmental phenotype. Taken together, these observations corroborate the autosomal dominant nature of CPVT and ARVD2 mutations *in vivo.*

These data provide confirmation that CPVT/ARVD2-linked RyR2 mutations expressed in a murine model replicate the disease phenotype observed in the human condition to some extent, although some different phenotypic characteristics were observed (Kannankeril *et al.*, 2006). Furthermore, there were differences of the phenotype of two different mouse models which expressed the same CPVT-linked R2474S mutation. However, there are obviously physiological differences between mouse and human, including altered ion channel expression levels, decreased heart size and significantly increased heart rate of mice (Cook *et al.*, 2009), which may or may not alter the phenotypic manifestation of the disease-linked mutation when compared across species.

1.3.4. Pathogenic mechanisms of RyR2 mutations

Given that disease-linked mutations are located throughout the RyR2 protein in several functionally important regions (Figure 1.11) and exhibit a degree of variable penetrance (Bauce *et al.*, 2002; Marjamaa *et al.*, 2009b), it is highly unlikely that all mutations result in an arrhythmogenic phenotype through a single unifying mechanism. Furthermore, as the number of functionally characterised arrhythmia-linked RyR2 mutations is increasing, it is hardly surprising that several mechanisms by which RyR2 mutations result in an arrhythmogenic phenotype have been proposed, each of which will be described here.

1.3.4.1. Altered RyR2 Ca^{2+} sensitivity

Arrhythmia-linked mutations have been shown to alter RyR2 sensitivity to both luminal and cytoplasmic Ca^{2+}, which can result in perturbed channel gating and dysregulated Ca^{2+} release.

Several N-terminal and central domain mutations have been shown to alter the Ca^{2+} dependence profiles of channel activation and inactivation in a heterologous cell system (Thomas *et al.*, 2005). The majority of characterised RyR2 disease-linked mutations have been shown to result in an increase in sensitivity to activation by cytoplasmic Ca^{2+}, when examined in single channel experiments, (S4565R, R3570W, Tester *et al.*, 2007; Marjamaa *et al.*, 2009b), in [^{3}H] ryanodine binding experiments (Jiang *et al.*, 2002) and when expressed in heterologous systems (Thomas *et al.*, 2005). However, an exception to this is the L433P ARVD2-linked RyR2 mutation which caused a decrease in Ca^{2+} sensitivity (Thomas *et al.*, 2005), suggesting that this mutation results in a decrease in channel activity, an observation that will be discussed further in section 3.1.3.

The effect of RyR2 mutations on Ca^{2+} sensitivity is further confounded by the fact that many mutations exhibit a similar cytoplasmic Ca^{2+} dependent activation profile compared to WT RyR2 (Jiang *et al.*, 2005; Tester *et al.*, 2007; Marjamaa *et al.*, 2009b) and has led to the emergence of the hypothesis that disease-linked RyR2 mutations preferentially alter the sensitivity of RyR2 to activation by luminal Ca^{2+} (Jiang *et al.*, 2004; Jiang *et al.*, 2005). Mutations from regions spanning the length of RyR2 were shown to increase RyR2 luminal Ca^{2+} sensitivity (Jiang *et al.*, 2005; Uchinoumi *et al.*, 2010), which manifested as an increase in spontaneous Ca^{2+} release coupled with a decrease in the levels of ER Ca^{2+} load when examined in heterologous systems (Jiang *et al.*, 2005; Jones *et al.*, 2008a). These observations have also been corroborated in single channel analysis and [^{3}H] ryanodine binding experiments (Jiang *et al.*, 2004; Jiang *et al.*, 2005). Although the majority of RyR2 disease-linked mutations increase luminal Ca^{2+} sensitivity, some mutations have been shown to decrease or completely ablate luminal Ca^{2+} sensitivity (Jiang *et al.*, 2007), suggesting the location and nature of the mutation can have profound effects on the extent of Ca^{2+} dysregulation. However, this is further complicated by the potential coupling between luminal and cytoplasmic Ca^{2+} activation and inactivation of RyR2 (section 1.2.3.1).

Although it may be difficult to envisage how a mutation located on the cytoplasmic face of the channel, such as R176Q, can alter luminal Ca^{2+} sensitivity, this could potentially be explained according to the disruption of RyR2 intra-molecular interactions described below. However, such mutations have been demonstrated to alter luminal Ca^{2+} sensitivity to a lesser extent than those located in the transmembrane region e.g. A4860G (Jiang *et al.*, 2007). The role of altered luminal Ca^{2+} regulation of RyR2 and the resulting effects on spontaneous SR Ca^{2+} release will be discussed in more detail in Chapter 5. The implication of dysfunctional luminal Ca^{2+} sensitivity also complements the implication of CSQ mutations in CPVT pathogenesis (CPVT2, see section 1.3.5).

1.3.4.2. Disruption of RyR2 inter-domain interactions

It has been proposed that regions of the RyR2 cytoplasmic assembly participate in inter-domain interactions, which are important in stabilising the closed state of the channel (Yamamoto & Ikemoto, 2002). Under resting conditions, a region of the N-terminus (residues 1-600) has been proposed to interact with a region of the central domain (residues 2000-2500), in a process termed domain "zipping" (Ikemoto & Yamamoto, 2000). Following stimulation of the channel, this interaction is proposed to be weakened, causing "unzipping" of this domain interaction and allowing channel opening and subsequent Ca^{2+} release (Ikemoto & Yamamoto, 2002). In support of this model, it has been shown that these two domains lie in close proximity to each other in sub-domain 5 of the cytoplasmic assembly (Figure 1.6, Liu *et al.*, 2005; Wang *et al.*, 2007). A recent FRET-based study confirmed that this interaction takes place between the N-terminal and central domains of separate RyR2 subunits rather than an intra-subunit interaction (Liu *et al.*, 2010). Furthermore, in support of this model, a short peptide corresponding to a region of the central domain (DPc10, G2460-P2495), has been shown to competitively bind the N-terminal domain, reversibly increasing channel activity and Ca^{2+} leak (Oda *et al.*, 2005), indicative of RyR2 destabilisation and this peptide was also shown to disrupt the FRET signal described above (Liu *et al.*, 2010).

Notably, these two interacting-domains correspond to regions of RyR2 in which disease-linked mutations have been shown to cluster (Medeiros-Domingo *et al.*, 2009). This led to the hypothesis that RyR2 mutations result in a CPVT/ARVD2 phenotype through the "unzipping" of these intramolecular interactions destabilising the channel and increasing

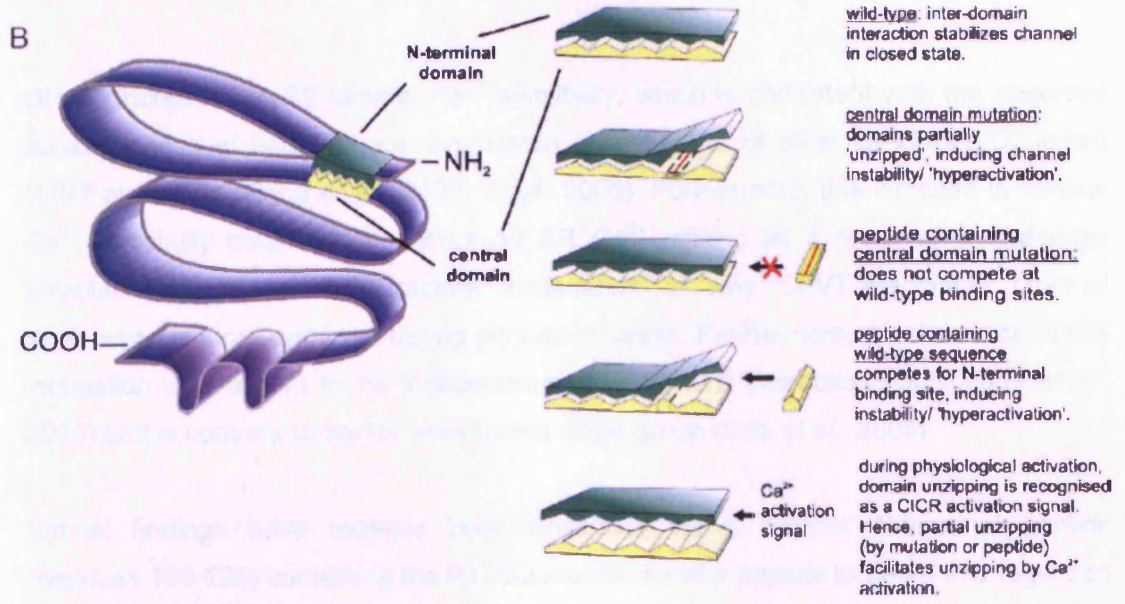

Figure 1.12. Schematic of peptide probe competition hypothesis of inter-domain interaction. *The N-terminal domain (green) interacts with the central domain (yellow). A central domain mutation results in the partial "unzipping" of the intra-domain interaction. DPc10-R2474S does not cause the disruption of this interaction. WT DPc10 competes for the N-terminal binding site, inducing domain unzipping and channel instability. Domain unzipping is involved in channel activation in CICR and partial unzipping facilitates further unzipping by Ca^{2+} activation. From Yang, (2006).*

RyR2 activity. This was supported by the observation that insertion of a CPVT-linked central domain RyR2 mutation, R2474S, into DPc10 prevented channel destabilisation. By extrapolation, this suggests that the presence of R2474S in RyR2 disrupts the interaction between the N-terminal and central domain, resulting in channel destabilisation and increased channel activity attributed to CPVT (Oda *et al.*, 2005; Yang *et al.*, 2006) and is consistent with recent results from an R2474S knock-in mouse (Uchinoumi *et al.*, 2010). In addition, the destabilisation of the channel caused by DPc10 resulted in an increase in RyR2 luminal Ca^{2+} sensitivity which was not observed when R2474S was present in the peptide, in accordance with the proposal that CPVT-linked mutations alter luminal Ca^{2+} sensitivity (section 1.3.4.1). Similar findings were obtained when DPc10 (10-50μM) was introduced into cardiac myocytes, in that DPc10 caused a sustained increase in resting cytoplasmic Ca^{2+} levels pertaining to increased SR Ca^{2+} leak and an increase in Ca^{2+} spark frequency associated with increased spontaneous Ca^{2+} release (Yang *et al.*, 2006).

DPc10 increased RyR2 luminal Ca^{2+} sensitivity, which is consistent with the observed consequences of heterologous expression of a number of other CPVT/ARVD2-linked RyR2 mutations (Jiang *et al.*, 2002; 2004; 2005). Furthermore, this increase in luminal Ca^{2+} sensitivity coupled with increased SR Ca^{2+} refilling as a result of β-adrenergic stimulation, provides an attractive explanation of why CPVT-associated channel dysfunction is more apparent during periods of stress. Furthermore, the disruption of this interaction was shown to be independent of FKBP12.6 interaction (Uchinoumi *et al.*, 2010) and is contrary to earlier work by the same group (Oda *et al.*, 2005).

Similar findings have recently been described using another N-terminal peptide (residues 163-195) containing the R176Q mutation and a peptide targeted to a region on the cytoplasmic side of the transmembrane domain (residues 4090 to 4123) containing the N4104K mutation (Tateishi *et al.*, 2009). This latter region is proposed to be involved in RyR2 autoregulation and is termed the I-domain (George, 2004, Mol. Biol. Cell). Both WT peptides resulted in increased Ca^{2+} leak manifesting as increased Ca^{2+} spark frequency, which was not observed with the mutated peptides, suggesting that these mutations also cause channel destabilisation by altering domain-domain interactions. Similarly, mutations in the I-domain (N4104K and R4497C) of the full-length channel were also shown to cause channel destabilisation and augmented Ca^{2+} release following agonist-evoked channel activation (George *et al.*, 2006), suggesting that disruption of interactions between the C-terminal and central domains can also result in channel dysfunction. This also provides a potential mechanism by which mutations in the cytoplasmic domain can alter luminal Ca^{2+} sensitivity.

1.3.4.3. RyR2 hyper-phosphorylation and FKBP12.6 dissociation

As described in section 1.2.3, the mechanism by which phosphorylation alters RyR2 activity (section 1.2.3.2.4) and the role of FKBP12.6 in RyR2 regulation (section 1.2.3.2.1) remains highly contentious, as do their roles in mutant RyR2 pathogenesis.

Marx et al proposed that CPVT-linked RyR2 mutations exhibit an increased sensitivity to β-adrenergic mediated PKA phosphorylation, resulting in a decreased affinity for FKBP12.6 and increased RyR2 destabilisation and SR Ca^{2+} leak (Marx *et al.*, 2000; Wehrens *et al.*, 2003). However, whether PKA hyperphosphorylation of CPVT-linked

mutant RyR2 channels causes the dissociation of FKBP12.6 and whether mutations alter the RyR2-FKBP12.6 interaction has been highly disputed by a number of other laboratories.

CPVT-linked mutations do not alter RyR2 phosphorylation status:

Firstly, equivalent levels of RyR2 phosphorylation were observed in heterologously expressed mutant and WT RyR2 using pan-phospho-specific (George *et al.*, 2003c) and a S2809-specific phospho-antibody (Tester *et al.*, 2007). Similarly, RyR2 isolated from heterozygous R4497C and R2474S knock-in mice exhibited equivalent S2809 phosphorylation levels compared to RyR2 isolated from WT mice (Fernandez-Velasco *et al.*, 2009; Sedej *et al.*, 2010; Xu *et al.*, 2010), providing further evidence that mutant RyR2 channels are not disproportionately phosphorylated or hyperphosphorylated. Recently, it was shown that R4497C myocytes exhibited spontaneous Ca^{2+} release and DADs independently of PKA phosphorylation as a result of oubain-induced SR Ca^{2+} overload (Sedej *et al.*, 2010), further questioning the role of RyR2 phosphorylation at S2808/S2809 in CPVT.

CPVT-linked mutations do not alter FKBP12.6 affinity:

There is also ambiguity over whether RyR2 mutations lead to the dissociation of FKBP12.6 from RyR2, as proposed by *Marks* and colleagues (Lehnart *et al.*, 2004; Sedej *et al.*, 2010). Several groups have shown that mutations from distinct regions of RyR2 exhibit a similar affinity for FKBP12.6 as that observed with WT RyR2 in heterologous expression systems (George *et al.*, 2003a; Jiang *et al.*, 2005; Tester *et al.*, 2007; Jones *et al.*, 2008a; Zissimopoulos *et al.*, 2009) and the R4497C knock-in mouse (Liu *et al.*, 2006). A recent study has also demonstrated that the N-terminal and central domain mutations, R176Q and S2246L, respectively, resulted in an increase in FKBP12.6 binding to RyR2 (Zissimopoulos *et al.*, 2009), adding further complexity to the effects of RyR2 mutations on RyR2-FKBP12.6 interaction.

Arrhythmia-associated phenomena are independent of FKBP12.6 interaction:

To further contest the role of FKBP12.6 dissociation in RyR2 mutant pathogenesis, CPVT/ARVD2-linked mutations have been shown to perturb intracellular Ca^{2+} handling without altering the RyR2-FKBP12.6 interaction or in the complete absence of FKBP12.6 from the experimental system. The R2474S and R4497C mice exhibited an unaltered RyR2-FKBP12.6 interaction, yet displayed increased susceptibility to DADs and

arrhythmia (Fernandez-Velasco *et al.*, 2009; Zissimopoulos *et al.*, 2009; Uchinoumi *et al.*, 2010). Similar results were obtained through heterologous expression of RyR2 containing several CPVT mutations, in that several RyR2 mutations altered luminal Ca^{2+} sensitivity or agonist-evoked SR Ca^{2+} release magnitude, despite normal levels of FKBP12.6 interaction (George *et al.*, 2003a; Jiang *et al.*, 2005).

These observations suggest that RyR2 is not hyperphosphorylated following β-adrenergic stimulation and CPVT/ARVD2 linked mutations do not cause increased FKBP12.6 dissociation from RyR2, making it highly unlikely that these are the mechanisms of RyR2 mutant pathogenesis.

1.3.5. Identification and pathogenic mechanisms of CSQ mutations

A CPVT-associated mutation in the cardiac isoform of CSQ (D307H) was first identified in a Bedouin family, in which several members exhibited stress-induced polymorphic VT on a background of a normal resting ECG (Lahat *et al.*, 2001a; Lahat *et al.*, 2001b). CPVT arising from mutations in the *CASQ2* gene is termed 'CPVT2', as opposed to CPVT (or CPVT1) arising from RyR2 mutations.

Homozygous R33Q and D307H knock-in mouse models presented similar phenotypes to those observed in human CPVT2, with myocytes isolated from these mice exhibiting decreased SR Ca^{2+} content and increased spontaneous Ca^{2+} release leading to DADs (Houle *et al.*, 2004; Dirksen *et al.*, 2007; Song *et al.*, 2007). These mutations were both shown to alter the tertiary structure of CSQ, disrupting polymerisation (Houle *et al.*, 2004; Song *et al.*, 2007; Bal *et al.*, 2010), suggesting that this is a common mechanism which contributes to the observed CPVT phenotype. Interestingly, similar observations were also made in CSQ-deficient mice, suggesting the homozygous inheritance of CSQ mutations causes near-complete ablation of normal CSQ function (Song *et al.*, 2007).

The precise mechanism by which mutations in CSQ result in a similar CPVT phenotype to that caused by RyR2-mutations remains unsolved, although there are two prominent hypotheses; a SR store-overload model proposed by *Chen* and colleagues and the ablation of CSQ-mediated RyR2 regulation model proposed by *Gyorke et al.* The first model of mutant CSQ pathogenesis is akin to the "SOICR" model (described in chapter

5), whereby the increase of SR Ca^{2+} load above a particular threshold level is proposed to result in spontaneous Ca^{2+} release through mutant RyR2 (MacLennan & Chen, 2009). In terms of mutant CSQ, this model proposes that the decreased Ca^{2+} binding affinity of mutant CSQ increases the level of free luminal Ca^{2+} above the threshold for diastolic Ca^{2+} leak (MacLennan & Chen, 2009). The level of SR Ca^{2+} is further increased during β-adrenergic stimulation, following an increase in PKA-mediated SERCA activity. This is proposed to result in increased spontaneous Ca^{2+} release, which can lead to DADs and arrhythmias observed in the autosomal recessive from of CPVT. The model proposed by Györke et al hypothesised that mutations in CSQ alter the protein-protein interactions between CSQ, junctin and triadin with RyR2, leading to dysfunctional regulation of RyR2 opening (Gyorke *et al.*, 2009). Like CPVT-linked mutations in RyR2, there does not appear to be a unifying mechanism by which CSQ mutations result in a CPVT phenotype i.e. D307H alters CSQ Ca^{2+} binding properties, whereas R33Q perturbs inter and intramolecular interactions between CSQ and RyR2.

1.3.6. Treatment of CPVT and ARVD2

The predominant therapeutic strategy currently employed to treat CPVT arrhythmogenesis is the administration of β-adrenergic receptor antagonists (β-blockers), including propranolol and atenolol (Priori *et al.*, 2002). This is intended to limit the stimulatory effect of circulating catecholamines on the β-adrenergic pathway (section 1.1.5), which has been widely implicated in models of arrhythmogenesis, with varying degrees of success. Some studies report high β-blocker efficacy in preventing further episodes (65%, Bauce *et al.*, 2002; 98%, Postma *et al.*, 2005), whereas others report a much lower success rate (Lahat *et al.*, 2001a), with ablation of arrhythmic episodes in just 41% of a Japanese CPVT cohort and 22% of patients dying during the 10 year follow-up period (Sumitomo *et al.*, 2003). The disparity in the success of β-blocker treatment in different patients could suggest that not all mutations result in CPVT through the same pathogenic, β-adrenergic-dependent mechanism or that other factors are involved in determining the penetrance of a particular mutation. The use of implantable cardioverter defribillators (ICD) is the usual course of treatment in patients in which β-blocker therapy is ineffective, although this treatment is also not always successful (Pizzale *et al.*, 2008).

K201 (also know as JTV-519) and S107 are compounds that have displayed several cardio-protective and anti-arrhythmic properties in the hands of a number of research groups, although there remains contention over the precise mechanism by which it elicits these benefits. K201 and S107 have been proposed to prevent arrhythmia by inhibiting spontaneous Ca^{2+} release from the SR by restoring the interaction between FKBP12.6 and RyR2 (Wehrens *et al.*, 2003; Yano *et al.*, 2003; Lehnart *et al.*, 2008), resulting in the stabilisation of the channel. *Marks et al* showed that K201 prevented arrhythmia in heterozygous FKBP12.6 knock-out mice, but not in FKBP12.6 null mice (Wehrens *et al.*, 2003; Lehnart *et al.*, 2006), suggesting that FKBP12.6 was essential for the therapeutic action of K201. However, given the ambiguity over the involvement of FKBP12.6 in CPVT, this hypothesis has been challenged by several other groups. K201 administration did not alter the FKBP12.6 interaction or the occurrence of DADs or arrhythmia in the R4496C heterozygous mouse model (Liu *et al.*, 2006). Furthermore K201 abolished the spontaneous Ca^{2+} release observed in myocytes and RyR-deficient cell lines, independently of FKBP12.6 association (Hunt *et al.*, 2007). It has also been suggested that SERCA is the main target of K201 (Loughrey *et al.*, 2007). Together, these findings indicate that further clarification is needed on the effects of K201 and S107 on RyR2 dysfunction.

Verapamil, an LTCC antagonist, has also been used to treat CPVT, although with limited success as it did not prevent arrhythmia, but increased the threshold of arrhythmia occurrence during exercise-stress testing (Sumitomo *et al.*, 2003). Verapamil has been shown to reduce spontaneous Ca^{2+} release when administered at high concentrations (intraperitoneal, 8μg/g mouse body weight, Wakimoto *et al.*, 2007), although this exceeded the toxic level in plasma and lower concentrations (0.5mM) had no observable effect on mutant RyR2 channel stabilisation (Liu *et al.*, 2010). A recent study demonstrated that verapamil did not affect disrupted intra-domain interactions between the N-terminal and central domains of RyR2 (Liu *et al.*, 2010).

Flecainide is a Na^{+} channel antagonist and has recently been shown to be effective in preventing arrhythmia in both CPVT1 and CPVT2 patients who were non responsive to β-blocker and verapamil therapy (Watanabe *et al.*, 2009) Flecanaide was demonstrated to decrease the frequency of spontaneous Ca^{2+} waves release in a CPVT2 mouse model (Watanabe *et al.*, 2009), which is proposed to be the result of a decreased in Ca^{2+} spark magnitude, despite an increase in spark frequency (Hilliard *et al.*, 2009).

Dantrolene is a compound that is used to treat malignant hypothermia in patients harbouring mutations in RyR1. A recent study demonstrated that dantrolene prevented diastolic Ca^{2+} leak and spontaneous Ca^{2+} release through RyR2 isolated from failing canine hearts (Kobayashi *et al.*, 2009), by restoring the defective inter-domain interactions in RyR2. Recently, the extent of the stabilising effect of dantrolene has been proposed to be dependent on the location of the mutation. Dantrolene was shown to stabilise inter-domain interactions weakened by a central domain mutation (R2474S, (R2474S, Liu *et al.*, 2010; Uchinoumi *et al.*, 2010), but had no effect on spontaneous Ca^{2+} release observed in cells expressing a C-terminal mutation (N4104K, Jiang *et al.*, 2008).

1.4. Single nucleotide polymorphisms in cardiac channelopathies.

Although both DNA polymorphisms and mutations are essentially changes in DNA sequence away from the "normal" or wild-type sequence, there are several differences between the precise definitions of these terms. Firstly, in order for a nucleotide substitution to be classified as a single nucleotide polymorphism (SNP), the least common allelic variant must be present in at least 1% of the population; otherwise the substitution is classed as a mutation. Secondly, SNPs are not usually causative of disease and although they may be identified in affected-individuals, they are also likely to be prevalent in the control population (Roses, 2000). For purposes of clarity in this thesis, missense nucleotide substitutions resulting in a disease-linked amino acid substitution will be referred to as "mutations", whereas substitutions that are not exclusively related to a disease-phenotype and are present in the healthy population will be referred to as "polymorphisms" or SNP's.

There is substantial evidence that rare nucleotide substitutions (mutations) in genes encoding several cardiac ion channels result in cardiomyopathies. Many of these mutations have been demonstrated to result in the alteration of ion channel structure and function, resulting in an arrhythmogenic phenotype (Zimmer & Surber, 2008; Medeiros-Domingo *et al.*, 2009).

However, since the advent of high throughput genotyping technologies such as SNP microarrays and genome wide association studies, common polymorphisms have received an increasing amount of interest. Genotyping of 29 cardiac genes in a large cohort (n = 1468) revealed three genes in which common SNPs were associated with subtle, but detectable, alterations in heart rate (cardiac sodium channel; SCN5A, calsequestrin; CASQ1 and β-adrenergic receptor; ADRB1, Wilton *et al.*, 2008), demonstrating that common sequence variants can modulate cardiac function. Furthermore, the inheritance of common SNPs in a number of cardiac ion channel genes has been demonstrated to cause subtle variation in QT interval (Pfeufer *et al.*, 2005).

There is an extremely strong link between a family history of HF and the likelihood of SCD and VT onset during myocardial infarction, suggesting that inherited genetic factors may pre-dispose to arrhythmia (Spooner *et al.*, 2001; Kaikkonen *et al.*, 2006). In support of this, genetic association studies have identified relationships between arrhythmia

susceptibility and SNPs in a number of genes encoding cardiac ion channels (Napolitano *et al.*, 2005; Albert *et al.*, 2010). SNPs in genes associated with long QT syndrome (LQTS) and related arrhythmogenic disease have been the focus of many of these studies and have revealed that these common sequence variants can have significant functional consequences on disease phenotype.

1.4.1. Congenital and acquired long QT syndrome

LQTS is a cardiac disorder which presents as a prolonged QT interval on an ECG, resulting from the prolongation of myocyte repolarisation during the cardiac action potential (Phase 0, Figure 1.3). Sustained myocyte repolarisation can result in the onset of early after-depolarisations (EADs), which can lead to Torsades de pointes (TdP), a specific variant of polymorphic VT. There are two variants of LQTS; termed congenital and acquired LQTS which exhibit a similar disease phenotype but are triggered by somewhat different mechanisms (van Noord *et al.*, 2010).

Congenital LQTS is caused by the inheritance of rare genetic mutations, predominantly in an autosomal dominant fashion, in a number of genes encoding proteins involved in myocyte repolarisation. The vast majority of congenital LQTS cases are due to mutations in cardiac Na^+ or K^+ channel genes (SCN5A, KCNQ1 and KCNH2, Tester *et al.*, 2005), however, there is emerging evidence that mutations in structural proteins e.g. AKAP9, caveolin-3 result in LQTS, although this has been observed in significantly fewer cases (Schulze-Bahr, 2006, 2008). Different subtypes of LQTS are described according to the gene in which the causative mutation is identified (LQT1-12), accompanied by differences in clinical phenotype e.g. Brugada syndrome, Timothy syndrome etc, (Schulze-Bahr, 2008; Webster & Berul, 2008). Congenital LQTS-associated mutations have been reported to have a variable penetrance (Priori *et al.*, 1999; Napolitano *et al.*, 2005), suggesting that like CPVT-associated mutations in RyR2, the inheritance of a LQTS-associated mutation does not necessarily result in a disease-phenotype, inferring that other genetic factors may be involved in modulating congenital LQTS pathogenesis.

Acquired LQTS (aLQTS) is significantly more prevalent than its congenital counterpart and aLQTS patients do not tend to inherit rare LQTS-associated genetic mutations. Instead, aLQTS onset is dependent on other mitigating factors including, but is not

limited to, female gender, congestive heart failure and ventricular hypertrophy, although by far the most common trigger is an adverse reaction to medication (Yang *et al.*, 2002; Schulze-Bahr, 2006, 2008). Many drugs have been linked to LQTS-onset including both anti-arrhythmic and non-anti-arrhythmic medications, with the majority of these drugs altering the duration of the QT interval by blocking repolarising I_{Kr} current (van Noord *et al.*, 2010). Given that aLQTS is observed in patients with no evidence of LQTS-associated mutations (Koo *et al.*, 2007), it is hypothesised that common sequence variation in the genes associated with congenital LQTS may pre-dispose individuals to QT prolongation and arrhythmia in response to other triggering factors. As such, it is regularly quoted that aLQTS is a "forme fruste" or masked variation of congenital LQTS.

1.4.2. Association of SNPs with LQTS

Genetic association and linkage studies have provided a great deal of evidence to support the above hypothesis and have demonstrated an apparent association of aLQTS with common SNPs (Yang *et al.*, 2002), some of which occur in up to 1 in 3 healthy individuals (Nof *et al.*, 2010). The relative abundance of these SNPS compared to rare congenital LQTS-associated mutations is a plausible explanation for the higher prevalence of aLQTS compared to the congenital form. Examples of the association of cardiac ion channel SNPs with LQTS and the functional consequences of SNP inheritance will be discussed in this section.

Splawski et al identified a SNP in the gene encoding the cardiac sodium channel, *SCN5A* (see section 1.4.4.1), encoding the S1102Y amino acid substitution, which was present in 11-13% of healthy African-Americans (Splawski *et al.*, 2002; Van Norstrand *et al.*, 2008). A subsequent study demonstrated that this SNP was more prevalent in an SCD-patient cohort of African origin, suggesting that S1102Y was associated with an increased risk of arrhythmia (Burke *et al.*, 2005). Functional characterisation of this SNP showed that S1102Y caused a slight prolongation of the QT interval by causing a modest negative shift in voltage dependence of channel activation (Splawski *et al.*, 2002). Another group demonstrated that S1102Y channels behaved comparably to WT channels under normal conditions, with a positive shift in channel inactivation only observed following cellular acidosis (Plant *et al.*, 2006). Taken together, these findings suggest that although the inheritance of the S1102Y SNP alone is not sufficient to result

in arrhythmia, it may pre-dispose carriers to acquired arrhythmia in response to secondary "trigger" factors.

Similarly, a SNP resulting in a non-synonymous K897T substitution in the gene encoding the cardiac potassium channel (*KCNH2,* hERG), responsible for the rapid inward rectifying K^+ current (I_{Kr}) during phase 3 of the AP, has been associated with a modest decrease in QT interval duration (1.6-10ms, Bezzina *et al.*, 2003; Marjamaa *et al.*, 2009c), which translated as a modest shift in I_{Kr} activation voltage dependence (-7mV, Bezzina *et al.*, 2003). This alteration in both QT duration and channel activation voltage dependence are comparatively small compared to those observed in congenital LQTS-associated mutations (30-40ms, Sanguinetti *et al.*, 1996) suggesting that K897T inheritance alone is unlikely to be of sufficient magnitude to result in EADs and TdP. This further suggests that the inheritance of common SNPs that cause subtle alterations in QT interval, may increase patient susceptibility to factors that also augment the QT interval e.g. QT interval prolonging drugs and LQTS associated mutations.

Of course, this could also suggest that the combinational effect of several co-inherited SNPs that each cause subtle alterations in QT interval, either in a single or several LQTS associated genes, could culminate in severe QT interval augmentation and arrhythmia. This proposal has been supported by a study in which affected members of several families suffering from congenital LQTS had not inherited a disease-linked mutation, but had inherited several common SNPs in several LQTS associated genes (Koo *et al.*, 2007).

1.4.3. Ethnicity-dependent variation in SNP prevalence

Association studies have also demonstrated that the prevalence of SNPs that are associated with increased arrhythmia-susceptibility vary significantly between populations of different ethnicity. Although, the S1102Y *SCN5A* polymorphism was relatively prevalent in individuals of African descent (section 1.4.2), this SNP was absent in large Asian, Caucasian or Hispanic control cohorts (n = 123 - 511, Splawski *et al.*, 2002). Interestingly, this same polymorphism was identified in SCD-affected individuals of a single Caucasian family (Chen *et al.*, 2002), but due to its absence from the healthy Caucasian population was classified as a mutation, rather than a SNP in this case. The

increased prevalence of S1102Y in populations of African descent (Splawski *et al.*, 2002; Van Norstrand *et al.*, 2008) could be a contributing factor to the observation that SCD is more frequent in African-descended populations compared to Caucasians (Zheng *et al.*, 2001). Furthermore, the K897T SNP in *KCNH2* that was present in ~32% of the Caucasian population was only found in 2% of a healthy Japanese cohort (Iwasa *et al.*, 2000).

In light of these observations, and the apparent susceptibility of certain populations to particular genetic arrhythmia-linked diseases i.e. increased prevalence of sudden unexplained death syndrome (SUDS) in Asian populations (Lizotte *et al.*, 2009), increased SCD in African-Americans etc (Zheng *et al.*, 2001), further suggests ethnicity-specific SNPs may predispose to arrhythmia.

1.4.4. Modulatory effects of SNPs on disease-linked mutations

Although association and linkage studies demonstrate that many SNPs are associated with increased arrhythmia susceptibility, an understanding of the mechanistic basis by which they result in arrhythmia pre-disposition is only obtained through their biophysical and intracellular characterisation.

Heterozygous inheritance of a *KCNH2* SNP (K897T) was shown to exacerbate the reduction in inward K^+ current caused by co-expression of a predicted stop codon (P926Ax14) in the same gene (Nof *et al.*, 2010). Interestingly, heterozygotic inheritance of either one of these alterations had no effect on clinical phenotype, yet co-inheritance of both alterations resulted in a severe arrhythmogenic phenotype (Nof *et al.*, 2010), suggesting the common K897T predisposes to arrhythmia caused by the co-inheritance of the stop codon mutation.

As well as increasing arrhythmia susceptibility by exacerbating the detrimental effects of ion channel mutations, common SNPs have been also been shown to offer protection against mutant phenotype (Viswanathan *et al.*, 2003; Ye *et al.*, 2003; Poelzing *et al.*, 2006). Although this phenomenon has been described in a number of cardiac ion channel genes, mutations and SNPs in *SCN5A* have been subjected to the most

rigorous combinatorial characterisation, and will be the focus of the next part of this introduction.

1.4.4.1. Cardiac sodium channel (hNav1.5)

The α-subunit of the human cardiac Na^+ channel (hNav1.5) is encoded for by the *SCN5A* gene and is expressed as a 260kDa transmembrane protein which constitutes the pore-forming region of the channel. The sodium channel β-subunits (NaVβ1 - 4) are much smaller, single transmembrane domain proteins that are proposed to be involved in the regulation and intracellular localisation of hNav1.5 (Abriel, 2010). hNav1.5 is responsible for the rapid depolarisation of the myocyte during phase 0 of the cardiac action potential, in which there is a rapid influx of Na^+ ions into the myocyte, causing the activation of the LTCC (Figure 1.3, Bers, 2008).

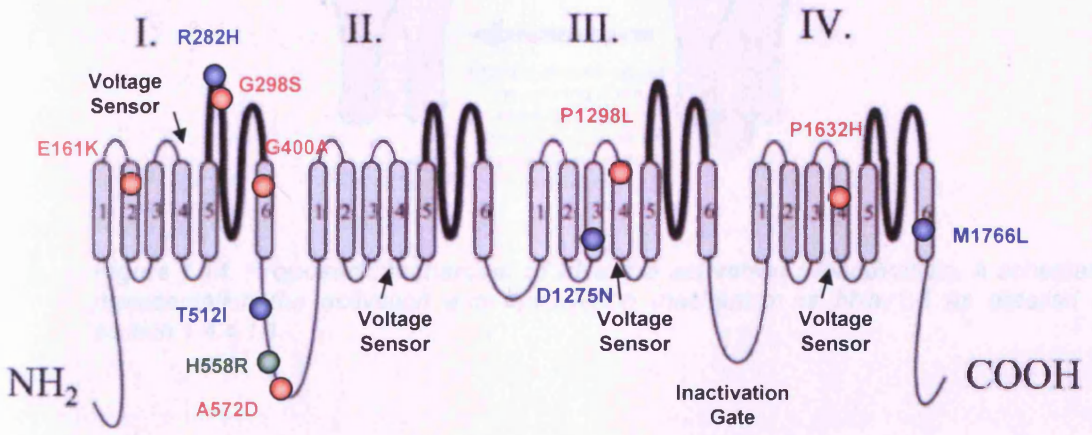

Figue 1.13. Schematic representation of the cardiac sodium channel protein (hNav1.5) α-subunit encoded for by the SCN5A gene. *The channel consists of four domains (DI-IV) connected by cytoplasmic linker sequences. Each domain contains six transmembrane segments (S1-S6) and a domain specific pore-forming loop (p-loop) between segments 5 and 6. S6 comprises the voltage sensor and the intracellular DIII-DIV loop comprises the inactivation gate. The common H558R SNP is indicated in green. Red residues are those whose functional consequences are exacerbated by H558R, whereas those whose normal function is restored by H558R (see section 1.4.4.1.2) are indicated in blue. Adapted from Balser (1999)*

hNav1.5 consists of four homologous transmembrane domains (I-IV) connected by cytoplasmic linker sequences, with each domain containing six transmembrane segments (S1-S6) as depicted in Figure 1.13. Residues between S5 and S6 of each

domain turn back into the protein to form the channel pore structure, which is termed the P-loop. (Balser, 1999; Grant, 2001) and is highly conserved between species and isoforms.

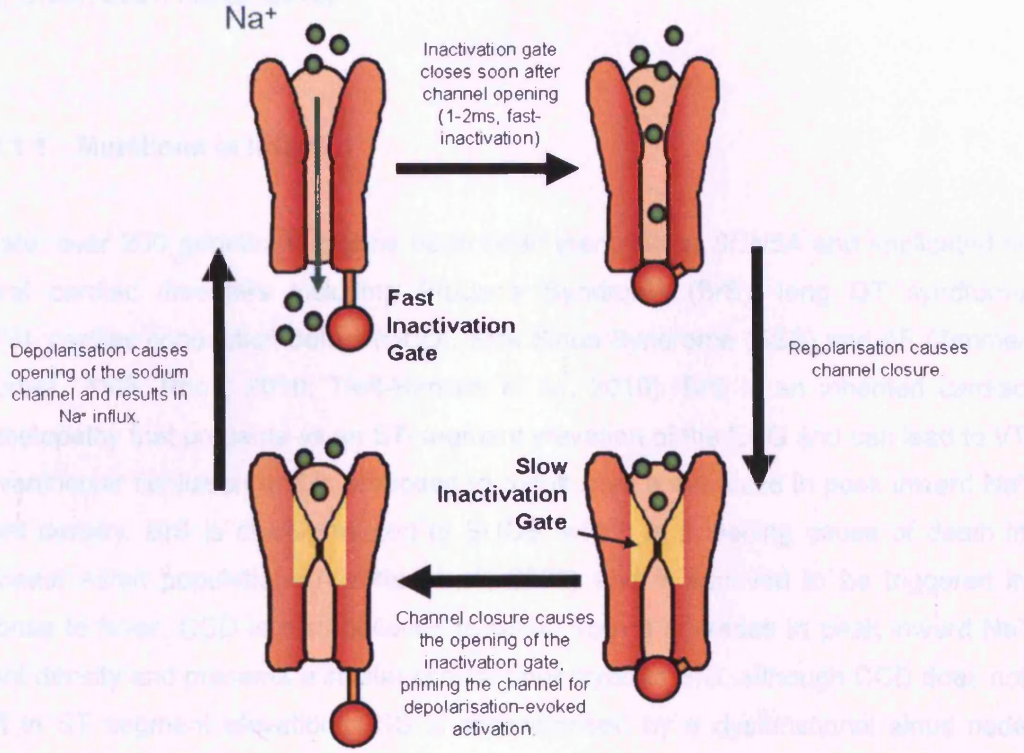

Figure 1.14. Proposed mechanism of hNav1.5 activation / inactivation. *A schematic representation the activation and inactivation mechanism of hNav1.5 as detailed in section 1.4.4.1.1.*

The S4 segment is proposed to contain the voltage sensor motif and undergoes a conformational change upon membrane depolarisation, resulting in protrusion of S4 into the cell and subsequent channel opening (Figure 1.14, Balser, 1999). The channel is inactivated within a few milliseconds of opening and the conformational change in S4 is proposed to act as the trigger for "fast-inactivation" of Nav1.5. The flexible intracellular loop between domain III and IV contains a cluster of hydrophobic amino acids which act as a pore-lid flanked by glycine and proline residues which function as molecular hinges and is collectively termed the "fast-inactivation gate". The flexibility of these flanker sequences allow the hydrophobic lid to bind to the its receptor site in the intracellular mouth of the pore, terminating inward Na^+ current and allowing membrane repolarisation. Repolarisation results in further conformational changes in S4, causing it

described above i.e voltage sensor, fast-inactivation gate and inactivation gate receptor sites (Zimmer & Surber, 2008).

Conversely, *SCN5A* mutations associated with BrS, SSS or CCD tend to confer a loss-of-function phenotype and have been shown to decrease or abolish inward Na^+ current by several mechanisms (Gui *et al.*, 2010a). Some mutations e.g. R282H, M1766L, R1232W/T1620M prevent correct hNav1.5 channel trafficking to the sarcolemmal membrane, retaining the protein within intracellular compartments (Baroudi *et al.*, 2002; Ye *et al.*, 2003; Poelzing *et al.*, 2006; Gui *et al.*, 2010a), completely ablating or decreasing inward Na^+ current as shown in Figure 1.15., indicating that different *SCN5A* mutations can affect the same mechanism to varying degrees.

Other loss-of-function *SCN5A* mutations correctly localise to the sarcolemmal membrane, but reduce inward Na^+ current by altering Nav1.5 biophysical properties. The G1406R mutation correctly localised to the sarcolemmal membrane, but caused complete ablation of Na^+ current (Kyndt *et al.*, 2001), presenting a severe cellular phenotype. The T512I CCD-linked mutation caused a hyperpolarisation of hNav1.5 activation and inactivation and enhanced slow channel inactivation, delaying channel recovery (Viswanathan *et al.*, 2003).

Interestingly, whether *SCN5A* mutations are expressed alone or are co-expressed with another *SCN5A* mutation can have a major impact on the severity of the resulting cellular phenotype. Both the R1232W and T1620M BrS-linked mutations have been shown to correctly localise to the sarcolemmal membrane, and both mutations exhibit enhanced channel inactivation properties when expressed alone. However, the co-expression of both R1232W and T1620M mutations resulted in complete ablation of Na^+ current and was attributable to incorrect membrane trafficking of the channel (Baroudi *et al.*, 2002), suggesting a detrimental combinational effect of some *SCN5A* mutations.

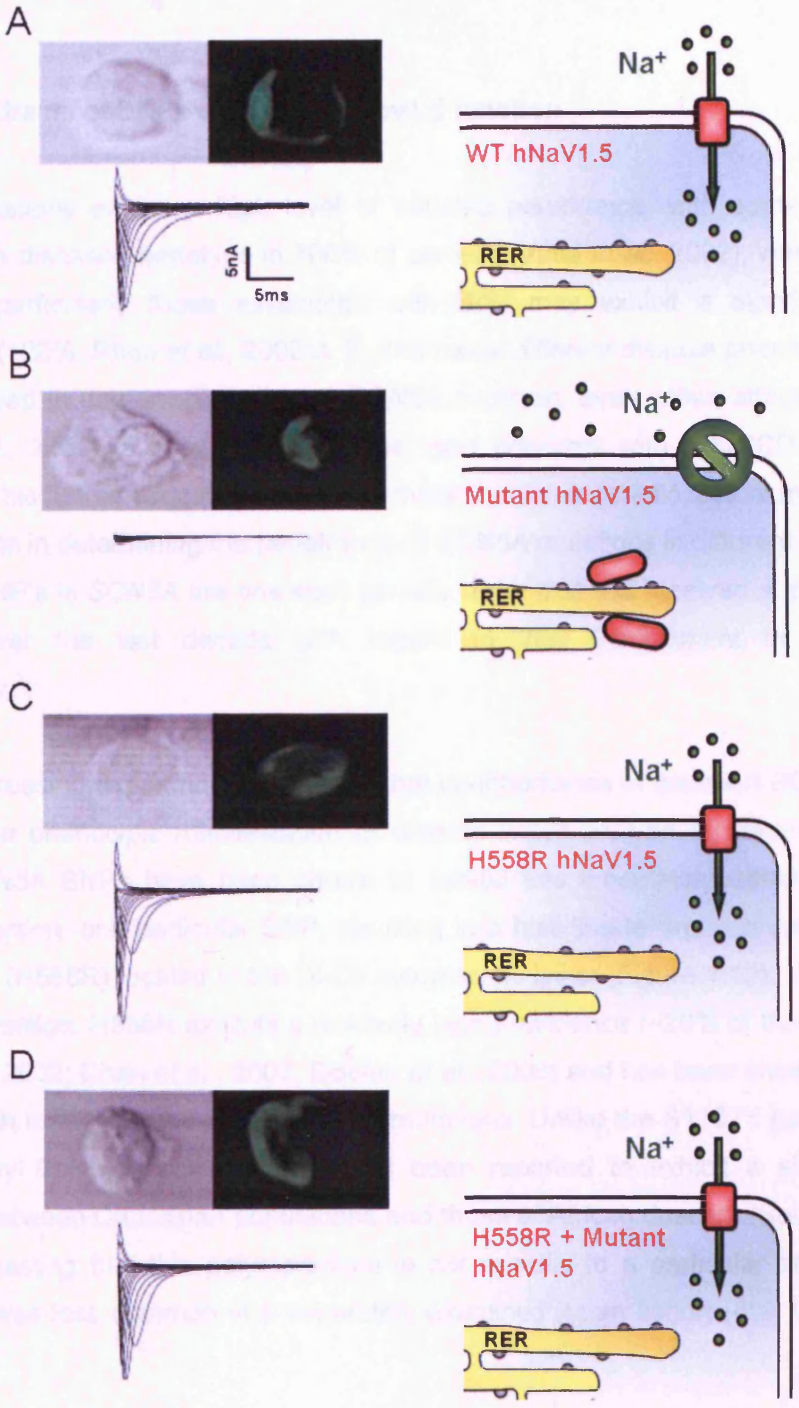

Figure 1.15. The H558R SCN5A SNP can restore normal I_{Na} current by correcting defective mutant channel trafficking, *see section 1.4.4.1.1and 1.4.4.1.2.. Heterologously expressed WT hNav1.5 and hNav1.5-H558R correctly localises to the cell periphery and exhibit normal Ina current (panel A and B). Several LQTS-associated mutations in SCN5A cause hNav1.5 to be retained in the ER, preventing correct membrane trafficking and abolishing I_{Na}. (panel C). Co-expression of H558R has been shown to correct membrane trafficking of several LQTS associated mutants and restore I_{Na} to normal levels. Each panel contains brightfield and immunofluorescent confocal images of recombinantly expressed hNav1.5, peak Na^+ density charts and schematic representation of hNav1.5 intracellular trafficking. Confocal images from Ye, (2003). Peak current traces from Poelzing, (2006).*

1.4.4.1.2. Effects of SNPs on mutant hNav1.5 function

SCN5A mutations exhibit a high level of variable penetrance, with some mutations resulting in a disease phenotype in 100% of carriers (Vatta *et al.*, 2002), whereas other mutations, particularly those associated with BrS, may exhibit a significantly low penetrance (~20%, Priori *et al.*, 2002a). Furthermore, different disease phenotypes have been observed in carriers of the same *SCN5A* mutation, even within affected families (Kyndt *et al.*, 2001); a phenomenon that is most prevalent with BrS/CCD-associated mutations. This further suggests that other environmental or genetic factors may have an important role in determining the penetrance of *SCN5A* mutations in different individuals. Common SNP's in *SCN5A* are one such genetic factor that has received a great deal of attention over the last decade with regard to their involvement in arrhythmia susceptibility.

There is increasing experimental evidence that co-inheritance of common *SCN5A* SNPs can alter the phenotypic manifestation of disease-linked *SCN5A* mutations. Although several *SCN5A* SNPs have been shown to exhibit this modulatory effect on mutant hNav1.5 function, one particular SNP, resulting in a histidine to arginine substitution at residue 588 (H558R) located in the DI-DII cytoplasmic linker (Figure 1.13), has received the most attention. H558R exhibits a relatively high prevalence (~20% of the population, Yang *et al.*, 2002; Chen *et al.*, 2007; Doolan *et al.*, 2008) and has been shown to be co-inherited with many disease-linked *SCN5A* mutations. Unlike the S1102Y polymorphism described by *Splawski et al*, H558R has been reported to exhibit a similar allelic frequency between Caucasian populations and those of African descent (Splawski *et al.*, 2002), suggesting that this polymorphism is not specific to a particular ethnic group, although it was less common in a separately examined Asian cohort (8%, Iwasa *et al.*, 2000).

Furthermore, heterologous expression of H558R alone consistently results in a similar biophysical phenotype to the WT channel (Makielski *et al.*, 2003; Viswanathan *et al.*, 2003; Poelzing *et al.*, 2006; Saito *et al.*, 2009; Gui *et al.*, 2010b). In addition, a cohort of *SCN5A* mutation carriers who had also inherited H558R, tended to exhibit improved ECG characteristics and fewer symptoms than subjects who did not carry this SNP (Lizotte *et al.*, 2009), suggesting a protective effect of this substitution, although this could very well be on a mutation-by-mutation basis. In contrast, a single genotyping

study identified a link between H558R inheritance and AF susceptibility (Chen *et al.*, 2007), questioning whether H558R is truly functionally benign in the absence of other *SCN5A* mutations.

The first experimental evidence that H558R altered the phenotypic manifestation of an *SCN5A* mutation was demonstrated through the heterologous co-expression of an LQTS mutation, M1766L, with H558R on the same recombinant protein (Ye *et al.*, 2003). Here, the presence of the H558R substitution was shown to restore correct trafficking of the protein to the sarcolemmal membrane and restored inward sodium current (as illustrated in Figure 1.15), although this current was persistent and characteristic of LQTS (Ye *et al.*, 2003). This suggests that although H558R was able to restore trafficking of the M1766L Nav1.5 to the sarcolemmal membrane, it did not restore the biophysical properties of the M1766L channel to normal levels.

This same polymorphism was able to restore the correct membrane trafficking and Na^+ current of another BrS-associated *SCN5A* mutation, R282H, which is found in the p-loop of DI (Poelzing *et al.*, 2006). The probands daughter, who had inherited R282H and H558R in a composite heterozygous fashion (Figure 1.16, patient D), was asymptomatic and displayed a normal ECG, whereas the proband did not co-inherit H558R and exhibited a BrS phenotype. In this case, the extent to which H558R restored normal channel function in heterologous systems was dependent on the precise mode of mutation and SNP co-expression and will be discussed further in section 3.1.2.

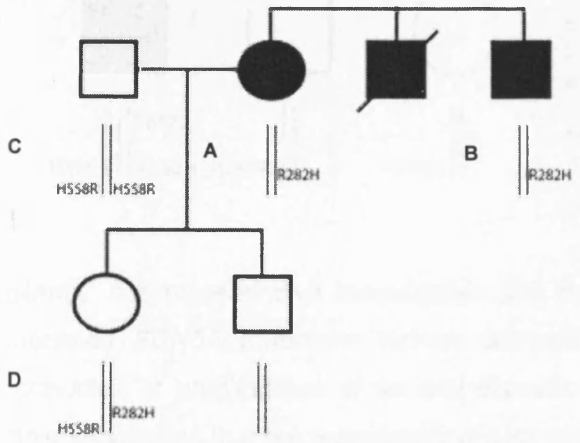

Figure 1.16. Pedigree of a family with Brugada syndrome, *BrS Affected individuals indicated in black. Patients A and B were heterozygous for the R282H mutation, patient C was homozygous for the H558R polymorphism and patient D was heterozygous for both R282H and H558R , with both substitutions on opposite alleles. From Poelzing, (2006).*

As well as restoring correct membrane trafficking of mutant Nav1.5 channels, H558R has been shown to alter the biophysical properties of mutant channels that exhibit normal membrane trafficking. The first example of this modulatory behaviour of H558R was demonstrated on the T512I mutation, which had been identified in CCD patient (Viswanathan *et al.*, 2003). In this case, the proband was homozygous for the H558R polymorphism and heterozygous for the T512I mutation, whereas the mother, who was asymptomatic, was heterozygous for both T512I and H558R, with both substitutions on the same allele (Figure 1.17).

Heterologous expression of Nav1.5 containing the T512I mutation altered activation and inactivation voltage-dependence and enhanced the level of channel slow-inactivation. These altered parameters were partially restored to normal levels when H558R was co-expressed with T512I on the same recombinant protein, inferring that this SNP was able to attenuate the detrimental biophysical effects of the T512I mutation (Viswanathan *et al.*, 2003). The fact that the mother of the proband had also inherited both substitutions on the same allele, but was asymptomatic, reiterates the variable penetrance of mutations occurring in *SCN5A* and the potential benefit of the inheritance of this SNP.

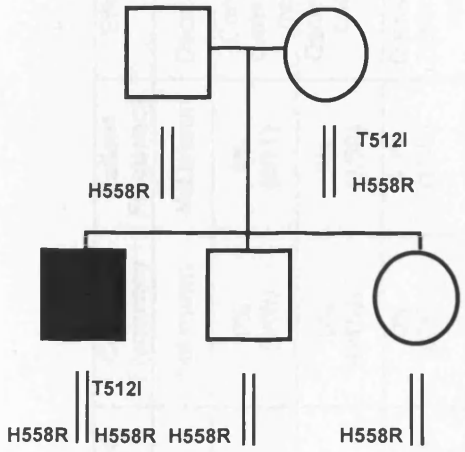

Figure 1.17. Family pedigree of a cardiac conduction disorder-affected proband who inherited H558R with a disease-linked SCN5A mutation, *A CCD affected patient was homozygous for the H558R polymorphism and heterozygous for the T512I mutation. The patients mother was asymptomatic and was heterozygous for both H558R and T512I, with both substitutions on the same allele. The probands father and siblings were asymptomatic and were heterozygous for H558R and did not carry T512I. Adapted from Viswanathan (2003).*

Recently, a comprehensive investigation into the effects of H558R on all known SSS-associated *SCN5A* mutations further demonstrated that this SNP resulted in both aggravation or amelioration of several disease causing mutations (Gui *et al.*, 2010b), further suggesting that the modulatory effects of H558R are mutation-specific.

Mutation	Associated Disease	Control Frequency	Patient Frequency	Effect of mutation on phenotype	Functional consequence of H558R co-expression	Reference
E161K	SSS	Not known	Not known	Decreased peak I_{Na} current.	Exacerbates decrease in I_{Na} current	Gui, 2010.
R282H	BrS	0% (0/60)	9% (1/11)	Complete ablation of I_{Na} current through abolition of membrane trafficking	Restores correct membrane trafficking and I_{Na}	Pitzalis, 2003; Poelzing, 2006.
G298S	IBS	0% (0/1500)	2% (1/50)	Decreased peak I_{Na} current and prolonged time to peak.	Exacerbates decrease in I_{Na} current and prolongation of time to peak.	Saito, 2009.
G400A	Acute myocardial infarction	0% (0/364)	5.3% (1/19)	Decreased peak I_{Na} current, hyperpolarised inactivation voltage-dependence.	Exacerbates decrease in peak I_{Na} current to near complete ablation.	Hu, 2007.
T512I	AV conduction block	Not known	Not known	Hyperpolarised voltage-dependent inactivation, decreased peak I_{Na}	Partial restoration of voltage-dependent inactivation and peak I_{Na} to WT levels	Viswanathan, 2003.
123A572D	LQT3	0.49%	0.45%	Similar to WT	Persistent late Sodium Current	Tester, 2010.
D1275N	SSS	Not known	Not known	Decreased peak I_{Na} current	Fully restores I_{Na} current	Gui, 2010.
P1298L	SSS	Not known	Not known	Decreased peak I_{Na} current	Exacerbates decrease in I_{Na} current	Gui, 2010.
R1632H	SSS	Not known	Not known	Prolonged channel recovery from inactivation	Exacerbated delay in channel inactivation	Gui, 2010.
M1766L	LQT3	0% (0/200)	n/a Single post-mortem	Decreased peak I_{Na} current through decreased membrane trafficking.	Fully restores correct membrane trafficking and I_{Na} current	Valdivia, 2002; Ye, 2003.

Table 1.3. Summary of the effects of H558R on mutant hNav1.5 channel function. *Several disease-linked SCN5A mutations have been characterized in the presence and absence of the H558R polymorphism, the functional consequences of which are indicated here. SSS = sick sinus syndrome, BrS = Brugada syndrome, IBS = irritable bowel syndrome, LQT3 = long WT syndrome type 3.*

Taken together, these examples suggest that depending on the specific nature of the co-inherited mutation and the precise mode of expression, the same common H558R polymorphism is able to restore normal channel function to varying degrees (see Table 1.3). However, the precise mechanism by which H558R can modulate the effects of an amino acid substitution that can be distant in the primary or 3D protein structure or on a separate protein monomer altogether remains unknown.

These examples of the effects of H558R on mutant channel function, clearly demonstrate that this polymorphism is capable of modulating mutant channel functionality through a variety of mechanisms, both when it is found on the same or opposite allele as the disease-linked mutations. Furthermore, this provides evidence that this SNP modulates the activity of several different mutations to a varying degree, depending on the precise mode of co-inheritance.

1.4.4.2. SNPs in CPVT-associated genes

There is increasing evidence that common SNPs in genes associated with CPVT and ARVD2 i.e. *CASQ2 and RyR2*, constitute rather more than benign natural sequence variation and such SNPs are sometimes associated with these disorders (de la Fuente *et al.*, 2008; Wong *et al.*, 2009), mirroring the implication of SNPs in other cardiac channelopathies.

1.4.4.2.1. CPVT-associated SNPs in *CASQ2*

Since the implication of CSQ mutations in CPVT pathogenesis (section 1.3.5), several non-synonymous mutations have been identified (de la Fuente *et al.*, 2008; Kirchhefer *et al.*, 2010). Recently, a study indentified a CPVT patient who had inherited two CSQ amino acid substitutions (Y55C and P308L) in a composite heterozygous manner (de la Fuente *et al.*, 2008). The inheritance of either of these mutations alone did not result in a CPVT phenotype and neither substitution was found in a large healthy cohort, suggesting that these substitutions are only pathogenic when co-inherited. This provides the first evidence that not all CSQ mutations are autosomal recessive and that co-inheritance of two apparently benign CSQ substitutions, can potentially alter protein function; however there is no biophysical evidence to support or refute this possibility.

Conversely, genetic screening of *CASQ2* of a CPVT cohort identified a CPVT-patient heterozygous for two non-synonymous SNPs resulting in T66A and V76M substitutions, both of which were located on the same allele (Laitinen *et al.*, 2003). This mode of SNP inheritance was also observed in 18 further CPVT patients and a large control cohort, suggesting that another confounding factor may be involved in this particular case. Subsequently, when expressed alone, T66A was shown to exhibit a similar Ca^{2+}-binding capacity and polymerisation Ca^{2+} dependency to WT CSQ (Kim *et al.*, 2007), whereas V76M decreased Ca^{2+} binding capacity and altered dimerisation propensity, but to a lesser degree than CPVT-linked mutations i.e. R33Q, L167H, D307H. This could suggest a combinatorial modulatory role of T66A and V76M SNPs in CPVT2 pathogenesis observed *in vivo* (Laitinen *et al.*, 2003). Like CPVT-linked mutations, V76M occurs at a residue highly conserved between species, suggesting that although it only has a modest role on CSQ function, V76M may evoke a predisposition to arrhythmia, questioning whether it should be classed as a SNP or a mutation.

1.4.4.2.2. Emerging role of SNPs in RyR2 function

There is little documented evidence of the prevalence and functional consequences of SNPs in RyR2, however there appears to be emerging interest in the roles that common sequence variation in RyR2 may have on channel function.

A rare non-synonymous RyR2 mutation located between the central and C-terminal mutation domains, N3308S, was recently identified in a patient exhibiting a typical CPVT phenotype (Figure 1.11, Marjamaa *et al.*, 2009a), suggesting this substitution is causative of the disease. However, this substitution was also identified in 1 out of 300 healthy individuals, suggesting that N3308S exhibits a variable penetrance or is mitigated by other, possibly genetic, factors. Biophysical characterisation of this substitution did not identify altered channel activity compared to WT RyR2, when subjected to increasing cytoplasmic Ca^{2+} (Marjamaa *et al.*, 2009a), providing an indication this is a rare, functionally benign substitution, however the extent of functional characterisation of N3308S was limited.

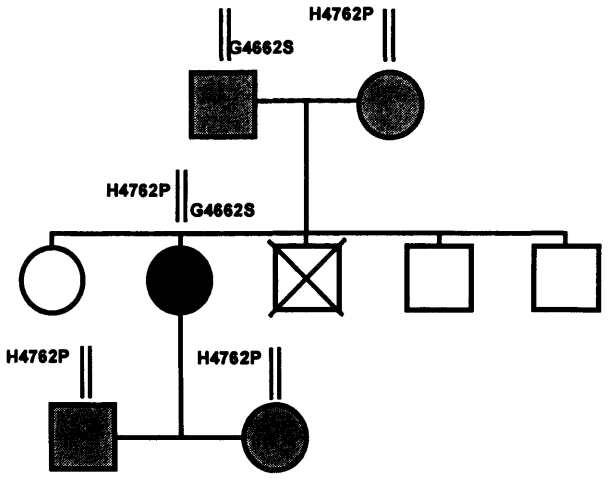

Figure 1.18. G4662S and H4726P result in a CPVT phenotype when inherited in a composite heterozygous fashion. *Grey symbols represent carriers of either asymptomatic G4662S or H4762P-carrying individuals. The black symbol represents the CPVT-affected patient harbouring both substitutions. Adapted from Postma (2005).*

A recent comprehensive genotyping study of a cohort of CPVT and gene-negative LQTS patients identified several RyR2 SNPs that were present in both patients and control subjects e.g. G1885E, G1886S, Q2958R, (Medeiros-Domingo *et al.*, 2009). However, this study provided no evidence that these SNPs exert any functional effects on the mutations with which they were co-inherited, and due to their prevalence in the control population they may just represent natural sequence variation. However, *Postma et al (2005)* identified a family in which a CPVT-affected individual inherited two rare substitutions (G4662S and H4726P) in a composite heterozygous manner i.e. one mutation from each parent (Figure 1.18). However, the probands parents and children had only inherited either one of these mutations and were completely asymptomatic (Postma *et al.*, 2005), suggesting that G4662S and H4726P are rare SNPs that only exhibit a detrimental phenotype when co-inherited.

Similarly, there is a reported case of ARVD2, whereby the affected individuals did not harbour a disease-linked RyR2 mutation, but had inherited the common G1885E and G1886S SNPs in a composite heterozygous fashion (Milting *et al.*, 2006). These polymorphisms are relatively common in the healthy Caucasian population (G1885E = 6% of individuals, G1886S = 20% of individuals, n=100-463, Milting *et al.*, 2006; Medeiros-Domingo *et al.*, 2009), but the inheritance of both SNPs simultaneously was only observed in an ARVD2 cohort (3.5%, 3/85 patients). Like the SNPs described by *Postma et al*, this suggests that inheritance of either SNP alone is not sufficient to result in an ARVD2 phenotype, yet these apparently benign SNPs are causative of disease when inherited in a composite heterozygous fashion. Subsequent biophysical

characterisation of single channels isolated from an ARVD2 patient harbouring both SNPs exhibited several sub-conductance states and an increased P_o at diastolic Ca^{2+} levels (Milting *et al.*, 2006), indicative of channel destabilisation and diastolic Ca^{2+} leak. The heterologous expression of recombinant RyR2 harbouring the G1885E and G1886S SNPs have further shown that these substitutions alter spontaneous Ca^{2+} release (Koop *et al.*, 2008), which will be discussed in greater detail in section 5.1.4.

These SNPs were also identified in Asian and African-American populations, although they were observed at different frequencies between populations. G1885E was only identified in a single SUDS patient (1/28) of Asian origin and was not present in the control population (0/95), whereas G1886S was present in 10.7% of SUDS cases (3/28 patients) and at similar levels in the control population (13.7%, 13/95 patients, (13.7%, 13/95 patients, Wong *et al.*, 2009). Similarly, G1885E was not identified in an African-American cohort, whereas G1886S present in 20% of healthy African-Americans (Medeiros-Domingo *et al.*, 2009). Although limited in number and cohort size, these studies suggest that there are differences between the prevalence of these SNPs between different ethnic populations, particularly in the Asian population.

1.4.4.2.3. Co-inheritance of SNPs with RyR2 mutations

Genotyping studies have identified several cases in which CPVT/ARVD2 patients carrying disease-linked RyR2 mutations have also inherited common, apparently functionally benign polymorphisms (Tiso *et al.*, 2001; Medeiros-Domingo *et al.*, 2009). The first documented case of this phenomenon describes three Italian families who inherited common, non-synonymous SNPs on the same allele as a disease-linked RyR2 mutation (Tiso *et al.*, 2001). In the first family identified, all ARVD2-affected individuals harboured a leucine to proline amino acid substitution at RyR2 residue 433 (L433P). Interestingly, all affected individuals also harboured a glycine to glutamate amino acid substitution at residue 1885 (G1885E) on the same allele as the L433P-coding nucleotide substitution, as shown in Figure 1.19. Similarly, affected members of two families harbouring an asparagine to isoleucine substitution at residue 2386 (N2386I) had also inherited the G1885E substitution described above, together with another RyR2 missense SNP encoding a glutamine to arginine substitution at residue 2958 (Q2958R). Neither disease-linked mutation was identified in a healthy control population (n = 200,

(n = 200, Tiso *et al.*, 2001), whereas the SNPs were, further suggesting that inheritance of these SNPs alone does not result in CPVT/ARVD2 pathogenesis. Both of these residues are highly conserved among species (Appendix 1, Figure 1), further suggesting a functional importance of both substitutions.

The Q2958R amino acid substitution was also co-inherited homozygously in all CPVT affected individuals from four Finnish families harbouring a range of RyR2-disease linked mutations: P2328S, V4653F and Q4201R (Laitinen *et al.*, 2001). Two individuals from one of these families (2/13 mutation carriers, 15.4%), who were heterozygous for the P2328S mutation and homozygous for the Q2958R polymorphism, were completely asymptomatic, whereas other family members with the same haplotype exhibited CPVT symptoms. The SNP encoding Q2958R exhibited an allelic frequency of 0.26 in the control population, confirming that the Q2958R amino acid substitution alone is not sufficient to cause a disease phenotype, which is not surprising considering that the Q2958R is the most common RyR2 polymorphism, particularly among Caucasians (34%, Medeiros-Domingo *et al.*, 2009).

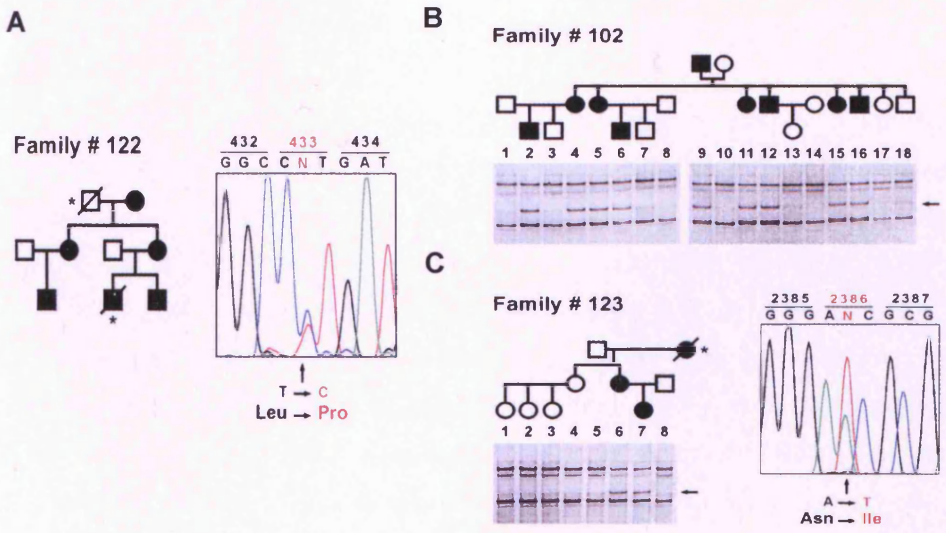

Figure 1.19. ARVD2 pedigrees of Italian families harbouring L433P and N2386I mutations and G1885E and Q2958R SNPs. *Asterisks indicate individuals whose DNA was not available for genotyping. Affected members of family A harboured the G1885E polymorphism on the same allele as the ARVD2-linked L433P mutation. Affected individuals of families B and C harboured both G1885E and Q2985R polymorphisms on the same allele as the N2386I mutation. Results of single strand conformation polymorphism analysis was used to detect substitutions and is indicated in panels B and C. Adapted from Tiso, (2001)*

Although the reported co-incidence of RyR2 polymorphisms with disease-linked RyR2 mutations appears to be relatively low, this could be artefactual due to targeted sequencing of mutation "hot-spots" in RyR2 (Laitinen *et al.*, 2001; Tiso *et al.*, 2001; Bagattin *et al.*, 2004; Marjamaa *et al.*, 2009b). Because the majority of CPVT cases do not undergo sequencing of the entire open reading frame, the prevalence of mutations and polymorphisms outside of the three "conventional" mutational domains remains unknown. The 61 exons that fall outside of the commonly targeted mutational domains encode 2570 amino acids, accounting for over half of the RyR2 protein. (Medeiros-Domingo *et al.*, 2009). Similarly, in some cases where SNP's are co-inherited with disease linked mutations, they are not always reported due to their incidence within the control population (Bauce *et al.*, 2002).

1.5. General Aims:

Some common SNPs in cardiac ion channel genes, exert a modulatory effect on disease-causing mutations within the same gene (Viswanathan *et al.*, 2003; Nof *et al.*, 2010). A group of ARVD2 patients were identified, in which all affected individuals had inherited the common G1885E SNP on the same allele as the ARVD2-linked RyR2 L433P mutation (Tiso *et al.*, 2001). The general aim of this thesis was to investigate the effects of G1885E co-expression on L433P mutant channel function.

Most functional characterisations of RyR2 mutations expressed in heterologous systems have been carried out on homotetrameric channels but this does not accurately represent the autosomal dominant nature of CPVT and ARVD2-linked RyR2 mutations. Furthermore, as is the case with other ion channels, SNPs often dictate the resultant channel behaviour depending on the precise mode of their co-inheritance i.e. *in cis* or *in trans* (Poelzing *et al.*, 2006). In light of these observations, characterisation of co-expressed WT, L433P and G1885E RyR2 was also carried out in RyR2-null HEK cells to better control the relative recombinant expression levels and subunit stoichiometry.

ARVD2 and CPVT-linked mutations in RyR2 have been shown to profoundly alter characteristics of agonist-evoked Ca^{2+} release when expressed in heterologous systems (George *et al.*, 2003a; Jiang *et al.*, 2005). Here, live-cell Ca^{2+}-imagining experiments were carried out to systematically analyse several parameters of caffeine-evoked Ca^{2+} release in HEK cells expressing L433P (Chapter 3). A major focus of this thesis was to determine whether these parameters were altered by G1885E co-expression. Analysis of small cytoplasmic Ca^{2+} fluxes is a useful tool for interrogating Ca^{2+} release dysfunction promoted by CPVT-linked RyR2 mutations (George *et al.*, 2003b; 2006; Fry, 2008). By quantifying these small Ca^{2+} fluxes using the index of Ca^{2+} signal variability the effects of L433P on basal and agonist-evoked Ca^{2+}-signalling were examined. This thesis investigated the influence of the G1885E SNP on Ca^{2+} handling mediated by L433P channels (Chapter 4). RyR2 mutations have also been reported to alter the propensity for spontaneous ER/SR Ca^{2+} release (Jiang *et al.*, 2005; Liu *et al.*, 2006), a phenomenon linked to DADs and arrhythmia. To this end, the extent and mode of spontaneous Ca^{2+} release of cells expressing L433P and the effects of G1885E co-expression were also examined (Chapter 5).

Chapter 2

Materials & Methods

2.1. Materials

2.1.1. General Lab Chemicals and Reagents

All chemicals and reagents used were of analytical grade and were obtained from Sigma-Aldrich, unless otherwise stated. All solutions were dissolved in deionised H_2O and stored at room temperature (RT) unless otherwise stated. All filtration was carried out using 0.2µM filters (Sartorious).

2.1.2. Molecular Biology Reagents

- QuikChange® site-directed mutagenesis Kit, obtained from Stratagene, stored at -20°C.
- Miniprep resuspension solution – 50mM Tris, 10mM EDTA, 100µg/ml RNAse A, pH adjusted to 7.5 with hydrochloric acid and filter sterilised.
- Miniprep Lysis solution – 0.2M sodium hydroxide, 1% (w:v) sodium dodecyl sulphate (SDS). Filter sterilised.
- Miniprep Neutralisation solution – 4.09M Guanidine-HCl, 0.759M acetic acid, pH adjusted to 4.2 with glacial acetic acid. Filter sterilised.
- Miniprep Column wash solution – 60mM potassium acetate, 8.3mM Tris-HCl (pH 7.5), 0.04mM EDTA, pH adjusted to 8.0, 60% (v:v) ethanol.
- Restriction enzymes – all enzymes and appropriate buffers were acquired from New England Biolabs (BamHI, BglII, EcoRI, HinDIII, KpnI) and Stratagene (SanDI). Stored at -20°C.
- Molecular Biology Grade Agarose – supplied by Eurogentec.
- EDTA – 0.5M stock prepared. 186.12g/L EDTA. pH adjusted to 10.0 with sodium hydroxide to dissolve EDTA. Once dissolved, pH adjusted to 7.5 using hydrochloric acid.
- TAE (50x) – 2M Tris, 2M acetic acid, 50mM EDTA.
- 1Kb DNA molecular weight ladder – supplied by Invitrogen, mixed with 2x Gel loading buffer and aliquots were stored at -20°C.
- Gel loading buffer (2x) – 5ml Glycerol, 5ml 1x TAE and 0.25% (w:v) Orange G to allow visualisation the progress of agarose gel electrophoresis.

- Maxiprep Resuspension Buffer (Buffer P1) - 50mM Tris, pH adjusted to 8.0, 10mM EDTA, 100µg/ml RNase A. Stored at 4-8°C.
- Maxiprep Lysis Buffer (Buffer P2) – 200mM sodium hydroxide, 1% SDS (w:v)
- Maxiprep Neutralisation Buffer (Buffer P3) – 3M potassium acetate, pH adjusted to 5.5.
- Column equilibration buffer (Buffer QBT) – 750mM NaCl, 50mM MOPS, pH adjusted to 7.0, 15% isopropanol (v:v) and 0.15% Triton® X-100 (v:v).
- Column wash buffer (Buffer QC) – 1M NaCl, 50mM MOPS, pH adjusted to 7.0 and 15% isopropanol (v:v).
- Elution buffer (Buffer QF) – 1.25M NaCl, 50mM Tris, pH adjusted to 8.5 and 15% isopropanol (v:v).
- QIAEX II gel extraction kit (Qiagen) – for the purification of DNA fragments resolved by agarose gel electrophoresis 2.2.1. Briefly, a slice of agarose gel containing resolved DNA is solubilised in a high salt buffer and is incubated with silica beads, to which the DNA binds. DNA-containing beads are collected and washed in another high salt buffer to remove residual agarose and are also washed with an ethanol containing buffer to remove salt contaminants. DNA was eluted from the silica beads in SDW.
- DNA sequencing Kit – BigDye terminator V5 obtained from Applied Biosystems. Briefly, DNA to be sequenced is incubated with standard deoxynucleotides as well as fluorescently-labelled, chain-terminating dideoxynucleotides which terminate DNA strand extension when incorporated into the newly synthesised DNA. This random incorporation of fluorescently-labelled dideoxynucleotides produces DNA fragments of varying lengths which can be resolved by high-resolution electrophoresis. Labelling of the dideoxynucleotides with fluorophores with distinct excitation/emission properties allows the determination of the specific terminating nucleotide.

2.1.3. Protein Biochemistry Reagents

- Protease inhibitor cocktail tablets – obtained from Roche. Contains several inhibitors of serine proteases (Pefabloc SC, aprotinin and leupeptin) proteases and inhibitors of cysteine proteases (E-64). Tablets were stored at 4-8°C. 1x

protease inhibitor cocktail tablet dissolved in 20mM Tris, 5mM EDTA and 0.05% (v:v) Triton-X-100 (25ml total volume), adjusted to pH7.4 with HCl.

- Hypo-osmotic cell lysis buffer – 20mM Tris, 1mM EDTA, pH adjusted to 7.4 with hydrochloric acid, protease inhibitor tablet (1 per 25ml, Roche) and 1% (v:v) Triton-X-100.
- Micro BCA™ protein assay kit – obtained from Thermo Scientific.
- BSA standards – 1mg/ml stock diluted to 200, 100, 50, 20 and 10µg/ml in sterile deionised H_20. Stored at -20°C
- SDS-PAGE Stack buffer (1x) - 0.5M Tris, pH adjusted to 6.8 with hydrochloric acid.
- SDS-PAGE Separating buffer – 1.5M Tris, pH adjusted to 8.8 with hydrochloric acid.
- 40% Acrylamide / bis-solution 37.5:1 – BioRad.
- Sodium Dodecyl Sulphate – 10% (w:v) solution prepared immediately before use.
- Ammonium persulphate (APS) – 10% (w:v) solution prepared immediately before use.
- Molecular weight markers – pre-stained (Kaleidoscope), obtained from BioRad.
- SDS-gel loading buffer (2x) 100mM Tris pH 6.8, 20% (v:v) glycerol, 4% (w:v) SDS, 0.2% (w:v) bromophenol blue, 10% (v:v) β-mercaptoethanol and filter sterilised. Prepared immediately prior to use.
- Running Buffer (1x) – 25mM Tris, 250mM Glycine, 0.1% (w:v) SDS
- Transfer Buffer (Semi-dry) - 48 mM Tris, 39 mM glycine, 0.037% (w/v) SDS.
- Tris-buffered saline (TBS, 1x) 20mM Tris, 137mM NaCl and pH adjusted to 7.6 with hydrochloric acid.
- TBS-T Buffer (1x) – 1x TBS, 0.1% (v:v) Tween-20.
- Blocking solution – 5% (w:v) non-fat dried milk (Marvel) dissolved in 1x TBS-T buffer

2.1.4. Oligonucleotides

SDM primers obtained from VH Bio were purified using reverse-phase HPLC and were supplied as lyophilised pellets. Pellets were resuspended in 250µl SDW and stored at -20°C. Primers were diluted to a concentration of 150ng/µl for use in site-directed

mutagenesis reactions (as detailed in manufacturers instructions). A list of all of the primers used in this study are detailed in Appendix I, Tables 2 and 3.

2.1.5. Plasmid Vectors

2.1.5.1. Mammalian Expression Vector

The mammalian expression vector, pcDNA3 (see Appendix I, Figure 3) containing full-length, human RyR2 which is tagged with eGFP at the N-terminus (pcDNA3-eGFP-hRyR2) was obtained from Dr. Christopher H. George. pcDNA3-eGFP-hRyR2 harbouring the CPVT-linked L433P mutation (pcDNA3-eGFP-hRyR2-L433P) was obtained from Dr. N. Lowri Thomas (see Appendix I, Table 1 and Figure 2 for construct nomenclature).

2.1.5.2. Intermediate Vector

The pSL1180 superlinker vector (GE Healthcare, see appendix 1, Figure 3) was used to clone fragments of RyR2 to undergo subsequent site-directed mutagenesis (George *et al.*, 2003c). This vector was used solely for the generation and propagation of mutagenised RyR2 and was not used for the expression of protein. pSL1180 containing the 2.1kb SanDI/KpnI fragment (pSL1180-SK1, hRyR2 DNA residue 5540-7678) was obtained from Dr. N. Lowri Thomas.

2.1.6. Microbiology

All growth media and antibiotics were obtained from Sigma-Aldrich. Sterile plasticware and glassware were obtained from Greiner and Fisher. All glassware was washed in detergent-free water and autoclaved prior to use. Aseptic technique was employed in all bacterial cell culture work and where possible work was carried out in a Class I containment safety cabinet.

- LB_{Amp} agar – 10g/L tryptone, 5g/L yeast extract, 10g/L NaCl, 15g/L agar. Autoclaved and allowed to cool before the addition of 100µg/ml of ampicillin. Stored at 4-8°C.
- LB_{Amp} broth – 10g/L Tryptone, 5g/L yeast extract, 10g/L NaCl. Autoclaved and allowed to cool prior to the addition of 100µg/ml of ampicillin. Stored at 4-8°C.
- NZY broth – 16g/L NZ, 5g/L yeast extract. Autoclaved and stored at 4-8°C.
- SOC medium – 20g/L Tryptone, 5g/L yeast extract, 0.5g/L NaCl, 0.18g/L KCl, 0.95g/L MgCl. Autoclaved and allowed to cool prior to the addition of glucose at 2% (w:v) from the stock solution.
- Glucose – 20% (w:v) in deionised H_20, filter sterilised.
- Ampicillin – 100mg/ml stock prepared in deionised H_20, filter sterilised, and aliquots were stored at -20°C.

2.1.7. Bacterial Cell Lines

Several strains of *Escherichia coli* and *Epicurian coli* were used in the generation and propagation of wild type and mutagenised eGFP-tagged hRyR2.

- XL1-Blue competent cells were obtained from Stratagene and were used solely for the transformation of single-stranded mutagenised plasmid DNA. XL1-Blue cells are deficient in endonuclease (*endA*) and recombination (*recA*), which improves the quality of purified DNA and insert stability. The *hsdR* mutation eliminates a methylation-specific restriction site, preventing cleavage of cloned DNA by the endogenous *Eco*K endonuclease system.
- XL10-Gold Ultracompetent cells were also obtained from Stratagene and were used for several stages of cloning of full length, pcDNA3-eGFP-RyR2 and pSL1180-SKI constructs. XL10-Gold cells are deficient in endonuclease (*endA-)* and recombination (*recA*-) genes, increasing plasmid quality and insert stability. These cells carry the *Hte* phenotype, which increases the transformation efficiency of large DNA molecules
- MAX Efficiency® Stbl2 competent cells were obtained from Invitrogen and are optimised for the transformation of unstable inserts with increased yield and and were used for the propagation of full-length mutagenised RyR2 plasmid. These cells contain the *endA*- and *recA1* phenotype described above.
- Aliquots of all bacterial stocks (25-50µl) were stored at -80°C.

2.1.8. Human Embryonic Kidney (HEK) 293 cell culture media and reagents.

HEK-293 cells (ATCC accession number CRL-1573) are derived from human embryonic kidney cells that have been immortalised through their transformation with sheared Adenoviral 5 DNA. They are an adherent cell line that exhibit epithelial morphology, in that they grow as a cellular monolayer, with a tendency to continue dividing after reaching confluency, forming aggregates or clumps of cells (Graham *et al.*, 1977). The phenotype of HEK-293 cells and the justification for the use of them in this study is discussed further in section 3.1.1.5.

All cell culture media and reagents were obtained from Invitrogen. All chemicals were obtained from Sigma-Aldrich, unless otherwise stated. Cell culture flasks and plates were obtained from Nunc (Fisher Scientific). Poly-D-Lysine coated glass coverslips were obtained from MatTek Corporation (www.mattek.com). All mammalian cell culture work was carried out under sterile conditions in Class I containment cabinets (Microflow).

- Foetal bovine serum (FBS) – heat-inactivated, filter sterilised and aliquots were stored at -20°C.
- Complete Dulbecco's Modified Eagles Medium (cDMEM) – DMEM containing 4.5g/L glucose and supplemented with 10% (v:v) foetal bovine serum (FBS), 2mM glutamine and 100µg/ml penicillin/streptomycin (all filter sterilised prior to addition). Stored at 4-8°C.
- Minimal Dulbecco's Modified Eagles Medium (mDMEM) – DMEM containing 5.4g/L glucose and supplemented with 2mM glutamine and 100µg/ml penicillin/streptomycin (all filter sterilised prior to addition). Stored at 4-8°C.
- Trypsin-EDTA – 1x in HBSS without Ca^{2+} or Mg^{2+}. Aliquots were made and stored at -20°C. Filter sterilised immediately prior to use.
- Saline solution – 0.9% (w/v) supplied by Baxter Medical Supplies.
- Phosphate buffered Saline (PBS) – Prepared a 10x stock, 1.37M NaCl, 27mM KCl, 100mM Na_2HPO_4 and 18mM KH_2PO_4. Diluted to 1x PBS and pH adjusted to 7.4.
- Effectene transfection reagent – obtained from Qiagen, stored at 4-8°C.
- Hepes buffered saline (HBS) 2x – 280mM NaCl, 10mM KCl, 1.5mM Na_2HPO_4, 10mM glucose, 50mM Hepes, pH adjusted to 7.05, filter sterilised and aliquots were stored at -20°C.

- Calcium chloride – 2M $CaCl_2.6H_2O$ was prepared, filtered and aliquots were stored -20°C.

2.1.9. Antibodies

- Ab-GFP (B-2), mouse monoclonal IgG, raised against the entire Green Fluorescent Protein of *Aequorea victoria*, and cross reacts with enhanced GFP. Obtained from Santa Cruz. Used at 1:5000 dilution for western blotting.
- pAb-1093, rabbit polyclonal antiserum, raised to residues 4454-4474 of the cardiac ryanodine receptor (EDKGKQKLRQLHTHRYGEPEC), and does not cross react with RyR1. Used a 1:5000 dilution for Western blotting, 1:100 for immunocytochemistry.

2.1.10. Ca^{2+} Imaging reagents and agonists

- Fluo3-AM – 50µg of Fluo-3 AM calcium dye dissolved in 15µl 20% (w:v) pluronic acid in DMSO to obtain a stock concentration of 3mM. Pluronic acid prevents aggregation of Fluo3-AM and increases loading efficiency. The 3mM solution was diluted 1:200 in mDMEM to obtain a working stock at 15µM. Fluo3-AM was prepared immediately prior to use.
- Caffeine solution – 100mM caffeine working stock was prepared in mDMEM. All subsequent dilutions were generated from this stock by dilution with mDMEM. Caffeine causes RyR2 activation by sensitising the channel to activation by luminal/cytoplasmic Ca^{2+} (section 3.1.5)
- Thapsigargin – 1mM stock solution prepared in DMSO, aliquots were stored at -20°C. Thapsigargin a sesquiterpene lactone isolated from the plant, *Thapsia garganica.* Thapsigargin raises cytoplasmic Ca^{2+} concentration by way of SERCA inhibition, leading to passive depletion of the ER Ca^{2+} store and is regularly used to estimate ER Ca^{2+} content (Lytton *et al.*, 1991; Tong *et al.*, 1999).
- Ionomycin – 1mM stock solution prepared in DMSO. Diluted 1/10 to prepare a 100µM stock and aliquots were stored at -20°C. Ionomycin is an ionophore that is produced by *Streptomyces conglobatus* and increases the permeability of the cell

membrane to Ca^{2+} ions, resulting in increased cytoplasmic Ca^{2+} levels if sufficient Ca^{2+} is present in the external medium.

- EGTA – 100mM stock solution of Na_2EGTA (ethylene glycol-bis (β-aminoethylether)-N,N,N',N'-tetraacetic acid) was prepared, pH adjusted to 10.0 with KOH until dissolved, pH adjusted to 7.0 with HCl and stored at 4-8°C. EGTA is a Ca^{2+} chelating agent that is routinely used to buffer Ca^{2+} in experimental systems and has a significantly higher affinity for Ca^{2+} than EDTA, which is a chelator of all divalent cations e.g. Ca^{2+}, Mg^{2+}, Mn^{2+} etc.

2.1.11. Data Analysis

DNA sequencing analysis was carried out on an Applied Biosystems DNA sequencing source file using Chromas Version 1.5 (Technelysium, http://www.technelysium.com.au). Homology alignments to the WT human RyR2 nucleotide sequence were performed using NCBI BLAST (http://blast.ncbi.nlm.nih.gov/Blast.cgi).

The analysis of Ca^{2+} imaging data will be discussed in further detail in sections 3.2, 4.2 and 5.2. Briefly, numerical data corresponding to the intensity of Ca^{2+}-dependent Fluo3-AM signal from defined cellular regions of interest were generated using Leica LAS AF software. Raw Ca^{2+}-imaging data was exported in a Microsoft Excel compatible format and was stored and manipulate using Microsoft Excel before graphical plotting and statistical analyses were performed using GraphPad Prism software (http://www.graphpad.com). Initial analyses of spontaneous Ca^{2+} oscillation parameters were carried out using synchrony – amplitude – length – variability of oscillations (SALVO) software (Silvester *et al.*, 2009), prior to data being transferred to Microsoft Excel. Appropriate statistical tests were performed using Microsoft Excel and GraphPad Prism software as detailed in section 2.2.4.

2.2 Methods

2.2.1. Molecular biology techniques

2.2.1.1. Agarose gel electrophoresis

DNA fragment size was analysed by agarose gel electrophoresis and comparison against concurrently run DNA molecular weight markers. All analysis of DNA fragments was carried out using a 1% (w:v) agarose gel prepared by dissolving the appropriate amount of agarose in TAE (1x) buffer and boiling in a microwave oven. The agarose was allowed to cool to ~50°C, before the addition of ethidium bromide to a final concentration of 0.1µg/ml and was then poured into a gel-tray according to manufacturer's instructions (Hoefer, Biorad). Once the gel was set, DNA samples were mixed with an equal volume of DNA loading buffer (2x) and loaded onto the gel and ran alongside a 1kB DNA molecular weight marker. Electrophoresis was typically carried out at constant voltage (80V) until the dye front had migrated two thirds of the way down the gel, which was sufficient to result in resolution of all DNA fragments. DNA was visualised using UV trans-illumination and imaged using a gel documentation system and Quantity One software.

2.2.1.2. Cloning of DNA fragments

Plasmid DNA (1-2µg) was digested with the appropriate restriction enzymes (5-10U per 20µl reaction) for 4 hours at 37°C to which ensured complete digestion. Concurrent double digests were carried out in the most appropriate buffers, as determined by the Double Digest Finder tool (New England Biolabs, http://tools.neb.com/NEBcutter2). Digest products were run on a 1% agarose gel (section 2.2.1.1). DNA fragments were physically excised from the agarose gel and purified using the QIAEX II gel extraction kit (Qiagen) according to the manufacturers instructions. The agarose-gel slice was weighed and nuclease free water (2x, v:w, 1µl:1mg of agarose), QX1 buffer (3x, v:w, 1µl:1mg of agarose) and 20µl of silica bead solution were added to the agarose gel containing the DNA fragments, which were then incubated at 50°C for 10 mins to solubilise the agarose. The mixture was centrifuged (20,000 xg, 1 min) and the supernatant was discarded. The resulting pellet was resuspended in 500µl QX1 buffer

and centrifuged (20,000 xg, 1 min). The supernatant was discarded and the pellet underwent two washes with 500µl PE buffer, centrifuging (20,000 xg, 1 min) after each wash. The supernatant was discarded and the pellet was incubated at RT for 10 mins to dry. DNA was eluted from the silica beads by the addition of 30µl elution buffer (10mM Tris, pH 8.8), which was incubated at 50°C for 5 mins before centrifugation (20,000 xg, 1 min) to remove the silica beads from solution. Product (5µl) was run on a 1% (w:v) agarose gel and visualized to validate purification (section 2.2.1.1 and section 2.2.1.4).

Although column-based purification methods tend to yield higher levels of DNA recovery, they are limited to DNA fragments between 0.1-10kb making them unsuitable for RyR2 purification. The amount of DNA recovered was estimated by visual comparison with the signal intensity of bands on an agarose gel corresponding to known amounts of pre - linearised DNA (Figure 2.1). Typically, ~150-200ng of DNA would be recovered from the restriction digest and QIAEX II purification of 4µg of plasmid DNA. Although there was a large loss of DNA, the remaining amount of DNA was sufficient to carry out ligations of mutagenesis cassettes into full-length RyR2.

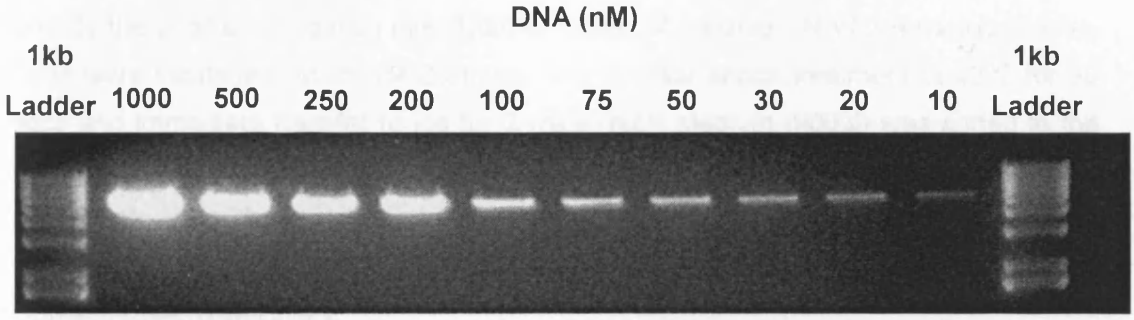

Figure 2.1. DNA dilution series for estimation of amount of DNA recovered from QIAEX II purification. *pSL1180 containing the SanDI/KpnI mutagenesis cassette (1µg) was digested with EcoRV for 4 hours at 37°C. EcoRV cuts the plasmid at a single site and linearises the plasmid DNA, preventing the effects of super-coiling on DNA fragment migration. A range of amounts of digest product (0.01 – 1µg) were run on an agarose gel (1%) containing ethidium bromide (1µl per 100ml of agarose) and were imaged by UV trans-illumination. The intensity of the resulting band of known molecular mass was used to estimate the amount of DNA recovered from QIAEX II purification.*

Ligations were carried out using the Rapid Ligation Kit (Roche) according to the manufacturer's instructions. The insert fragment was mixed with the plasmid vector (50ng) in a 3:1 molar ratio together with T4 DNA ligase and Ligase Buffer and was incubated at 4-8°C for 16 hours. Ligation product (15µl) was used to transform XL10-Gold cells (50µl) according to the protocol in section 2.2.1.3.

2.2.1.3. Transformation of competent bacterial cell lines

Three strains of *Escherichia coli* were used in this study: XL10-Gold (Stratagene), XL1-Blue (Stratagene) and MAX Efficiency Stbl2 (Invitrogen) competent cells (see section 2.1.7). The adherence to stringent protocols was essential for successful propagation of full-length RyR2 plasmid cDNA, as the large plasmid (~21kb) is fragile and prone to spontaneous intra-plasmid recombination. Bacteria transformed with full-length RyR2 plasmid were cultured at 30°C for less than 18 hours to minimize the likelihood of spontaneous plasmid DNA rearrangements (George *et al.*, 2003c). Bacteria transformed with the smaller intermediate vector containing mutagenesis cassettes were cultured at 37°C. All bacteria were cultured in LB media containing ampicillin (100µg/ml, LB_{Amp}) for transformant selection, either in suspension with shaking at 225rpm or on LB-agar plates.

Propagation of full-length RyR2 plasmid DNA and the intermediate vector containing mutagenesis cassettes was carried out by the transformation of XL10-Gold cells. Briefly competent cells (25µl) were thawed on ice and treated with β-ME (1µl, 0.5M) for 10 mins prior to the addition of ligation mix (15µl) or 100ng of plasmid DNA for retransformation. Cells were incubated on ice for 30 mins, prior to hear shock treatment at 42°C for 30 secs and immediate transfer to ice for 2 mins. NZY medium (900µl) was added to the cells which were then incubated at 37°C for 1 hour with shaking at 225rpm. Cells were plated onto LB_{Amp} agar plates and were incubated overnight at 30°C or 37°C for cells transformed with full-length RyR2 or intermediate vector containing mutagenesis cassette DNA respectively.

Site-directed mutagenesis products (5µl) were treated with DpnI to digest the methylated, non-mutated DNA template (see section 2.2.1.7 and Figure 2.2) and were transformed into XL-1 Blue supercompetent cells (25µl). A similar method was employed to that used in the transformation of XL10-Gold cells, although β-ME treatment of cells was not carried out in this protocol. XL1-Blue cells are capable of repairing the resulting 'nicks' in plasmid DNA resulting from site-directed mutagenesis primer elongation.

MAX Efficiency Stbl2 cells were used for the propagation of full-length RyR2 plasmid DNA, as they produced a significantly higher yield and no observable differences in restriction digest patterns compared to plasmid DNA propagated in XL10-Gold cells.

Full-length RyR2 plasmid DNA (200pg) was added to Stbl2 cells (50µl) and incubated on ice for 30 mins. Cells were heat-shocked at 42°C for 25 secs before being returned to ice for a further 2 mins. SOC medium (900µl) was added to the cells, which were incubated at 30°C for 90 mins with shaking at 225rpm. Bacteria were spread onto LB_{Amp} plates and incubated overnight at 30°C, before being examined for colony growth. Stbl2 cells tended to produce slightly smaller and significantly more individual colonies, when compared XL10 Gold cells.

2.2.1.4. Small scale plasmid isolation ("Miniprep")

Individual bacterial colonies were picked into LB_{Amp} medium (4ml) and incubated for 16h at 30°C (full-length RyR2 plasmid DNA) or 37°C (intermediate vector containing mutagenesis cassettes).

A proportion of the bacterial culture (3mls) was subsequently centrifuged (20,000 xg, 1 min) to pellet the bacteria. Plasmid DNA was then purified using the Wizard Mini-Prep System (Promega) according to the manufacturer's instructions. Briefly, the bacterial pellet was resuspended in resuspension solution (250µl) containing RNase A. Cell lysis solution (250µl) was added to the resuspended cells which were incubated at RT for 2 mins. Neutralisation solution (350µl) was added to the lysed bacteria which were then centrifuged (20,000 xg, 1 min) RT to pellet insoluble material. The clear lysate was transferred to a Wizard Mini-Prep spin column, containing a silica membrane to which the DNA became bound after centrifugation (20,000 XG, 1 min). The flow-through was discarded and the column was washed with wash solution (700µl) and centrifuged (20,000 xg, 1 min). The supernatant was discarded and the column underwent a further wash with wash solution (250µl) and was centrifuged (20,000 xg, 1 min). The column flow-through was discarded and the column was centrifuged (20,000 xg, 2 mins) to dry the silica membrane. The column was transferred to a collection tube and plasmid DNA was eluted in dH_20 (30µl) by centrifugation (20,000 xg, 1 min).

2.2.1.5. Large scale plasmid isolation ("Maxiprep")

The remaining miniprep culture was refreshed with 3ml LB_{AMP} broth and incubated at 30°C (full-length RyR2 constructs) or 37°C (intermediate vector containing mutagenesis cassette) with shaking at 225 rpm for 1 hour prior to seeding a larger culture (200ml) at a 1 in 400 dilution. Larger cultures were incubated at 30°C (full-length RyR2 constructs) or 37°C (intermediate vector containing mutagenesis cassettes) with shaking at 225rpm for 16 hours before being centrifuged at 15,000 xg for 10 mins at 4°C to pellet the bacterial cells. Plasmid DNA was isolated from the bacteria using the Qiagen Maxi-prep kit according to the manufacturer's instructions. The supernatant was discarded and the cell pellet was resuspended in 10ml of resuspension buffer (Buffer P1). Cells were lysed by the addition of 10mls of lysis buffer (Buffer P2) followed by inversion of the tube until the lysate became clear. Neutralisation buffer (Buffer P3, 10ml) was added to the solution which was incubated on ice for 30 mins to precipitate insoluble material. The lysate was centrifuged at 20,000 xg for 30 mins to remove the insoluble material. A Qiagen-tip 500 was equilibrated with 10ml of column equilibration buffer (Buffer QBT), prior to the addition of the cleared supernatant to the column. The supernatant was allowed to flow through the column before undergoing two washes with 30mls of wash buffer (Buffer QC). The column was transferred to a 30ml collection tube and DNA was eluted in 15ml of elution buffer (Buffer QF). 10.5mls of isopropanol was added to the DNA which was allowed to precipitate for 16 hours at -20°C. DNA was collected by centrifugation at 20,000 xg, 4°C for 30 mins. The DNA pellet was washed with 5ml of 80% ethanol and was centrifuged for a further 10 mins at 20,000 xg at 4°C. The supernatant was discarded and the pellet was allowed to air-dry for 10 mins before being resuspended in 500µl of SDW. DNA was incubated at 37°C for 2 mins to aid resuspension, before being transferred to a 1.5ml micro-centrifuge tube. Plasmid DNA was quantified (see 2.2.1.6) and 1µg of "Maxiprep" DNA was analysed for sequence integrity (see 2.2.1.3) and stored at -20°C.

2.2.1.6. Analysis of recombinant plasmid DNA

DNA concentration was determined using a spectrophotometer to measure the absorbance at 260nm (Abs_{260}) of a 1:50 dilution of "Maxiprep" DNA in SDW. Duplicate

measurements were made to allow the calculation of the average Abs_{260}, which was used to calculate DNA concentration according to the following formula:

Abs_{260} x dilution factor x 50 = DNA Concentration (ng/µl)

An Abs_{260} value of 1 corresponds to 50µg/ml double stranded DNA, hence this multiplication step is incorporated into the above formula. Tyrosine and tryptophan residues absorb strongly at 280nm, and as such the absorbance at 280nm (Abs_{280}) is measured and used as an indicator of contaminating protein levels. The Abs_{260} : Abs_{280} ratio was determined and used as a measure of the purity of the DNA prep, with a ratio of >1.8 being indicative of a preparation of high purity.

Restriction enzyme mapping was used to confirm that transformations were successful and that no gross plasmid rearrangement events had occurred during transformation, which would be presented as an altered DNA fragment banding pattern when run on an agarose gel. Several restriction enzymes were available for the mapping of full-length human RyR2 due to the presence of multiple restriction sites for an individual restriction enzyme in the RyR2 DNA sequence. Hin*DIII* was used for restriction mapping of pSL1180-SK1 constructs, due to the presence of numerous Hin*DIII* restriction sites in this construct.

2.2.1.7. Site-directed mutagenesis of pSL1180-SK1

The site-directed mutagenesis (SDM) method employed in the generation of full-length RyR2 cDNA constructs containing the single nucleotide polymorphisms utilises the polymerase chain reaction (PCR) and is limited to DNA sequences of ~6-8kb in length (Figure 2.2). The pcDNA3-eGFP-RyR2 plasmid is approximately 21kb making it too large for PCR amplification. Therefore, a method utilising an intermediate vector, pSL1180, containing the *SanDI/KpnI* hRyR2 mutagenesis cassette (psL1180-SK1) was adopted for the generation of constructs containing the G1885E polymorphism. The cassette in the intermediate vector is only 5,455bp, a suitable length for reliable PCR amplification.

Site-directed mutagenesis was carried out on the pSL1180 intermediate vector containing the *SanDI/KpnI* RyR2 fragment using the QuikChange® SDM kit (Stratagene) according to the manufacturers instructions (Figure 2.2). A schematic overview of the methods employed in the incorporation of single nucleotide substitutions and their subsequent verification is shown in Figure 2.3. Complementary oligonucleotide primers were designed that complemented the WT RyR2 DNA sequence, apart from a single mis-matched nucleotide that resulted in the required amino acid substitution.

When designing primers for use in SDM reactions, there are several factors that need to be considered. Firstly, both mutagenic primers need to contain the proposed base substitution and anneal to the same sequence on opposite strands of the template plasmid. Secondly, primers need to be between 25 and 45 base pairs long, with the mutation site as central as possible, to ensure complete specific annealing of the primer to the template DNA. Thirdly, the primers must have a melting temperate (T_m) of >78°C and should terminate with a guanine or cytosine base to ensure primer stability. Finally, the primers must have a high level of purity, such as that obtained by HPLC purification, as a decrease in primer purity results in a significant decrease in mutation efficiency. The primers used are detailed in Appendix 1, Table 2. The SDM reaction mix was prepared as detailed in Table 2.1. and underwent thermal cycling according to the protocol in Table 2.2.

Reagent	Volume	Final Concentration
10x Reaction Buffer	5µl	1x
DNA Plasmid Template	0.5µl of 90ng/µl stock	45ng total (0.9ng/µl)
Forward Primer (G1885E For)	1µl of 150ng/µl stock.	150ng total (3ng/µl)
Reverse Primer (G1885E Rev)	1µl of 150ng/µl stock.	150ng total (3ng/µl)
dNTP Mix	1µl of 10mM stock	0.2mM
PfuTurbo DNA Polymerase	1µl of 2.5U/µl stock	2.5U (0.5U/µl)
Nuclease Free H_2O	To total volume of 50µl	40.5µl

Table 2.1. G1885E Site-directed mutagenesis reaction mix.

Step	Temperature	Duration	Cycles
Initial Denaturation	95°C	30 secs	1
Denaturation	95°C	30 secs	18
Annealing	55°C	1 min	
Elongation	68°C	6 mins	
Hold	4°C	Indefinitely	1
The length of the elongation step is determined by the size of the template plasmid, requiring 1 min per 1kb to be amplified.			

Table 2.2. Site-directed mutagenesis thermal cycling protocol.

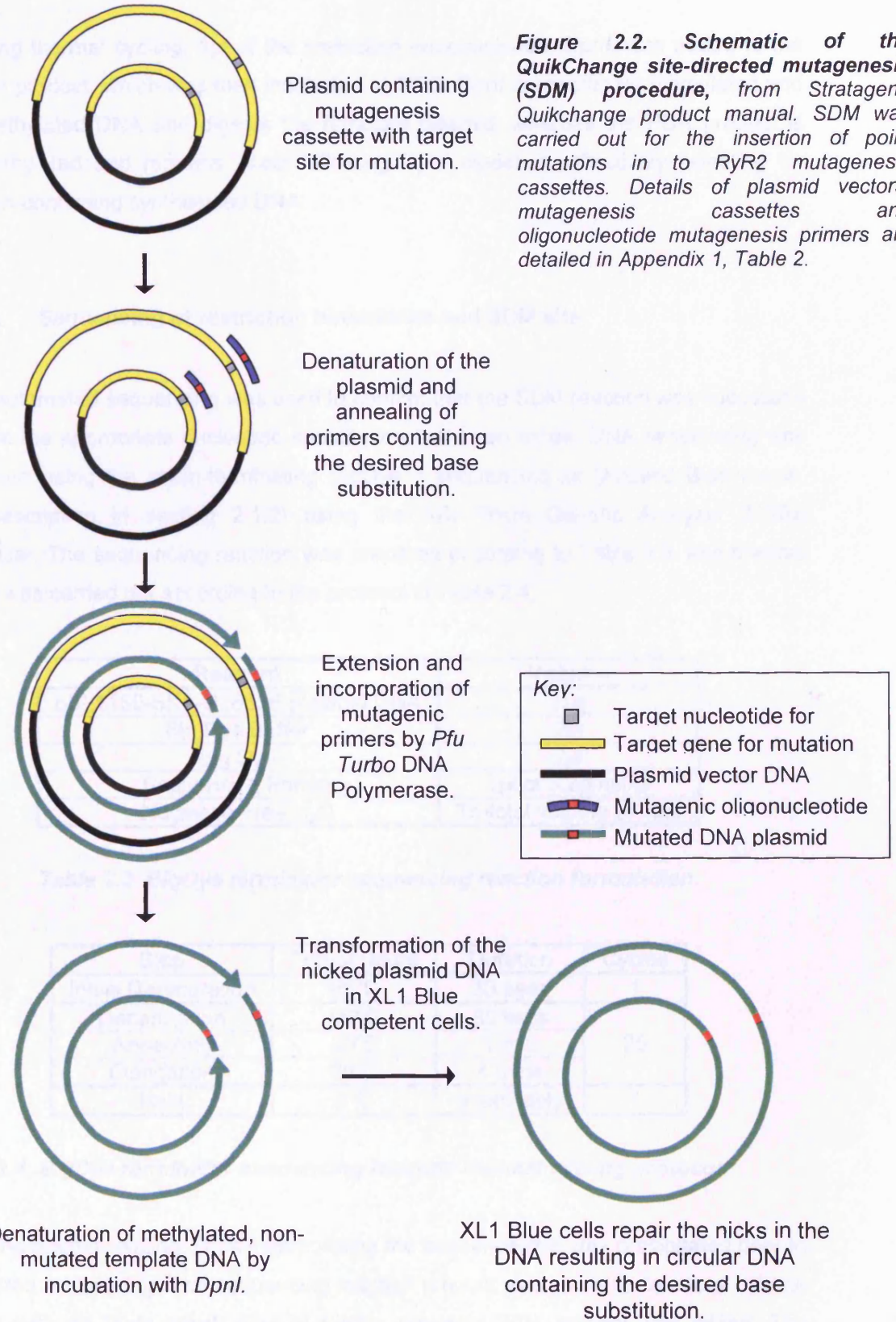

Figure 2.2. Schematic of the QuikChange site-directed mutagenesis (SDM) procedure, *from Stratagene Quikchange product manual. SDM was carried out for the insertion of point mutations in to RyR2 mutagenesis cassettes. Details of plasmid vectors, mutagenesis cassettes and oligonucleotide mutagenesis primers are detailed in Appendix 1, Table 2.*

Following thermal cycling, 1µl of the restriction endonuclease, Dpn*I*, was added to the reaction product, which was then incubated at 37°C. Dpn*I* is specific for methylated and hemimethylated DNA and digests the template plasmid, whereas the PCR product is non-methylated and remains intact following Dpn*I* digestion, effectively selecting for mutation-containing synthesised DNA.

2.2.1.8. Sequencing of restriction boundaries and SDM site

Direct automated sequencing was used to confirm that the SDM reaction was successful and that the appropriate nucleotide substitution had been made. DNA sequencing was performed using the chain-terminating BigDye™ sequencing kit (Applied Biosystems, brief description in section 2.1.2) using the ABI Prism Genetic Analyzer 3130xl sequencer. The sequencing reaction was prepared according to Table 2.3. and thermal cycling was carried out according to the protocol in Table 2.4.

Reagent	Volume
pSL1180-SK1-G1885E plasmid DNA	1µg
Big Dye Buffer	2µl
Big Dye	2µl
Sequencing Primer	1µl of 3.2pmol/µl
Nuclease Free H_2O	To total volume of 10µl

Table 2.3. BigDye terminator sequencing reaction formulation.

Step	Temperature	Duration	Cycles
Initial Denaturation	96°C	30 secs	1
Denaturation	96°C	30 secs	25
Annealing	50°C	1 min	
Elongation	60°C	4 mins	
Hold	4°C	Indefinitely	1

Table 2.4. BigDye terminator sequencing reaction thermal cycling protocol.

Following thermal cycling, DNA incorporating the sequence-dye was precipitated prior to automated sequencing. The sequencing reaction product was made up to a total volume of 20µl with dH_2O, to which 80µl of freshly prepared 75% ethanol was added. The reaction mix was then incubated in the dark, at RT for 1 hour. The sequencing reaction

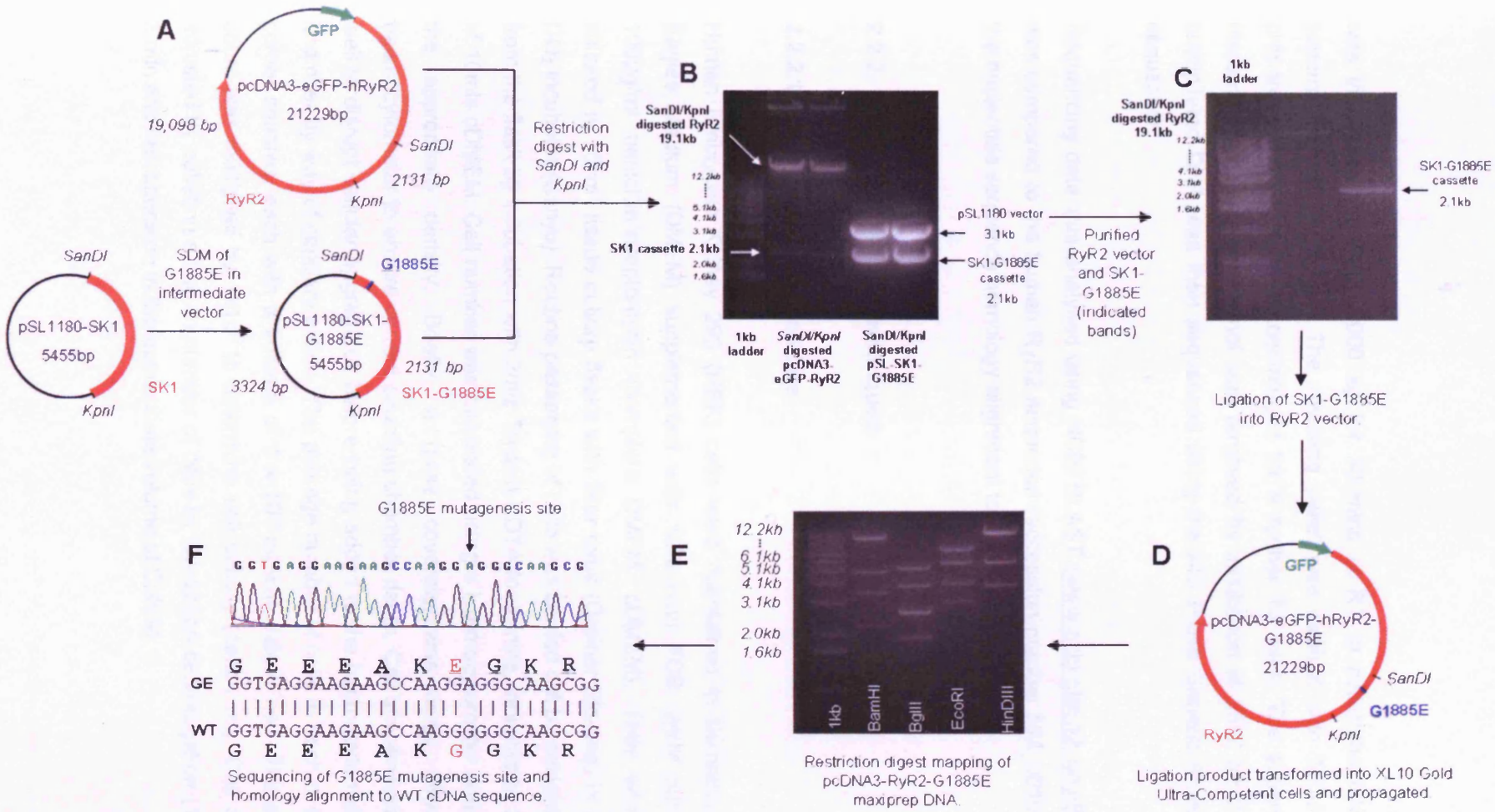

Figure 2.3. Cloning strategy for inserting nucleotide substitutions into full-length RyR2 cDNA. *Site directed mutagenesis was used to insert a SNP (G1885E) into the SanDI/KpnI mutagenesis cassette (SK1) in the intermediate vector (panel A, section 2.2.1.7). The expression vector containing full-length RyR2 and intermediate vector containing the mutagenesis cassette were both digested with SanDI/KpnI (panel B, section 2.2.1.2) and DNA fragments corresponding to the RyR2 "vector" and mutagenesis cassette containing G1885E were purified (panel C). The cassette containing G1885E was ligated into the full-length RyR2 "vector" (panel D), which was then propagated in XL10-Gold or Stbl2 cells (section 2.2.1.3 - 2.2.1.5). Successful ligation was confirmed by restriction mapping (panel E) and direct sequencing of the SDM site. The resulting codon change is indicated in red. (panel F, section 2.2.1.8).*

was then centrifuged at 20000 xg for 30 mins at RT to pellet the DNA and the supernatant was discarded. The resulting pellet was washed with 180µl of freshly prepared 75% ethanol and centrifuged for a further 15 mins. The supernatant was discarded and residual ethanol was removed by incubation at 95°C for 2 mins. The precipitated DNA was then sequenced using the ABI Prism Genetic Analyzer 3130xl sequencer.

Sequencing data was analysed using NCBI BLAST (www.ncbi.nlm.nih.gov/BLAST) and was compared to the human RyR2 sequence (accession number NM_001035.2) using the nucleotide sequence homology alignment tool.

2.2.2. Cell biology techniques

2.2.2.1. HEK-293 cell culture

Human Embryonic Kidney 293 (HEK) cells were maintained in Dulbecco's Modified Eagles Medium (DMEM) supplemented with 10% (v:v) FCS, 2mM glutamine and 100µg/ml penicillin/streptomycin (complete DMEM, cDMEM). They were routinely cultured in 75cm^2 tissue culture flasks with filter caps (Greiner Bio-one) in a 37°C, 5% CO_2 incubator (Sanyo). Routine passaging of cells was carried out by detaching the cells from the flask by incubation with 2mls Trypsin-EDTA for 2 mins, inhibited by the addition of 10mls cDMEM. Cell number was calculated using a haemocytometer and adjusted to the appropriate density. Briefly, a glass coverslip was firmly affixed to the haemocytometer to ensure correct counting chamber depth. Cell suspension was mixed well to disrupt cellular aggregates before being added to the haemocytometer counting chamber by way of capillary action. The average number of cells in each of the four 4x4 corner squares, each with a volume of 1 x 10^{-4} ml was determined. The average cell count was multiplied by 1x10^5 to determine cell density (cells / ml). Cell density was adjusted by pelleting a known number of cells by low-speed centrifugation (1000 xg) for 5 min and resuspension in the appropriate volume of DMEM.

2.2.2.2. Heterologous RyR2 expression

In order to heterologously express full-length recombinant RyR2 in HEK-293 cells, two methods of transfection were employed with the downstream experimental application being the deciding factor of which methodology was used. Calcium phosphate ($CaPO_4$) mediated transfection was used for the transfection of cells from which RyR2 protein was to be used in SDS-PAGE and western blot-analysis as this method results in high levels of RyR2 expression per individual cell. However, high-levels of RyR2 expression can be cytotoxic and result in increased cell-death (George et al., 2003a) and also leaves a residual precipitate on the cells, which is not ideal for live-cell Ca^{2+} imaging. $CaPO_4$ transfection also tended to exhibit a high level of variation between separate transfection experiments, possibly due to the sensitivity to variation in transfection reagents e.g. HBS, CaCl. Furthermore, $CaPO_4$-mediated transfection requires a significantly greater amount of DNA (~10 fold) for successful transfection compared to a commercially available lipid-mediated transfection reagent, Effectene (Qiagen).

Effectene Reagent (Qiagen) was more suitable for the transfection of cells for live cell imaging, as it produced highly reproducible transfection efficiencies (40-45 %, Figure 3.10), did not leave a precipitate and was less cytotoxic than $CaPO_4$-mediated transfection, possibly due to lower levels of RyR2 expression per individual cell. However, transfection of large numbers of cells for RyR2 with Effectene reagent was not feasible due to the expense of sufficient reagent for large scale transfection. Also, when large scale transfection was attempted, the amount of RyR2 that was isolated was not sufficient to exhibit sufficient signal for accurate determination of relative levels of RyR2 expression by SDS-page and western blot analysis.

2.2.2.2.1. Calcium phosphate-mediated transfection of HEK cells

HEK cells ($1x10^6$) were seeded into a T75 flask and were incubated for 24 hours at 37°C, 5% CO_2 prior to transfection with full-length, pcDNA3-eGFP-RyR2 plasmid DNA. Plasmid DNA (28µg) was mixed with sterile dH_2O and 259µl of 2M $CaCl_2$ to a total volume of 1050µl and vortexed vigorously. This mixture was added a drop at a time to 1050µl of warmed 2x HBS in a sterile 14ml capacity polypropylene tube (Greiner) with continuous mixing to achieve a final $CaCl_2$ concentration of 125mM and a volume of

2050µl. Transfection complexes were incubated at RT for no longer than 30 mins to allow precipitates to form. These were subsequently mixed by vortexing and added a drop at a time to cells in cDMEM (20ml), which were incubated at 37°C, 5% CO_2 for 24 hours. Transfection media was then removed and replaced with cDMEM and cells were incubated for a further 24 hours before harvesting by trypsinisation as in section 2.2.2.1.

2.2.2.2.2. Effectene-mediated transfection of HEK cells

Transfection of HEK cells for subsequent live-cell Ca^{2+}-imaging using confocal microscopy was achieved using the lipid-based Effectene Reagent (Qiagen) according to manufacturer's instructions. HEK cells were seeded onto 154mm^2, poly-D-lysine coated coverslips (154mm^2 growth area, MatTek) at a density of 1x10^5 cells/coverslip in a meniscus volume of 150µl. Cells were incubated at 37°C, 5% CO_2 for 1 hour prior to transfection, to allow them to adhere to the coverslip. To transfect 14 coverslips, 3.2µg of pcDNA3-eGFP-RyR2 plasmid DNA was made up to a total volume of 400µl with EC Buffer, to which 25.6µl enhancer solution was added to "condense" the DNA. The solution was mixed by vortexing and incubated at RT for 4 mins. 80µl of Effectene reagent was added to the solution, which was mixed by vortexing and incubated at RT for 10 mins to produce condensed Effectene-DNA complexes. 2.4mls of cDMEM was added to the transfection solution containing the Effectene-DNA complexes, 200µl of which was added to the meniscus on each coverslip. Cells were incubated at 37°C, 5% CO_2 for 24 hours before being topped up with 2mls cDMEM and returned to the incubator for a further 24 hours (48 hours total incubation post-transfection). Cells were then examined for eGFP fluorescence using fluorescent microscopy (Zeiss) for confirmation of successful protein expression.

2.2.2.2.3. Co-transfection with multiple RyR2 cDNAs

To investigate the functional consequences of co-expression of two distinct recombinant RyR2s, cells were transfected with equimolar ratios of two distinct RyR2 cDNAs using Effectene reagent as detailed in section 2.2.2.2.2. When transfecting cells on 14 coverslips for single-cell Ca^{2+} imaging, 1.6µg of each RyR2 cDNA (3.2µg total) was mixed, prior to incubation with enhancer and Effectene reagents. Transfection with a

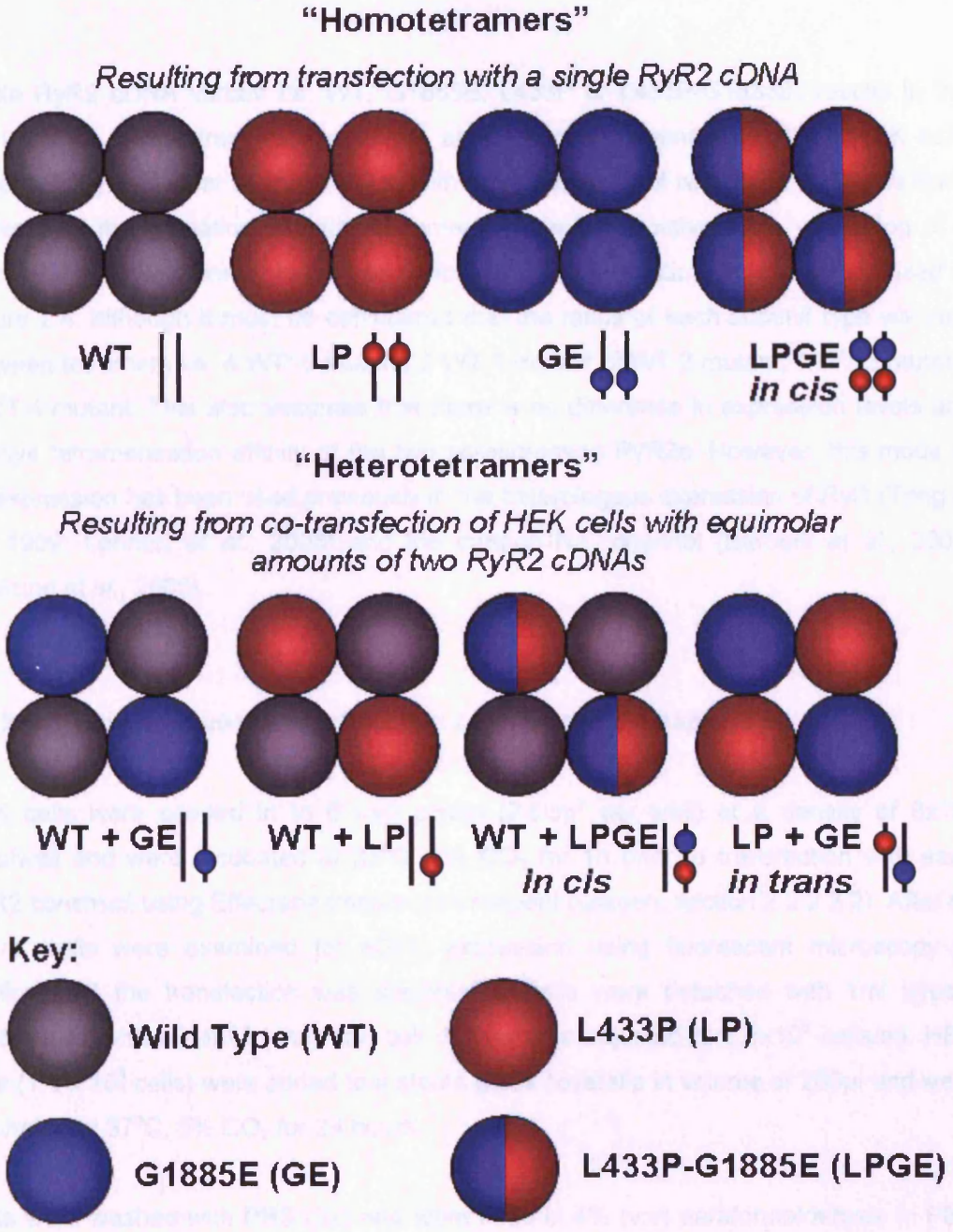

Figure 2.4. Schematic representation of recombinant RyR2 tetramerisation. *HEK cells transfected with a single RyR2 result in the formation of homotetramers, with each monomeric subunit containing identical amino acid substitutions (panel A). Co-transfection of HEK cells with equimolar ratios of two distinct RyR2 cDNAs likely results in the formation of heterotetramers containing a mixture of RyR2 subunits (panel B). Although tetramers consisting of 2 of each type of RyR2 subunit are illustrated here, RyR2 tetramers will likely be of varying stoichiometry, including the formation of homotetrameric channels, although this can not be determined in these experiments. Tetramers described as "in cis" indicate the mode of expression replicative of inheritance of the two substitutions on the same allele in vivo, whereas those described as "in trans" are representative of the inheritance of two substitutions on opposite alleles in vivo. The hypothetical modes of inheritance i.e. (in cis and in trans) are indicated in each case.*

single RyR2 cDNA variant i.e. WT, G1885E, L433P or L433P-G1885E, results in the formation of homotetramers due to the absence of endogenous RyR2 in HEK cells (Figure 3.11). However co-transfection with equal amounts of two RyR2 cDNAs is likely to result in the formation of heterotetramers of varying stoichiometry, consisting of a mixture of the two different monomeric subunits in varying ratios. This is summarised in Figure 2.4, although it must be considered that the ratios of each subunit type will vary between tetramers i.e. 4 WT: 0 Mutant, 3 WT:1 mutant, 2 WT:2 mutant, 1 WT:3 mutant, 0 WT:4 mutant. This also assumes that there is no difference in expression levels and relative tetramerisation affinity of the two co-expressed RyR2s. However, this mode of co-expression has been used previously in the heterologous expression of RyR (Tong *et al.*, 1999; Lehnart *et al.*, 2008) and the cardiac Na^+ channel (Baroudi *et al.*, 2002; Poelzing *et al.*, 2006).

2.2.2.2.4. Immunofluorescent detection of RyR2 protein expression

HEK cells were seeded in to 6 well plates (9.6cm^2 per well) at a density of 8x10^5 cells/well and were incubated at 37°C, 5% CO_2 for 1h prior to transfection with each RyR2 construct using Effectene transfection reagent (Qiagen, section 2.2.2.2.2). After 48 hours, cells were examined for eGFP expression using fluorescent microscopy to confirm that the transfection was successful. Cells were detached with 1ml trypsin 'inactivated' with cDMEM (4ml) and cell density was adjusted to 7.5x10^5 cells/ml. HEK cells (1.5 x 10^5 cells) were added to a sterile glass coverslip in volume of 200µl and were incubated at 37°C, 5% CO_2 for 24 hours.

Cells were washed with PBS (3x) and were fixed in 4% (v:v) paraformaldehyde in PBS for 10 mins in the dark at RT. Cells were washed with PBS and rehydrated in PBS for 24 hours at 4-8°C. Following rehydration, cells were washed with PBS and permeabilised with 0.1% (v:v) Triton-X-100 diluted in PBS for 30 mins at RT. Cells were incubated in 10% (v:v) FCS diluted in PBS for 30 mins at RT. Following washing with PBS, cells were incubated with an anti-hRyR2 antibody (pAb1093, 1:100 v:v) at RT for 90 mins. Following three 10 min washes in PBS, cells were incubated with the secondary Alexa^{546} goat anti-rabbit antibody (1:250) in PBS in the dark at RT for 90 mins. Coverslips were washed in PBS and SDW and mounted on glass slides using a drop of Fluorsave and were allowed to dry for 30 mins. Cells were imaged using an SP5 confocal microscope

(Leica) with an oil immersion, 63x objective. eGFP fluorescence was excited with an Argon laser (peak excitation of 488nm) and emission between 520±28nm was detected. Alexa^{546} fluorescence was excited at 561nm with a diode-pulsed solid state (DPSS) laser was detected over 655±65nm range.

The direct overlay of eGFP- and Alexa^{546} images was used to determine the extent of co-localisation of eGFP and antibody signals (calculated for each construct and expressed as the 'percentage overlap' as described previously (George *et al.*, 2003a)

2.2.2.3. Confocal microscopy

HEK cells transfected with full-length pcDNA3-eGFP-hRyR2 constructs using Effectene reagent, were examined using a SP5 confocal microscope (Leica). 48 hours post-transfection (2.2.2.2.2) cells were loaded with Fluo3-AM (15μM in mDMEM, see section 2.1.10) for 1h at 37°C, 5% CO_2, before addition of excess mDMEM. Cells were returned to the incubator for a further 15 mins to allow de-esterification of Fluo3-AM. Media was aspirated from the coverslip and was replaced with mDMEM (1ml) prior to examination using the confocal microscope using an oil-immersion, 63x magnification objective, using an Argon laser. Excitation was at 488nm and fluorescence was detected over the range of 525±25nm. Data was acquired from regions of interest representing global intracellular environments using Leica LAS AF confocal software. Analysis of exported Ca^{2+} imaging data was performed using Microsoft Excel and GraphPad Prism software.

2.2.3. Protein biochemistry techniques

2.2.3.1. Preparation of mixed membranes from transfected HEK cells

Following $CaPO_4$ mediated transfection of HEK cells (as in section 2.2.2.2.1) cells were harvested by trypsinisation and pelleted by centrifugation (1,000 xg, 5 mins). Cells were resuspended in hypo-osmotic buffer (see section 2.1.3, 1ml buffer per 1x10^6 cells). Cells were homogenized by 10 strokes with a glass homogenizer on ice, before passing the cells through a 23G needle ten times. Lysed cells were centrifuged at low speed (1,000 xg, 15 mins) to remove un-lysed cells and nuclei. The supernatant was collected and

centrifuged at high speed (30,000 xg, 90 mins, 4°C) to pellet a microsomal fraction. Supernatant was removed and the microsomal pellet was resuspended in 0.4M sucrose, 20mM HEPES solution (20µl per $1x10^6$ cells). Microsomal preparations were aliquoted, snap frozen and stored at -80°C.

2.2.3.2. Micro-BCA protein assay

The first step of the micro bicinchoninic acid (BCA) protein assay is the chelation of copper with protein in an alkaline environment to form a blue-coloured complex. Peptides containing three or more amino acid residues form a coloured chelate complex with cupric ions in an alkaline environment containing sodium potassium tartrate. The second step of the colour development process involves the reaction of BCA, a highly sensitive colourimetric detection reagent, with the cupric cation formed in the first stage of the assay. The purple coloured reaction product is formed by the chelation of two molecules of BCA with one cuprous ion. The BCA/copper complex is water-soluble and exhibits a strong linear absorbance at 562nm directly proportional to increasing protein concentration.

Protein samples were diluted 1:200 (v:v) in SDW and 100µl was added in duplicate to a 96 well plate. This dilution of sample proteins was necessary to ensure that protein concentrations were in the linear range of the relationship between protein concentration and absorbance as demonstrated by the generation of a BSA standard curve (Figure 2.5). Bovine serum albumin (BSA) was diluted to a range of concentrations (10, 25, 50, 75, 100, 200 µg/ml) and added in duplicate to the 96 well plate. BCA solution was prepared by combing reagents A, B and C in a ratio of 50:49:1 respectively and 100µl of the prepared solution was added to each well. The samples were incubated at 37°C for 1 hour before reading the absorbance at 560nm on a plate reader (Labsystems, Multiskan Ex). A standard curve of BSA protein concentration was generated using the absorbance at 560nm of the range of known BSA concentrations (Figure 2.5). The equation of the linear regression line was used to determine the protein concentration from the OD_{560} of sample protein. Typical protein yields from $1x10^6$ cells harvested 48 hours post-transfection with full-length RyR2 was typically between approximately 8mg-10mg and approximately 5-6mg in $1x10^6$ untransfected HEK cells.

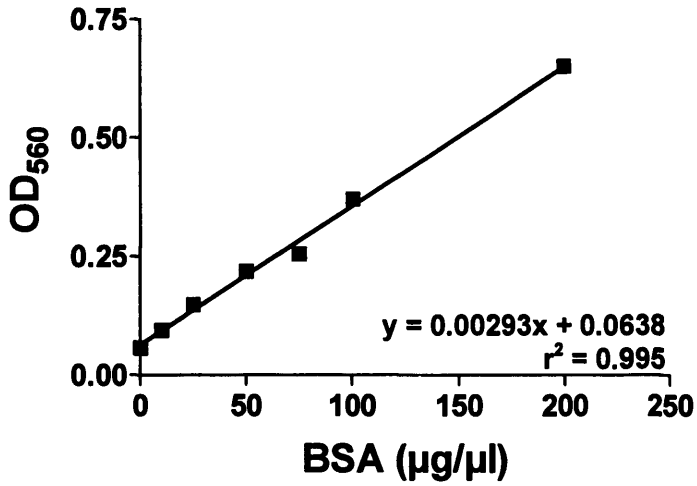

Figure 2.5. Linear regression analysis of the relationship between BSA concentration and absorbance at 560nm. *Linear regression analysis was used to generate a standard curve from which sample protein concentration (µg/µl) could be estimated. Absorbance readings at each BSA concentration were taken in duplicate.*

2.2.3.3. SDS Polyacrylamide gel electrophoresis

RyR2 protein expression levels were analysed by discontinuous SDS-polyacrylamide gel electrophoresis (Laemmli, 1970, Nature) and subsequently, by western blot analysis. A 4% (v:v) acrylamide separating gel was prepared according to Table 2.5. A 4% gel is suitable for the resolution of proteins greater than 500 kDa. It was imperative that TEMED and APS were added to the separating gel immediately prior to the pouring of the gel to prevent premature acrylamide polymerization. A fresh working stock of APS was made immediately prior to preparation of the separating gel.

Reagent	Volume	Final Concentration
40% bis-Acrylamide	3ml	4% (v:v)
Tris 1.5M pH8.8	7.5ml	25% (v:v)
SDS, 10% (w:v)	3ml	1% (v:v)
Ammonium persulphate, 10% (w:v)	150µl	0.5% (v:v)
TEMED	15µl	0.05% (v:v)
dH_2O	16.335ml	60.45% (v:v)
Total	30ml	

Table 2.5. 4% SDS-PAGE separating gel formulation.

The polyacrylamide gel mixture was poured into the gel casing (Hoefer), which had been assembled according to the manufacturer's instructions, and covered with a 1cm layer of SDW and allowed to set. Once the polyacrylamide gel had set, the water was removed and replaced with 4% stacking gel prepared according to Table 2.6.

Reagent	Volume	Final Concentration
40% bis-Acrylamide	2ml	4% (v:v)
Tris 0.5M pH6.8	5ml	25% (v:v)
SDS, 10% (w:v)	200µl	0.1%
Ammonium persulphate, 10% (w:v)	100µl	0.5%
TEMED	20µl	0.1% (v:v)
dH_2O	16.28ml	69.4% (v:v)
Total	20ml	

Table 2.6. 4% SDS-PAGE stacking gel formulation.

While the stacking gel was setting, mixed membrane protein samples (100µg) were incubated with equal volumes of 2x SDS-gel loading buffer at 42°C for 30 mins to linearise proteins. Once the stacking gel had set, mixed membrane protein samples (100µg) were loaded alongside protein molecular weight markers (Invitrogen). Electrophoresis was carried out at constant current (10mA) until only the two largest markers (150 and 250 kDa) remained on the gel. The RyR2 monomer is 565 kDa and migrates through the gel at a slower rate than even the largest Kaleidoscope protein molecular weight markers, and presents as a band above those corresponding to these markers following western blot analysis.

2.2.3.4. Transfer of proteins onto a PVDF membrane

Proteins separated on SDS-PAGE gels were transferred onto a polyvinylidene difluoride (PVDF) membrane (Millipore) using a semi-dry blotting system (Bio-Rad). PVDF membranes were prepared by soaking in methanol for 1 min and subsequently in semi-dry transfer buffer for 30 mins. The semi-dry transfer apparatus was assembled according to the manufacturers instructions and transfer was carried out at constant current (400mA, limited to 25V) for 2 hours at 4°C.

2.2.3.5. Western blot analysis of RyR2 protein

Following protein transfer, the membrane was incubated in 5% (w:v) non-fat dried milk protein (Marvel) in TBS-T buffer (5% blocking buffer) overnight at 4°C. An RyR2-specific primary antibody (pAb1093) was diluted 1:5000 (v:v) in blocking buffer and was applied to the membrane for 2 hours at RT or overnight at 4°C. The membrane was then washed three times (10 mins each wash) in 1% blocking buffer. A horseradish peroxidase (HRP)-conjugated secondary antibody (raised against the species corresponding to source of primary antibody was produced) was applied in a 1:10000 dilution in 1% blocking buffer for 2 hours at RT. The blot was then washed with TBS-T buffer (5x 10mins). Immunoreactive protein bands were visualised by enhanced chemiluminescence detection (ECL, GE Healthcare) according to manufacturer's instructions (Figure 2.6). Briefly, HRP conjugated to the secondary antibody catalyses the peracid-mediated oxidation of luminol. Oxidation causes luminol to enter an excited state which decays to a ground state via a light emitting pathway (428nm). The presence of enhancer molecules, including phenols, enhances this light emission up to 1000-fold, making it readily detectable by exposure to blue-light sensitive autoradiography film. The blot was exposed to X-ray film (Hyperfilm, GE Healthcare) for a suitable length of time which was determined by the level of the chemiluminescence signal.

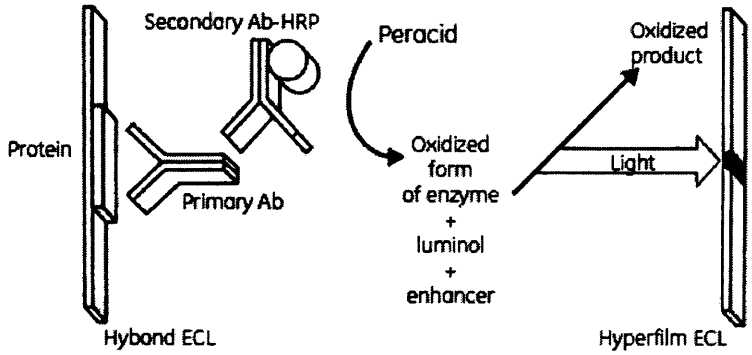

Figure 2.6. Principle of Enhanced Chemiluminescent (ECL) protein detection, *from GE healthcare ECL Western Blotting Detection Manual. Horseradish peroxidase on the secondary antibody catalyses the peroxidase-mediated oxidation of luminol, which emits low levels of light (428nm) which is enhanced by the presence of phenols. This enhances emitted-light levels up to 1000-fold and is readily detectable by exposure to blue-light sensitive autoradiography film.*

2.2.4. Statistical analysis

Appropriate statistical analyses were carried out using Microsoft Excel and GraphPad Prism software. Data was assessed for Gaussian distribution by way of Kolmogorov-Smirnoff test ($p>0.10$ indicating a normal distribution) and through investigation of the frequency histogram. Homogeneity of variance testing of normally distributed data was carried out using Bartlett's test for equal variances. Comparison of independent sample means from normally distributed data was carried out using Students T-test to compare two means, or by One-Way analysis of variance (ANOVA) to compare multiple sample means. Tukey-Kramers post-hoc test was used to compare multiple sample means to each other, providing that the ANOVA result indicated a significant difference between sample means ($p<0.05$). Comparison of independent sample means from data which did not fit a Gaussian distribution were carried out using non-parametric tests. The Mann-Whitney test was used to compare two sample medians and the Kruskal-Wallis test with Dunn's post-hoc tests were used to compare median values of multiple samples. Unless otherwise stated, the level of significance reported as a result of statistical testing is reported by a number of asterisks with a single asterisk representing $p < 0.05$ (*), two asterisks representing $p < 0.01$ (**) and three asterisks representing $p < 0.001$(***). The absence of an asterisk represents that $p > 0.05$, indicating that no significant difference at the 95% confidence level was observed.

2.2.5. Linear regression analysis

Linear regression analysis was used to determine whether relationships existed between two variables and to determine the nature of any relationships. All linear regression analysis was carried out using the least-squares method using GraphPad Prism analytical software. Several key statistics were determined from the linear regression analysis, which are detailed below and were used to examine the relationship between two variables.

Gradient: The gradient (Δ) quantifies the steepness of the line-of-best-fit and indicates the change in one variable (y) for each unit change in another variable (x). If the gradient is positive, it indicates that an increase in

variable x results in an increase in variable *y* (positive relationship). If the gradient is a negative value, it infers that as variable *x* increases, variable *y* decreases (negative relationship).

r^2: This is the goodness-of-fit value and represents how well the data fits the line-of-best-fit. This value is always between 0 and 1, with values a value of 1 indicating that all data points lie exactly on the line-of-best-fit. A value of 0 indicates that there is no linear relationship between two variables. An arbitrary threshold value of 0.3 was chosen to represent a weak significant relationship, 0.5 - 0.7 to represent a moderate relationship and greater than 0.7 to represent a strong relationship.

p-value: The null hypothesis predicts that the slope of the linear regression line is zero. If this the p-value was less than 0.05, the null hypothesis is rejected and it would suggest that the slope of the linear regression line is significantly different to zero and there is a significant positive or negative relationship between the two variables, *x* and *y*.

The r^2 and p-values must be interpreted together to determine whether a significant relationship between two variables exists.

Chapter 3

Functional characterisation of the L433P ARVD2 linked mutation and associated G1885E polymorphism in a heterologous cell system.

3.1. Introduction

To date, there have been over 124 single nucleotide substitutions identified in the *RyR2* gene of patients diagnosed with CPVT/ARVD2 (Medeiros-Domingo *et al.*, 2009). Despite the continuing identification of arrhythmogenic disease-linked RyR2 mutations (Thomas *et al.,* 2010), the precise mechanism by which these mutations result in an arrhythmogenic phenotype remains unknown, although several mechanisms have been proposed (section 1.3.4). Although the majority of RyR2 mutations that have been functionally characterised have been shown to increase channel activity under various experimental conditions, there is emerging evidence that not all mutations confer a gain-of-functionality (Thomas *et al.*, 2004; 2005; Jiang *et al.*, 2007). This suggests that there may not be a unifying mechanism by which RyR2 mutations result in channel dysfunction. Together with the fact that the location of the mutation in the RyR2 protein sequence does not dictate the resulting phenotype (Jiang *et al.*, 2005), this reiterates the need to functionally characterise mutations on an individual basis.

3.1.1. RyR2 functional characterisation methodologies

Given that the number of identified RyR2 mutations is increasing dramatically (Thomas *et al.*, 2010), comprehensive functional characterisation tends to be prioritised to those mutations which present an 'interesting' phenotype i.e. R4497C, R2474S etc. The characterisation of disease-linked RyR2 mutations has been carried out using several experimental systems, each capable of investigating different pathophysiological mechanisms of mutant channel function, several of which will be discussed here.

3.1.1.1. Lipid bilayer single channel analysis

Unlike whole-cell patch-clamp analysis of cell-surface ion channels which measures multiple channel currents, the reconstitution of channels into lipid bilayers allows the investigation of the gating and conductance properties of single RyR2 and other intracellular membrane channels (Holmberg & Williams, 1989). These experiments allow the precise control of the ionic environment surrounding the cytoplasmic and luminal face of the channel and as such can be used to monitor RyR2 biophysical properties

under a range of physiological conditions i.e. high luminal Ca^{2+} and low cytoplasmic Ca^{2+}, concentrations characteristic of diastole. As such, lipid bilayer analysis of single RyR2 channels has allowed the investigation into the effects of physiological and non-physiological ligands, regulatory proteins, cellular processes and RyR2 mutations on channel gating and conductance properties (Rousseau *et al.*, 1986; Holmberg & Williams, 1989; Tester *et al.*, 2007; Kong *et al.*, 2008).

Although this methodology allows for the precise control of the ionic conditions surrounding the channel, it is not without its limitations. Isolation of RyR2 channels from a cellular environment is likely to subject the channel to non-physiological conditions, such as oxidative stress, which may alter channel properties (Meissner, 2004). Similarly, detergent lysis of cellular expression systems may lead to the dissociation of accessory proteins from the RyR macromolecular complex or alteration of inter- and intramolecular interactions.

3.1.1.2. [^{3}H]ryanodine binding assays

Ryanodine is a highly toxic plant alkaloid found in the *Ryania speciosa* plant and binds all three RyR isoforms with high affinity. The radio-labelling of ryanodine has provided an indispensible tool that was used in the identification and isolation of RyR2 (Inui *et al.*, 1987) and has been used extensively in the functional characterisation of RyR2. Given that ryanodine only binds RyR2 when the channel is in the open state, the measurement of the level of bound ryanodine is an accurate measure of channel activity. In this sense, the [^{3}H]ryanodine binding assay has been used to investigate the effects on RyR channel activity of physiological ligands e.g. Ca^{2+}, Mg^{2+}, ATP (Holmberg & Williams, 1989; Du *et al.*, 1998) non-physiological ligands e.g. caffeine, K201 (Holmberg & Williams, 1989; Hunt *et al.*, 2007) and accessory proteins e.g. FKBP12.6 (Yano *et al.*, 2003). Furthermore ryanodine binding analysis has been instrumental in elucidating the mechanisms by which CPVT/ARVD2 linked mutations alter RyR2 gating parameters. Typical gain-of-function mutations that are proposed to exhibit diastolic Ca^{2+} leak are regularly characterised by an increase in sensitivity to Ca^{2+}-dependent [^{3}H]ryanodine binding (Jones *et al.*, 2008a; Fernandez-Velasco *et al.*, 2009) due to the increased open probability compared to WT RyR2.

3.1.1.3 SR vesicle Ca^{2+} uptake and leak assays

Given the proposed role of diastolic Ca^{2+} leak in RyR2 mutant pathogenesis, assays have been developed to measure the rates of Ca^{2+} uptake and release into and out of the SR (Yano *et al.*, 2000; Doi *et al.*, 2002; Yano *et al.*, 2003; Oda *et al.*, 2005). Briefly, isolated SR vesicles are loaded with Ca^{2+} through incubation in a Ca^{2+}-containing buffer, with SERCA-mediated Ca^{2+} uptake being initiated through the addition of ATP. By monitoring the decrease in Ca^{2+}-indicator signal intensity (e.g. Fluo3, see section 3.1.1.4), the rate of Ca^{2+} uptake into the SR can be monitored. Once Ca^{2+} uptake had plateaued, a small amount of thapsigargin (typically 1μM) was added to the SR vesicles to inhibit SERCA activity and cause a passive release of Ca^{2+} from the SR through RyR2, which can be measured by monitoring the increase in Fluo3 signal intensity (Yano *et al.*, 2000). This approach has been used to examine the effects of both RyR2 accessory proteins e.g. FKBP12.6 (Yano *et al.*, 2000; Yano *et al.*, 2003), and arrhythmia-linked mutations e.g. R2474S (Oda *et al.*, 2005), on the rates of Ca^{2+} uptake and release, with decreased rates of Ca^{2+} uptake and increased rates of Ca^{2+} release pertaining to SR Ca^{2+} leak.

3.1.1.4 Ca^{2+} imaging in intact cells

Since the advent of Ca^{2+} sensitive fluorescent dyes and improvements in microscopy and computing technology, intracellular Ca^{2+} imaging has become a powerful and widely used technique in the investigation of RyR2 function. Although the examination of RyR2 in intact cells does not allow the precise control of the environment surrounding the channel, as afforded in experiments where RyR2 is isolated from the cell (section 3.1.1.1), this method allows the characterisation of RyR in more physiologically relevant setting. Of course, the precise nature of this cellular environment is entirely dependent on the cell-line in which Ca^{2+} imaging experiments are carried out (see section 3.1.1.5).

High-powered laser scanning confocal microscopy is widely used in the characterisation of RyR2, as by utilising fluorescent Ca^{2+}-indicator dyes e.g. Fluo3, fura-2, it allows the direct monitoring of free intracellular Ca^{2+} levels in intact cells in a relatively non-invasive fashion. Confocal microscopy has many advantages over conventional fluorescence microscopy in that it:

- Removes light that has not originated from the focal plane, resulting in the generation of a sharper image.
- Causes sample excitation on a point-by-point basis, decreasing the effects of global photo-bleaching.
- Allows 3D reconstruction of samples by computationally assembling "stacks" of 2D images.

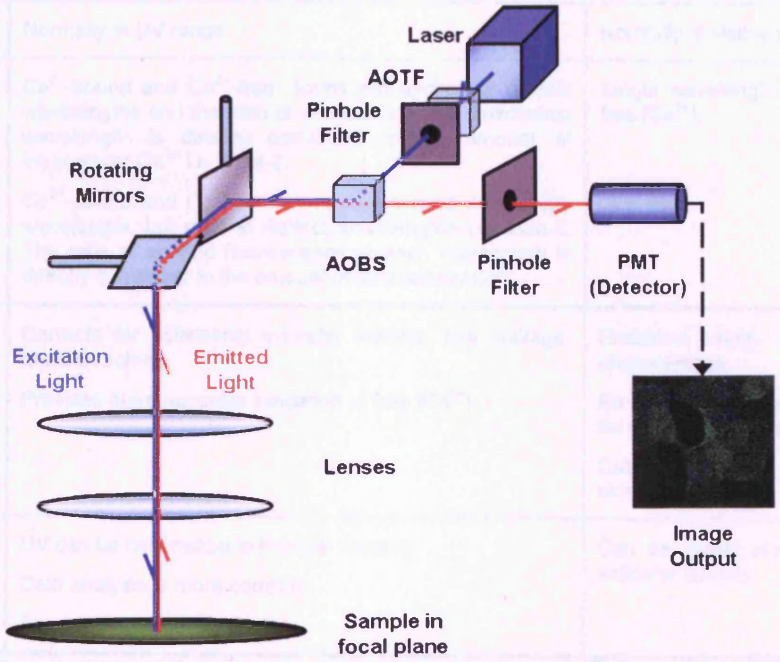

Figure 3.1. Schematic representation of the workings of a confocal microscope.

Briefly, "excitation light" from a high-powered laser of known wavelength emission passes through a pinhole filter and is directed towards a series of horizontally and vertically rotating mirrors by the acousto-optical beam splitter (AOBS). These mirrors allow the excitation light to be systematically scanned across the sample, causing excitation of the fluorescent indicator on a point-by-point basis. Emitted fluorescent light is descanned by the same rotating mirrors and is 'tuned' to a particular wavelength by the AOBS. Light that did not originate from the focal point is removed by passing the emitted light through a pinhole filter, prior to detection by a photomultiplier tube (PMT). The PMT effectively amplifies the fluorescent signal through a process termed "secondary emission" and converts it to a measurable current pulse that is indicative of the magnitude of the initial fluorescence level.

There are many Ca^{2+} indicator dyes that are commercially available, each with unique excitation and emission profiles. These dyes fall in to two categories; ratiometric or single-wavelength, the properties of which are detailed in Table 3.1.

	Ratiometric Dyes	Single Wavelength Dyes
Examples	Fura-2, Fura Red, Indo-1.	Fluo-3, Fluo-4, Ca^{2+} Orange.
Excitation	Normally in UV range	Normally in visible spectrum range
Emission	Ca^{2+}-bound and Ca^{2+}-free forms are excited at distinct wavelengths and the ratio of emissions at each excitation wavelength is directly correlated to the amount of intracellular Ca^{2+} i.e. Fura-2. Ca^{2+}-bound and Ca^{2+}-free forms are excited at a single wavelength, but emit at distinct wavelengths i.e. Indo-1. The ratio of emitted fluorescence at each wavelength is directly correlated to the amount of intracellular Ca^{2+}.	Single wavelength, dependent on free $[Ca^{2+}]$.
Advantages	Corrects for differential indicator loading, dye leakage, photobleaching. Provides more accurate indication of free $[Ca^{2+}]$	Excitation energy is low, reducing photodamage Emission of multiple indicators can be carried out in the same cell. Data analysis is comparatively simple
Disadvantages	UV can be detrimental in live-cell imaging. Data analysis is more complex. Expensive equipment costs.	Can be influenced by differential indicator loading.

Table 3.1. Comparison ratiometric and single wavelength Ca^{2+} indicator properties.

Acetoxymethyl (AM)-conjugated forms of Ca^{2+} dyes are able to traverse the cell membrane and are passively taken up by cells into the cytoplasm. The Ca^{2+}-sensitive form of the dye is liberated through hydrolysis of the AM-conjugated form by the action of endogenous esterases. As well as rendering the dye sensitive to Ca^{2+}, this restores the hydrophobic properties of the dye, preventing it from leaking from the cell (Kao *et al.*, 1989). In the case of single-wavelength Ca^{2+} indicators, an increase in cytoplasmic Ca^{2+} concentration results in dramatic increase in indicator emission intensity (Kao *et al.*, 1989; Gee *et al.*, 2000).

Live-cell Ca^{2+}-imaging has been widely used to investigate many aspects of the consequences of arrhythmia-linked RyR2 mutations on intracellular Ca^{2+} handling. In cardiac myocytes, spontaneous Ca^{2+} release events associated with arrhythmia, namely Ca^{2+} sparks and waves, manifest as localised and propagating increases in intracellular Ca^{2+}-dependent signal intensity respectively (Lehnart *et al.*, 2008; Fernandez-Velasco *et*

al., 2009; Uchinoumi *et al.*, 2010). Although sparks and waves are not observed in non-myocyte cells expressing RyR2, similar spontaneous ER Ca^{2+} release events have been observed in HEK cells recombinantly expressing RyR2 and have been implicated in CPVT pathogenesis (see Chapter 5, (Jiang *et al.*, 2002; 2004; 2005; Koop *et al.*, 2008). The quantification and characterisation of all of these types of spontaneous Ca^{2+} release events are measured as an indication of the propensity for mutations to increase DAD susceptibility.

Intracellular Ca^{2+}-imaging is also routinely used to measure parameters of agonist-evoked ER/SR Ca^{2+} release to determine differences in sensitivity between WT and mutant RyR2 (George *et al.*, 2003a; Thomas *et al.*, 2004; Jiang *et al.*, 2005; Thomas *et al.*, 2005). Unlike in experiments where RyR2 is isolated from the cellular environment, in order for agonists to directly activate RyR2, they must be able to rapidly traverse the cell membrane or activate RyR2 via receptor-coupled mechanisms. Such RyR2 agonists that are routinely used include Ca^{2+} itself, caffeine (section 3.1.5) and 4-chloro-m-cres (4-cmc). Additionally, RyR2 in cardiomyocytes is also indirectly activated by the addition of activators of the β-adrenergic signalling cascade such as isoproterenol and epinephrine.

3.1.1.5. Heterologous expression in mammalian cell lines

There are many cell lines in which human RyR2 can be recombinantly expressed, although it could be argued that none of them provide the perfect system in which to characterise the functional effects of RyR2 mutations. Perhaps the preferred cell type in which to characterise RyR2 mutations would be the primary cardiac myocyte, as this cell type retains the contractile phenotype exhibited *in vivo* and expresses a multitude of cardio-specific regulatory proteins e.g. FKBP12.6, junctin, triadin, etc (section 1.2.3.2 – 1.2.3.3). However, transfection of primary cardiac myocytes with recombinant RyR2 has proved problematic due to the size (~20kb) and fragility of the plasmid and tends to yield low levels of protein expression (George *et al.*, 2005), making the study of mutant RyR2 function in primary myocytes difficult. Immortalised myocyte cell lines, such as HL-1 cells (Claycomb *et al.*, 1998), have been developed, as have transgenic mice harbouring RyR2 mutations (section 1.3.3, Cerrone *et al.*, 2005; Kannankeril *et al.*, 2006; Goddard *et al.*, 2008; Lehnart *et al.*, 2008), which go some way to alleviating this problem. Like

primary cardiac myocytes, HL-1 cells retain a contractile phenotype and express the full complement of cardio-specific accessory proteins (Claycomb *et al., 1998)*, although they are not without their disadvantages in terms of studying RyR2 mutant channel function. Due to the endogenous expression of RyR2 in cardiac myocytes, transfection with RyR2 cDNA may result in the expression of either two discrete populations of recombinant and endogenous RyR2 or the formation of heterotetramers of unknown stoichiometry, adding an undefined element to RyR2 mutation functional characterisation. Furthermore, work carried out in this laboratory has shown that the contractile phenotype exhibited by HL-1 cells tends to be ablated following transfection with RyR2.

Another cell line that has been used in the functional characterisation of RyR1 and RyR3 is the dyspedic skeletal myotube, 1B5, cell line (Moore *et al.*, 1998). These cells have been engineered to be deficient in all three RyR isoforms, yet they express the full complement of skeletal muscle RyR accessory proteins that are involved in RyR1 regulation e.g. FKBP12, CSQ etc (Moore *et al.*, 1998). However, a similar cell line from a transgenic cardiac lineage has not been developed to date, meaning alternative expression systems must be used in the investigation of RyR2.

RyR2-deficient cell lines provide another attractive system in which to investigate the functional effects of RyR2 mutations. The lack of endogenous RyR2 protein in such cell lines means that transfection with RyR2 cDNA results in the expression of a homotetrameric population of recombinant RyR2 channels. This effectively abolishes the possibility of heterotetramerisation and reduces the complexity of RyR2 mutant characterisation. Furthermore, the investigation of RyR mutations in a manner replicative of heterozygotic inheritance has been carried out by co-transfecting RyR-deficient cells with equimolar ratios of WT and mutant RyR2 (Tong *et al.*, 1999; Wehrens *et* al., 2003; Lehnart *et al.*, 2008), which is likely to result in the formation of RyR heterotetramers. This is supported by the finding that an [^{3}H]ryanodine-binding-deficient RyR2 mutant, I4827T, co-precipitated with WT RyR2 and restored [^{3}H]ryanodine binding, suggesting heterotetramerisation of WT and I4827T mutant subunits (Xiao *et al.*, 2002). Furthermore, single-channel analysis of ho motetrameric G48 24A ch annels exhibited near-complete ablation of channel conductance, yet RyR2 purified from cells co-expressing G4824A and WT RyR2 subunits exhibited a range of conductances, which were proposed to represent channels consisting of each possible combination of WT and mutant subunits (Zhao *et al.*, 1999).

	Immortalised Cardiac Myocytes (HL-1) *(Claycomb, 1998)*	CHO *(Tijo, 1958)*	COS *(Jensen, 1964)*	HEK-293 *(Graham, 1977)*
Species	Mouse	Hamster	African Green Monkey	Human
Tissue	Cardiac Myocyte	Ovary	Kidney	Kidney
Endogenous RyR2 expression	Yes	No	No	No
Contractile Phenotype	Contractile	Non-contractile	Non-contractile	Non-contractile
RyR2 accessory proteins	Full complement	n/a	n/a	n/a
Advantages	Full complement of cardiac-specific accessory proteins. Recombinant RyR2 co-expression reflects autosomal dominant nature of RyR2 mutations. Human-derived cell line	Allows homotetrameric expression of recombinant RyR2. Effects of recombinant RyR2 expression separated from effects of accessory proteins. Effects of recombinant RyR2 expression separated from modulation by accessory proteins.	Allows homotetrameric expression of recombinant RyR2. Effects of recombinant RyR2 expression separated from effects of accessory proteins. Effects of recombinant RyR2 expression separated from modulation by accessory proteins.	Can express RyR2 to relatively high levels. Allows homotetrameric expression of recombinant RyR2. Widely used in RyR2 characterisation. Functional RyR2 data produced complements that from other experimental systems (section 3.1.1.6). Effects of recombinant RyR2 expression separated from modulation by accessory proteins. Human derived cell line.
Disadvantages	Endogenous RyR2 expression complicates interpretation of effects of recombinant RyR2 expression. Exhibit a variable contractile phenotype. Loses contractile phenotype following transfection. Non-human derived cell line.	Low levels of stable RyR2 expression (Imagaw, 1998). High levels of RyR2 expression decreased cell viability (George, 2003). Non-human derived cell line.	Lacks many RyR2 accessory proteins and myocyte ultra-structure. Little functional RyR2 characterisation data available. Non-human derived cell line	Lacks many RyR2 accessory proteins and myocyte ultra-structure e.g. FKBP12.6, Junctin, Triadin.

Table 3.2. A summary of cell-lines used in the heterologous expression and functional characterisation of RyR2.

Several RyR2-deficient cell lines have been used in the functional investigation of RyR2 mutations including Chinese hamster ovary cells (CHO, (CHO, Imagawa *et al.*, 1992; George *et al.*, 2003b), African Green Monkey cells (COS) and human embryonic kidney cells (HEK-293 cells). CHO cells are routinely used in the investigation of recombinantly expressed proteins. However, stable RyR2 expression has been shown to result in limited RyR2 expression levels (Imagawa *et al.*, 1992) whereas driving transient RyR2 expression in CHO cells dramatically decreased cell viability (George *et al.*, 2003b), making these cells less than ideal for RyR2 expression and subsequent characterisation. HEK-293 cells are the most widely used RyR2-deficient cell line in the study of recombinant RyR2 in single-channel electrophysiological studies (Jiang *et al.*, 2002; 2004; 2005; 2010) or for the investigation of RyR2 Ca^{2+}-handling dynamics in a mammalian cell environment (Jiang *et al.*, 2002; 2004; Thomas *et al.*, 2004; 2005). Although HEK cells are lacking in many of the regulatory RyR2 accessory proteins expressed in cardiac myocytes, functional data produced from experiments in which RyR2 is expressed in HEK cells complements that produced from experiments carried out in cardiac myocytes (section 3.1.1.6). Similarly, functional characterisation of recombinant RyR2 isolated from HEK cells also appears to be highly comparable to those results obtained using RyR2 isolated from native tissue (Du *et al.*, 1998). It is for the reasons described above, coupled with the fact that the majority of RyR2 mutation characterisation has been carried out in HEK cells by several groups, that this cell line will be used in this study of the effects of L433P and G1885E expression on intracellular Ca^{2+} handling.

3.1.1.6. Comprehensive characterisation of R4497C, R2474S and R176Q RyR2 mutations.

The R4497C mutation was one of the first and more severe CPVT-linked mutations identified through the genetic screening of a CPVT-affected cohort (Priori *et al.*, 2001) and as such has been subjected to extensive functional investigation in a variety of experimental systems (summarised in Table 3.3). Patients who inherited the R4497C mutation presented structurally normal hearts and bidirectional VT that was reproducibly induced by exercise-stress testing or isoproterenol infusion (Priori *et al.*, 2001).

Heterologous expression of R4496C (mouse equivalent of R4497C) in HEK-293 cells increased the propensity of spontaneous ER Ca^{2+} release, which was associated with an increased sensitivity to activation by luminal Ca^{2+} and increased single channel P_o at low cytosolic Ca^{2+} concentrations, compared to WT RyR2 (Jiang *et al.*, 2002; 2004). Furthermore, R4496C expression resulted in an increase in caffeine sensitivity, indicating that the R4496C channel was sensitised to both Ca^{2+} and caffeine-activation (Jiang *et al.*, 2004). Similarly, immortalised cardiomyocytes (HL-1 cells) transfected with RyR2 containing the R4497C mutation displayed an increased Ca^{2+} transient amplitude following agonist-evoked RyR2 activation, whereas comparable intracellular Ca^{2+} transient amplitudes were observed following β-adrenergic stimulation. However, both modes of channel activation produced significantly prolonged Ca^{2+} transients (George *et al.*, 2003a), which can result in the prolongation of elevated cytoplasmic Ca^{2+} concentration, which can create a premature inward depolarising current through the NCX, increasing the likelihood of DAD occurrence (Bers, 2008; Gyorke & Carnes, 2008).

The $R4496C^{+/-}$ mouse exhibited a similar phenotype to that observed in CPVT patients (section 1.3.3), with an increased susceptibility to VT under conditions of physical stress or β-adrenergic stimulation, despite a structurally normal heart and normal resting ECG (Cerrone *et al.*, 2005). Myocytes isolated from $R4496C^{+/-}$ mice and subjected to electrical pacing or β-adrenergic stimulation displayed an increased frequency of DAD's compared to WT mice (Liu *et al.*, 2006; Fernandez-Velasco *et al.*, 2009). This was attributed to an observed increase in Ca^{2+} spark frequency and an increase in sensitivity to Ca^{2+}-dependent activation of RyR2, which culminated in an increase in intracellular Ca^{2+} wave propagation (Fernandez-Velasco *et al.*, 2009). Myocytes isolated from these mice also displayed increased Ca^{2+} spark frequency under non-stimulated conditions and an increased level of basal activity at low Ca^{2+} concentrations. Not only does this reconcile with the increase in R4496C basal activity observed in channels isolated from HEK cells (Jiang *et al.*, 2002), but this suggests that the effects of the R4496C mutation are evident at rest and are exacerbated following β-adrenergic stimulation (Liu *et al.*, 2006; Fernandez-Velasco *et al.*, 2009).

Similar findings have been observed for a central domain mutation (R2474S), that was identified in a single, CPVT-affected individual who suffered from syncope and exhibited non-sustained VT during exercise-stress testing, despite exhibiting a normal resting ECG (Priori *et al.*, 2002). Heterologous expression of R2474S demonstrated that this

mutation had no effect on the Ca^{2+}-dependence of [^{3}H]ryanodine binding, but significantly increased spontaneous Ca^{2+} release propensity attributed to an observed increase in luminal Ca^{2+} sensitivity (Jiang *et al.*, 2005). Myocytes isolated from two R2474S heterozygous mouse models (section 1.3.3), exhibited an increase in spontaneous Ca^{2+} sparks and waves following β-adrenergic stimulation (Lehnart *et al.*, 2008; Uchinoumi *et al.*, 2010; Xu *et al.*, 2010), corroborating the increase in spontaneous Ca^{2+} release observed through heterologous R2474S expression and the stress-induced nature of human CPVT.

Although there were similarities in Ca^{2+} handling observed in myocytes isolated from each of these mouse models, there were several differences between findings from each group (section 1.3.3, summarised in table 1.2) i.e. normal phosphorylation vs hyperphosphorylation, normal FKBP12.6:RyR2 interaction vs decreased FKBP12.6:RyR2 interaction). As such, *Uchinoumi et al* proposed that R2474S resulted in an increase in spontaneous Ca^{2+} release through the destabilisation of an inter-domain interaction coupled with a decrease in CaM-binding, leading to increased Ca^{2+} leak and arrhythmia (section 1.3.4.2) (Uchinoumi *et al.*, 2010; Xu *et al.*, 2010). However, *Lehnart et al* proposed R2474S caused SR Ca^{2+} leak through PKA-mediated "hyper-phosphorylation" of the mutant RyR2 causing increased FKBP12.6 dissociation and channel destabilisation (section 1.3.4.3, Lehnart *et al.*, 2008). There is extensive evidence supporting the destabilisation of the domain-interaction hypothesis which is discussed in greater detail in section 1.3.4.2.

Similar findings have been observed for an N-terminal RyR2 mutation (R176Q) that has been identified in a number of ARVD2-affected individuals, both as the only identified mutation (Tester *et al.*, 2005) or on the same allele as a second T2504M mutation (Tiso *et al.*, 2001; Bauce *et al.*, 2002; Tester *et al.*, 2005). The equivalent mutation in RyR1 (R163C) has been shown to result in both MH and CCD disease phenotypes in different individuals, without the presence of a second RyR1 mutation (Robinson *et al.*, 2002), suggesting R176Q alone is likely to result in the ARVD2 phenotype. Interestingly, R163C was shown to result in different disease phenotypes (i.e. MH or CCD) in different individuals, as was R176Q in RyR2 (Bauce *et al.*, 2002) which has been implicated in both ARVD2 and CPVT, suggesting other genetic or environmental factors are important in determining the resulting disease phenotype of these mutations.

	R176Q	R2474S	R4497C (R4496C)
Patient Phenotype	ARVD2, fibro-fatty infiltration of the right ventricle, stress induced pVT. *(Tiso, 2001).*	CPVT, structurally normal heart and ECG, stress-induced bVT or pVT (Priori, 2002)	CPVT, structurally normal heart and ECG, exercise-induced bVT *(Priori, 2001).*
Mouse Phenotype	Structurally normal heart and resting ECG. Decreased RV end-diastolic volume. Stress, β-AR stimuation or agonist-induced bVT. *(Kannankeril, 2006, Mathur, 2009)*	Structurally normal heart. Stress or β-AR induced bVT and pVT. (Lehnart, 2008, Uchinoumi, 2010). Spontaneous clonic/tonic seizures (Lehnart, 2008)	Structurally normal heart and resting ECG. Stress or β-AR stimulation-induced VT *(Cerrone, 2005)*
Isolated myocyte characteristics	Increased basal and β-AR induced spontaneous Ca^{2+} release. *(Kannankeril, 2006)*	Increased β-AR-induced spontaneous Ca^{2+} release (Uchinoumi, 2010) and Ca^{2+} wave propagation, (Lehnart, 2008)	Increased basal and β-AR-induced spontaneous Ca^{2+} release and Ca^{2+} wave propagation (*Liu 2006, Verlasco, 2009).*
Recombinant expression in immortalised myocytes	n/a	n/a	Increased caffeine-evoked Ca^{2+} release magnitude and duration. (George, 2003). Prolonged Ca^{2+} release transient duration following β-AR stimulation. (George, 2003)
Recombinant expression in RyR2 deficient cell lines (HEK293)	Increased caffeine-evoked Ca^{2+} release magnitude (Thomas, 2004) **Homotetrameric expression with T2504M:** Increased caffeine-evoked Ca^{2+} release magnitude (Thomas, 2004) and spontaneous Ca^{2+} release (Jiang, 2005).	Increased spontaneous Ca^{2+} release in cells expressing mouse RyR2 (Jiang, 2005)	Increased spontaneous Ca^{2+} release (SOICR) Increased luminal Ca^{2+} sensitivity. Increased sensitivity to caffeine-evoked channel activation. (Jiang, 2002, Jiang, 2004)
Single Channel Analysis	**Homotetrameric expression with T2504M:** Increased luminal Ca^{2+} sensitivity. (Jiang, 2005)	Increased luminal Ca^{2+} sensitivity. (Jiang, 2005, Uchinoumi, 2010). β-AR stimulation increased P_o (Wehrens, 2003, Lehnart, 2008), restored to WT after S107 treatment (Lehnart, 2008).	Increased P_o at low $[Ca^{2+}]$. Slight increase in luminal Ca^{2+} sensitivity. (Jiang, 2004)
[^{3}H] Ryanodine binding	**Homotetrameric expression with T2504M:** Normal Ca^{2+} dependent activation (Jiang, 2005)	Normal Ca^{2+} dependent activation (Jiang, 2005)	Increased basal activity at low $[Ca^{2+}]_c$. Increased Ca^{2+} sensitivity and caffeine sensitivity.(Jiang, 2002, Jiang, 2004)
Effects on RyR2 phosphorylation level	n/a	Equal phosphorylation levels (Wehrens, 2003, Lehnart, 2008), but increased sensitivity to phosphorylation activation (Uchinoumi, 2010)	No effect on RyR2 phosphorylation in HL1 cells. (George, 2003)
Effects on FKBP12.6 interaction	**Homotetrameric expression with T2504M:** No alteration in FKBP interaction when heterologously co-expressed (Jiang, 2005).	Decreased interaction in heterozygous mouse, exacerbated by β-AR stimulation, restored to WT after S107 treatment (Lehnart, 2008) No alteration in heterozygous myocytes (Ucinoumi, 2010) **Interaction in heterologous expression:** No alteration (Jiang, 2005), but β-AR causes dissociation (Wehrens, 2003).	FKBP interaction similar to WT at rest and after β-AR stimulation. (George, 2003). β-AR dissociates FKBP12.6 (Wehrens, 2003). Normal FKBP12.6 interaction in knock-in mouse (Liu, 2006, Verlasco, 2009)

Table 3.3. A summary of the functional characterisation of three CPVT/ARVD2-linked mutations in a variety of experimental systems. *R176Q was first identified in a patient who also inherited a T2504M mutation, as such characterisation of R176Q is often carried out in the presence of this second mutation. SIDS = Sudden infant death syndrome, RV = right ventricle, VT = ventricular tachycardia pVT = polymorphic ventricular tachycardia, bVT = bi-directional ventricular tachycardia*

When heterologously expressed in HEK-293 cells, R176Q increased the magnitude of caffeine-evoked Ca^{2+} release compared to that observed in cells expressing WT RyR2 (Thomas *et al.*, 2004). When both R176Q and T2504M were co-expressed on the same RyR2 subunits in HEK293 cells, there was an increase in channel sensitivity to caffeine activation compared to WT RyR2 (Thomas *et al.*, 2004) and an increase in spontaneous Ca^{2+} release frequency (Jiang *et al.*, 2005). This was associated with an increased sensitivity to luminal Ca^{2+} and suggests the increased spontaneous Ca^{2+} release observed in HEK cells is due to a decreased luminal Ca^{2+} activation threshold (Jiang *et al.*, 2005). Mice heterozygous for the R176Q mutation ($R176Q^{+/-}$) exhibited a normal resting ECG and exhibited bidirectional VT in response to β-adrenergic stimulation or caffeine and epinephrine administration (section 1.3.3, Kannankeril *et al.*, 2006; Mathur *et al.*, 2009). Myocytes isolated from the $R176Q^{+/-}$ mouse displayed increased spontaneous Ca^{2+} release under both non-stimulated conditions and following β-adrenergic stimulation (Kannankeril *et al.*, 2006), similar to observations in HEK cells expressing recombinant R176Q.

The comprehensive functional characterisation of the R176Q, R4497C and a central domain mutation, R2474S, in a multitude of experimental systems reveals the benefit of such complementary investigation in determining the mechanism of mutant channel dysfunction (Table 3.3). The fact that data derived from each experimental system exhibits similarities with that obtained from other methodologies and results in similar mechanistic conclusions being made, suggests that cell based assays can be reliably used to gain an insight into how the specific RyR2 mutations result in a disease-phenotype *in vivo*.

3.1.2. The effects of SNP expression on mutant hNav1.5 function depends on the mode of co-inheritance

As described in section 1.4.4.1.2, the common H558R *SCN5A* SNP exhibited profound effects on mutant hNav1.5 functionality and has been shown to both alleviate or exacerbate the detrimental consequences of several disease-linked *SCN5A* mutations (Ye *et al.*, 2003; Poelzing *et al.*, 2006; Gui *et al.*, 2010b). Furthermore, H558R was also shown to ameliorate mutant channel function to varying degrees (Viswanathan *et al.*, 2003; Poelzing *et al.*, 2006; Gui *et al.*, 2010b), suggesting that the precise nature and

location of the co-inherited mutation may be an important factor in determining the extent to which H558R altered mutant channel function. This hypothesis has been supported through the biophysical characterization of recombinant hNav1.5 channels containing the H558R SNP in combination with several disease-linked mutations.

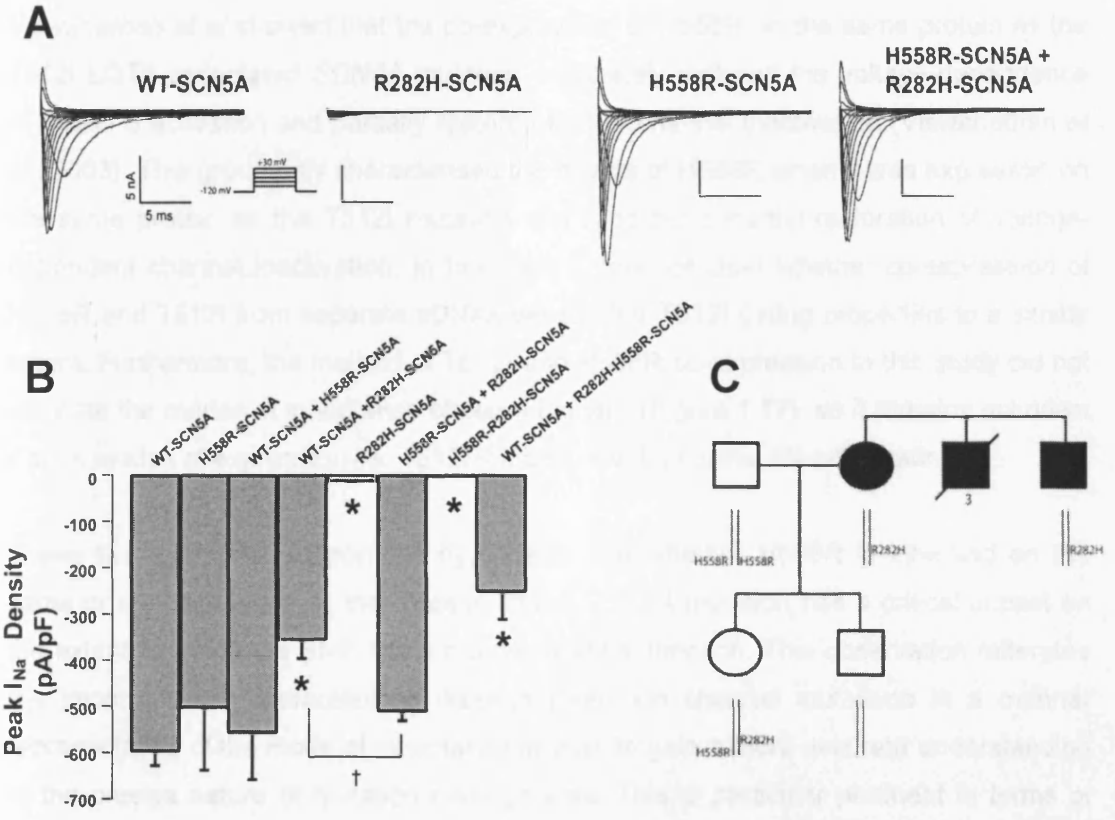

Figure 3.2. H558R restores R282H I_{Na} current only when both substitutions are on the same protein. *R282H abolished I_{Na} current, which was partially restored (~50%) when H558R was co-expressed on separate protein to the mutation (panel A). Co-expression of H558R on the same protein as R282H had no restorative effect on I_{Na} current (panel B). These findings corroborate those observe in vivo (panel C). From Poelzing, (2006).*

Poelzing et al demonstrated that the H558R SNP was able to restore I_{Na} current through R282H channels by restoring correct membrane trafficking, as illustrated schematically in Figure 1.15. I_{Na} currents were only completely restored to normal levels when H558R and R282H were expressed on separate hNav1.5 molecules through co-transfection with equimolar ratios of *H558R-SCN5A and R282H-SCN5A cDNA* (Figure 3.2, Poelzing

et al., 2006). These findings correlate with the observation that individuals who inherited R282H and H558R in a composite heterozygous fashion, did not exhibit a LQTS-related phenotype, whereas those who inherited R282H were symptomatic. This restoration of I_{Na} current was not observed when H558R and R282H were expressed on the same protein, was partially restored when co-expressed with WT hNav1.5.

Viswanathan et al showed that the co-expression of H558R on the same protein as the T512I LQTS-associated *SCN5A* mutation completely restored the voltage-dependence of hNav1.5 activation and partially restored that of channel inactivation (Viswanathan *et al.*, 2003). This group only characterised the effects of H558R when it was expressed on the same protein as the T512I mutation and reported a partial restoration of voltage-dependent channel inactivation. In this case it was not clear whether co-expression of H558R and T512I from separate cDNAs would alter T512I gating properties to a similar extent. Furthermore, the method of T512I and H558R co-expression in this study did not replicate the modes of inheritance observed *in vivo* (Figure 1.17), so it remains unknown if such modes of expression i.e. T512I+H558R, exhibit normal hNav1.5 gating.

These two examples support the hypothesis that whether H558R is inherited on the same or opposite allele as the disease-linked *SCN5A* mutation has a critical impact on the extent to which the SNP alters mutant channel function. This observation reiterates the importance of characterising disease-linked ion channel mutations in a manner representative of the mode of inheritance *in vivo,* to gain a more accurate understanding of the precise nature of mutation pathogenesis. This is particular pertinent in terms of RyR2 mutations, which are predominantly investigated when expressed as homotetramers which is representative of autosomal recessive inheritance, although RyR2 mutations exhibit autosomal dominant pathogenesis. The few studies that have investigated the functional consequences of heterologous co-expression of mutant RyR with WT RyR, observe a diluted form of the mutant cellular phenotype (Tong *et al.*, 1999; Wehrens *et al.*, 2003; Lehnart *et al.*, 2008). As described in section 3.1.1.5, the transfection of RyR-null cell lines with equimolar ratios of mutant and WT RyR2 cDNA allows the greatest control over the relative levels of mutant and WT RyR2 protein expression. However, at present it is difficult to accurately determine relative levels of each recombinant protein and precise RyR2 channel stoichiometry.

3.1.3. Characterisation of homotetrameric L433P and G1885E

Although a group of ARVD2 patients were identified who were heterozygous for both L433P and G1885E, functional characterisation has only been carried out when either one of these substitutions were heterologously expressed. Furthermore, both L433P and G1885E have only been characterised when expressed as homotetramers, which is not truly representative of the autosomal dominant nature of CPVT/ARVD2-linked RyR2 mutations (see section 1.3.2)

Functional characterisation of L433P revealed that it does not exhibit the typical phenotype associated with gain-of-function RyR2 disease-linked mutations (Thomas, 2004). Heterologous expression of human RyR2 channels harbouring the L433P mutation exhibited a decreased sensitivity to caffeine activation (EC_{50} = 4.84 ± 0.58mM) compared to WT RyR2 (EC_{50} = 1.56 ± 0.2mM). Furthermore, L433P increased the rate at which Ca^{2+} was released from the ER and decreased the rate at which Ca^{2+} was removed from the cytosol following caffeine-evoked Ca^{2+} release from the ER (Thomas *et al.*, 2004) and a caused a modest decrease in ER Ca^{2+} levels. Taken together, these data suggest that L433P is not a typical gain-of-function mutation in terms of channel activation and that the decreased Ca^{2+} store load and rate of Ca^{2+} removal and increased rate of Ca^{2+} release could be indicative of "leaky" RyR2 channels associated with delayed after depolarisations and arrhythmia (Bers, 2006, 2008; Gyorke & Carnes, 2008; Santiago *et al.*, 2010).

However, another group has disputed that L433P is associated with a different intracellular Ca^{2+} handling phenotype compared to that observed through the heterologous expression of other gain-of-function RyR2 mutations (Jiang *et al.*, 2005). They demonstrated that single channel analysis of isolated mouse RyR2 channels harbouring L433P exhibited an increase in channel sensitivity to caffeine-induced activation (EC_{50} = 2.4mM) compared to cells expressing WT RyR2 (EC_{50} = 4.5mM, Jiang *et al.*, 2005). They also observed an increase in "store-overload induced Ca^{2+} release", as well as a decrease in ER Ca^{2+} store load after heterologous expression of L433P (Jiang *et al.*, 2005), both of which are phenomena characteristic of gain-of-function mutations. This disparity between findings could be a result of the different experimental systems in which the data was obtained (single-cell Ca^{2+}-imaging versus mixed-membrane [^{3}H]ryanodine binding), RyR2 species differences (mouse vs human),

different HEK cell lineage and the different functional end points being measured (magnitude of Ca^{2+} release rather than channel activation).

Single RyR2 channels isolated from a CPVT patient who inherited G1885E and G1886S in a composite heterozygous fashion exhibited several subconductance states (Figure 3.3, Milting *et al.*, 2006), indicative of a destabilised channel with altered conduction properties. The recent heterologous expression and functional characterisation of G1885E and G1886S revealed that expression of either one of these substitutions alone exhibited similar Ca^{2+} and caffeine sensitivity to WT channels accompanied by a normal store load (Koop *et al.*, 2008). However, expression of homotetrameric G1885E also increased the occurrence of spontaneous Ca^{2+} release, which was suggested to be a result of an increased sensitivity to luminal Ca^{2+} (Koop *et al.*, 2008) although this remains to be verified directly. This is the only characterisation that has been carried out on G1885E expressed alone and provides the first indication that G1885E has mutation-like properties.

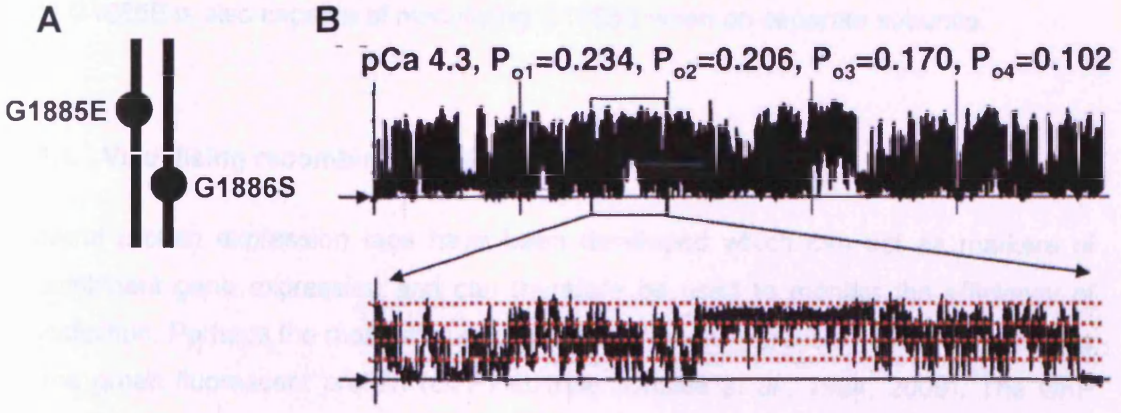

Figure 3.3. Composite heterozygotic inheritance of G1885E/G1886S results in channel sub-conductance states. *An ARVD2 patient inherited G1885E and G1886S on opposite alleles as shown in panel A. Single channel analysis of RyR2 isolated from this patient, shown in panel B, illustrated that this mode of G1885E and G1886S inheritance resulted in 4 sub-conductance states under conditions representative of systole. The open probabilities of each sub-conductance state are detailed above the trace. From Milting, (2006)*

Interestingly, expression of homotetramers containing both G1885E and G1886S substitutions resulted in near-complete ablation of spontaneous Ca^{2+} release and severely augmented Ca^{2+} and caffeine sensitivity (Koop *et al.*, 2008), accompanied by an increase in ER Ca^{2+} levels pertaining to a decrease in luminal Ca^{2+} sensitivity (see

section 5.1.3). However, this mode of homotetrameric expression is not representative of the observed mode of expression *in vivo*, where heterotetramers containing G1885E and G1886S monomeric subunits would be present. The fact that homotetrameric expression of the two substitutions exhibited a 'loss-of-function' phenotype, whereas single channel studies of heterotetrameric RyR2 made up of G1885E and G1886S subunits exhibited a phenotype more characteristic of gain-of function RyR2 mutations. This disparity in findings between the two modes of expression highlights the importance of functionally characterising RyR2 mutations when expressed in a manner more closely representative of the mode of inheritance observed *in vivo*.

A common finding from these studies is the G1885E SNP is able to modify the function of another nearby SNP, G1886S, in terms of agonist activation and spontaneous Ca^{2+} release. Furthermore, the fact that inheritance of G1885E and G1886S in a composite heterozygous fashion exhibited an ARVD2 phenotype, yet association studies did not establish a link between the inheritance of either one of the SNPS and ARVD2 suggests that G1885E is also capable of modulating G1886S when on separate subunits.

3.1.4. Visualising recombinant RyR2 using eGFP

Several protein expression tags have been developed which can act as markers of recombinant gene expression and can therefore be used to monitor the efficiency of transfection. Perhaps the most ubiquitous marker of gene expression in cellular systems is the green fluorescent protein (GFP) epitope (Chalfie *et al.*, 1994; 2009). The GFP protein comprises 238 amino acid residues (26.9 kDa) and was first isolated from the jellyfish *Aequorea victoria* in which it was coupled with a bio-luminescent Ca^{2+}-sensing protein, *aequorin*. Native GFP has two excitation peaks: a maximal peak at 395nm (UV light) and a smaller excitation peak at 470nm (blue light) and has an emission peak at 509nm (green light). *In vivo,* in the presence of Ca^{2+}, *aequorin* emits blue light (469nm), which causes the emission of green light from the neighbouring GFP chromophore (Chalfie *et al.*, 1994).

Subsequently, work was carried out to show that isolated GFP was a relatively stable protein, was active as a monomer, fluoresced independently of any cofactors or accessory proteins, was not easily photo-bleached and retained functionality in all species in which it was examined. More importantly, GFP fluorescence can be examined

in both live and fixed cells using fluorescent or confocal microscopy and can be detected by an anti-GFP antibody during western blotting, making it a versatile fluorescent biomarker (Cubitt *et al.*, 1995). Since its discovery and isolation, GFP has undergone significant refinement to alter and improve its photo-properties. By introducing specific amino acid substitutions into GFP, a whole palette of chromophores have been developed with varying excitation and emission wavelengths (Zimmer, 2009). Enhanced GFP (eGFP) was one of the first derivatives and was developed by inserting P64L and S65T amino acid substitutions into the WT chromophore, causing a shift in the maximal excitation peak to 488nm and a 35-fold increase in fluorescence intensity compared to WT GFP (Zhang *et al.*, 1996). The coding sequence of eGFP has also been altered to contain 190 silent-base substitutions corresponding to human codon-usage preferences, as opposed to jellyfish, increasing expression levels in mammalian cell systems (Zhang *et al.*, 1996).

Determining the successful transfection of RyR into mammalian cells with a relatively high efficiency has proved difficult due to the high molecular weight of the RyR2 plasmid DNA. As such, *Treves et al* generated a number of full-length eGFP-tagged recombinant RyR1 proteins, with the eGFP chromophore fused to the N and C termini and subsequently characterised them in COS cells (Treves *et al.*, 2002). Fusion of eGFP to the extreme C-terminus ablated channel caffeine sensitivity. However, eGFP-tagging at the extreme N-terminus retained correct channel trafficking to the ER and formed functional channels as determined by way of caffeine-sensitivity when heterologously expressed in COS and CHO cells (Bhat *et al.*, 1999; Treves *et al.*, 2002). Taken together this suggests that the precise location of GFP in RyR is critical in determining whether the channel retains functionality.

As such, a mammalian expression vector containing the human RyR2 gene with eGFP fused to the extreme N-terminus (pcDNA3-eGFP-hRyR2) has been created, as described previously (George *et al.*, 2003c), which allows the monitoring of RyR2 transfection efficiency. This construct has been used in the functional studies of RyR2 mutations in mammalian cell systems in which the resulting RyR2 protein that was expressed formed functional, tetrameric channels which correctly localised to the endoplasmic reticulum (Thomas *et al.*, 2004; 2005) and exhibited similar functionality to untagged RyR2. GFP has also been used in the mapping of particular amino acid residues in the 3D structure of RyR2 (section 1.2.1). GFP has been introduced into

several regions of the cytoplasmic domain of RyR2, with the resulting channels retaining functionality by way of caffeine and [^{3}H]ryanodine sensitivity (Zhang *et al.*, 2003; Wang *et al.*, 2007; Jones *et al.*, 2008b). This is somewhat surprising, as the intra-molecular insertion of eGFP doesn't appear to significantly alter RyR2 function, yet the insertion of a single point mutation can be catastrophic.

3.1.5. Caffeine as an RyR2 agonist.

Caffeine is an RyR2 agonist that is regularly used to examine Ca^{2+} handling properties of RyR2 in many experimental methods described in section 3.1.1. It is widely believed that rather than directly activating RyR, caffeine sensitises the channel to activation by Ca^{2+} (Sitsapesan & Williams, 1990; Kong *et al.*, 2008). Despite the RyR-activating properties of caffeine first being described in 1985 (Fabiato, 1985), the precise mechanism of caffeine activation of RyR is still uncertain. Analysis of sheep RyR2 in planar lipid bilayers in physiological cytoplasmic Ca^{2+} (0.1μM), demonstrated that addition of caffeine (1mM) to the cytosolic side of RyR2 in lipid bilayers, resulted in an increased open probability from effectively 0 to 0.25, but did not alter channel conductance (Sitsapesan & Williams, 1990). This increase in channel P_o was due to an increase in the frequency of channel opening events and a reduction in the duration of channel closed

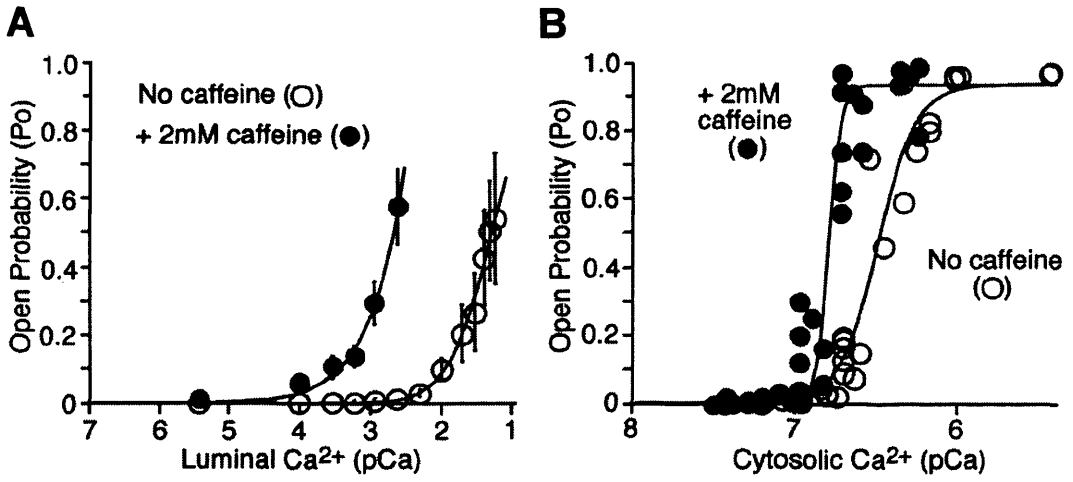

Figure 3.4. Caffeine preferentially increases the sensitivity of RyR2 to activation by luminal Ca^{2+}. *Single channel activities were recorded with increasing luminal or cytosolic Ca^{2+} concentration in the presence and absence of caffeine (2mM). Cytosolic or luminal Ca^{2+} concentrations were 46nM in panel A and B respectively. Data represents the mean (± S.E.M) channel open probabilities (n = 5 - 9 channels). From Kong, (2008).*

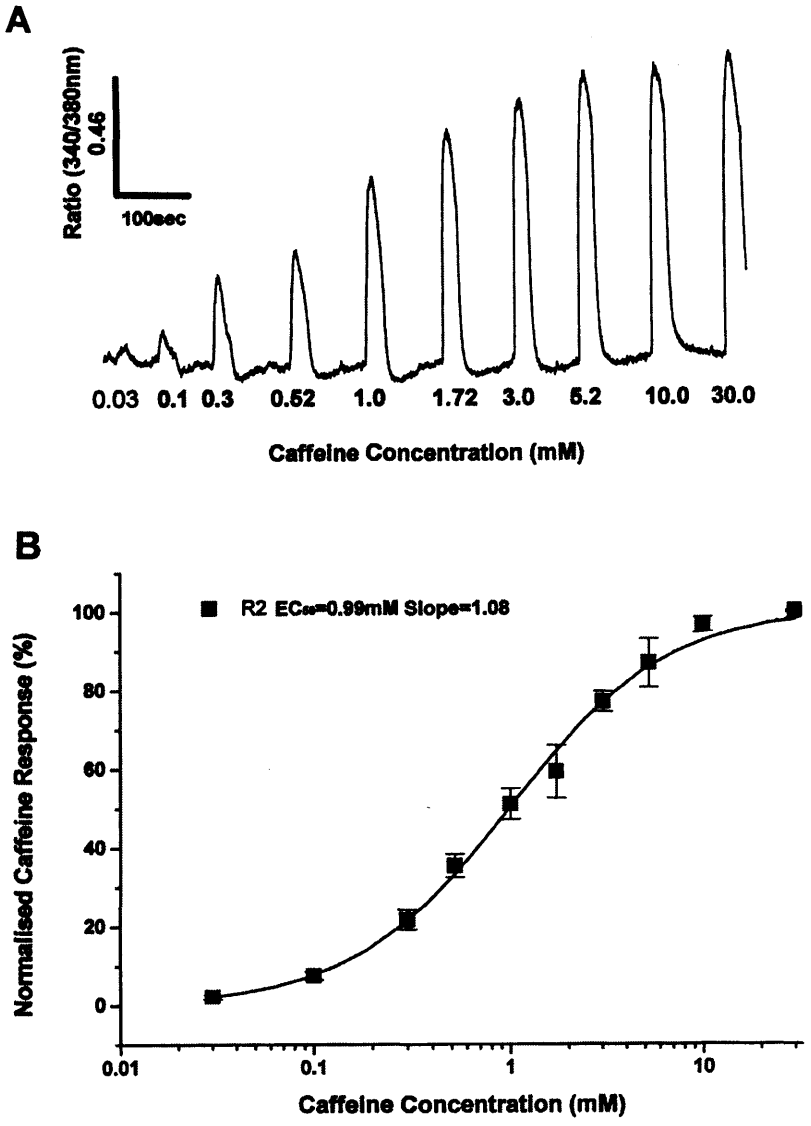

Figure 3.5. Caffeine activation profiles of rabbit RyR2 heterologously expressed in HEK-293 cells. *HEK-293 cells transiently expressing rabbit RyR2 were loaded with the ratiometric Ca^{2+}-indicator dye, Fura-2, and were examined using microfluoriometry. Individual peak amplitudes of 340/380nm ratio (of peak fluorescence divided by basal fluorescence) following activation with 0.03 - 30mM, with a wash step between sequential caffeine additions to restore resting SR Ca^{2+} levels, as shown in panel A. Resulting data was normalised to the peak Fura-2 340/380nm ratio obtained at 30mM caffeine and was expressed as mean ± S.E.M and was used to plot a caffeine activation profile, shown in panel B. Half maximal channel activation (EC_{50}) was observed at 1.00mM. From Du et al, (1998).*

events. In the presence of subactivating cytoplasmic Ca^{2+} (80pM) and extremely high free-luminal Ca^{2+} (80mM), caffeine (<10mM) was not sufficient to induce channel openings, although 40mM caffeine increased the P_o to 0.1 (Sitsapesan & Williams, 1990). Similarly, experiments on canine RyR2 showed that the addition of caffeine (6mM) on the cytosolic side of the channel in 60nM cytosolic Ca^{2+} and 50mM luminal Ca^{2+} increased the channel P_o from practically zero to 0.22 (Rousseau & Meissner, 1989). Addition of caffeine to the luminal side of RyR2 had no effect on channel open probability (Rousseau & Meissner, 1989), suggesting that the site of interaction of caffeine with the channel is found on the large cytoplasmic domain. These data propose that caffeine enhances channel activation by sensitising the channel to activation by cytosolic Ca^{2+}, although a recent study has suggested the mechanism of caffeine activation is not entirely straightforward.

By directly measuring ER Ca^{2+} concentration of HEK-293 cells expressing recombinant RyR2, the exposure of cells to increasing concentrations of caffeine decreased the luminal Ca^{2+} threshold at which spontaneous ER Ca^{2+} release occurred (Kong *et al.*, 2008). Subsequently, single channel analysis of RyR2 in 46nM cytosolic Ca^{2+} and 300nM luminal Ca^{2+} (reflecting diastolic cellular conditions), caffeine was shown to preferentially sensitise the channel to activation by luminal, rather than cytosolic Ca^{2+} (Figure 3.4), demonstrated by a ~100 fold increase in channel sensitivity to activation by luminal Ca^{2+} compared to a ~2 fold increase in sensitivity to activation by cytoplasmic Ca^{2+} (Figure 3.4, Kong *et al.*, 2008). Whether this is due to a direct increase in sensitivity of the luminal Ca^{2+} binding site to activation or a result of increased luminal Ca^{2+} flow-through-dependent activation at the cytoplasmic activation site remains unknown (Laver, 2007).

Despite the uncertainty of the precise mechanism of caffeine activation of RyR2, it has been widely used in functional studies of RyR2 mutations to measure both channel activation properties and ER/SR Ca^{2+} store load in heterologous systems. The expression of recombinant rabbit RyR2 in HEK-293 cells demonstrated an increase in cytoplasmic Ca^{2+} concentrations in response to caffeine, as indicated by a substantial increase in Ca^{2+}-dependent Fura-2 fluorescence ratio (Figure 3.5, Du *et al.*, 1998). These experiments demonstrated that in HEK-293 cells, rabbit RyR2 exhibited a half maximal level of channel activation in response to approximately 1mM caffeine, slightly lower than that observed in HEK cells expressing eGFP-tagged human RyR2 (1.5mM,

Thomas *et al.*, 2004) and that peak caffeine-induced Ca^{2+} release was achieved at approximately 10mM caffeine.

In light of the potency of caffeine in activating RyR2, and the prevalence of its use in functional characterisation of RyR2, particularly of the L433P and G1885E substitutions, caffeine will be used as an activating ligand to monitor RyR2 Ca^{2+} release parameters in this study.

3.1.6. Chapter aims

It is evident from recent studies of RyR2 and other cardiac ion channels that in some cases, SNPs exert a modulatory effect on mutant channel function. In some instances the SNP rescues mutant channel function, whereas in others it exacerbates the detrimental effects of the co-inherited mutation. Furthermore, whether the SNP is present on the same protein subunit as the mutation or on separate subunits (i.e. *in cis* or *in trans,* see Figure 2.4) can influence the extent to which the SNP modifies mutant channel function. The G1885E polymorphism has been shown to modulate the effects of another RyR2 SNP, G1886S, and has also been identified *in cis* of the ARVD2-linked L433P mutation in an affected family.

It is hypothesised that:

- HEK-293 cells provide a suitable heterologous system in which to investigate intracellular Ca^{2+} handling dynamics following expression of recombinant eGFP tagged human RyR2 using single-cell Ca^{2+} imaging techniques.

- Expression of L433P and G1885E RyR2 alter intracellular Ca^{2+} handling parameters to varying degrees depending on whether they are expressed as homotetramers or heterotetramers.

- The G1885E SNP modulates the detrimental effects of L433P on intracellular Ca^{2+} handling characteristics and the mode of co-expression (*'in cis'* or *'in trans'*) influences the extent of this modulatory effect.

In summary, this chapter will aim to determine whether the heterologous expression of L433P and G1885E substitutions alters intracellular Ca^{2+} handling characteristics and subsequently, whether the presence of G1885E alters the cellular Ca^{2+} handling phenotype of cells expressing the L433P ARVD2-linked mutation.

3.2. Methods

3.2.1. Cloning and Site-Directed Mutagenesis

Full-length RyR2 cDNA constructs containing the nucleotide substitution that results in the G1885E substitution were generated using the cassette-based mutagenesis strategy summarised in Figure 2.3. This strategy was adopted for the generation of constructs containing the G1885E polymorphism alone (pcDNA3-eGFP-RyR2-G1885E) or on the same cDNA construct as the L433P mutation (pcDNA3-eGFP-RyR2-L433P-G1885E). Construct nomenclature is detailed in Appendix I, Table 1 and Figure 2).

The SDM reaction to introduce the appropriate codon change into the *San*DI/*Kpn*I mutation cassette (SKI) resulting in the G1885E substitution (GGG to GAG at nucleotide 5454) was carried out using the oligonucleotide primers detailed in Appendix 1, Table 2, according to the thermal cycling protocol in Table 2.2. The G1885E substitution was introduced into the full-length WT and hRyR2-L433P sequence by purifying the SK1-G1885E mutagenesis cassette and ligating it into pcDNA3-eGFP-hRyR2 and pcDNA3-eGFP-hRyR2-L433P respectively (section 2.2.1.2).

Constructs were verified at each stage of cloning by restriction digest mapping of 1µg of plasmid DNA using a battery of restriction enzymes: *Bam*HI, *Bgl*II, *Eco*RI and *Hin*DIII (section 2.2.1.6). Correct nucleotide-substitution insertion and the SK1-G1885E mutagenesis cassette 5' and 3' insertion boundaries were verified by direct-automated sequencing and subsequent nucleotide-nucleotide sequence homology alignment (section 2.2.1.8). Sequencing primers are detailed in Appendix 1, Table 3.

3.2.2. Single-cell Ca^{2+} imaging of HEK cells expressing hRyR2

HEK-293 cells on poly-D-lysine coated glass coverslips were loaded with Fluo3-AM as detailed in section 2.2.2.3. The volume of minimal DMEM on the coverslip was adjusted to 1ml immediately prior to imaging. Cells were imaged with a 63x oil immersion lens on a Leica SP5 confocal microscope controlled by Leica LAS AF software. Excitation of Fluo3 was achieved using an Argon laser at 488nm and emitted Fluo3 fluorescence was collected over the range 525 ± 25nm.

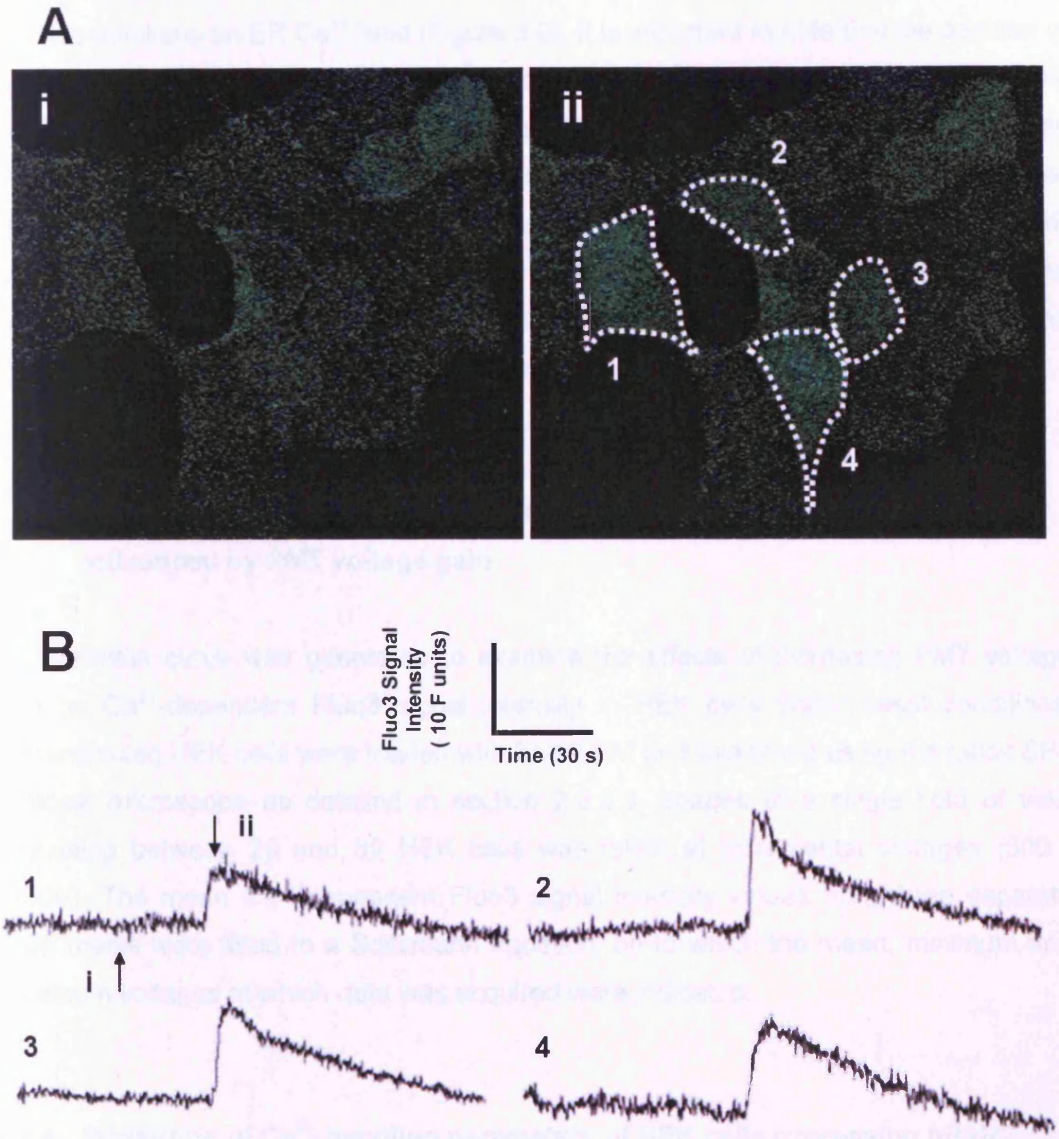

Figure 3.6. Heterogeneous caffeine-induced Ca^{2+} release in HEK cells transfected with RyR2. *HEK cells expressing eGFP-hRyR2 were loaded with Fluo3-AM and examined using confocal microscopy (panel A). Cells were imaged before and after caffeine (0.1-40mM) addition, denoted by i and ii respectively. The Ca^{2+} -dependent increase in Fluo3 signal intensity following caffeine activation of RyR2 can be seen in the numbered traces (panel B1-4) corresponding to the highlighted cells in the confocal images (panel A, ii 1-4).*

Images were acquired every 200ms for a period of 2 minutes 30 seconds (750 frames total). Basal Fluo3 signal intensity was measured for the first 30 seconds of the series before a caffeine addition (0.1-10mM) was made to activate RyR2. A single addition of

caffeine was made to each individual coverslip to remove the effects of sequential caffeine additions on ER Ca^{2+} load (Figure 3.6). It is important to note that the addition of caffeine as a bolus to the cells is likely to alter RyR2 inactivation properties, which will have implications on store refilling and subsequent intracellular handling. These effects will be discussed in more detail throughout this chapter. 'Global' regions of interest representing whole single-cell environments were generated using Leica LAS AF software and there was no significant difference between ROI area in cells expressing each RyR (45 - 46.5μm^2, p=0.96, ANOVA). Data analysis was carried out using Microsoft Excel and GraphPad Prism software.

3.2.3. Boltzmann curve generation to determine if Fluo3 signal intensity was influenced by PMT voltage gain

A Boltzmann curve was generated to examine the effects of increasing PMT voltage gain on Ca^{2+}-dependent Fluo3 signal intensity in HEK cells under basal conditions. Untransfected HEK cells were loaded with Fluo3-AM and examined using the Leica SP5 confocal microscope as detailed in section 2.2.2.3. Images of a single field of view containing between 29 and 39 HEK cells was taken at incremental voltages (500 - 1250V). The mean Ca^{2+}-dependent Fluo3 signal intensity values from three separate experiments were fitted to a Boltzmann equation, on to which the mean, minimum and maximum voltages at which data was acquired were indicated.

3.2.4. Measuring of Ca^{2+}-handling parameters of HEK cells expressing hRyR2

Several parameters of the caffeine-induced Ca^{2+}-transient were measured in HEK cells expressing each of the RyR2 constructs which are described below and illustrated in Figure 3.7. Single-cell Ca^{2+} imaging data was exported from Leica LAS AF confocal software and Ca^{2+} transient parameters were determined using Microsoft Excel.

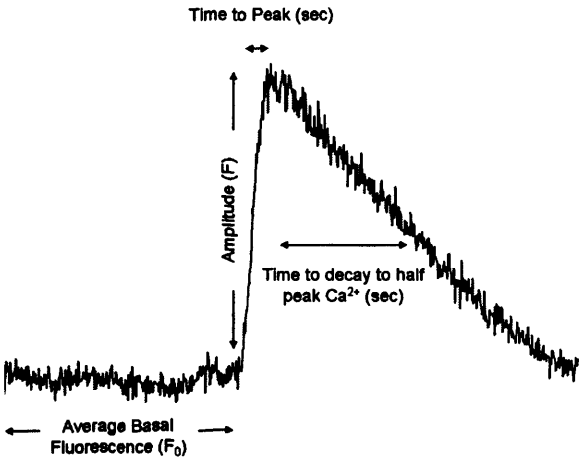

Figure 3.7. Measurement of intracellular Ca^{2+} handling parameters. *The average basal Ca^{2+}-dependent Fluo3 signal intensity (F_0) was determined over a period of 60 seconds prior to caffeine addition (0.1-40mM). The amplitude of Ca^{2+} release (F), time to peak Ca^{2+} and time to decay to half maximal Ca^{2+} were determined and used to determine rates of Ca^{2+} release and Ca^{2+} extrusion as described in section 3.2.4.*

Basal Ca^{2+}-dependent signal intensity

The average basal Ca^{2+}-dependent Fluo3 signal intensity (F_0) was measured by calculating the mean average signal intensity of the first 300 frames (60 seconds) of the time series. This provided an indication of the relative level of basal cytoplasmic Ca^{2+} prior to caffeine activation of RyR2 in cells expressing each mutation/polymorphism and was integral in determining the other Ca^{2+} transient parameters.

Magnitude of Ca^{2+} release

The magnitude of Ca^{2+} release following caffeine activation was determined by measuring the height of the peak Fluo3 signal (F) and subtracting the average basal Fluo3 signal (F_0) from this. As peak magnitude may be influenced by differences in basal signal intensity, the magnitude of Ca^{2+} release was normalised to the average basal intensity, i.e. $[(F-F_0) / F_0]$.

Rate of Ca^{2+} Release $(\Delta F-F_0/F_0)sec^{-1}$

The rate of Ca^{2+} release was determined by first measuring the time from caffeine addition at which peak Fluo3 signal intensity was achieved. This allowed the subsequent calculation of the rate at which Ca^{2+} released i.e. $[(F-F_0) / F_0] / T_{Peak}$.

Rate of Ca^{2+} removal from the cytoplasm

The rate of removal of Ca^{2+} from the cytoplasm was determined by first measuring the time taken for the Fluo3 signal to decrease to that of half the maximal signal intensity

achieved following caffeine addition. The half maximal value was used rather than the time taken for the signal intensity to return to resting levels, as not all Ca^{2+} transients returned to baseline levels following caffeine addition. This was then used to calculate the rate at which the Fluo3 signal decreased and represents the removal of Ca^{2+} from the cytosol by extrusion from the cell via plasma membrane pumps and exchangers or uptake into intracellular stores.

3.2.5. Estimation of ER Ca^{2+} store load

ER Ca^{2+} load was estimated by the measurement of peak Ca^{2+} release following the addition of thapsigargin (10μM) to HEK cells expressing recombinant RyR2 (Figure 3.8). Thapsigargin is a selective and irreversible blocker of the sarco-endoplasmic reticulum Ca^{2+} ATPase (SERCA) and upon inhibition of SERCA by thapsigargin, the ER store is passively emptied (Lytton *et al.*, 1991). As only a proportion of cells in a particular field of view were expressing RyR2, transfected cells were first identified by the addition of a low concentration caffeine bolus (0.5mM).

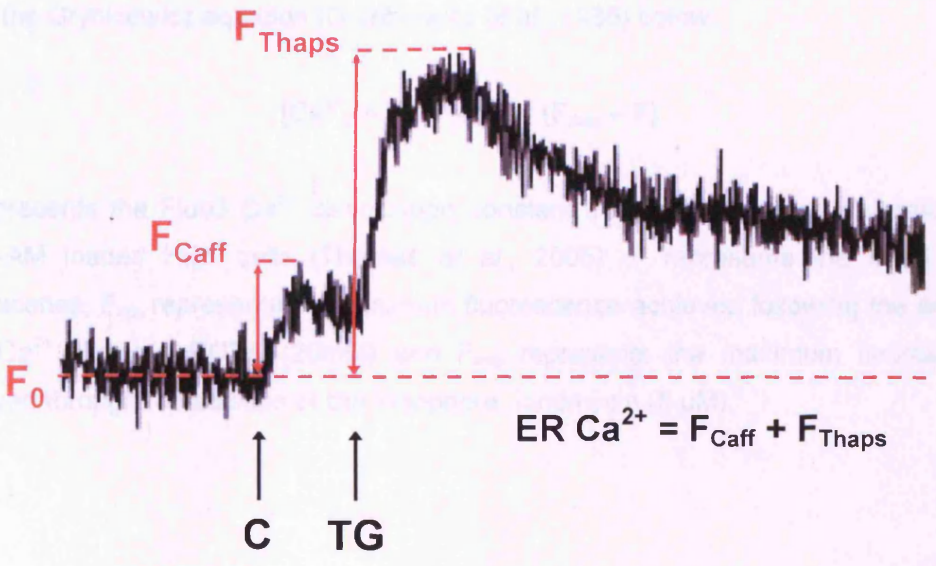

Figure 3.8. Estimation of ER Ca^{2+} store load. *HEK cells expressing recombinant RyR2 were loaded with Fluo3-AM and examined using confocal microscopy. The mean basal Ca^{2+}-dependent Fluo3 signal was determined for the 40 second period prior to exposure of cells to a low concentration of caffeine (0.5mM, C) to identify transfected cells. Thapsigargin (10μM, TG) was added to the cells after approximately a further 10 seconds. The magnitude of caffeine (F_{Caff}) and thapsigargin (F_{Thaps}) evoked Ca^{2+} release were combined to determine the total ER store Ca^{2+} load. Cells were imaged every 200ms for a total of 5 minutes.*

To minimise the effects of Ca^{2+} reuptake into the ER, thapsigargin addition was made immediately after the caffeine addition. The same method of loading cells with Fluo3-AM and single-cell Ca^{2+} imaging was used as detailed in section 2.2.2.3. Thapsigargin was used to estimate store load instead of caffeine, as the ER store in HEK cells is functionally compartmentalised and contains a significant caffeine-insensitive component (Tong *et al.*, 1999). However, it is important to note that caffeine and thapsigargin only allow the indirect estimation of ER Ca^{2+} load by measuring the amount of Ca^{2+} release following their application, rather than directly measuring ER Ca^{2+} content *in situ*.

3.2.6. Determination of resting cytoplasmic Ca^{2+} concentration.

Increased cytosolic basal Ca^{2+} levels can be indicative of Ca^{2+} leak from the ER/SR and as such, resting cytosolic Ca^{2+} levels were determined in HEK cells expressing each recombinant RyR2. Cells were loaded with Fluo3-AM as detailed in section 2.2.2.3. and the intracellular fluorescence signal was used to determine the basal Ca^{2+} concentration using the Grynkiewicz equation (Grynkiewicz *et al.*, 1985) below:

$$[Ca^{2+}] = K_d (F-F_{min}) / (F_{max} - F)$$

K_d represents the Fluo3 Ca^{2+} dissociation constant that was previously determined in Fluo3-AM loaded HEK cells (Thomas *et al.*, 2005), F represents the initial basal fluorescence, F_{min} represents the minimum fluorescence achieved following the addition of a Ca^{2+} chelator, EGTA (20mM) and F_{max} represents the maximum fluorescence achieved through the addition of the ionophore, Ionomycin (5 μM).

3.3. Results

3.3.1. Generation of ARVD2-linked RyR2 mutant/polymorphism constructs

GFP-tagged RyR2 mutants harbouring the G1885E polymorphism (pcDNA3-eGFP-hRyR2-G1885E), the L433P mutation (pcDNA3-eGFP-hRyR2-L433P) or both substitutions (pcDNA3-eGFP-hRyR2-L433P-G1885E) were successfully generated and propagated. Restriction digest mapping and direct automated sequencing of the 5' and 3' restriction boundaries were carried out to confirm correct ligation of mutated cassettes into full-length pcDNA3-eGFP-hRyR2 constructs (Figure 3.9B and 3.9C respectively). Restriction digests of all pcDNA3-eGFP-hRyR2 constructs with a battery of restriction enzymes produced the correct banding pattern of fragments with expected molecular weights as determined by *in silico* digestion using NEBcutter. (Figure 3.9A)

Direct automated sequencing of the mutagenesis site and sequence homology alignment to the WT sequence was carried out to confirm that the correct nucleotide substitution had taken place (Figure 3.9C). This was also used to verify that no additional base substitutions had inadvertently been inserted into the cDNA sequence. Taken together, these data confirm that full-length, eGFP-tagged human RyR2-encoding constructs containing the nucleotide substitutions resulting in the L433P and G1885E amino acid substitutions have been successfully cloned and propagated.

3.3.2. Expression of recombinant RyR2 in HEK Cells

HEK-293 cells were routinely transfected with full-length RyR2 cDNA constructs according to the method described in section 2.2.2.2.2. Calculation of the percentage of cells exhibiting eGFP fluorescence following transfection with each RyR2 construct demonstrated equivalent efficiencies of transfection (40 - 45%, $p = 0.88$, ANOVA, Figure 3.10). SDS-PAGE and western blot analysis was carried out as detailed in section 2.2.3 in order to determine relative expression levels of each RyR2 construct and to ensure that the full-length protein was being expressed. Western blot analysis using an antibody probe targeted to the C-terminus of RyR2 (pAb1093) and a goat, anti-rabbit HRP-conjugated secondary antibody produced a single, high molecular weight protein band in

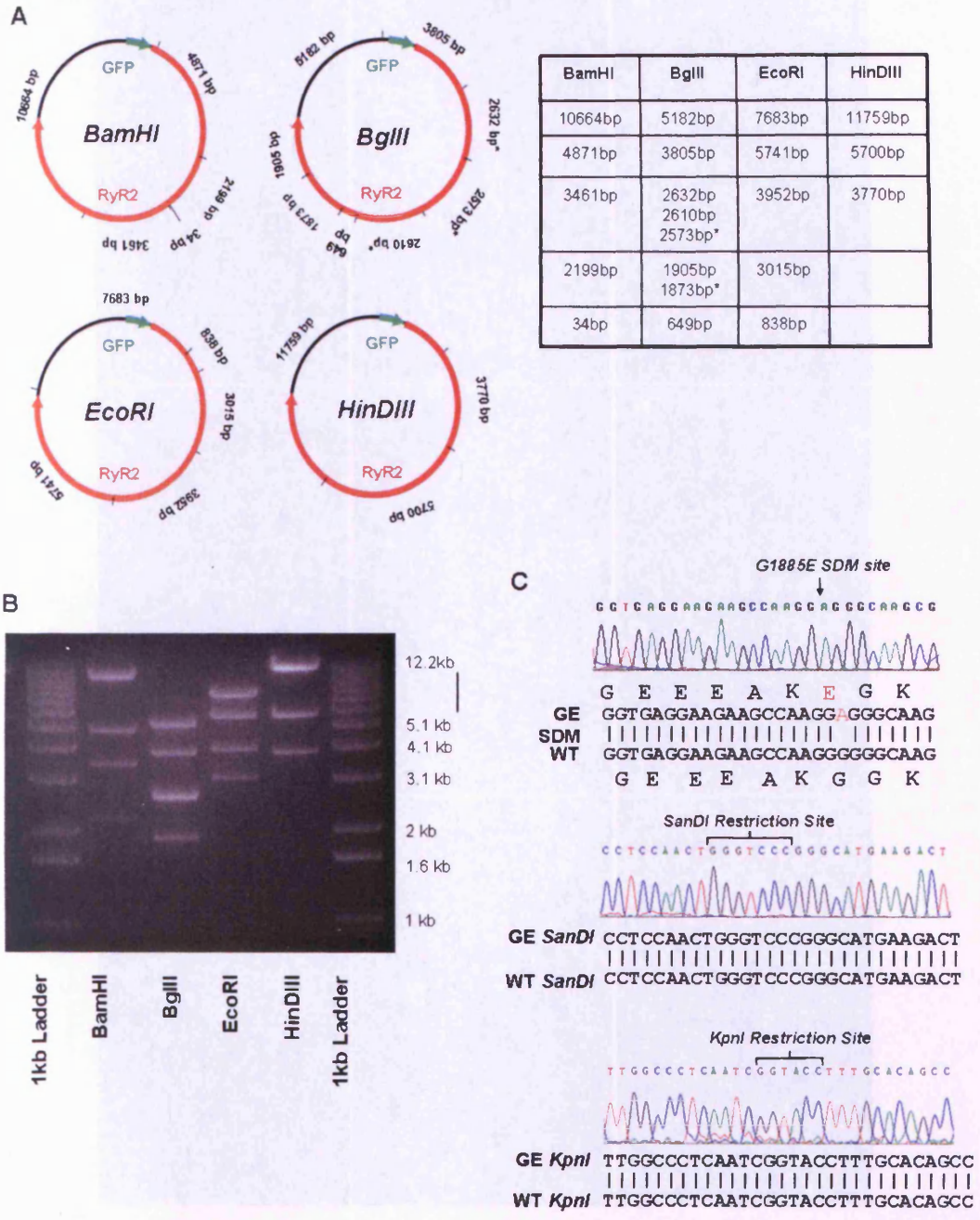

BamHI	BglII	EcoRI	HinDIII
10664bp	5182bp	7683bp	11759bp
4871bp	3805bp	5741bp	5700bp
3461bp	2632bp 2610bp 2573bp*	3952bp	3770bp
2199bp	1905bp 1873bp*	3015bp	
34bp	649bp	838bp	

Figure 3.9. Restriction digest mapping of full-length eGFP-hRyR2 plasmid. *Full-length WT and mutant pcDNA3-eGFP-hRyR2 cDNA (1µg) were digested with restriction enzymes (BamHI, BglII, EcoRI and HinDIII), the products of which were run on a 1% agarose gel with a 1kb DNA ladder (Panel B). The restriction digest pattern was compared to the expected fragment sizes, as determined by in silico digest of the WT and mutant RyR2 cDNA sequence using NEBcutter (Panel A). Asterisked fragments are of similar molecular weight and appear as a single band on a 1% agarose gel. DNA sequencing of the G1885E mutagenesis site and the SanDI/KpnI restriction sites was carried out and compared to the WT sequence by nucleotide homology alignment as shown in panel C. Nucleotide substitutions did not disrupt any restriction sites. (Panel C).*

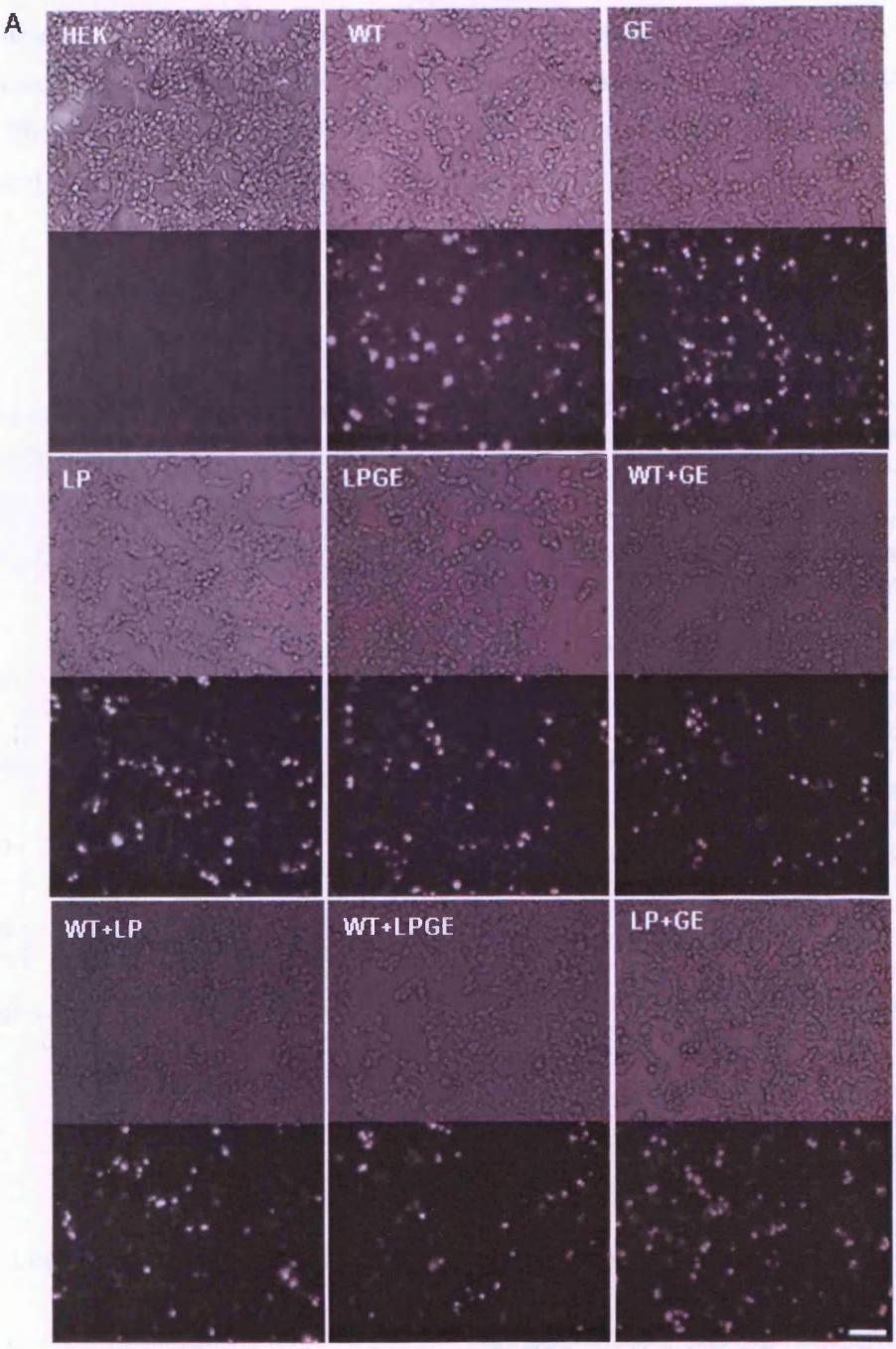

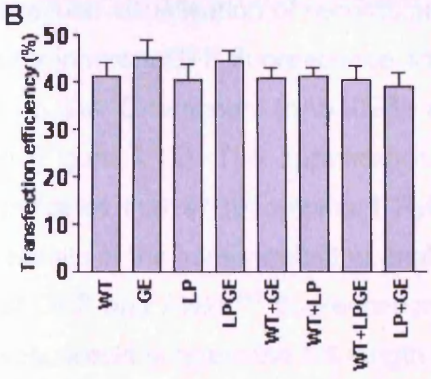

Figure 3.10. Expression of recombinant GFP-tagged hRyR2 in HEK cells following Effectene-mediated transfection. *Transfection efficiencies were calculated using fluorescence (panel A, lower panels) and phase (Panel B, upper panels) images. Untransfected HEK cells did not exhibit intracellular eGFP fluorescence. Similar transfection efficiencies (40-45%) were achieved with all RyR2 constructs, (panel B, ANOVA, $p>0.05$). Data was obtained from between 7 and 15 separate transfections with 554±11.5 cells per coverslip. Scale bar represents 100μm.*

each case. Each RyR2 produced a band of equal molecular weight (565 kDa) and there was no significant difference in relative levels of expression ($p > 0.35$, ANOVA, Figure 3.11). There was no RyR2 protein detected in untransfected HEK cells, which is consistent with this being an RyR2-deficient cell line.

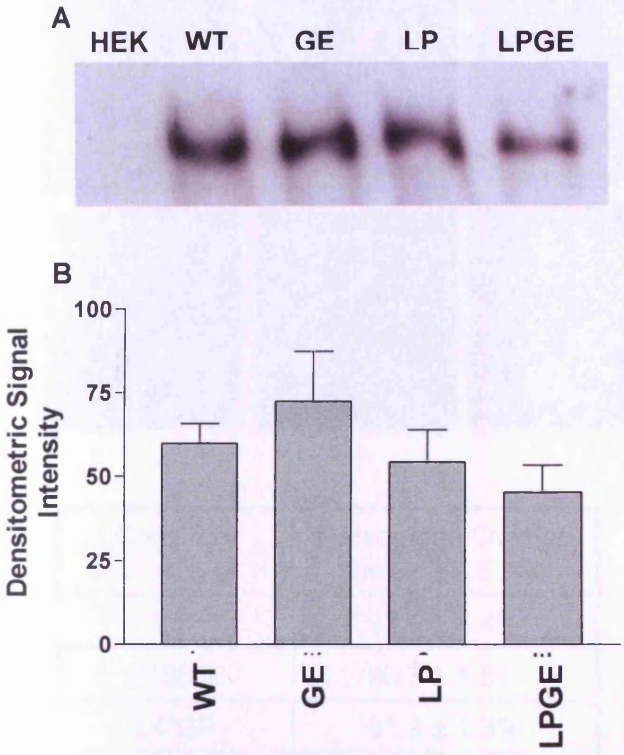

Figure 3.11. All recombinant RyR2 expressed to equivalent levels. *Mixed membrane vesicles isolated from HEK cells transiently expressing WT and mutant/polymorphism were resolved by SDS-PAGE as shown in panel A. Western blotting with a RyR2 specific rabbit-polyclonal antibody (pAb1093) produced a single, high molecular weight band was detected for each RyR2 construct. Densitometric analyses were carried out on 5 experiments, the results of which are presented in panel B. There was no significant difference in RyR2 expression levels of any mutant RyR2 (one-way ANOVA, $p>0.05$). Untransfected HEK cells did not display RyR2 this large molecular weight band. Data is presented as mean ± S.E.M. and is from 5 experiments.*

3.3.3. Localisation of recombinant RyR2 to the endoplasmic reticulum

The intracellular visualisation of recombinant RyR2 protein was performed by examining the cells for inherent GFP fluorescence and also via immunodetection using an antibody targeted to the C-terminus (pAb1093) and Alexa^{546}-conjugated secondary antibody detection (Figure 3.12). The appearance of the characteristic lattice-like fluorescence pattern indicates that all recombinant RyR2s correctly localised to the ER. Consistent with the results of the immunoblotting analysis, the high degree of colocalisation (89.1 to 93.6%) of GFP and Alexa^{546} fluorescence, targeted to the amino and carboxyl regions respectively, would suggest the full-length protein is being expressed.

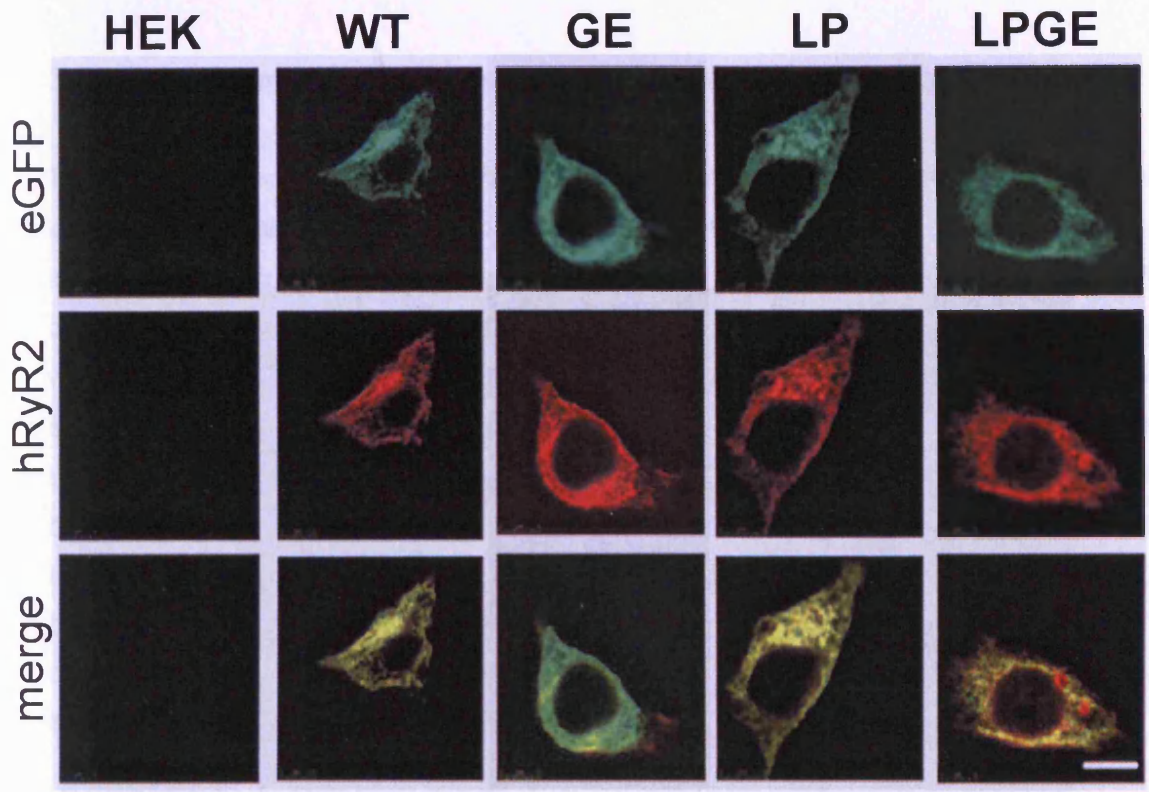

B

Construct	Percentage Overlap (mean±S.E.M)
WT	93.6 ± 2.4%
G1885E	90.7 ± 1.8%
L433P	91.9 ± 1.3%
L433P-G1885E	89.1± 3%

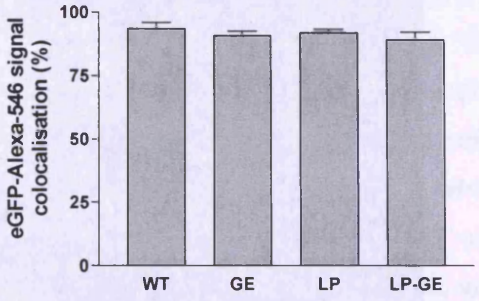

Figure 3.12. L433P and G1885E exhibit correct ER trafficking. *Cells expressing recombinant eGFP-hRyR2 were examined for endogenous eGFP fluorescence (top panels, excitation 488nm, emission collection = 525±25nm) and immunofluorescence of Alexa^{546} secondary antibody used with an anti-RyR2 primary antibody targeted to the C-terminus (pAB1093, middle panels, excitation = 546nm, emission 572±30nm) as shown in panel A. Both GFP and Alexa^{546} signals were localised to the ER as characterised by the lattice-like appearance. The scale bar represents 10μM. Extent of antibody and GFP colocalisation was quantified as the percentage of GFP pixels (green) that were directly coincident with Alexa^{546} pixels (red), presenting as yellow pixels when the two images were overlayed ('Merged', bottom panels, George, 2003). The mean ± S.E.M. extent of colocalisation is presented in panel B. Data was collected from between 7-11 cells.*

3.3.4. Voltage-independent measurement of Fluo3 signal intensity

The examination of the effects of PMT voltage gain on the Ca^{2+}-dependent Fluo3 signal intensity demonstrated a clear positive relationship between the two parameters, indicating that increasing PMT voltage resulted in an increase in signal intensity. In HEK cells loaded with Fluo3-AM, the effects of increasing voltage on Fluo3 signal intensity was fitted to a Boltzmann distribution, as illustrated in Figure 3.13. The Boltzmann curve exhibited a flat section when voltage gain was between approximately 0-750V, where the Ca^{2+}-dependent Fluo3 signal was relatively voltage-independent. This was followed by a steep section where Fluo3 signal intensity exhibited a high voltage-dependence, between voltages of approximately 800 and 1200V. The Boltzmann curve appears to begin to plateau at voltages in excess of 1250V, although the plateau phase was not completely observed here due to the maximum voltage gain in this experimental system being limited to 1250V.

Given the voltage-dependence of Fluo3 signal intensity (Figure 3.13A), variation in voltage gain at which data was collected could lead to artefactual differences in signal intensity being misinterpreted as having biological significance. In light of this it was essential to determine whether all experimental data was collected at comparable voltages. The mean voltage at which all Ca^{2+}-imaging data was acquired was normally-distributed about a mean of 730 ± 3.2V (Figure 3.13). The average voltage at which Ca^{2+}-imaging data was acquired from cells expressing each recombinant RyR2 was between 717.2 and 739.6 V and the minimal and maximal voltages at which data was acquired were 643 and 815 V respectively.

There were significant differences between the voltage gain at which Ca^{2+}-imaging data was acquired from HEK cells expressing each RyR2 (Figure 3.14, ANOVA, $p < 0.05$). However, this was likely attributable to the high sample number (216-760 cells, 34-70 coverslips per RyR2 construct) coupled with the fact that the majority of data was collected at voltages close to the mean, although some data was collected at extreme voltages.

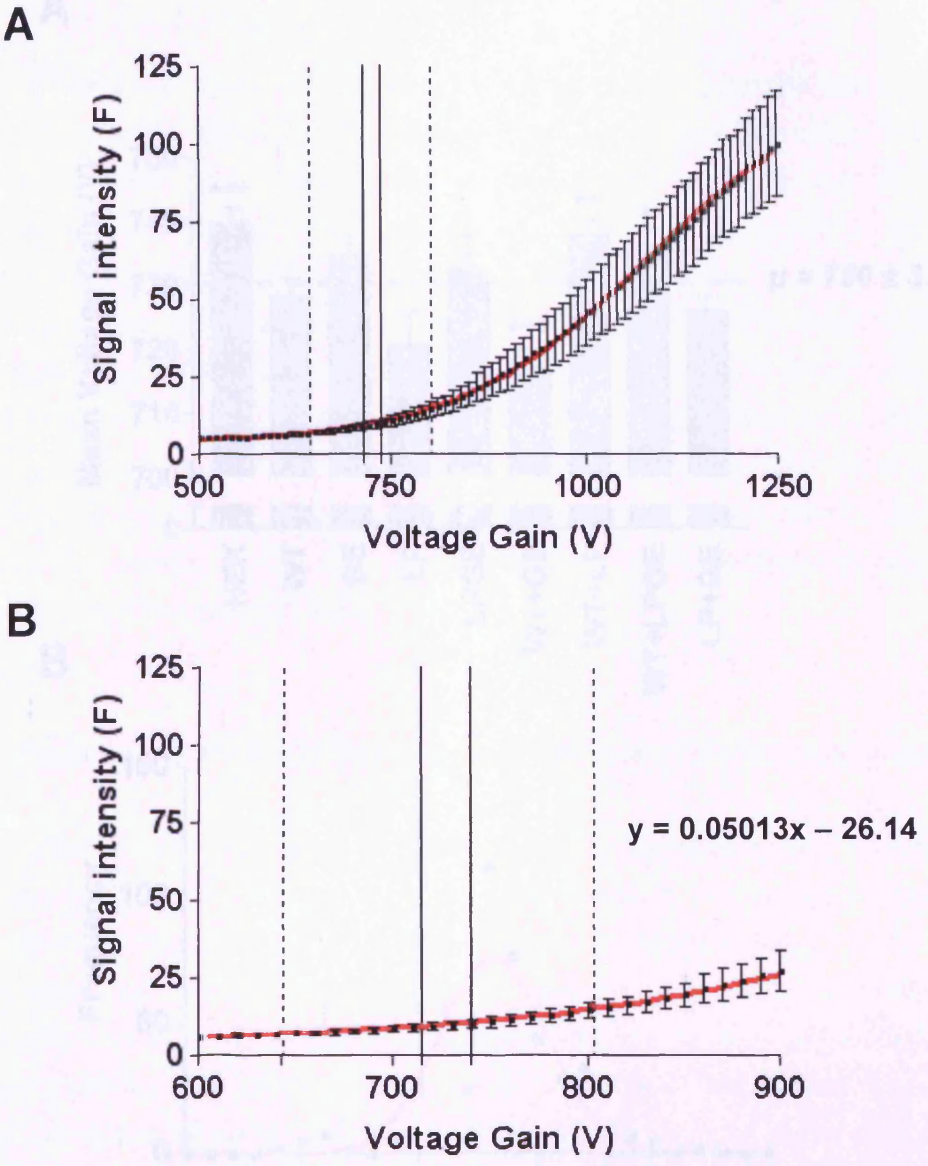

Figure 3.13. Boltzmann curve of HEK cells loaded with Fluo3-AM. *A Boltzmann curve was generated to examine the effects of increasing voltage gain (V) on Ca^2-dependent Fluo3 signal intensity in untransfected HEK cells. The mean ± S.E.M. signal intensity of HEK cells loaded with Fluo3-AM was determined at each voltage gain, increasing voltage in 10V increments from 500 – 1250V and is plotted in panel A. Data was generated from between 29-39 cells in 3 separate experiments. Solid black lines represent the lowest and highest average data acquisition voltages (714.9 and 739.6V respectively). Dotted black lines represent the minimal and maximal voltage at which Ca^{2+}-imaging data was acquired. Panel B shows the portion of the Boltzmann curve across which Ca^{2+} imaging data was collected. The portion of the linear regression line between the minimal and maximal voltages at which data was collected (dotted lines) approximates to a straight line represented by the formula y = 0.05013x – 26.14.*

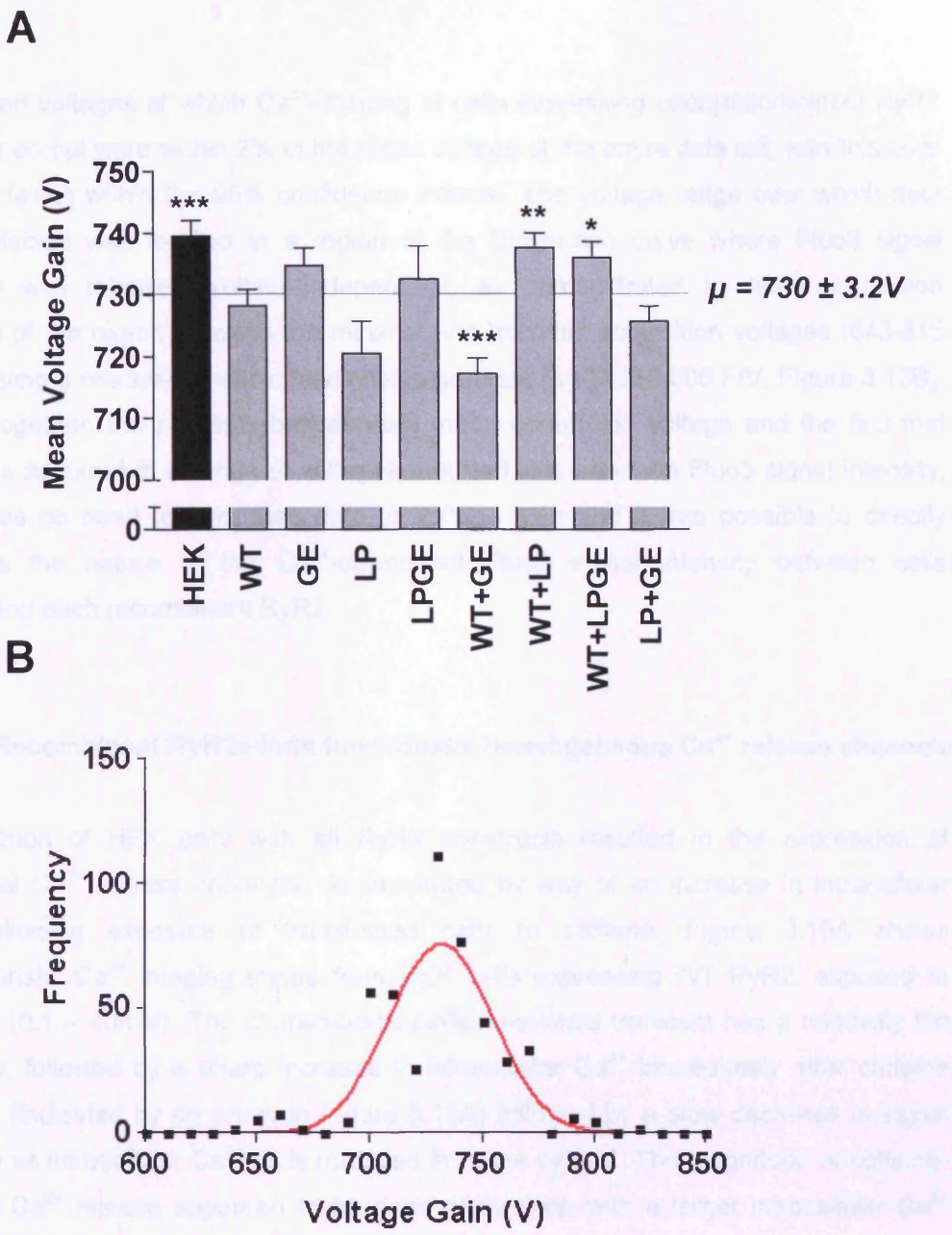

Figure 3.14. Ca^{2+} imaging data was acquired at comparable PMT voltage gain. *Voltage gain at which Ca^{2+} imaging data was acquired was normally distributed. The mean voltage gain at which data was acquired is displayed in panel A and ranged from between 717.2 – 737.7 V for cells expressing each RyR2. Asterisked data indicates a significant differences to the mean voltage gain ($p < 0.05$) The voltage gain at which Ca^{2+} imaging data was collected followed a Gaussian distribution about the mean of 730 ± 3.2V. Although data were collected at significantly different voltages to the mean, the majority of data was collected at voltages within 2% of the mean voltage gain and 96% of experiments were carried out at voltages within the normal distribution voltage range. Data was collected from a total of 457 separate coverslips.*

The mean voltages at which Ca^{2+}-imaging of cells expressing each recombinant RyR2 was carried out were within 2% of the mean voltage of the entire data set, with this level of error falling within the 95% confidence interval. The voltage range over which data was collected was located in a region of the Boltzmann curve where Fluo3 signal intensity was relatively voltage-independent, as demonstrated by linear-regression analysis of the region between the minimal and maximal acquisition voltages (643-815 V) revealing a relatively shallow relationship gradient (Δ=0.05±0.006 F/V, Figure 3.13B). Taken together, the similarity between the mean acquisition voltage and the fact that data was acquired at a range of voltages that had little effect on Fluo3 signal intensity, there was no need to normalise data to voltage gain and it was possible to directly compare the nature of the Ca^{2+}-dependent Fluo3 signal intensity between cells expressing each recombinant RyR2.

3.3.5. Recombinant RyR2s form functionally heterogeneous Ca^{2+} release channels.

Transfection of HEK cells with all RyR2 constructs resulted in the expression of functional Ca^{2+} release channels, demonstrated by way of an increase in intracellular Ca^{2+} following exposure of transfected cells to caffeine. Figure 3.15A shows characteristic Ca^{2+} imaging traces from HEK cells expressing WT RyR2, exposed to caffeine (0.1 – 40mM). The characteristic caffeine-evoked transient has a relatively flat baseline, followed by a sharp increase in intracellular Ca^{2+} immediately after caffeine addition (indicated by an arrow in Figure 3.15A) followed by a slow decrease in signal intensity as intracellular Ca^{2+} as is removed from the cytosol. The magnitude of caffeine-induced Ca^{2+} release appeared to be dose dependent, with a larger intracellular Ca^{2+} transient being observed following activation with increasing concentrations of caffeine.

The average magnitude of Ca^{2+} release following activation of WT RyR2 with each concentration of caffeine was calculated and used to generate a caffeine-activation curve (Figure 3.15B). The magnitude of Ca^{2+} release ($F-F_0$) was normalised to the basal signal intensity to account for differences in resting Ca^{2+} levels ($F-F_0 / F_0$). Under these experimental conditions, WT RyR2 produced half maximal caffeine-activation (EC_{50}) at 1.28±0.19mM caffeine, which is comparable to data produced from a study using a similar experimental system (1.56 ± 0.24mM, Thomas *et al.*, 2004).

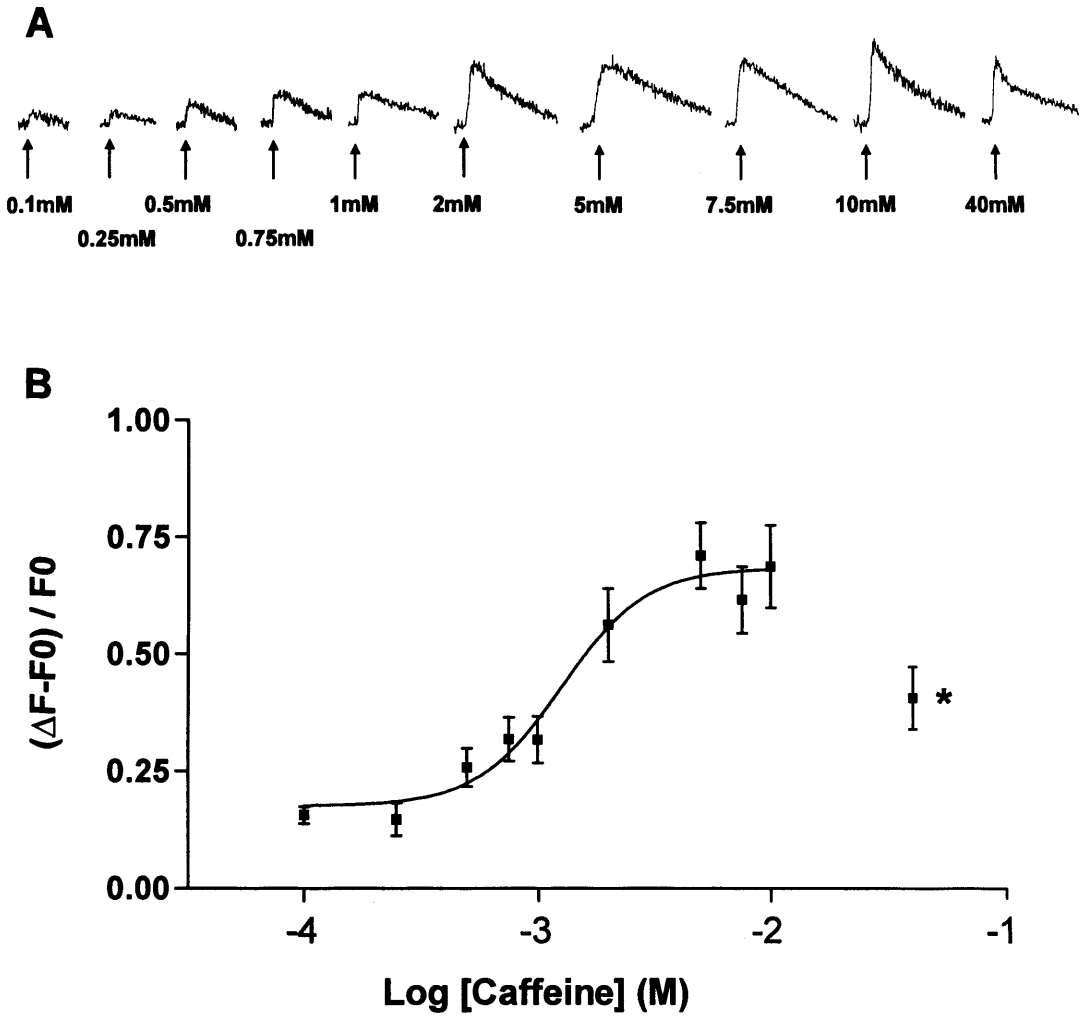

Figure 3.15. WT RyR2 exhibits a sigmoidal caffeine activation curve when expressed in HEK cells. *Representative Ca^{2+} transients following the addition of caffeine (0.1-40mM) at the points indicated in A. The average magnitude of Ca^{2+} release following activation with each caffeine concentration was used to produce a caffeine-activation curve (Panel B). The EC_{50} value (1.27mM) was calculated from a non-linear regression sigmoidal dose response curve and represents the caffeine concentration evoking half-maximal Ca^{2+} release. The 40mM caffeine data point (*) was excluded from non-linear regression due to quenching of Fluo3 signal as the fluorescence at this caffeine concentration was typically 10-40% lower than that observed following activation with 10mM caffeine. Data was collected form between 11 and 49 cells per caffeine concentration from 12 separate experiments.*

Although the majority of caffeine sensitive cells exhibited these "normal" transients, a significant percentage (~15-40%) of cells expressing each RyR2 construct exhibited spontaneous basal Ca^{2+} oscillations prior to caffeine addition. Cells exhibiting spontaneous basal Ca^{2+} oscillations were analysed as a separate data set and will be discussed in Chapter 5 of this thesis and are excluded from the analysis described in this chapter (see Figure 3.16).

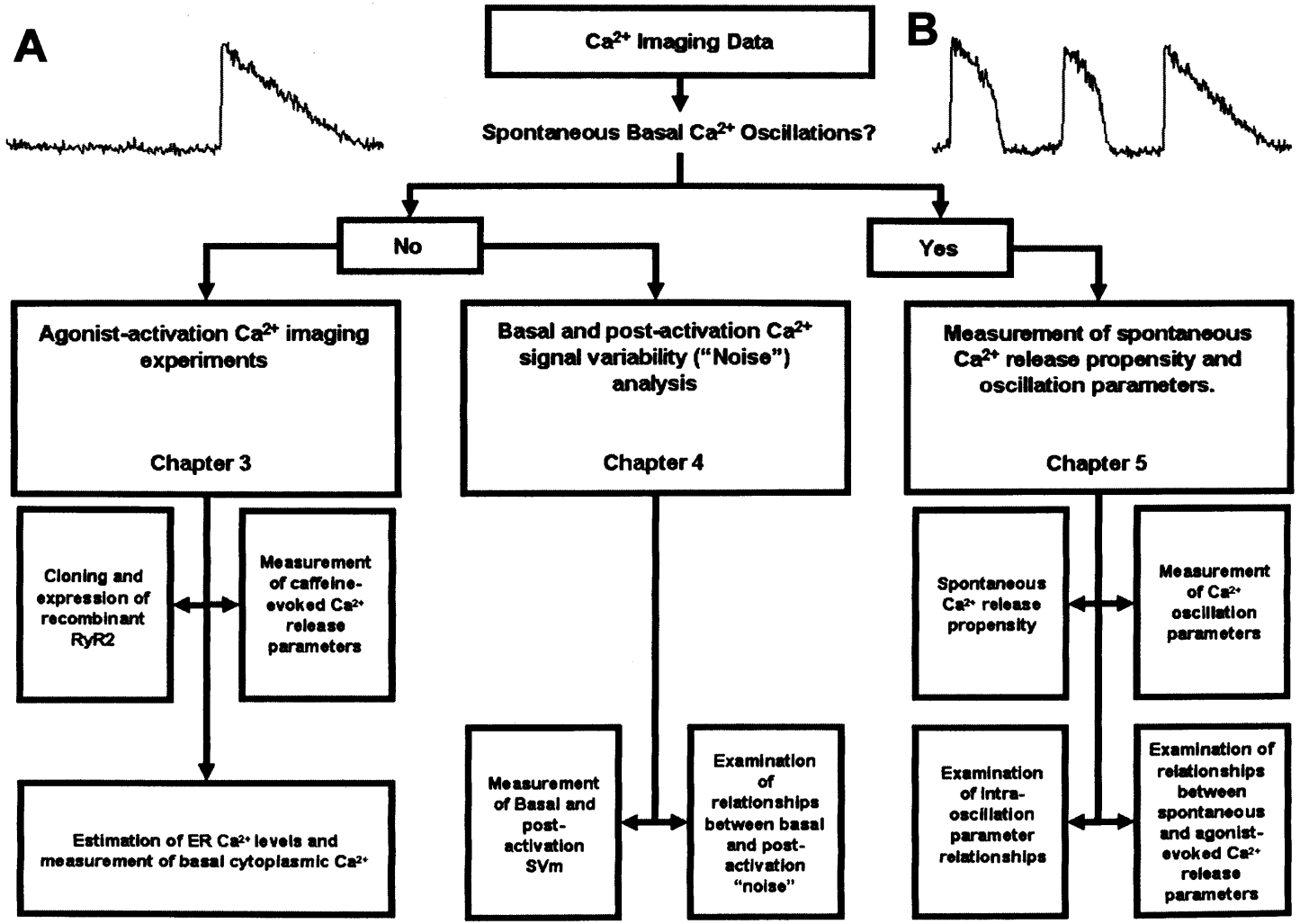

Figure 3.16. Single cell Ca^{2+} imaging analysis work-stream. *Data from non-oscillating cells underwent analysis of caffeine-evoked Ca^{2+} release parameters (Chapter 3) and analysis of basal and post-activation Ca^{2+} signal variability (Chapter 4). Data from cells that exhibited spontaneous basal Ca^{2+} oscillations were analysed as a separate data-set and the incidence and characteristics of spontaneous Ca^{2+} release events were determined (Chapter 5).*

Identical Ca^{2+} imaging experiments were carried out on cells expressing each recombinant RyR2, alone or co-expressed with WT RyR2. These experiments demonstrated significant heterogeneity in terms of the magnitude of caffeine-induced Ca^{2+} release and channel sensitivity to caffeine activation. Figure 3.17 shows the caffeine-activation curves of cells expressing RyR2 homotetramers containing L433P, G1885E or L433P-G1885E (LP, GE or LPGE respectively). Figure 3.18 shows the caffeine activation curves obtained from cells co-expressing WT RyR2 with L433P (WT+LP), G1885E (WT+GE) or L433P-G1885E (WT+LPGE) or co-expressing L433P with G1885E on separate subunits (LP+GE), in a fashion mimicking the expression of heterotetramers (see Figure 2.4 for visual representation of RyR2 homo- and heterotetramers). For clarity in describing the various combinations of recombinant RyR2 expression, the nomenclature described in Figure 2.4 will be adopted for the duration of this thesis.

From the EC_{50} values produced (Figures 3.17 and 3.18) it is evident that the expression of GE homotetramers or WT+GE heterotetramers produced channels with similar caffeine-sensitivity to WT (1.00 ± 0.15mM and 1.61 ± 0.42mM respectively, Figure 3.17 and Figure 3.18). Cells expressing LP homotetramers exhibited a significantly higher EC_{50} value (2.17 ± 0.35mM) than cells expressing WT RyR2 ($p < 0.05$, Figure 3.17), indicating that LP channels are desensitised to caffeine activation compared to WT RyR2, reaffirming the notion that L433P is a not a typical gain-of-function RyR2 mutation. Expression of LPGE homotetramers produced an EC_{50} value of 0.11 ± 0.07mM, which would suggest that homotetrameric LPGE channels are sensitised to caffeine activation compared to WT RyR2 ($p < 0.01$, Figure 3.17). However, the inclusion of G1885E on the same subunit as L433P (LPGE) appears to have abolished the sigmoidal caffeine dose response that was exhibited in cells expressing all other RyR2s, suggesting this EC_{50} may be artefactual. Additionally, the only significant difference between the magnitudes of Ca^{2+} release at a particular activating caffeine concentration in cells expressing LPGE compared to those expressing LP alone was observed following activation by 0.1mM caffeine ($p < 0.05$, Figure 3.17).

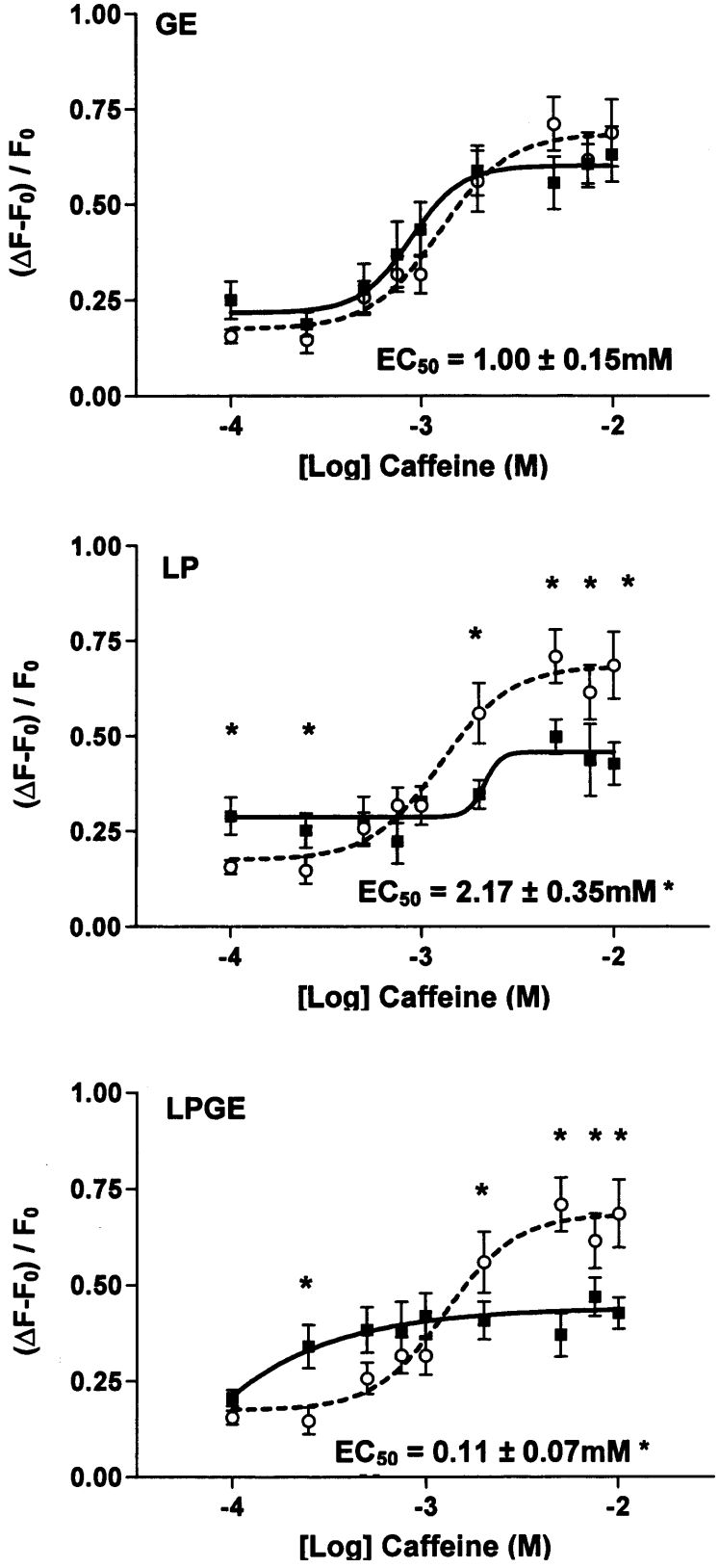

Figure 3.17. Homotetrameric L433P or L433P-G1885E alter the RyR2 caffeine activation profile. *Caffeine-activation dose response curves (0.1-10mM caffeine) were generated using HEK cells expressing G1885E, L433P or L433P-G1885E, homotetramerically. Data is represented as the mean ± S.E.M. magnitude of caffeine-induced Ca^{2+} release (ΔF-F0 / F0) and was obtained from between 10 - 84 cells at each caffeine concentration from >3 experiments. WT data is represented by open circles (○)* and a dashed line and mutant/polymorphism data is represented by closed squares (■) and a solid line. The EC_{50} value of WT RyR2 is 1.27mM as shown in Figure 3.11. Asterisked data points denote a significant difference to WT ($p < 0.05$).

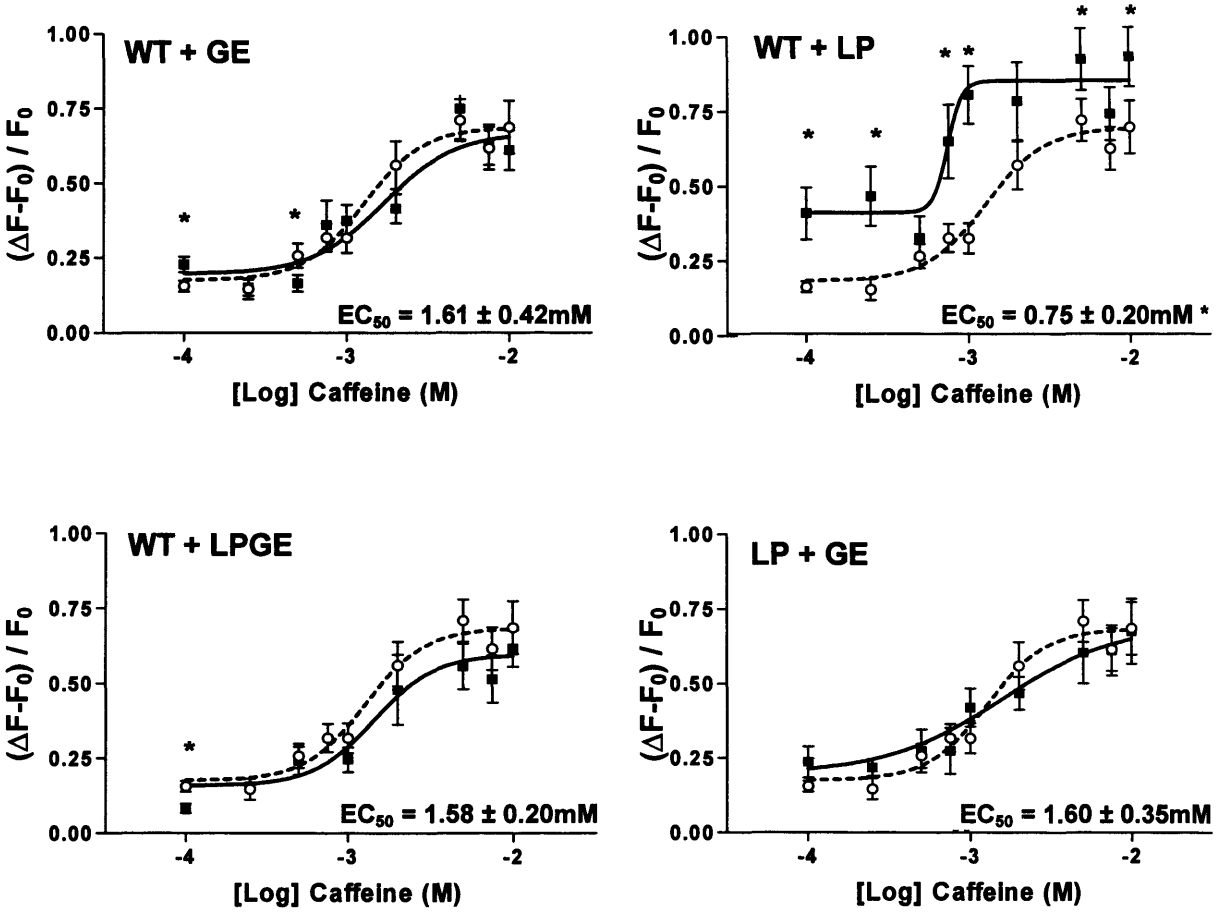

Figure 3.18. G1885E negates the altered caffeine activation profile of WT+LP co-expression. *Caffeine-activation dose response curves (0.1-10mM caffeine) were generated using HEK cells co-expressing WT RyR2 with G1885E, L433P or L433P-G1885E or co-expressing L433P with G1885E. Data is represented as the mean ± S.E.M. magnitude of caffeine-induced Ca^{2+} release (ΔF-F0 / F0) and was obtained from between 11 - 67 cells at each caffeine concentration from >3 experiments. WT data is represented by open circles (○) and a dashed line and mutant/polymorphism data is represented by closed squares (■) and a solid line. The EC_{50} value of WT RyR2 is 1.27mM as shown in Figure 3.11. Asterisked data points and EC_{50} values denote a significant difference to WT ($p < 0.05$).*

Co-expression of L433P with WT RyR2 (WT+LP), appeared to cause the caffeine activation curve to shift in the opposite direction to when LP was expressed alone, producing a significantly lower EC_{50} value than of WT RyR2 (0.75 ± 0.2mM, $p < 0.05$, Figure 3.18), inferring increased sensitivity to caffeine activation. Interestingly, the co-expression of L433P-G1885E with WT RyR2 (WT+LPGE, representative of *'in cis'* inheritance) produced a caffeine-activation curve that was significantly right-shifted (1.58 ± 0.2mM, $p < 0.05$, Figure 3.18) compared to that observed in cells co-expressing WT+LP, indicating that the presence of the G1885E polymorphism prevented the sensitisation of the channel to caffeine activation caused by WT+LP expression. Similarly, the increased caffeine-sensitivity of heterotetrameric WT+LP channels was not observed when G1885E was co-expressed on separate subunits to L433P (LP+GE, representative of *'in trans' inheritance*). This mode of expression resulted in a caffeine activation profile that was similar to that obtained from cells expressing WT RyR2 ($p = 0.70$), indicating the presence of G1885E restored normal caffeine sensitivity to WT+LP channels.

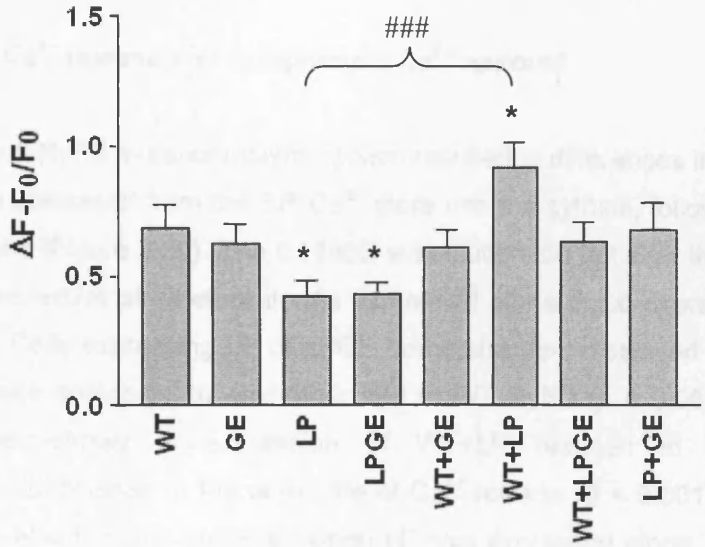

Figure 3.19. Heterogeneity in peak caffeine-induced Ca^{2+} release magnitude. *The average peak magnitude of Ca^{2+} release following activation with caffeine (10mM), representing maximal RyR2 activation was determined in HEK cells expressing each combination of recombinant RyR2. Data is presented as the mean magnitude of Ca^{2+} release ± S.E.M. Data was acquired from between 29 and 62 cells expressing each RyR2 construct.* * indicates a statistically significant difference compared to WT RyR2 ($p < 0.05$). **###** indicates a statistically significant difference compared to the homotetrameric counterpart of heterotetrameric substitution ($p < 0.001$) *i.e. WT+GE vs GE or WT+LP vs LP or WT+LPGE vs LP.*

Heterogeneity between caffeine-induced Ca^{2+}-release was observed between cells expressing each construct following maximal RyR2 activation with 10mM caffeine (Figure 3.19). Expression of GE or WT+GE exhibited similar peak Ca^{2+} release magnitude compared to WT RyR2 ($p=0.62$). Homotetrameric expression of LP or LPGE exhibited a significantly decreased peak Ca^{2+} release compared to cells expressing WT RyR2 ($p < 0.05$), although the magnitude of this decrease did not differ between cells expressing LP or LPGE ($p = 0.96$). This suggests that inclusion of G1885E on the same sub-unit as L433P had no significant effect on peak caffeine-induced Ca^{2+} release compared to that observed when L433P was expressed alone. Co-expressing WT+LP resulted in a significant increase in the magnitude of peak caffeine-induced Ca^{2+} release compared to WT RyR2 ($p < 0.05$), although this increase did not reach statistical significance when compared to other G1885E or L433P containing RyR2s ($p = 0.07$, Figure 3.19). However, co-expression of WT+LPGE resulted in a non-significant decrease in the peak magnitude of Ca^{2+} release compared to cells co-expressing WT+LP ($p = 0.07$), indicating that G1885E caused modest alterations in L433P peak Ca^{2+} release magnitude, but only in the heterotetrameric state.

3.3.6. Rates of Ca^{2+} release and cytoplasmic Ca^{2+} removal

Expression of each RyR2 mutation/polymorphism resulted in differences in the peak rate at which Ca^{2+} was released from the ER Ca^{2+} store into the cytosol, following activation with 10mM caffeine (Figure 3.20). The G1885E substitution did not alter the peak rate of Ca^{2+} release, irrespective of whether it was expressed alone or co-expressed with WT RyR2 ($p = 0.31$). Cells expressing LP or LPGE homotetramers displayed a similar peak rate of Ca^{2+} release compared to eachother and to WT RyR2 ($p = 0.06$ and $p = 0.07$ respectively). Interestingly, co-expression of WT+LP resulted in a significant, approximately 2-fold increase in the peak rate of Ca^{2+} release ($p < 0.001$) compared to WT, the opposite effect to that observed when LP was expressed alone. However, this increase in peak rate of caffeine-induced Ca^{2+} release was not observed following WT+LPGE or LP+GE co-expression. Taken together, these data suggest that the G1885E polymorphism has a modulatory effect on the peak rate of caffeine-induced Ca^{2+} release of WT+LP mutant channels, but not on homotetrameric L433P channels (Figure 3.20).

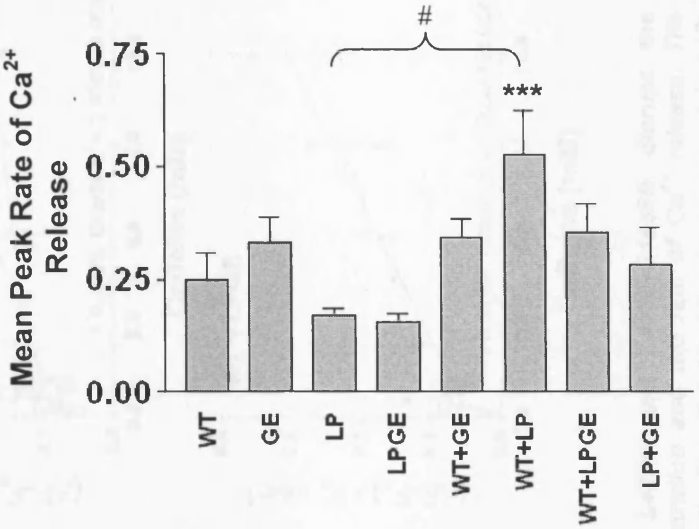

Figure 3.20. Mean peak rate of Ca^{2+} release following caffeine (10mM) activation. *The mean peak rate of Ca^{2+} release was measured following channel activation with caffeine (10mM), representing maximal channel activation. Data is presented as mean rate of Ca^{2+} release ± S.E.M. Data comprises of between 29 and 67 cells expressing each RyR2 construct.* *** indicates a statistically significant difference compared to WT RyR2 ($p<0.001$). # indicates a statistically significant difference compared to the homotetrameric counterpart of heterotetrameric substitution *i.e. WT+GE vs GE or WT+LP vs LP or WT+LPGE*

Linear regression analysis was carried out to determine if there was a relationship between the rate of Ca^{2+} release and the concentration of activating caffeine in cells expressing each recombinant RyR2 (Figure 3.21). Cells expressing WT RyR2 exhibited a strong, positive correlation between the concentration of activating-caffeine and the average rate of resulting Ca^{2+} release ($r^2 = 0.89$, $\Delta = 0.019 \pm 0.003$, $p < 0.001$). Expression of the G1885E polymorphism produced a similar relationship between activating caffeine concentration and the rate of Ca^{2+} release compared to WT, both when homotetrameric GE ($r^2 = 0.89$, $\Delta = 0.024 \pm 0.003$, $p < 0.0001$) or heterotetrameric WT+GE ($r^2 = 0.89$, $\Delta = 0.027 \pm 0.004$, $p < 0.0001$) were expressed.

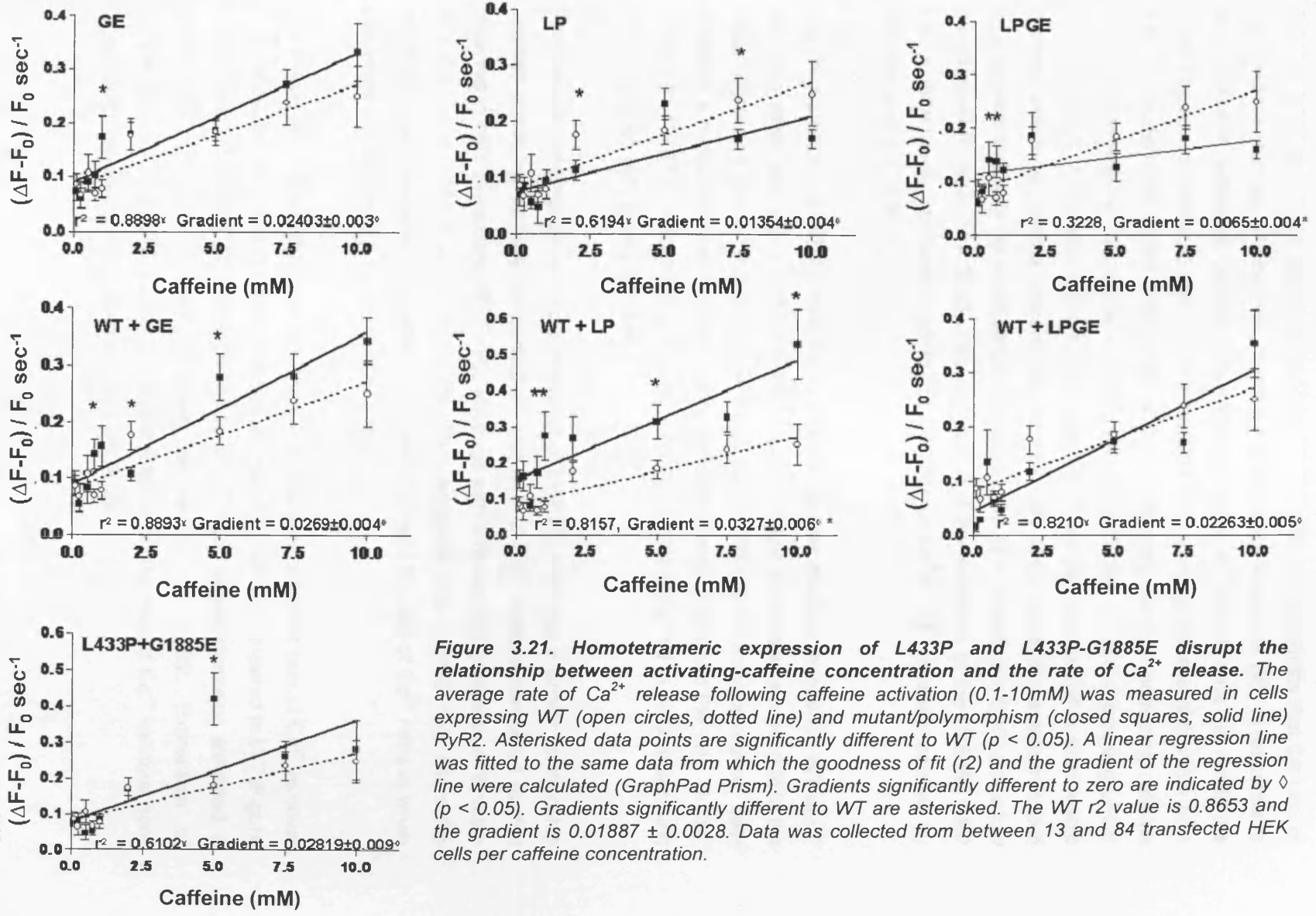

Figure 3.21. Homotetrameric expression of L433P and L433P-G1885E disrupt the relationship between activating-caffeine concentration and the rate of Ca^{2+} release. *The average rate of Ca^{2+} release following caffeine activation (0.1-10mM) was measured in cells expressing WT (open circles, dotted line) and mutant/polymorphism (closed squares, solid line) RyR2. Asterisked data points are significantly different to WT ($p < 0.05$). A linear regression line was fitted to the same data from which the goodness of fit (r2) and the gradient of the regression line were calculated (GraphPad Prism). Gradients significantly different to zero are indicated by ◊ ($p < 0.05$). Gradients significantly different to WT are asterisked. The WT r2 value is 0.8653 and the gradient is 0.01887 ± 0.0028. Data was collected from between 13 and 84 transfected HEK cells per caffeine concentration.*

Expression of LP homotetramers produced a similar gradient of the line-of-best-fit (Δ = 0.014 ± 0.004, $p < 0.05$) compared to that of WT RyR2. This suggests that the rate of Ca^{2+} release through LP channels increases to the same extent as WT, in response to an increase in activating caffeine concentration. However, the LP data did not fit the linear regression model so well, which manifests as a lower goodness-of-fit value (r^2 = 0.62). This decrease in the robustness of the relationship between activating caffeine concentration and the rate of Ca^{2+} release was exacerbated in cells expressing LPGE homotetramers. Cells expressing LPGE homotetramers did not exhibit a relationship between activating caffeine concentration and the rate of Ca^{2+} release as demonstrated by a gradient that was not significantly different to zero (Δ = 0.0065, $p = 0.12$) and a low goodness-of-fit value (r^2 = 0.32). This suggests that the presence of the G1885E SNP has a detrimental modulatory effect on the dysfunctional Ca^{2+} release caused by homotetrameric L433P expression.

The co-expression of WT+LP resulted in a much steeper gradient than when WT or LP were expressed alone (Δ = 0.033 ± 0.006, $p < 0.001$), and the data was a good fit to the linear regression line (r^2 = 0.82). Interestingly, when WT+LPGE was expressed, cells exhibited a relationship between activating caffeine concentration and the rate of Ca^{2+} release (r^2 = 0.82, Δ = 0.02263, $p < 0.001$) similar to that observed in cells expressing WT RyR2 or co-expressing WT+LP.

Furthermore, heterotetrameric co-expression of LP+GE, exhibited a similar relationship between activating caffeine concentration and rate of Ca^{2+} release compared to that observed in cells expressing WT RyR2, although with a decreased goodness of fit value (r^2 = 0.61, Δ = 0.028 ± 0.009, $p < 0.05$). This suggests that G1885E only alters the relationship between activating caffeine concentration and the rate of Ca^{2+} release when expressed with L433P in a homotetrameric state.

Expression of most recombinant RyR2 variants displayed a similar rate of Ca^{2+} removal from the cytosol following caffeine-evoked Ca^{2+} release (10mM) compared to WT (Figure 3.22). Cells expressing GE homotetramers or WT+GE heterotetramers, exhibited a similar rate of Ca^{2+} removal as cells expressing WT RyR2. Expression of homotetrameric LP or LPGE had no significant effect on the rate of Ca^{2+} removal from the cytosol compared to cells co-expressing WT RyR2.

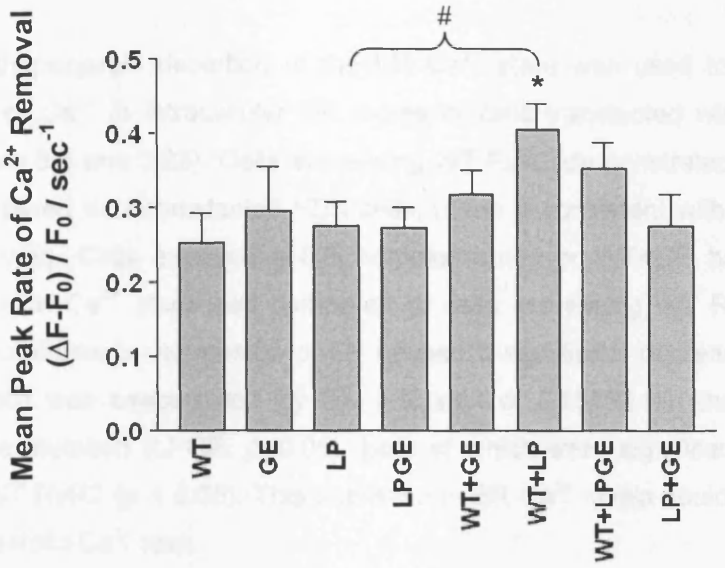

Figure 3.22. WT+LP heterotetrameric expression increases the rate of Ca^{2+} removal from the cytoplasm following RyR activation. *Data presented is the mean rate of Ca^{2+} removal following RyR2 activation with 10mM caffeine ± S.E.M., representing the rate of Ca^{2+} removal from the cytosol following maximal RyR2 activation. Data was collected from between 29 and 62 cells expressing each RyR2 construct.* * indicates a statistically significant difference in the mean peak rate of Ca^{2+} release compared to WT RyR2. # indicates a statistically significant difference compared to the homotetrameric counterpart of heterotetrameric substitution *i.e. WT+GE vs GE or WT+LP vs LP or WT+LPGE vs LP.*

However, co-expression of WT+LP resulted in a significant increase in the rate of Ca^{2+} removal from the cytosol, compared to WT or LP homotetramers were expressed ($p < 0.05$). Co-expression of WT+LPGE exhibited a similar rate of Ca^{2+} removal compared to that observed in cells expressing WT RyR2. It is important to note that differing magnitudes of caffeine-induced Ca^{2+} release observed in cells expressing each recombinant RyR2 may contribute to the varying rates of Ca^{2+} removal from the cytosol. Also worth noting is that the addition of a caffeine bolus to the cells may alter RyR2 gating following Ca^{2+} release (Gaburjakova *et* al, 2006) and may presumably perturb ER store refilling with the majority of Ca^{2+} likely being removed from the cell through various cell membrane bound Ca^{2+} pumps and exchangers.

3.3.7. Differential ER Ca^{2+} store load

Caffeine and thapsigargin depletion of the ER Ca^{2+} store was used to estimate the relative levels of Ca^{2+} in intracellular ER stores of cells transfected with each RyR2 construct (Figure 3.8 and 3.23). Cells expressing WT RyR2 demonstrated an increased store load compared to untransfected HEK cells, which is consistent with previous data (Tong *et al*, 1999). Cells expressing GE homotetramers or WT+GE heterotetramers displayed a similar Ca^{2+} store load compared to cells expressing WT RyR2 ($p=0.69$). However, homotetrameric expression of LP caused a significant decrease in ER Ca^{2+} store load which was exacerbated by the inclusion of G1885E on the same RyR2 subunits as the mutation (LPGE, $p<0.05$), both of which were significantly decreased compared to WT RyR2 ($p < 0.05$). This decrease in ER Ca^{2+} levels could potentially be indicative of diastolic Ca^{2+} leak.

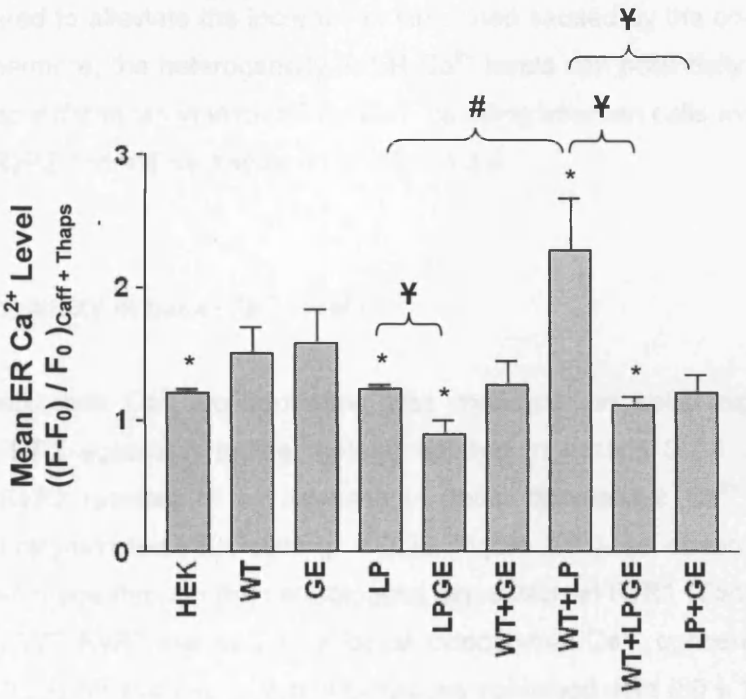

Figure 3.23. Heterogeneity in ER Ca^{2+} load as estimated by thapsigargin depletion of ER Ca^{2+}. *Transfected cells were indentified by caffeine-sensitivity (0.5mM). Passive ER store depletion was achieved by thapsigargin (10μM) inhibition of SERCA, preventing store refilling. Data represents mean ± S.E.M magnitude of thapsigargin and caffeine induced Ca^{2+} release. Data was obtained from 20-74 cells per recombinant RyR2, or from 272 untransfected cells.* * indicates a statistically significant difference compared to WT RyR2. # indicates a statistically significant difference compared to the homotetrameric counterpart of heterotetrameric substitution *i.e. WT+GE vs GE or WT+LP vs LP or WT+LPGE vs LP.* ¥ indicates a statistically significant difference compared to the respective recombinant RyR2 without G1885E co-expression. *i.e. LP-GE vs LP or WT+LPGE vs WT+LP or LP+GE vs WT+LP.*

Co-expression of heterotetrameric WT+LP had the opposite effect to when homotetrameric LP was expressed, exhibiting a significantly increased ER Ca^{2+} store load compared to cells expressing WT ($p < 0.05$). Conversely, co-expression of WT+LPGE heterotetramers resulted in a significant decrease in ER Ca^{2+} levels compared to cells expressing either WT or WT+LP ($p < 0.05$). Heterotetrameric LP+GE expression exhibited a comparable ER Ca^{2+} store load to WT RyR2, although this was significantly decreased compared to that of cells co-expressing WT+LP ($p < 0.05$).

In summary, the presence of G1885E appears to alters ER Ca^{2+} load irrespective of whether it is expressed on the same or separate subunits as L433P in a heterotetrameric fashion or whether it is expressed with homotetrameric L433P. Homotetrameric expression of LPGE appeared to exacerbate the effects of L433P on Ca^{2+} store load, whereas co-expression of G1885E with L433P in a heterotetrameric fashion appeared to alleviate the increase in store load caused by the co-expression of WT+LP. Furthermore, the heterogeneity in ER Ca^{2+} levels can potentially explain some of the observed differences in intracellular Ca^{2+} handling between cells expressing each recombinant RyR2 and will be discussed in section 3.4.

3.3.8. Heterogeneity in basal Ca^{2+} levels

The free cytoplasmic Ca^{2+} concentration was measured in cells expressing each recombinant RyR2 according to the method detailed in section 3.2.6. Expression of recombinant RyR2 resulted in an increase in basal cytoplasmic Ca^{2+} concentration compared to untransfected HEK cells ($p < 0.05$, Figure 3.24), an observation that has previously been made through the heterologous expression of RyR1 (Tong *et al.*, 1999). Expression of WT RyR2 resulted in a basal cytoplasmic Ca^{2+} concentration (108 ± 19nM, Figure 3.24) comparable to that of previously published data (80 ± 13nM, Thomas *et al.*, 2005). Expression of homotetrameric GE or heterotetrameric WT+GE did not significantly alter the basal cytoplasmic Ca^{2+} concentration compared to that of cells expressing WT RyR2. When homotetrameric L433P was expressed, a basal cytoplasmic Ca^{2+} concentration of 110 ± 14nM (101.8±13% of WT) was observed, which is similar to WT ($p = 0.94$) and previously published data (86 ± 13mM, 107.5±15%, Thomas *et al.*, 2005). However, expression of homotetrameric LPGE resulted in a significant increase in basal cytoplasmic Ca^{2+} concentration (268±37nM, 248±13.8% of WT) compared to

that observed in cells expressing homotetrameric LP, which suggests that the presence of G1885E increases the level of cytoplasmic Ca^{2+} and coupled with the observed decreased Ca^{2+} store load, could be indicative of ER Ca^{2+} leak.

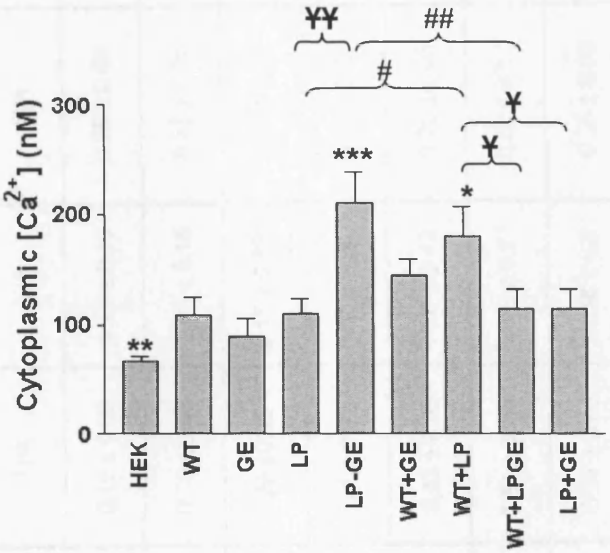

Figure 3.24. Heterogeneity in basal cytoplasmic Ca^{2+} levels in cells expressing each recombinant RyR2. *Transfected cells were indentified by caffeine-sensitivity (0.5mM) before determination of the maximal (Ionomycin 10μM) and minimal (EGTA, 20mM) Ca^{2+}-dependent signal intensities. These values were used to determine the basal cytoplasmic Ca^{2+} concentration of cells expressing each RyR2. Data is plotted as mean ± S.E.M. which is and was generated from between 21 and 73 transfected cells and 130 untransfected cells.* * indicates a statistically significant difference compared to WT RyR2. # indicates a statistically significant difference compared to the homotetrameric counterpart of heterotetrameric substitution *i.e. WT+GE vs GE or WT+LP vs LP or WT+LPGE vs LP.* ¥ indicates a statistically significant difference compared to the respective recombinant RyR2 without G1885E co-expression. *i.e. LP-GE vs LP or WT+LPGE vs WT+LP or LP+GE vs WT+LP.*

Co-expression of WT+LP also significantly increased basal cytoplasmic Ca^{2+} levels compared to WT RyR2 (184.4 ± 32.5nM, 170.7±17.6% of WT, $p < 0.05$). Interestingly, co-expression of WT+LPGE restored basal cytoplasmic Ca^{2+} levels to those observed in cells expressing WT RyR2 or homotetrameric LP, as did the expression of LP+GE heterotetramers. Taken together this data indicates that the G1885E also alters the basal cytoplasmic Ca^{2+} levels of cells expressing the L433P mutation, both when it is expressed in a homotetrameric or heterotetrameric manner. Given that altered cytoplasmic Ca^{2+} concentration has been implicated in impaired cardiac function, the differences in cytoplasmic Ca^{2+} levels observed here may be an indication that L433P and G1885E have a role in arrhythmia pathogenesis.

RyR2	ER Ca^{2+} Store Load $[(F_{caff} + F_{thaps})-F_0] / F_0$	Cytoplasmic $[Ca^{2+}]$ (mM)	Peak Ca^{2+} release	Minimal Ca^{2+} release	Caffeine EC_{50} (mM)	Peak Rate of Ca^{2+} release $\Delta(F-F_0/F_0)$ sec^{-1}	Rate of Ca^{2+} removal $\Delta(F-F_0/F_0)$ sec^{-1}
Untransfected	1.21 ± 0.03 *	67.2 ± 3.7 *	N/A	N/A	N/A	N/A	N/A
Wild Type	1.51 ± 0.19	108.7 ± 16.2	0.68 ± 0.09	0.15 ± 0.02	1.27 ± 0.19	0.25 ± 0.06	0.25 ± 0.04
G1885E	1.58 ± 0.26	88.5 ± 16.8	0.63 ± 0.07	0.19 ± 0.03	1.00 ± 0.15	0.33 ± 0.05	0.3 ± 0.06
L433P	**1.1 ± 0.1 ***	110.7 ± 13.2	**0.43 ± 0.06 ***	**0.25 ±0.05 ***	**2.17 ± 0.35 ***	0.17 ± 0.02	0.28 ± 0.03
L433P - G1885E	**0.89 ± 0.11 ***	**193.4 ± 13.8 ***	**0.43 ± 0.04 ***	**0.21 ± 0.02 ***	**0.11 ± 0.07 ***	0.16 ± 0.02	0.27 ± 0.03
WT + G1885E	1.27 ± 0.18	145.1 ± 14.0	0.61 ± 0.07	0.15 ± 0.03	1.6 ± 0.42	0.26 ± 0.03	0.32 ± 0.03
WT + L433P	**2.29 ± 0.39 ***	**180.0 ± 28.0 ***	**0.92 ± 0.1 ***	**0.37 ± 0.09 ***	**0.75 ± 0.2 ***	**0.53 ± 0.1 ***	**0.41 ± 0.04 ***
WT + L433P-G1885E	**1.11 ± 0.06 ***	114.2 ± 18.0	0.64 ± 0.07	0.11 ± 0.02	1.58 ± 0.2	0.35 ± 0.06	0.35 ± 0.04
L433P + G1885E	1.21 ± 0.14	114.2 ± 18.5	0.68 ± 0.11	0.22 ± 0.03	1.6 ± 0.35	0.28 ± 0.08	0.28 ± 0.04

Table 3.4. A summary of the Ca^{2+} handling parameters observed in cells expressing each recombinant RyR2. *Asterisked data indicates a significant difference to WT RyR2 ($p < 0.05$). Green values indicate a significant increase and red values indicate a significant decrease compared to WT RyR2.*

3.4. Discussion

3.4.1. RyR2 constructs harbouring ARVD2-linked mutations/polymorphisms were successfully generated and expressed in HEK-293 cells.

Non-liposomal lipid-mediated transfection was shown to be an effective method of transiently expressing recombinant RyR2 in HEK cells. This method of transfection routinely resulted in transfection efficiencies of ~40-45% for all cDNA constructs, as determined by monitoring cells for eGFP expression. Co-transfection of cells with two different RyR2 cDNAs in a 1:1 molar ratio produced comparable transfection efficiencies to when cells were transfected with a single RyR2 construct. This suggests that transfection with two distinct RyR2 cDNA constructs results in the same number of cells expressing RyR2 protein and there is no obvious detrimental effect of co-transfection on eGFP expression. This method of co-transfection has been routinely used in the investigation of cardiac sodium channel gene (*SCN5A*) mutations (Viswanathan *et al.*, 2003; Poelzing *et al.*, 2006), RyR1 CCD/MH-linked mutations (Tong *et al.*, 1999; Du *et al.*, 2004) and RyR2 mutations (Wehrens *et al.*, 2003; Lehnart *et al.*, 2008). HEK-293 cells transfected with each RyR2 construct exhibited eGFP fluorescence, indicating that the chromophore was correctly folded, as eGFP only fluoresces when the correct secondary structure has been adopted.

Western blot analysis of mixed membrane vesicles isolated from HEK cells transfected with each RyR2 construct, and subsequently probed with an anti-RyR2 antibody confirmed that the full-length 565kDa protein was being expressed, since the pAb1093 antibody binds to RyR at the C-terminus (residues 4455-4474). The densitometric analysis of western blots also showed that the relative levels of expression did not differ between cells expressing each RyR2 mutation/polymorphism, consistent with published data in the cases of G1885E (Koop *et al.*, 2008) and L433P (Thomas *et al.*, 2004). As all RyR2 mutants/polymorphisms were expressed to comparable levels, any observed functional consequences of RyR2 mutations/polymorphisms do not stem from differences in relative expression levels.

The high degree of co-incident localisation (89-94%) of endogenous eGFP fluorescence with pAb1093 immunofluorescence also suggests that the full-length RyR2 protein is being expressed. This is corroborated by the fact that the eGFP epitope is located at the extreme N-terminus of the protein and the pAb1093 antibody is targeted to a region near

the C-terminus, with the two signals exhibiting high levels of co-localisation. Interestingly, all recombinant RyR2's exhibited an expression pattern similar to that characteristic of immunofluorescent markers targeted to other ER proteins i.e. sarcolipin (Gramolini *et al.*, 2004), SERCA (Bobe *et al.*, 2004). This confirms the correct membrane trafficking of recombinant RyR2's to the ER, meaning that any observed functional consequences of mutant channel expression are not caused by protein mis-trafficking. The correct trafficking of RyR2 to the ER also confirms that the fusion of the eGFP chromophore to the N-terminus of the RyR2 peptide does not prevent correct protein targeting. The lack of pAb1093-dependent signal demonstrated by western blot analysis of membrane vesicles isolated from untransfected HEK cells, coupled with the absence of pAb1093 immunofluorescence confirms that HEK cells do not endogenously express RyR2.

Transfection of HEK-293 cells with each of the RyR2 cDNAs resulted in the formation of functional recombinant RyR2 channels, as demonstrated by caffeine-evoked Ca^{2+} release in single-cell Ca^{2+}-imaging experiments. This confirms that the fusion of the eGFP epitope at the extreme N-terminus does not prevent the formation of functional Ca^{2+} release channels. This is consistent with previous functional studies using similar N-terminal eGFP-tagged RyR2 cDNA constructs in HEK-293 cells (Thomas *et al.*, 2004; 2005) and 3D-mapping studies in which the GFP epitope was inserted into various locations within the RyR2 protein (Zhang *et al.*, 2003; Liu *et al.*, 2005; Wang *et al.*, 2007). Insertion of GFP into regions spanning the length of the protein (Figure 1.6, regulatory motif localisation), including at the N-terminus (Wang *et al.*, 2007), resulted in channels that presented similar Ca^{2+} and caffeine activation sensitivities to untagged WT RyR2 channels. This makes it unlikely that the insertion of a GFP tag at the extreme N-terminus will cause gross perturbation of channel function. Untransfected HEK cells did not exhibit caffeine-induced Ca^{2+} release, reconfirming that HEK cells do not endogenously express RyR2.

Cells expressing WT RyR2 exhibited similar basal cytoplasmic Ca^{2+} levels and ER Ca^{2+} store load compared to previously published data produced from a similar experimental system (Thomas *et al.*, 2004; 2005). Similarly, the resting cytoplasmic Ca^{2+} levels of cells expressing RyR2 (108.7±16.2nM) were comparable to those observed as a result of expression of RyR1 in a HEK-293 cell model (112.1±11nM, Tong *et al.*, 1999). Also in accordance with this study, cells expressing recombinant RyR2 exhibited a marked increase in cytoplasmic Ca^{2+} concentration compared to untransfected HEK cells

(97±5nM, 15.5% increase, Tong *et al.*, 1999), although this increase was not as pronounced as that observed here (67.2±3.7nM, 38.2% increase). *Tong et al* proposed that expression of RyR1 causes an increase in the permeability of the ER Ca^{2+} store, accounting for the observed rise in basal cytoplasmic Ca^{2+} levels and also observed a compensatory increase in SERCA expression levels and activity, culminating in an increased store load (Tong *et al.*, 1999), similar to observations made here.

The caffeine activation profile of cells expressing recombinant WT RyR2 was also similar to previously published data obtained from the heterologous expression of recombinant human (Thomas *et al.*, 2004) and rabbit (Du *et al.*, 1998) RyR2. Cells expressing WT RyR2 also displayed a strong relationship between activating caffeine concentration and the rate of subsequent Ca^{2+} release, suggesting that increasing the level of channel activation increases the rate at which Ca^{2+} is released from the ER.

All of this data taken together would suggest that HEK-293 cells provide a suitable model system in which to express human RyR2 and study the functional consequences of mutant channel expression on intracellular Ca^{2+} handling. The similarities observed between the Ca^{2+} handling properties of HEK-293 cells expressing WT RyR2 in this study and that of *Thomas et al* suggest that direct comparison of experimental data from the two studies is plausible. The measurement of the intracellular Ca^{2+} handling parameters discussed here were determined for cells expressing each recombinant RyR2 and the data generated is summarised in Table 3.4.

3.4.2. G1885E channels are functionally similar to WT RyR2

Single-cell Ca^{2+} imaging of HEK cells expressing RyR2 containing G1885E indicates that this polymorphism did not cause gross perturbation of RyR2 Ca^{2+} handling in a cellular environment. Unlike the vast majority of CPVT/ARVD2-associated mutations and consistent with previous investigation of this polymorphism (Koop *et al.*, 2008), G1885E expression did not result in a decreased ER Ca^{2+} store load. This, coupled with the fact that it did not lead to increased basal cytoplasmic Ca^{2+} levels, suggests that it is unlikely that G1885E results in diastolic Ca^{2+} leak, one of the mechanisms by which RyR2 mutations are proposed to result in arrhythmia. The magnitude of caffeine-induced Ca^{2+} release in cells expressing G1885E was similar to that observed in cells expressing WT

RyR2 across the entire caffeine concentration range (0.1-10mM), which suggests the G1885E channel had a similar activation profile to that of WT RyR2. This is corroborated by the similarity between WT and G1885E EC_{50} values in previously published data of mouse RyR2-G1885E caffeine activation profiling (Koop *et al.*, 2008). The similarity in the rates of Ca^{2+} release and subsequent Ca^{2+} removal, coupled with the comparable magnitudes of Ca^{2+} release suggests that following channel activation, the cytoplasmic Ca^{2+} concentration profile is comparable between cells expressing G1885E or WT RyR2. Similarly, when G1885E was co-expressed with WT RyR2 there was no significant difference in ER Ca^{2+} store load, basal cytoplasmic Ca^{2+} levels, caffeine activation profile and the rates of Ca^{2+} release and subsequent Ca^{2+} removal when compared to WT or G1885E data. Collectively, these data suggest that G1885E does not cause any gross perturbation of intracellular Ca^{2+} handling parameters, regardless of whether it is expressed as homotetramers or heterotetramers.

The G1885E polymorphism is located in DR3 (Zhang *et al.*, 2003), a region of the cytoplasmic domain that has been proposed to be involved in the Ca^{2+} dependent regulation of RyR activity (Hayek *et al.*, 1999). Given the role of DR3 in RyR2 inactivation (Hayek *et al.*, 2000), the substitution of the non-polar glycine residue for a negatively charged glutamate residue (G1885E) could potentially alter the Ca^{2+} binding affinity of this domain and subsequently alter Ca^{2+}-dependent regulation of the channel. However, in these experiments G1885E did not appear to exhibit an altered caffeine activation profile, suggesting that the G1885E substitution is unlikely to alter Ca^{2+} dependent channel activation when it is the only substitution present, however this would need to be examined in single channel studies. The effects of G1885E on Ca^{2+} dependent channel inactivation could not be accurately determined in this experimental system as the addition of caffeine as a bolus is likely to alter channel gating parameters following activation (Gaburjakova *et al.*, 2006).

Although several groups have demonstrated that CPVT/ARVD2-linked RyR2 mutations do not reduce FKBP12.6 binding (George *et al.*, 2003a; Stange *et al.*, 2003; Zissimopoulos *et al.*, 2009), G1885E is in a region directly adjacent to the proposed FKBP12.6 binding site (Zhang *et al.*, 2003; Sharma *et al.*, 2006), meaning that functional consequences of G1885E on FKBP12.6 binding or activity cannot be ruled out. If G1885E did alter FKBP12.6 regulation of RyR2, it would not have been observed in these experiments as HEK-293 cells do not endogenously express FKBP12.6. The

potential effects of the G1885E substitution on FKBP12.6 activity would therefore need to be investigated when co-expressed with FKBP12.6 or in a cardiac system in which FKBP12.6 is endogenously expressed.

3.4.3. L433P functional consequences depend on mode of expression

The L433P ARVD2-linked mutation resulted in significant perturbation of intracellular RyR2 Ca^{2+} handling dynamics compared to G1885E. Cells expressing L433P homotetramers exhibited a decrease in Ca^{2+} store load and similar basal cytoplasmic Ca^{2+} levels to cells expressing WT RyR2, in agreement with findings from several studies (Thomas *et al.*, 2004; Jiang *et al.*, 2005) and observations made through heterologous expression of RyR1 MH-linked mutations (Bobe *et al.*, 2004; Brini *et al.*, 2005). Interestingly, when L433P channels were fully activated by high concentrations of caffeine, the magnitude of Ca^{2+} release was significantly decreased compared to cells expressing WT RyR2. The caffeine activation profile of L433P appeared to be right shifted compared to WT (EC_{50} = 2.17 ± 0.35), suggesting that L433P caused a desensitisation of the channel to caffeine activation, which is in accord with previous work (Thomas *et al.*, 2004), although the extent of caffeine desensitisation was more pronounced in their experiments (EC_{50} = 4.86 ± 0.58mM).

The observed decrease in Ca^{2+} store load could be indicative of passive Ca^{2+} leak from the ER, as has been observed through heterologous expression of several MH and CCD-linked RyR1 mutations (Brini *et al.*, 2005), resulting in a decreased level of ER Ca^{2+} available for release following caffeine activation of RyR2 (Bers, 2008). Although the Ca^{2+} store load was decreased, the level of cytoplasmic Ca^{2+} was unchanged compared to WT, suggesting that a compensatory mechanism of Ca^{2+} extrusion may have come into effect. However, the precise mechanism of extrusion of cytoplasmic Ca^{2+} from HEK cells remains unknown as HEK cells do not endogenously express NCX (Hurtado *et al.*, 2006). Coupled with the fact that ER Ca^{2+} store refilling may be chronically perturbed by the activating-caffeine bolus, this suggests that Ca^{2+} is most likely removed from the cytoplasm by the "slow" mechanisms described in section 1.2.3.3.4. The observed increase in the magnitude of Ca^{2+} release at low activating caffeine concentrations could be a result of increased L433P sensitivity to caffeine activation, which is not presented at

higher activating caffeine concentrations due to the decreased Ca^{2+} availability resulting from the reduced ER store load.

The significant decrease in the rate at which Ca^{2+} was released from the ER following caffeine activation of RyR2 could potentially be due to the observed decrease in peak Ca^{2+} release magnitude, both of which are likely attributable to the decreased ER Ca^{2+} load. The decreased ER Ca^{2+} store load coupled with the unaltered basal cytoplasmic Ca^{2+} concentration would result in a decreased Ca^{2+} gradient from the ER to the cytoplasm, potentially decreasing the rate of calcium release from the ER. Alternatively, the L433P mutation may alter channel conductance properties, although this would not have been evident in these experiments and was not observed in previous biophysical characterisation of L433P (Jiang *et al.*, 2005). The L433P mutation did not alter the rate of Ca^{2+} removal from the cytoplasm following caffeine-evoked Ca^{2+} release compared to that of WT, suggesting under these experimental conditions, this mutation has little observable effect on Ca^{2+} extrusion or channel inactivation. However, subtle differences in channel inactivation properties pertaining to ER Ca^{2+} leak through incomplete activation may well be masked by the continued presence of caffeine following channel activation. Data presented in Chapter 5 of this thesis, which examines Ca^{2+} handling parameters in the absence of caffeine-evoked channel activation, will discuss the effects of mutations on channel inactivation in further detail. However, collectively this data is consistent with the view that L433P is not a typical gain-of-function mutation (Thomas *et al.*, 2004; Thomas *et al.*, 2005).

It is extremely important to note that the homotetrameric expression of L433P in HEK-293 cells is not truly representative of the mode of mutant RyR2 protein expression *in vivo* (Tiso *et al.*, 2001). All CPVT/ARVD2-linked RyR2 mutations are inherited in an autosomal dominant fashion (apart from a single case of compound heterozygosity, Postma *et al.*, 2005), meaning that all patients express both WT and mutant RyR2 subunits, which are likely to form heterotetramers of varying stoichiometry. To replicate this *in vitro*, HEK-293 cells were co-transfected with equimolar amounts of WT and L433P plasmid DNA, leading to the expression of both WT and L433P RyR2 monomers. Whether the distinct RyR2 monomers tetramerise to form two distinct homotetrameric channel populations or form heterotetramers of varying stoichiometry remains unknown. However, the fact that co-expression of WT+LP or WT+LPGE didn't simply result in a "diluted" cellular phenotype half way between that observed in cells expressing either

WT, LP or LPGE, suggests that heterotetramers are being expressed which present a rather complex phenotype. Furthermore, it has been demonstrated that RyR1 and RyR2 monomers, which have a certain degree of sequence divergence (~30%) are capable of heterotetramerisation (Xiao *et al.*, 2002), making it likely that recombinant RyR2 with a single amino acid substitution will form heterotetramers with WT RyR2.

Regardless of the stoichiometry of the RyR2 channels resulting from WT RyR2 and L433P co-expression, there were drastically different functional consequences compared to those observed in cells expressing homotetrameric L433P. Here, WT+LP co-expression resulted in a dramatically increased Ca^{2+} store load, the complete opposite effect of that observed in cells expressing L433P alone, and was coupled with an increase in basal cytoplasmic Ca^{2+} levels. Co-expression of WT+LP not only resulted in an increased caffeine sensitivity as demonstrated by the left-shifted caffeine activation curve (EC_{50} = 0.75 ± 0.2mM), but also significantly increased the magnitude of caffeine-evoked Ca^{2+} release across the range of activating caffeine concentrations. This is most likely a consequence of the increased ER Ca^{2+} store load, as increasing SR store load has been shown to result in Ca^{2+} transients of increased amplitude. It would be useful to determine whether SERCA activity is upregulated in cells co-expressing WT+LP, to determine whether this causes the observed increase in ER Ca^{2+}, which likely drives the increased channel sensitivity to activation and the increased magnitude of Ca^{2+} release.

The increase in peak rate of Ca^{2+} release is likely attributable to the observed increase in ER Ca^{2+} load, resulting in increased Ca^{2+} transient magnitude. Similarly, the rate of Ca^{2+} removal following caffeine-evoked Ca^{2+} release was significantly increased, perhaps driven by upregulation of Ca^{2+} extrusion mechanisms due to the increased cytoplasmic Ca^{2+} concentration, rather than a functional consequence of the presence of the L433P mutation. An alternative hypothesis could be that Ca^{2+} extrusion mechanism activity is somehow down-regulated and/or SERCA activity is upregulated, resulting in a net decrease in Ca^{2+} removal from the cell and enhanced store refilling. However, without measuring the activity of the various Ca^{2+} extrusion/sequestration proteins it is impossible to draw conclusions on the precise mechanism responsible for the increased Ca^{2+} store load and basal cytoplasmic Ca^{2+}.

Given the disparity between the basal cytoplasmic Ca^{2+} level, ER Ca^{2+} load and Ca^{2+} release parameters in cells co-expressing WT+LP compared to cells expressing L433P

or WT RyR2 homotetramers, the experimental system was scrutinised to ascertain whether these results were artefactual or biologically significant. However, after further experimentation using fresh DNA preparations, cell culture and transfection reagents, lower passage HEK cells etc., comparable results were consistently obtained from cells expressing WT+LP, confirming that the observed phenotype is functionally relevant.

The differences between the results observed in cells expressing L433P homotetramers expressing WT+LP suggest the mechanisms by which RyR2 mutations perturb RyR Ca^{2+} handling dynamics are a complex phenomenon. Co-expression of L433P with WT RyR2 did not simply result in a "diluted" response of L433P channel perturbation, but displayed a shift in the opposite direction in terms of ER Ca^{2+} store content, magnitude of caffeine-evoked Ca^{2+} release, caffeine-sensitivity etc. This provides an indication that co-transfection of HEK cells with distinct RyR2 cDNAs results in the formation of heterotetramers that convey a complex functional phenotype. This is consistent with the recent observation that heterotetrameric expression of two *SCN5A* mutations presented very different I_{Na} current characteristics to when either mutation was expressed alone (Medeiros-Domingo *et al.*, 2009). Furthermore the inheritance of two apparently benign RyR2 mutations in a composite heterozygotic manner was demonstrated to result in CPVT/ARVD2 pathogenesis (Postma *et al.*, 2005), although cellular characterisation of this particular case has not been carried out. Interestingly, although homotetrameric LP expression appeared to result in a decreased ER store load and a decrease in Ca^{2+} transient amplitude, when co-expressed with WT RyR2 the resulting phenotype was more characteristic of the gain-of-function phenotype exhibited by the majority of CPVT/ARVD2-linked mutations i.e. increased caffeine sensitivity, increased peak Ca^{2+} release.

3.4.4. G1885E alters L433P Ca^{2+} handling properties.

To determine whether the G1885E SNP had any beneficial or detrimental consequences on L433P mutant channel function, several modes of L433P and G1885E co-expression were investigated (see Figure 2.4), namely; L433P and G1885E on every subunit of the RyR2 tetramer (LPGE, homozygous '*in cis*'), L433P and G1885E on the same RyR2 construct co-expressed with WT RyR2 (WT+LPGE, heterozygous '*in cis*') which is most representative of the observed mode of inheritance in ARVD2 patients (Tiso *et al.*, 2001)

and finally, L433P co-expressed with G1885E on distinct RyR2 subunits (LP+GE, heterozygous '*in trans*'). This co-expression of LP+GE on different sub-units would have the most relevance in terms of the potential therapeutic benefits of polymorphism gene transfer in patients who inherited the disease linked-mutation.

3.4.4.1. Homotetrameric co-expression of L433P and G1885E exacerbates L433P mutant channel function.

Homotetrameric expression of G1885E on the same subunit as L433P (LPGE) appeared to modulate the severity of channel dysfunction caused by the L433P mutation. The decrease in ER Ca^{2+} levels caused by the expression of LP homotetramers was exacerbated when G1885E was expressed on the same RyR2 subunits as the mutation in a homotetrameric fashion (LPGE). A dramatic increase in basal cytoplasmic Ca^{2+} concentration was observed in cells expressing homotetrameric LPGE, which coupled with the decreased luminal Ca^{2+} concentration, could suggest a Ca^{2+} leak more severe than that caused by L433P alone.

L433P is located in the N-terminal mutation domain (Wang *et al.*, 2007) and is in close proximity to the central mutation domain (Liu *et al.*, 2005). It has been proposed that mutations in the central and N-terminal domains destabilise the channel by disrupting an interaction between these two domains (Yang *et al.*, 2006). In line with this model, it is plausible that the N-terminal L433P mutation causes unzipping from the central domain, resulting in a destabilised channel prone to Ca^{2+} leak, resulting in the decreased ER Ca^{2+} load seen here.

Although not in the central mutation domain, G1885E is in sub-domain 9 in relatively close proximity to the L433P-containing N-terminal mutation domain (between sub-domains 5 and 9) in the RyR2 3D structure (Zhang *et al.*, 2003; Wang *et al.*, 2007). The presence of G1885E on the same subunit as L433P may cause further channel destabilisation and increased Ca^{2+} leak, resulting in the observed further decrease in ER Ca^{2+} load and increased basal cytoplasmic Ca^{2+} in cells expressing LPGE homotetramers. Although it appears that homotetrameric LPGE expression resulted in sensitisation of the channel to caffeine activation (EC_{50} = 0.11 ± 0.07), this is likely to be artefactual as LPGE expression caused the abolition of the sigmoidal caffeine activation

profile exhibited by all other RyR2 mutations investigated in this study. It would appear that having both G1885E and L433P on every RyR2 subunit perturbs the activation profile of RyR2 and results in an "all-or-nothing" release of ER Ca^{2+} following caffeine activation of RyR2. This observation is corroborated by the fact that the relationship between the activating caffeine concentration and the rate of caffeine induced Ca^{2+} release was weakened in cells expressing L433P alone, but was completely abolished in cells expressing both substitutions on every subunit (Figure 3.21).

The significantly lower magnitude of Ca^{2+} release observed in response to minimal caffeine activation (0.1mM) in cells expressing LPGE compared to those expressing LP is likely due to a proportion of RyR2 channels remaining insensitive to this low concentration of caffeine, resulting in a decreased magnitude of Ca^{2+} release in response to 0.1mM caffeine. Expression of homotetrameric LPGE did not alter the rate at which Ca^{2+} was removed from the cytoplasm or released from the ER, compared to when L433P was expressed alone, suggesting that the G1885E polymorphism doesn't further alter L433P Ca^{2+} handling kinetic parameters when expressed in this manner.

3.4.4.2. Heterotetrameric WT+LPGE and LP+GE expression restores normal intracellular Ca^{2+} handling

Despite the presence of G1885E only causing subtle differences in homotetrameric L433P Ca^{2+} handling parameters, when the two substitutions were expressed in a heterotetrameric manner (WT+LPGE or LP+GE), the modulatory effect of G1885E on L433P channel function was much more pronounced.

Perhaps the most relevant heterologous RyR2 expression pattern results from the co-expression of WT+LPGE, as the ARVD2 patients expressing these substitutions were heterozygous for both L433P and G1885E, with both encoding nucleotide substitutions on the same allele (Tiso *et al.*, 2001). Co-expression of WT+LPGE caused a dramatic difference in intracellular Ca^{2+} handling compared to that observed through heterotetrameric WT+LP expression i.e. without the G1885E polymorphism. When WT+LPGE heterotetramers were expressed, despite exhibiting a significant decrease in Ca^{2+} store load compared to WT, the basal cytoplasmic Ca^{2+} levels, caffeine activation profile (EC_{50} = 1.58 ± 0.2mM) and kinetic parameters of caffeine induced Ca^{2+} release

same or separate subunits appeared to have little bearing on the extent to which G1885E modified L433P Ca^{2+} handling.

A recent study has demonstrated that the central and N-terminal domains participate in an inter-subunit interaction (Liu *et al.*, 2010). This makes it easier to envisage how G1885E alters L433P function when the two substitutions are expressed on separate subunits (LP+GE) or on all subunits (LPGE), which likely places the two substitutions in relatively close proximity in the RyR2 structure. However, this makes it harder to visualise how G1885E alters L433P function when it is expressed in a manner representative of heterozygous inheritance of both substitutions on the same allele i.e. WT+LPGE, which presumably increases the physical distance between the two substitutions. However, the fact that G1885E has previously been shown to alter RyR2 functionality when found on the opposite allele to another substitution, G1886S (Milting *et al.*, 2006), or when expressed on the same subunits as this SNP (Koop *et al.*, 2008), adds credence to the hypothesis that G1885E can modulate the functional consequences of a mutation that is not in close proximity in the RyR2 structure.

3.4.5. Chapter Summary

The data produced through the heterologous expression of WT RyR2, G1885E and L433P was comparable to that obtained in previous functional studies, suggesting that the experimental system employed here is suitable for the characterisation of these substitutions.

The results of the characterisation of L433P are consistent with the notion that L433P is not a typical gain-of-function mutation, as it exhibited decreased caffeine sensitivity, decreased ER Ca^{2+} store load and decreased kinetic parameters of ER Ca^{2+} release. However, when co-expressed with WT RyR2, L433P presented an intracellular Ca^{2+} handling phenotype more characteristic of a gain-of-function mutation.

These observed differences between LP and WT+LP expression suggests the mode of expression is critical in determining the extent of channel dysfunction and highlights the importance of characterising RyR2 mutations in a homotetrameric and heterotetrameric form, with the latter being a more faithful representation of the autosomal dominant nature of CPVT-linked RyR2 mutation inheritance.

G1885E exhibited a highly comparable intracellular Ca^{2+} handling phenotype compared to WT RyR2, both when expressed as homotetramers (GE) and heterotetramers (WT+GE). This suggests that when expressed alone, G1885E is more characteristic of a SNP, rather than a disease-linked mutation.

Although G1885E appeared functionally benign when expressed alone, this SNP was shown to alter the functional consequences of L433P co-expression. This provides the first documented evidence that a common RyR2 SNP can modulate the severity of mutant RyR2 Ca^{2+} handling dysfunction.

Furthermore, G1885E was shown to modulate the effects of L433P to varying degrees depending on the precise mode of co-expression. Homotetrameric expression of LPGE appeared to exacerbate the decrease in ER Ca^{2+} store load caused by homotetrameric LP expression, but had little effect on intracellular Ca^{2+} handling parameters. Conversely, heterotetrameric expression of WT+LPGE or LP+GE appeared to restore the majority of intracellular Ca^{2+} handling parameters that were perturbed by WT+LP

expression, to WT levels. This suggests that heterotetrameric co-expression of G1885E may offer protective benefits against dysfunctional Ca^{2+} handling caused by WT+LP expression.

However, the work detailed in this chapter does not provide a clear mechanism by which the co-expression of WT+LPGE, representative of the ARVD2-assoicated genotype *in vivo*, results in a disease-phenotype. Recent reports have demonstrated that CPVT-linked mutations alter basal and post-activation cytoplasmic Ca^{2+} flux and display subtle alterations in basal Ca^{2+} handling (Jiang *et al.*, 2002; Liu *et al.*, 2006; Fernandez-Velasco *et al.*, 2009). In light of this, the next chapter of this thesis will investigate whether there are any subtle, underlying alterations in intracellular Ca^{2+} handling and whether these can explain the differences in agonist-evoked Ca^{2+} release parameters observed here.

Chapter 4

Characterisation of the effects of L433P and G1885E on cytoplasmic Ca^{2+} flux.

4.1 Introduction

4.1.1. Myocyte Ca^{2+} homeostasis

In order to maintain the relatively low level of cytoplasmic Ca^{2+} (~100nM) in the cardiac myocyte, an extensive network of interplaying Ca^{2+} channels, pumps and exchangers work together to move Ca^{2+} ions in and out of the cell and it's intracellular Ca^{2+} compartments (Bers, 2002; Dibb *et al.*, 2007). Even though the level of cytoplasmic Ca^{2+} appears to remain relatively constant during diastole, this apparent steady state is maintained by equilibrium in the influx and efflux of Ca^{2+} into and out of the cytoplasm during the period between CICR events (Figure 4.1, Piacentino *et al.*, 2003). Even at peak cytoplasmic Ca^{2+} concentrations (~1-2μM), the extracellular Ca^{2+} concentration (~1mM) is much greater, creating a steep inward Ca^{2+} gradient *(Schaub et al., 2006).* Cells hydrolyse ATP to generate the energy required to extrude Ca^{2+} from the cell against the direction of the Ca^{2+} gradient through PMCA, whereas the NCX utilises the

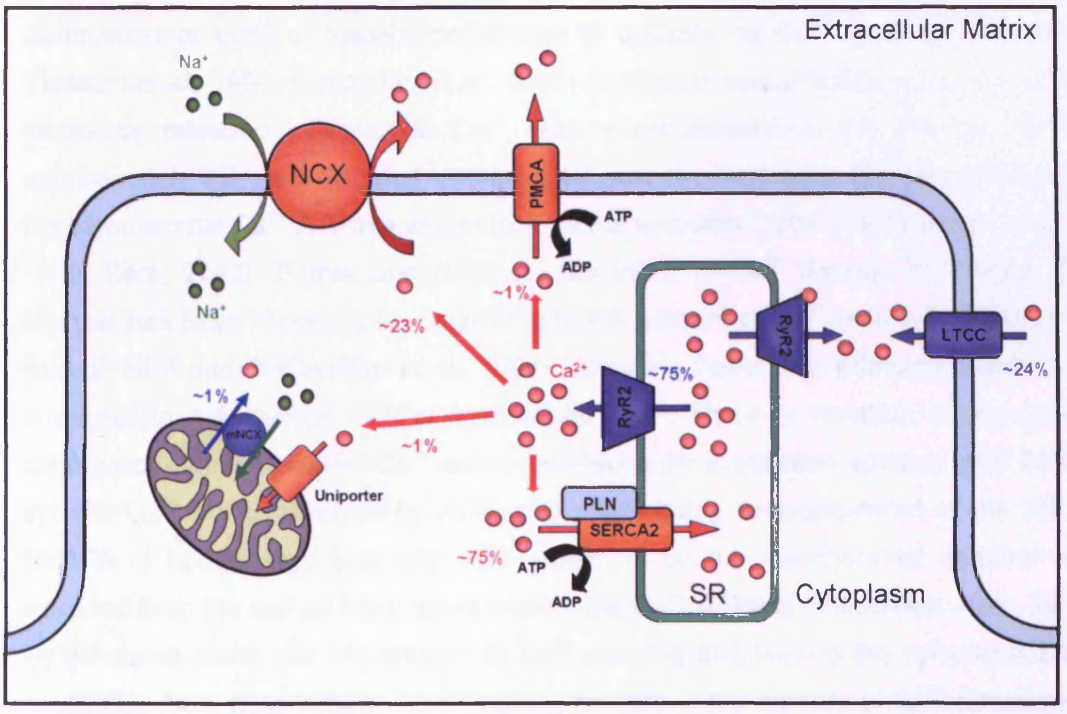

Figure 4.1. Proteins involved in CICR and maintaining myocyte Ca^{2+} homeostasis. *Inotropic mechanisms and their approximate relative contribution to increasing cytoplasmic Ca^{2+} levels in human myocytes are indicated in blue. Lusitropic mechanisms and their relative contribution to removing cytoplasmic Ca^{2+} are indicated in red (Piacentino et al., 2003). Under resting conditions, the net influx and efflux of Ca^{2+} are in equilibrium.*

electrochemical Na^+ gradient to drive Ca^{2+} removal from the cell *(3 Na^+ ions: 1 Ca^{2+} ion, Berridge et al., 2000; Laude & Simpson, 2009).* It is imperative that myocyte Ca^{2+} release and extrusion mechanisms work in a highly orchestrated manner to ensure that intracellular Ca^{2+} homeostasis and correct Ca^{2+} cycling are maintained (Dibb et al., 2007), to ensure correct functioning of the heart on a beat-to-beat basis. Abnormal basal Ca^{2+} cycling and perturbation of intracellular Ca^{2+} homeostasis have implications in terms of cardiac pathology which will be discussed later in the chapter (section 4.1.3).

4.1.2 Basal Ca^{2+} cycling

In order to lower cytoplasmic Ca^{2+} concentration following CICR, several extrusion pathways come into effect; namely SR and sarcolemmal Ca^{2+}-ATPases, sarcolemmal NCX and the mitochondrial uniporter (Bers, 2008). Selective inhibition of the activity of each of these Ca^{2+} handling proteins allowed the elucidation of the approximate contribution of each of these mechanisms to cytoplasmic Ca^{2+} removal (Figure 4.1, (Bassani *et al.*, 1994; Piacentino *et al.*, 2003). In mouse myocytes approximately 90% of transiently released cytoplasmic Ca^{2+} was re-sequestered in the SR by SERCA, approximately 9% was extruded through NCX and the remaining 1% was removed by the sarcolemmal Ca^{2+}-ATPase and mitochondrial uniporter ('slow mechanisms', Li *et al.*, 1998; Bers, 2002). Rather unsurprisingly the influx of Ca^{2+} through the L-type Ca^{2+} channel has been shown to be equivalent to the amount of Ca^{2+} removed from the cell through NCX and PMCA (Diaz *et al.*, 2004), indicating that under resting conditions there is negligible net change in total intracellular Ca^{2+}. There is variation in the relative contributions of cytoplasmic Ca^{2+} extrusion mechanisms between species, with 23% of systolic Ca^{2+} being removed by NCX and ~75% being re-sequestered in the SR via SERCA in human myocytes and ~2% taken up by the mitochondrial uniporter and extruded from the cell by the plasma membrane Ca^{2+} ATPase (Piacentino *et al.*, 2003). By the same token that the amount of Ca^{2+} entering and leaving the cytoplasm are in equilibrium from beat-to-beat, under resting conditions the amount of Ca^{2+} sequestered in the SR following CICR is comparable to the amount that was released during the previous CICR event (Trafford *et al.*, 2001). Together this provides a mechanism by which intracellular Ca^{2+} homeostasis is maintained, allowing the myocyte to achieve a constant resting state between each heart beat.

However, this assumes that the myocyte is subject to consistent conditions, which is not always the case i.e. following β-AR stimulation during periods of physical or emotional stress, in which a temporary amplification of Ca^{2+} fluxes is evident (Bers, 2008). In such situations, the presence of a compensatory negative feedback mechanism is apparent, which is briefly described here. β-AR stimulation causes an increase in the uptake of Ca^{2+} into the SR though PKA-mediated dissociation of PLB from SERCA (Periasamy & Huke, 2001). The PKA-mediated increase in Ca^{2+} influx through the L-type Ca^{2+} channel, coupled with the increased SR Ca^{2+} content, results in a larger systolic Ca^{2+} transient during CICR (Bers, 2002). The increased systolic Ca^{2+} transient amplitude results in a greater increase in cytoplasmic Ca^{2+} concentration. Consequently, this increases the amount of Ca^{2+} extruded from the cell via the NCX and results in a smaller influx of "trigger" Ca^{2+} due to increased Ca^{2+}-dependent inactivation of the L-type Ca^{2+} channel (Dibb, 2007). Collectively, this results in a net increase in the amount of Ca^{2+} removed from the cell and consequently reduces the amount of subsequent SR Ca^{2+} uptake. This decrease in SR Ca^{2+} content results in a slightly smaller systolic Ca^{2+} transient than that of the previous CICR event, causing a slight decrease in Ca^{2+} extrusion by NCX and a slight increase in inward L-type Ca^{2+} current. This auto-regulative process continues until a steady state of intracellular Ca^{2+} and SR Ca^{2+} content is re-established (Trafford *et al.*, 2001; Dibb *et al.*, 2007).

4.1.3. Chronic Ca^{2+} flux imbalance in cardiac pathology

In HF, it is widely accepted that the altered characteristics of the systolic Ca^{2+} transient are pathogenic, with several HF models demonstrating a significant decrease in systolic Ca^{2+} transient magnitude (Piacentino *et al.*, 2003). Selective inhibition of several Ca^{2+} extrusion mechanisms demonstrated that in a model of left ventricular hypertrophy, the rate of Ca^{2+} uptake into the SR by SERCA was decreased and the rate of Ca^{2+} removal from the myocyte through NCX and the sarcolemmal Ca^{2+}-ATPase was increased (Diaz *et al.*, 2004), an observation that has been described by several groups (Bassani *et al.*, 1994; Piacentino *et al.*, 2003; Dibb *et al.*, 2007). Ultimately, this net Ca^{2+} efflux resulted in a decrease in SR Ca^{2+} content, accounting for the observed decrease in systolic transient amplitude observed in HF (Bers, 2006).

Although the mechanisms by which they do so remain contentious, it is generally reported that gain-of-function CPVT/ARVD2-linked RyR2 mutations increase channel open probability resulting in diastolic SR Ca^{2+} leak or spontaneous Ca^{2+} release (Jiang *et al.*, 2005; Tester *et al.*, 2007; Lehnart *et al.*, 2008; Marjamaa *et al.*, 2009b; Tateishi *et al.*, 2009), suggesting basal Ca^{2+} handling dysfunction. Although the majority of this leaked Ca^{2+} would be re-sequestered by SERCA (Piacentino *et al.*, 2003), the increased cytoplasmic Ca^{2+} levels resulting from this diastolic leak could increase the net Ca^{2+} efflux from the myocyte through increased NCX activity and increased L-type Ca^{2+} channel inactivation. This could potentially result in the decreased steady state SR Ca^{2+} levels observed in CPVT mouse models (Fernandez-Velasco *et al.*, 2009; Uchinoumi *et al.*, 2010) or through the heterologuous expression of RyR2 containing CPVT/ARVD2-linked mutations (Jiang *et al.*, 2004; Jiang *et al.*, 2005).

It has been demonstrated in single channel experiments that increased RyR2 open probability alone is not sufficient to maintain diastolic Ca^{2+} leak (Dibb *et al.*, 2007), presumably due to the adaptation of SR Ca^{2+} levels to a lower steady state through the mechanisms described above (section 4.1.2). However, the maintenance of increased SR Ca^{2+} content, such as that which occurs during PKA-mediated dissociation of PLN from SERCA during β-AR stimulation (Periasamy *et al.*, 2008), results in sustained diastolic Ca^{2+} leak between systolic Ca^{2+} transients (Dibb *et al.*, 2007). It is the persistence of this altered SR-to-cytoplasmic Ca^{2+} flux that can lead to DADs through increased NCX activity, potentially resulting in arrhythmia. Furthermore, the dependence of this persistent diastolic Ca^{2+} leak on increased SR Ca^{2+} content corroborates the fact that CPVT/ARVD2 mutations only result in arrhythmia following β-AR stimulation when SERCA activity and SR Ca^{2+} levels are increased (Leenhardt *et al.*, 1995; Priori *et al.*, 2001; 2002b).

Interestingly, the comprehensive functional characterisation of the R4497C mutation has demonstrated that this mutation results in subtle alterations in basal Ca^{2+} cycling, (Jiang *et al.*, 2002; Liu *et al.*, 2006; Fernandez-Velasco *et al.*, 2009) which are exacerbated following β-AR stimulation. This suggests that underlying alterations in basal cytoplasmic Ca^{2+} handling are likely to originate from the diastolic Ca^{2+} leak caused by this mutation, providing a rationale for the further investigation into the alterations in the subtleties of basal Ca^{2+} cycling caused by RyR2 mutations.

4.1.4. Effects of altered basal Ca^{2+} signal variability in heterologous systems

Although there is little published data detailing the investigation of basal Ca^{2+} signal variability in heterologous systems expressing RyR2, a handful of studies have demonstrated that subtle variations in basal cytoplasmic Ca^{2+} variability have profound cellular consequences.

The stable expression of RyR2 in CHO cells was shown to result in an increase in cell death and was associated with an increase in resting Ca^{2+} flux, manifesting as an increase in resting Ca^{2+}-dependent signal variability or 'noise', set against a background of normal cytoplasmic Ca^{2+} concentration (Figure 4.2, George *et al.*, 2003b). Interestingly, the co-expression of FKBP12.6 with RyR2 was shown to decrease the level of Ca^{2+} flux, restoring the level of cell viability to those observed in untransfected cells, implicating the level of SR-to-cytoplasmic Ca^{2+} flux in cell death.

Relative signal variability (RSV) is a measure of relative change in Ca^{2+} dependent signal variability before and after agonist-evoked RyR2 channel activation in the same cell (George *et al.*, 2006). *George et al* subsequently used this method of signal variability or "noise" analysis to examine the effects of CPVT-linked mutations (R4497C and N4104K, George *et al.*, 2007b) on basal and post-activation cytoplasmic Ca^{2+} fluxes. Using fluorescence energy transfer (FRET) analysis, they demonstrated that CPVT-linked RyR2 mutations caused destabilisation of an int ra-RyR2 interaction following agonist-activation of the channel, which was accompanied by an increase in Ca^{2+}-dependent signal RSV. Given that the disruption of this interaction is proposed to result in increased Ca^{2+} leak from the ER/SR, it is likely that the increase in Ca^{2+} leak and subsequent extrusion or reuptake is responsible for this increase in Ca^{2+} signal variability.

Together these data suggest that the analysis of subtle variations in basal and post activation Ca^{2+}-dependent signal variability can provide mechanistic insights into altered RyR2 mutant channel function.

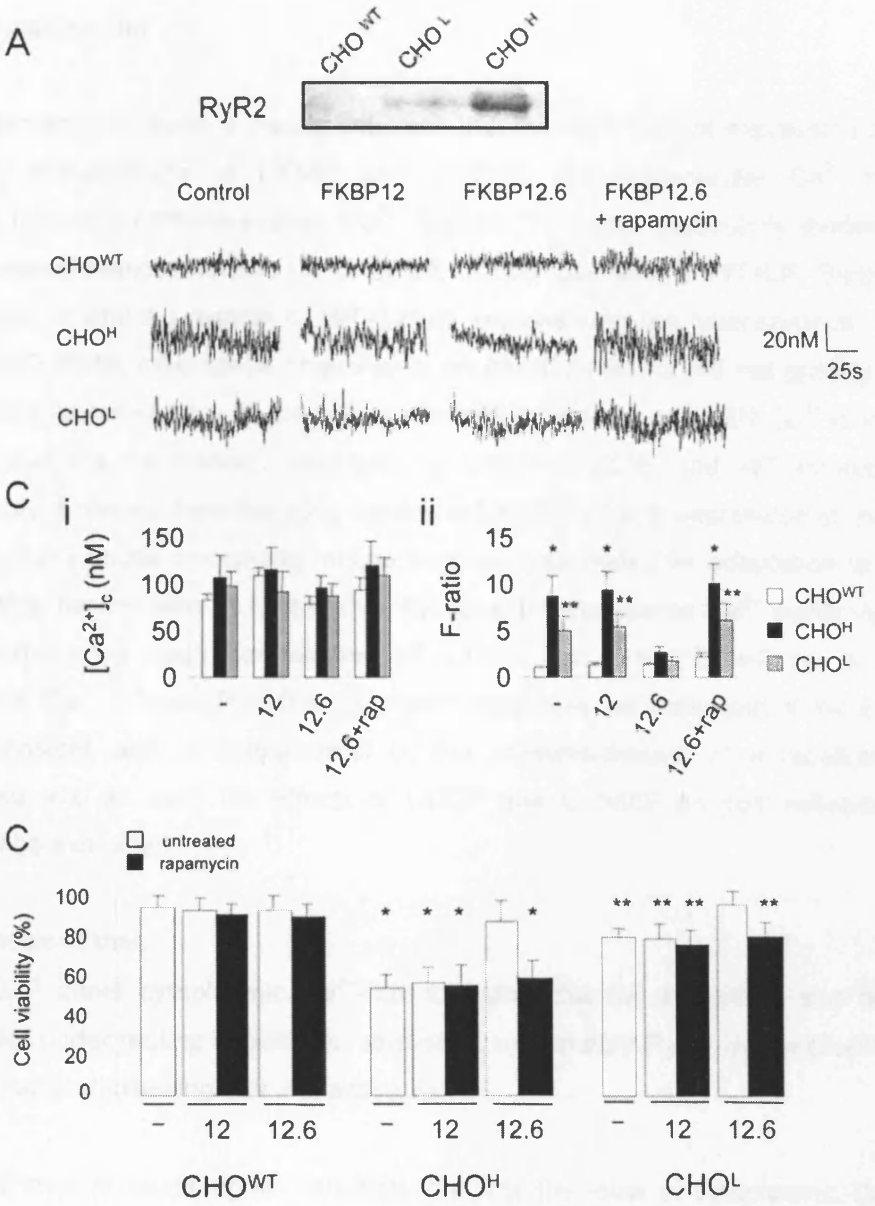

Figure 4.2. Increased Ca^{2+} signal variability associated with RyR2 expression results in decreased cell viability. *CHO cell lines stably expressing discrete levels of hRyR2 were generated, confirmed by western blot analysis and designated CHO^{WT} (untransfected CHO cells), CHO^{L} (low levels of relative RyR2 expression) and CHO^{H} (high levels of relative RyR2 expression), as shown in panel A. Resting Ca^{2+} dependent Fluo3 signal intensity was measured in each cell line with and without transient FKBP or FKBP12.6 expression as shown in panel B. Rapamycin (5μM, 15 hour exposure) was used to dissociate FKBP12.6. Data presented in panel C shows that despite comparable resting cytoplasmic Ca^{2+} levels (i), expression of RyR2 increased the level of cytoplasmic Ca^{2+} signal variability, which was restored to normal levels following FKBP12.6 interaction (F-ratio, ii). In panel C, * represents $p<0.005$ compared to CHO^{WT} and CHO^{L} cells, ** represents $p<0.001$ compared to CHO^{WT} and CHO^{H} cells. The increase in F-ratio resulting from RyR2 expression and absence of FKBP12.6 interaction were associated with decreased cell viability, as determined by Alamar Blue cell viability assays, shown in panel D (* represents $p<0.005$ compared to CHO^{WT} and CHO^{L} cells and ** represents $p<0.01$ when compared with CHO^{WT} and CHO^{H} cells. From George, (2003b).*

4.1.5. Chapter aims

Data presented in Chapter 3 clearly indicates that the recombinant expression of RyR2 containing combinations of L433P and G1885E alter intracellular Ca^{2+} handling dynamics following caffeine-evoked Ca^{2+} release. This was particularly evident when cells expressed homotetrameric LP or LPGE or heterotetrameric WT+LP. Surprisingly, the heterotetrameric expression of WT+LPGE, representing the heterozygous mode of L433P and G1885E inheritance observed in an ARVD2 patient, did not grossly perturb Ca^{2+} handling parameters, with the notable exception of decreasing ER Ca^{2+} levels. This suggests that the mechanism underpinning L433P-G1885E and WT co-expression pathogenicity is distinct from the other modes of L433P/G1885E expression or manifests through a more subtle underlying mechanism such as defective adaptation to altered Ca^{2+} handling parameters. In light of this, the level of cytoplasmic Ca^{2+} signal variability in cells expressing each combination of L433P and G1885E will be examined. Furthermore, Ca^{2+} removal from the cytoplasm comprises the major part of the ER Ca^{2+}-release transient and is instrumental in the reestablishment of intracellular Ca^{2+} homeostasis and as such the effects of L433P and G1885E on post-activation Ca^{2+} cycling will be examined.

It is hypothesised that:

- L433P alters cytoplasmic Ca^{2+}-flux following channel activation, and has little effect under resting conditions, consistent with mutant RyR2 dysfunction tending to manifest following channel activation.

- The level of basal signal variability predicts the level of cytoplasmic Ca^{2+} flux following channel activation, and this coupling is modified by L433P.

- There is variation in the level of cytoplasmic Ca^{2+} flux during re-establishment of Ca^{2+} homeostasis following channel activation and this is perturbed by L433P.

- G1885E has little effect on basal and post-activation cytoplasmic Ca^{2+} flux when expressed alone, but modulates the level of Ca^{2+} flux in cells expressing L433P.

- Alterations in cytoplasmic Ca^{2+} flux may reconcile the alterations in Ca^{2+} handling parameters caused by L433P described in Chapter 3.

4.2. Methods

4.2.1. Ca^{2+}-imaging data collection

The same Ca^{2+} imaging data set as that described in Chapter 3 was used to investigate the effects of expressing combinations of WT, L433P and G1885E on the relative levels of cytoplasmic Ca^{2+} signal variability as that described in Chapter 3. Analysis of Ca^{2+} signal variability was only carried out on cells that exhibited characteristic Ca^{2+} transients and did not exhibit spontaneous Ca^{2+} oscillations prior to caffeine-evoked channel activation which will be discussed in Chapter 5 (see Figure 3.1.6). Together, this allowed direct comparison of the results obtained from the noise analysis experiments detailed in this chapter with the observations following the measurement of intracellular Ca^{2+} handling parameters following caffeine-evoked Ca^{2+} release, as detailed in Chapter 3.

4.2.2. Calculation of SV and SVm

There are several commonly used measures of signal variation in Ca^{2+} signal intensity including RSV, F-ratio and the coefficient of variation (CoV), all of which require a variance-based component. Previous work from this laboratory has demonstrated that variance based measurements of signal variability are not appropriate for determining the level of Ca^{2+}-dependent signal variation in these experiments (Fry, 2008).

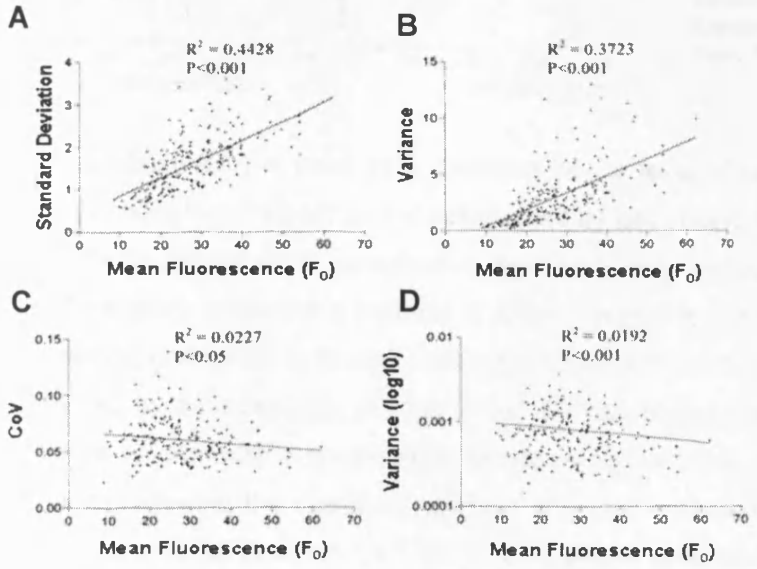

Figure 4.3. Correlation between mean signal intensity and variance based noise-analysis parameters. *Increased basal signal intensity was associated with an increase in standard deviation and variance. This positive relationship was abolished by normalising variance to the mean signal intensity (CoV) or log transforming the data prior to calculating the variance. Adapted from Fry, (2008)*

Both standard deviation and variance of Ca^{2+}-dependent signal intensity were highly dependent on the mean level of Ca^{2+}-dependent fluorescence (Figure 4.3A-B), indicating that these measurements of signal variability would not account for differential Ca^{2+} indicator loading nor variation in cytoplasmic Ca^{2+} levels, which inevitably occur in single cell Ca^{2+} imaging experiments. Although the effect of mean signal intensity on these values was mitigated by normalisation to the mean signal intensity, (coefficient of variance, CoV, Figure 4.3C) or by log transformation of the data (Figure 4.3D), these measurements were also highly biased by the gradient or 'drift' of the signal trace (Figure 4.4A-B), which was another inevitable factor in Ca^{2+} imaging experiments. In light of this CoV and variance (Log10) were deemed unsuitable for the analysis of Ca^{2+}-depedent signal variability in these experiments (Figure 4.4C-D). Similarly, the F-ratio was unsuitable for analysis of Ca-dependent signal variability in these experiments, due to its derivation from signal variance.

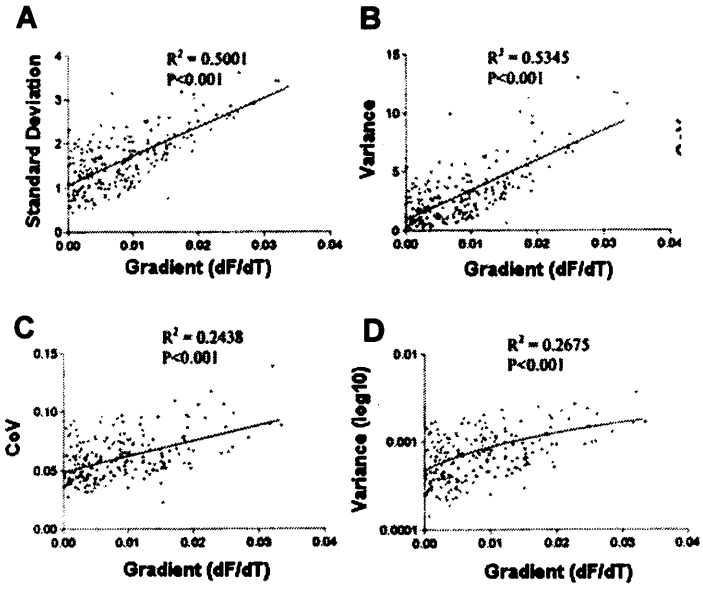

Figure 4.4. Correlation between signal gradient and variance based noise-analysis parameters. *Increased basal signal gradient was associated with an increase in standard deviation, variance, CoV and log transformed variance. Adapted from Fry, (Fry, 2008).*

Signal variability (SV) is used as a measure of the level of variability or "noise" in the Ca^{2+} dependent Fluo3 signal and is determined by calculating the sum of the magnitude of the differences between consecutive signal intensity measurements (George *et al.*, 2006). This group utilised this method of noise analysis to compare the levels of "noise" under resting conditions to those following channel activation by calculating RSV and is represented by a percentage change in SV. SV can be normalised to the length of the time series to generate a single value representing the level of signal noise in a given time series, allowing the direct comparison of SV of data collected over different time periods. The method by which Ca^{2+} SV is calculated is detailed in Figure 4.5.

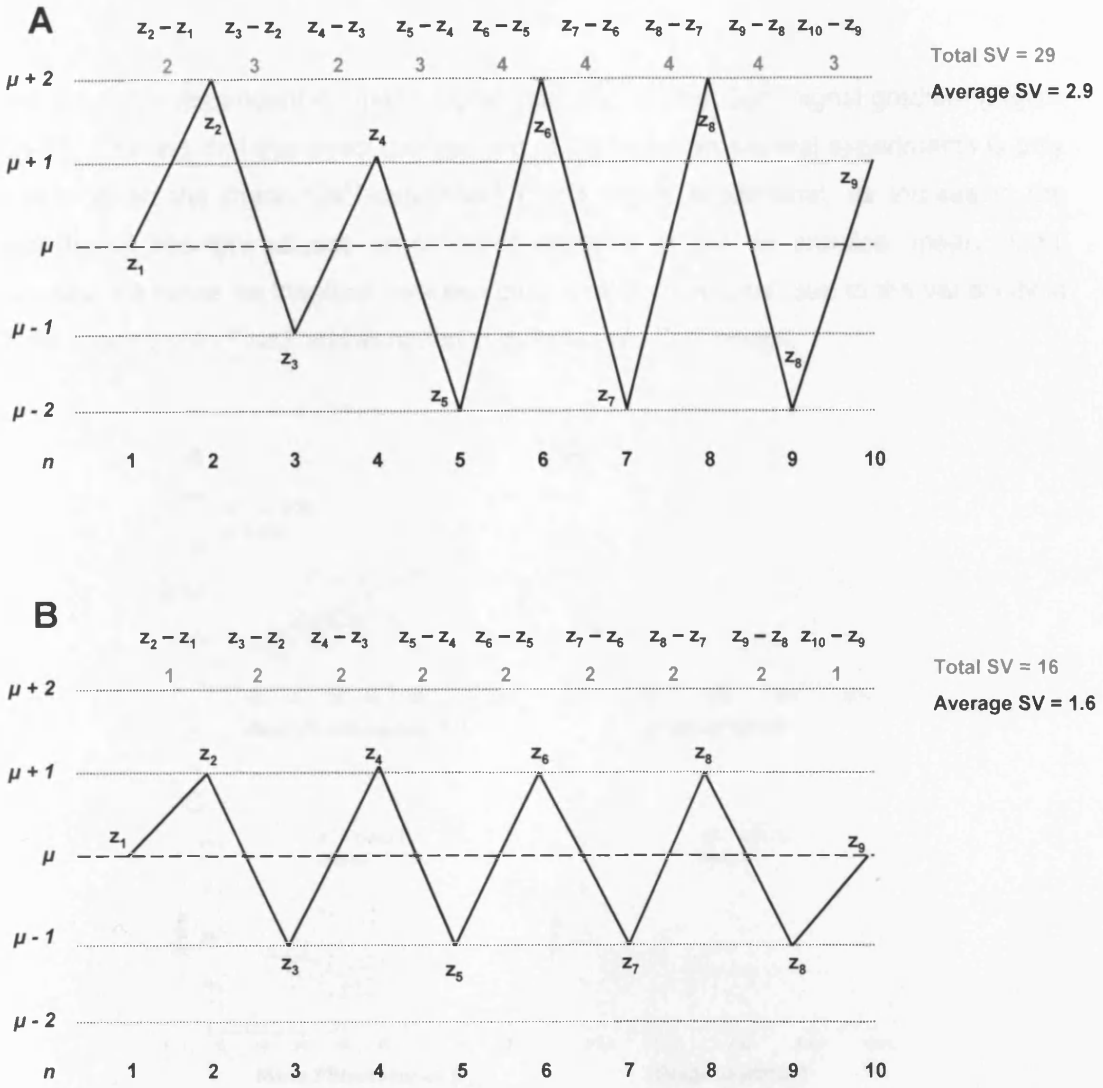

C

$$SV = \sum_{n=1}^{n=k-1} | Z_n - Z_{n-1} |$$

For k values Z_1, Z_2, Z_3... ... Z_k

Figure 4.5. Determining Ca^{2+}-dependent Fluo3 signal variability (SV). *Total signal variability (SV) was determined by measuring the average magnitude of the difference between consecutive data points i.e. $(n_2 - n_1) + (n_3 - n_2) + \ldots + (n_{10} - n_9)$. The average SV for a given series was determined by dividing the total SV by the number of data points in the series. Panel A illustrates an example of a series exhibiting relatively high SV compared to that illustrated in panel B. SV is represented by the formula described in panel C.*

However, SV is dependent on mean signal intensity, but not Ca^{2+} signal gradient (Figure 4.6A-B), meaning that the direct comparison of SV between several experiments is only possible when the mean Ca^{2+}-dependent Fluo3 signal is identical, as increasing the mean signal intensity causes an inherent increase in SV. In practice, mean signal intensities will never be identical between cells and/or coverslips, due to the variability in cellular loading with Fluo3 and variation in cytoplasmic Ca^{2+} levels.

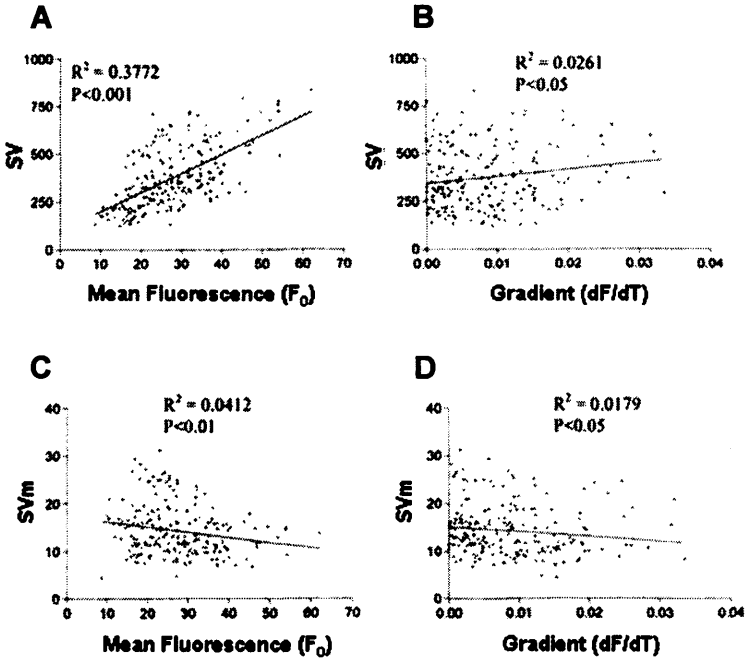

Figure 4.6. SV normalised to mean signal intensity (SVm) is independent of mean fluorescence and basal signal gradient. *SV is dependent on mean signal intensity and basal signal gradient (panel A and B), whereas SVm is independent of mean signal intensity and basal gradient (C and D). Adapted from Fry, (2008).*

To circumvent this problem, the average SV is normalised to the mean signal intensity (SVm) to take into account differential Ca^{2+} indicator loading and the subsequent necessity to record data using different PMT voltage gain to alter Fluo3 signal intensity. SVm is independent of both mean signal intensity and the Ca^{2+}-dependent signal gradient (Figure 4.6C-D) and is a robust indicator of Ca^{2+}-dependent signal variability in these experiments.

The level of basal SVm was determined for the period 30 seconds prior to the addition of caffeine to the cells. In order to examine whether SVm varied following caffeine-evoked

Ca^{2+} release (as intracellular Ca^{2+} concentration returned to a steady state), the post-activation data was divided into groups representing the period immediately after caffeine activation (early, 0-30 seconds post-activation), an intermediate period (middle, 30-60 seconds post-activation) and the final section when Ca^{2+}-dependent signal intensity was approaching basal levels (late, 60-90 seconds post-activation), as demonstrated in Figure 4.7. The sub-division of the post activation time series was carried out to determine whether there were changes in the level of cytoplasmic Ca^{2+} flux from peak caffeine-evoked Ca^{2+} release to the restoration of a steady-state representing a relative equilibrium of the movement of Ca^{2+} ions into and out of the cytoplasm.

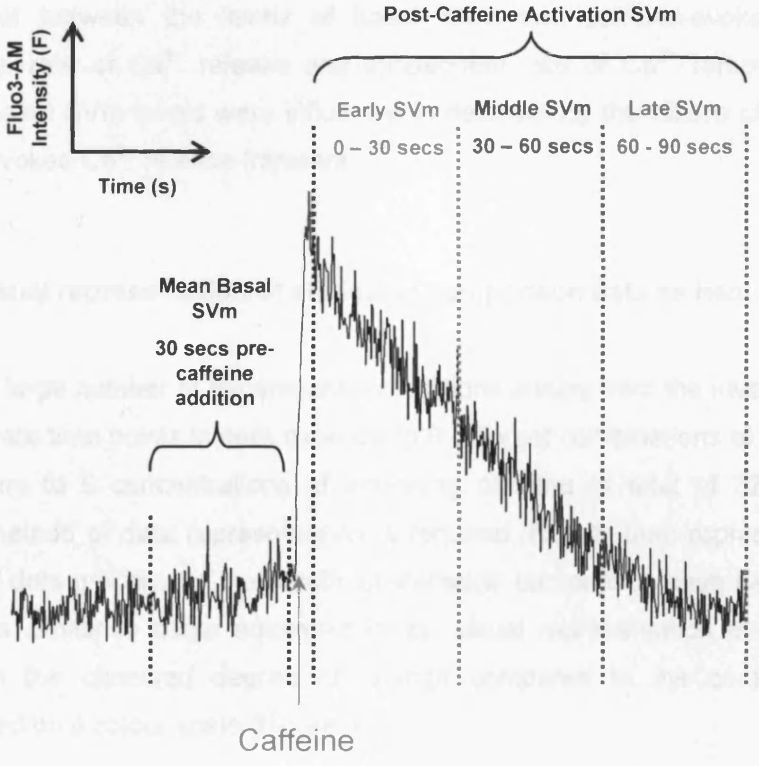

Figure 4.7. Division of post-activation intracellular Ca^{2+} recovery period into early, middle and late phases. *To determine whether the level of SVm differed over the period in which cytoplasmic Ca^{2+} levels returned to a steady, resting state the post-activation data was split into three distinct groupings representing the period immediately after peak signal intensity was reached (Early, 0-30 sec post-activation, red), an intermediate period (Middle, 30-60 sec post-activation, blue) and the period when intracellular Ca^{2+} was approaching the steady resting state (Late, 60-90 sec post-activation, green). The mean basal SVm was determined for the 30 second period prior to caffeine-evoked activation of RyR2 to allow direct comparison of SVm levels between each time grouping.*

4.2.3. Examination of the relationship between basal and post-activation SVm

To ascertain whether the level of RyR2 activation and the magnitude of subsequent Ca^{2+} release influenced the level of post-activation Ca^{2+} signal variability, linear regression analysis was carried out on caffeine concentration and SVm at each of the post-activation time points. Regression analysis was also carried out to identify whether relationships existed between the level of basal SVm and the level of SVm following caffeine activation (0.1-10mM), to determine whether L433P or G1885E altered the coupling between basal and post-activation SVm. Linear regression analysis was also carried out between the levels of basal SVm and caffeine-evoked Ca^{2+} release magnitude, rate of Ca^{2+} release and subsequent rate of Ca^{2+} removal to determine whether basal SVm levels were influential in determining the nature of the subsequent caffeine-evoked Ca^{2+} release transient.

4.2.4. Visual representation of statistical comparison data as heat maps

Given the large number of experimental conditions arising from the investigation of SVm at 4 separate time points in cells expressing 9 different combinations of RyR2, subjected to exposure to 9 concentrations of activating caffeine (a total of 324 conditions), a suitable method of data representation is required. Rather than representing the large amount of data graphically, the results of statistical comparison have been presented as heat maps similar to those employed in the visual representation of DNA microarray data, with the observed degree of change compared to the control group being represented on a colour scale (Figure 4.8).

To generate the heat map, the mean SVm value at a given time point and activating caffeine concentration was compared to the corresponding mean SVm value in the control group i.e. WT, to determine whether there was a significant difference between the two SVm values. The observed difference between SVm in cells expressing mutant RyR2 was expressed as a percentage change compared to the level of SVm observed in cells expressing WT RyR2. If statistically significant ($p < 0.05$), this percentage change in SVm was allocated a colour according to the scale illustrated in Figure 4.8. Statistical comparison of relationship gradients observed when comparing the linear relationships between basal and post-caffeine activation SVm were also summarised using heat

maps, through statistical comparison of linear regression gradients. Only statistically significant differences were illustrated on the heat maps ($p < 0.05$).

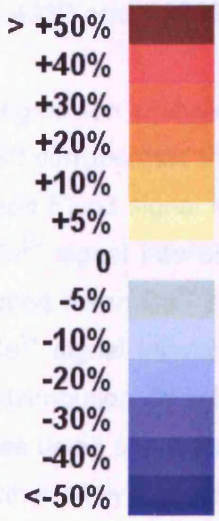

Figure 4.8. Heat map colour scale. *The percentage change between SVm or linear regression gradient was represented in heat maps according to the heat map colour scale bar. The white-to-red transition represents an increase in SVm or linear regression gradient, whereas the white-to-blue transition represents a decrease.*

Only statistically significant data ($p < 0.05$) is indicated on heat maps and white tabular cells indicate that there was no significant difference between the compared values.

4.3. Results

4.3.1. L433P and G1885E do not grossly perturb basal signal variability.

Linear regression analysis of SVm data produced in HEK cells expressing recombinant WT RyR2 corroborated the findings of *Fry et al (2008)*, in that SVm was independent of both mean Fluo3 signal intensity and the basal Fluo3 signal gradient (Figure 4.9). The mean Ca^{2+} signal intensity-independence of SVm was evident for both raw and log-transformed mean Ca^{2+} signal intensity data, however, only data produced when mean basal Ca^{2+} signal intensity was log-transformed prior to linear regression exhibited a normal distribution. In light of this, to allow statistical comparison of mean basal signal intensities using parametric tests, only Log transformed basal Ca^{2+} signal intensity data were further analysed and described in this chapter.

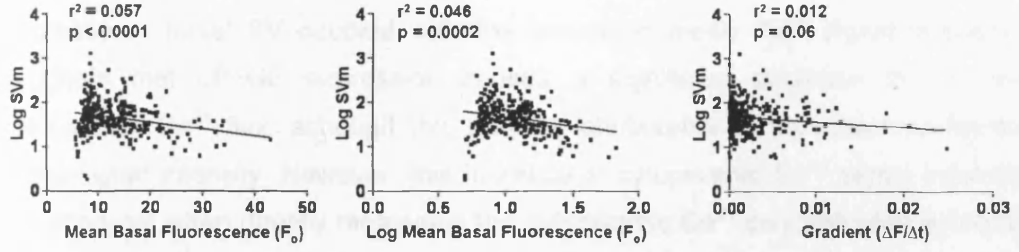

Figure 4.9. SVm is independent of mean basal signal intensity and signal gradient. *Linear regression analysis of data produced in HEK cells expressing recombinant RyR2 demonstrated that SVm was independent of mean signal intensity (both untransformed and log transformed data) and basal Ca^{2+} signal gradient. Data was collected from 299 cells.*

Representative traces of basal Ca^{2+} levels for the 30 second period prior to channel activation in untransfected HEK cells and those expressing RyR2 are illustrated in Figure 4.10 and basal signal intensity, SV and SVm values are summarised in Figure 4.11. Consistent with the measurement of absolute basal cytoplasmic Ca^{2+} levels described in section 3.3.8, cells expressing recombinant RyR2 exhibited an increase in basal Ca^{2+}-dependent Fluo3 signal intensity compared to that observed in untransfected HEK cells (Figure 4.11A, $p < 0.001$). This increase in mean signal intensity was coupled with a significant decrease in basal SV (Figure 4.11B, $p < 0.001$), which manifested as a decrease in basal SVm ($p < 0.05$, Figure 4.11C) in cells expressing recombinant RyR2. Also consistent with the measurement of basal Ca^{2+} levels, homotetrameric expression of WT RyR2, GE or LP all exhibited comparable mean basal Ca^{2+}-dependent signal

intensities (Figure 4.11A) and comparable basal SVm (Figure 4.11C), indicating these substitutions had little effect on basal Ca^{2+} flux. Despite homotetrameric LPGE expression causing a significant increase in mean basal signal intensity (Figure 4.11A), which could pertain to increased ER Ca^{2+} leak, an equivalent SVm was observed (Figure 4.11C) due to an observed increase in basal SV (Figure 4.11B). This suggests that although homotetrameric LPGE expression increases basal Ca^{2+} flux, this increase is not apparent when taking into account the increase in resting cytoplasmic Ca^{2+} levels. The same observation was made in cells expressing WT+LP or WT+LPGE heterotetramers, which exhibited an increase in resting signal intensity but an equivalent cytoplasmic Ca^{2+} SVm levels compared to WT RyR2 (Figure 4.11A and C).

Conversely, heterotetrameric LP+GE expression resulted in a significant increase in mean basal signal intensity ($p<0.001$, Figure 4.11A), indicating a higher level of cytoplasmic Ca^{2+}, which was coupled with a significant decrease in the level of cytoplasmic Ca^{2+} SVm (Figure 4.11C). This decrease in SVm was attributed to a decrease in basal SV coupled with the increased mean Ca^{2+} signal intensity. This suggests that LP+GE expression causes a significant decrease in the level of cytoplasmic Ca^{2+} flux, although this may be attributable to the observed increase in basal signal intensity. However, this increase in cytoplasmic Ca^{2+} signal intensity was not apparent when directly measuring the cytoplasmic Ca^{2+} concentration as detailed in section 3.3.8, suggesting that the observed increase may be artefactual and possibly due to other factors. i.e. differential Ca^{2+} indicator loading.

G1885E only appeared to alter L433P mean basal signal intensity or basal SVm, when co-expressed as heterotetrameric LP+GE and not when expressed on the same RyR2 monomers as the mutation (LPGE or WT+LPGE, Figures 4.10 and 4.11). However, the mean signal intensity and SVm levels in cells expressing LP+GE were not significantly different from those observed in cells co-expressing WT+LP or WT+LPGE, suggesting that G1885E only exerts a modest effect on L433P basal Ca^{2+} cycling.

In summary, L433P and/or G1885E did not cause gross perturbation of the level of basal cytoplasmic Ca^{2+} flux in HEK cells expressing recombinant RyR2, when accounting for mean cytoplasmic Ca^{2+} levels under resting conditions.

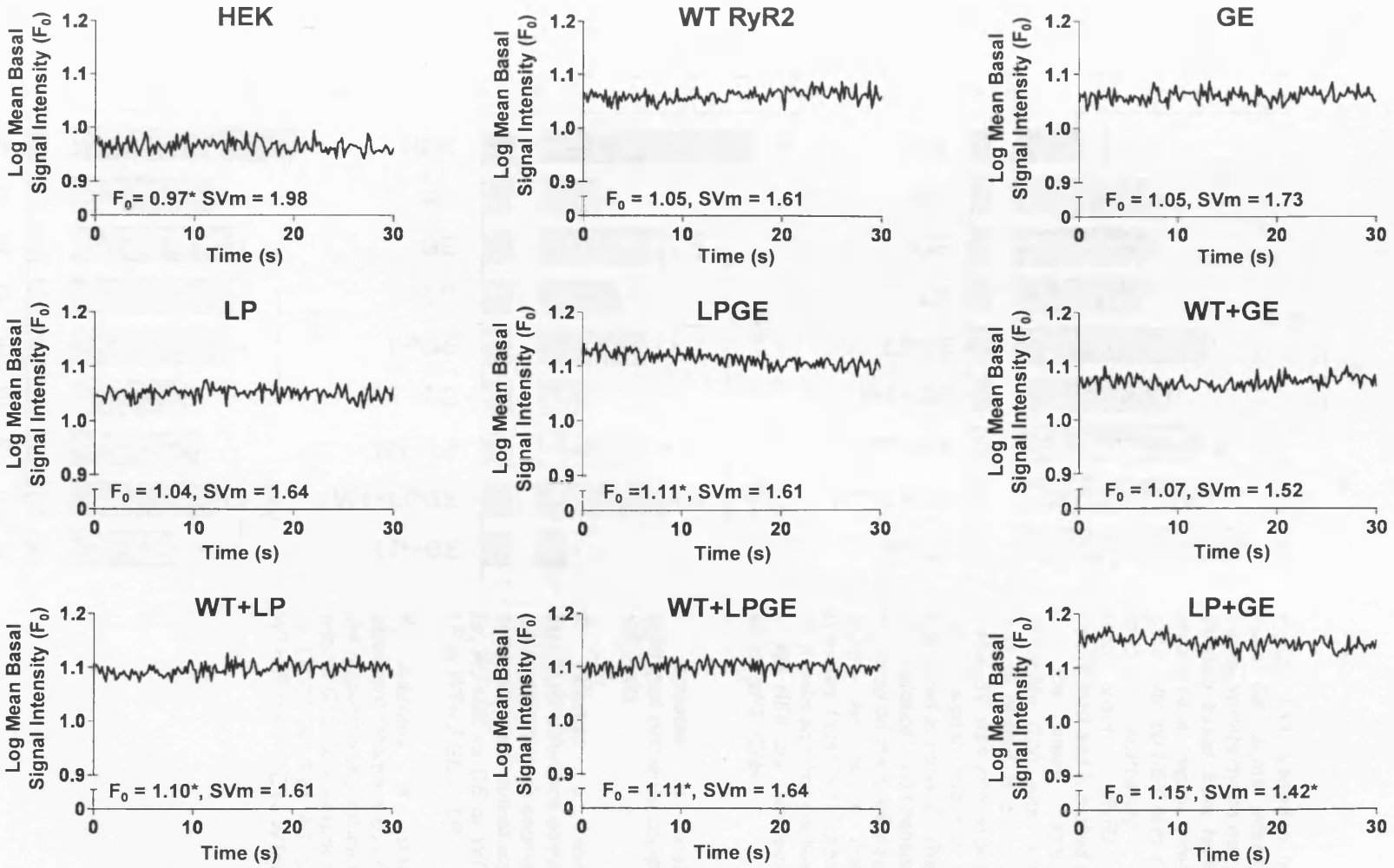

Figure 4.10. Representative basal Ca^{2+} traces illustrate heterogeneity in mean basal signal intensity and basal Ca^{2+} SVm. *Traces represent the Ca^{2+}-dependent Fluo3 signal intensity for the period 30 seconds immediately prior to caffeine addition. Mean signal intensities and basal SVm values are displayed. Asterisked data represents a significant difference to WT RyR2 ($p<0.05$)*

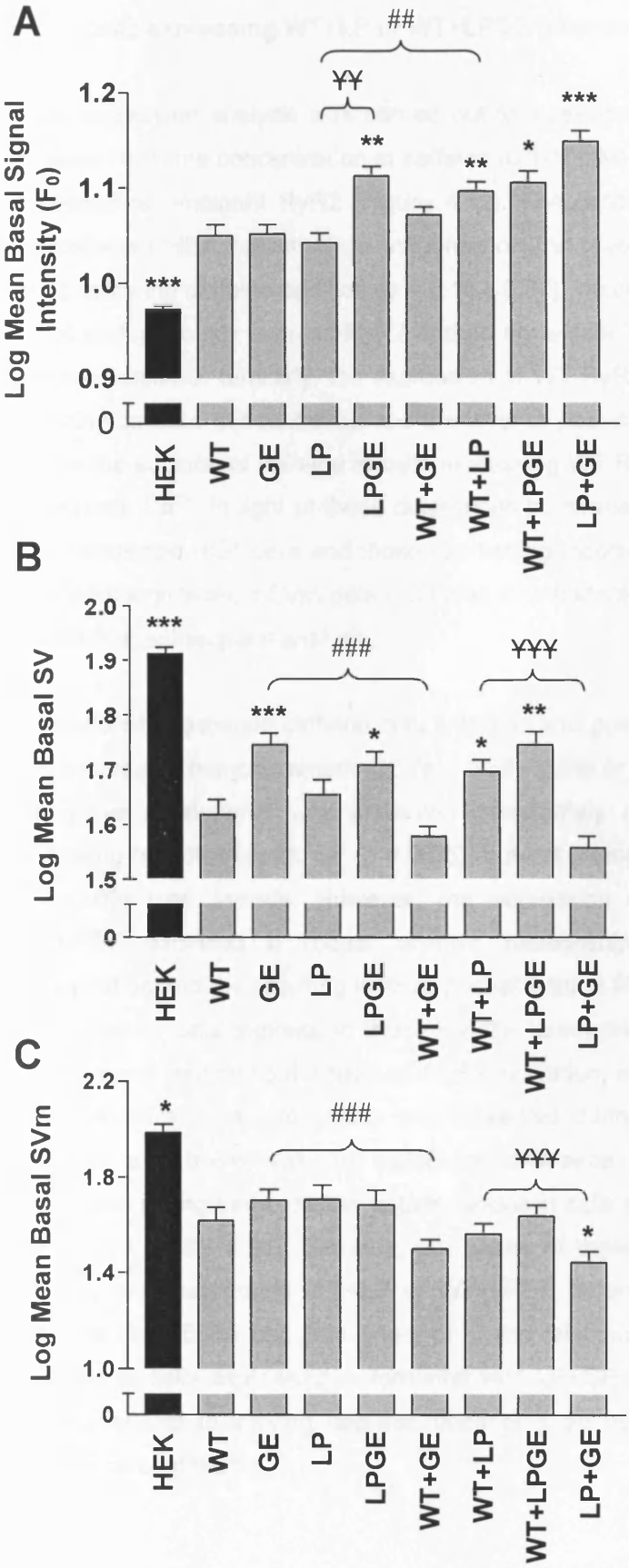

Figure 4.11. Variation in mean basal Ca^{2+} signal intensity and signal variability do not grossly perturb basal SVm levels. *The mean basal signal intensity of untransfected HEK cells and HEK cells expressing each recombinant RyR2 was determined and is plotted in panel A. The mean basal signal variability (SV) was determined and is plotted in panel B. The basal SV was normalised to the mean signal intensity and is presented in panel C. The results of statistical comparisons are indicated on the graphs according to the key above. Data was collected from 792 untransfected HEK cells and from between 269 – 388 HEK cell transfected with each RyR2 cDNA.*

** indicates a statistically significant difference compared to WT RyR2.*

 # indicates a statistically significant difference compared to the homotetrameric counterpart of heterotetrameric substitution i.e. WT+GE vs GE or WT+LP vs LP or WT+LPGE vs LP.

¥ indicates a statistically significant difference compared to the respective recombinant RyR2 without G1885E co-expression. i.e. LP-GE vs LP or WT+LPGE vs WT+LP or LP+GE vs WT+LP

4.3.2. Post-activation SVm is dependent on activating-caffeine concentration in cells expressing WT+LP or WT+LPGE heterotetramers

Linear regression analysis was carried out to investigate whether post-activation SVm correlated with the concentration of caffeine (0.1-10mM) used to activate heterologously expressed recombinant RyR2 (Figure 4.12). The concentration of caffeine applied to untransfected HEK cells had no influence on the level of observed SVm during any period following caffeine addition ($p = 0.14 - 0.87$), which is not surprising as HEK cells do not endogenously express RyR2 and do not exhibit ER Ca^{2+} release in response to caffeine exposure. Similarly, the expression of WT RyR2 did not exhibit a link between activating-caffeine concentration and the level of post-activation SVm ($p = 0.07 - 0.19$), despite the addition of caffeine to cells expressing WT RyR2 resulting in the elevation of cytoplasmic Ca^{2+}. In light of these differences in intracellular Ca^{2+} handling phenotypes of untransfected HEK cells and those expressing recombinant RyR2, the comparison of post-caffeine activation SVm data produced in untransfected HEK cells will no longer be described in subsequent analysis.

No relationship between caffeine concentration and post-activation SVm was evident in cells expressing homotetrameric GE ($p = 0.58 - 0.99$) or LPGE ($p = 0.2 - 0.92$) However, a negative relationship was observed immediately after caffeine addition in cells expressing homotetrameric LP ($p < 0.05$), but not during the middle ($p = 0.24$) and late ($p = 0.09$) time periods. However, the expression of heterotetrameric WT+LP or WT+LPGE exhibited a robust positive relationship between activating caffeine concentration and the resulting level of post-activation SVm ($p < 0.05$, Figure 4.12). This implies that in cells expressing these RyR2s, increasing the concentration of caffeine, and therefore increasing the level of RyR2 activation, results in a greater level of post-activation SVm. This relationship was observed during all periods following channel activation and there was no significant difference between the gradient of this relationship during early, middle or late periods in cells expressing either combination of RyR2s ($p = 0.88 - 0.96$). Similarly, the nature of these relationships was comparable between cells expressing WT+LP or WT+LPGE heterotetramers, suggesting that the presence of G1885E had little effect on these relationships. This relationship was not observed in cells expressing heterotetrameric LP+GE, suggesting that G1885E alters this relationship to varying degrees depending on the precise mode of L433P and G1885E co-expression.

A

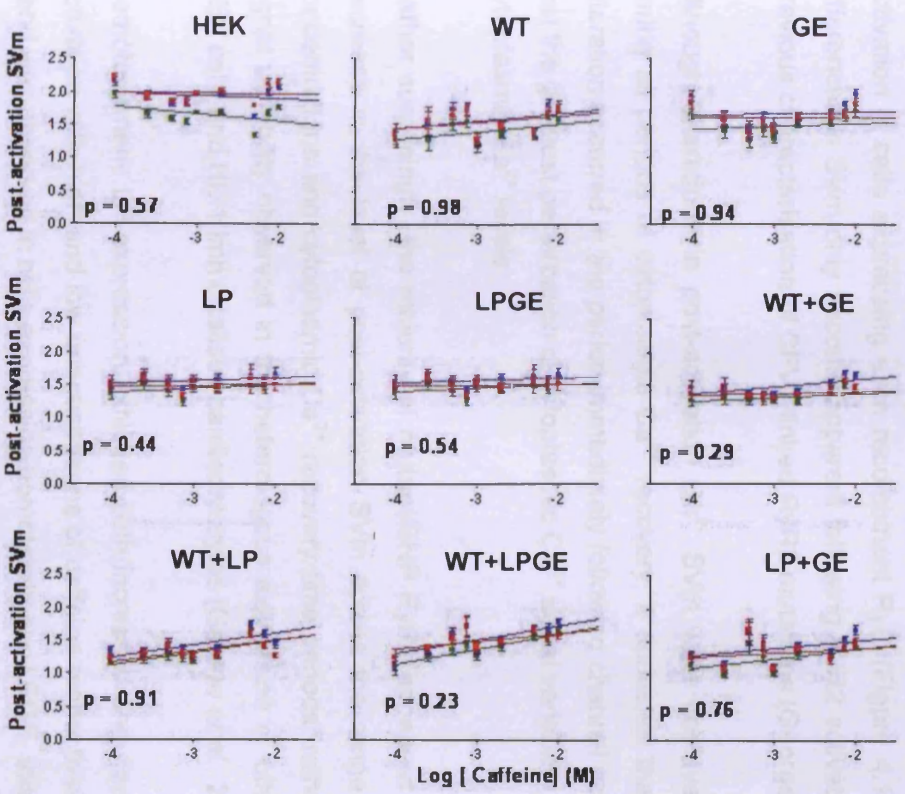

B

Caffeine (mM)		[Caffeine] vs post-activation SVm		
		Early	Middle	Late
HEK	Δ	-0.01 ± 0.06	-0.05 ± 0.06	-0.10 ± 0.06
	p	0.87	0.48	0.14
	r^2	0.01	0.06	0.25
WT	Δ	0.09 ± 0.07	0.11 ± 0.08	0.11 ± 0.06
	p	0.21	0.21	0.48
	r^2	0.19	0.19	0.07
GE	Δ	-0.001 ± 0.07	0.02 ± 0.08	0.04 ± 0.06
	p	0.99	0.82	0.58
	r^2	0.01	0.007	0.04
LP	Δ	-0.17 ± 0.07	-0.1 ± 0.14	-0.06 ± 0.06
	p	0.04*	0.15	0.40
	r^2	0.44	0.24	0.09
LP-GE	Δ	0.003 ± 0.03	0.04 ± 0.03	0.06 ± 0.04
	p	0.92	0.22	0.2
	r^2	0.01	0.18	0.19
WT+GE	Δ	0.02 ± 0.04	0.11 ± 0.04	0.06 ± 0.04
	p	0.53	0.02*	0.22
	r^2	0.05	0.51	0.18
WT+LP	Δ	0.16 ± 0.06	0.19 ± 0.05	0.19 ± 0.064
	p	0.02*	0.005*	0.001*
	r^2	0.52	0.65	0.74
WT+LPGE	Δ	0.13 ± 0.05	0.21 ± 0.06	0.23 ± 0.03
	p	0.03*	0.005*	0.001*
	r^2	0.46	0.64	0.91
LP+GE	Δ	0.07 ± 0.08	0.11 ± 0.07	0.14 ± 0.06
	p	0.40	0.16	0.06
	r^2	0.09	0.23	0.40

Figure 4.12. Linear regression analysis of the relationship between activating caffeine concentration and post-activation SVm. *Linear regression analysis was carried out to determine if the level of post-activation SVm was dependent on activating caffeine concentration. Linear regression line gradient (Δ), goodness-of-fit value (r^2) and significance values (p) are indicated in the table in panel B. Asterisked data indicates a significant relationship between caffeine concentration and post-activation SVm. There was no significant difference between the gradients in early, medium and late in cells expressing the same RyR2 (p-values indicated in panel A). Data was collected from between 7 and 78 cells per experimental condition.*

4.3.3. L433P and G1885E decrease the level of post-activation SVm compared to WT RyR2

The level of post-activation SVm was measured to determine whether expression of L433P and/or G1885E altered the level of cytoplasmic Ca^{2+} signal variability following caffeine-evoked ER Ca^{2+} release. SVm levels were recorded in cells expressing each RyR2, at each post-activation time point (early, middle and late), following activation with the range of caffeine concentrations (0.1-10mM). All raw SVm values are detailed in Appendix II, Tables 1 and 2.H eat maps were used to illustrate the statistical comparison of SVm levels in HEK cells expressing combinations of L433P and G1885E compared to WT RyR2 (Figure 4.13).

Despite the heterologous expression of mutant RyR2 having very little effect on cytoplasmic Ca^{2+} SVm under resting conditions, there was significant heterogeneity between the levels of cytoplasmic Ca^{2+} SVm following caffeine-evoked channel activation in cells expressing each recombinant RyR (Figure 4.13). This suggests that differences in SVm only become apparent following RyR2 activation, which agrees with previous characterisation of CPVT-linked RyR2 mutations (George *et al.*, 2006).

Although alterations in post-activation Ca^{2+} SVm were observed to varying degrees during all periods of cytoplasmic Ca^{2+} recovery, it appeared that the majority of SVm alteration occurred in the period immediately following channel activation. This suggests that the greatest perturbation of cytoplasmic Ca^{2+} signal variability tends to occur at peak cytoplasmic Ca^{2+} levels.

Rather surprisingly, the majority of mutant/SNP RyR2 appeared to cause a significant decrease in the level of post-activation SVm across the range of activating caffeine concentrations and cytoplasmic Ca^{2+} recovery time periods, rather than an increase in signal variability observed in the heterologous expression of other CPVT-mutations in HEK cells and HL-1 immortalised cardiomyocytes (George *et al.*, 2006).

Homotetrameric LP expression exhibited both increased and decreased SVm following activation with high and low concentrations of caffeine respectively. Given that a similar trend was observed in cells expressing homotetrameric LPGE, this could be attributable

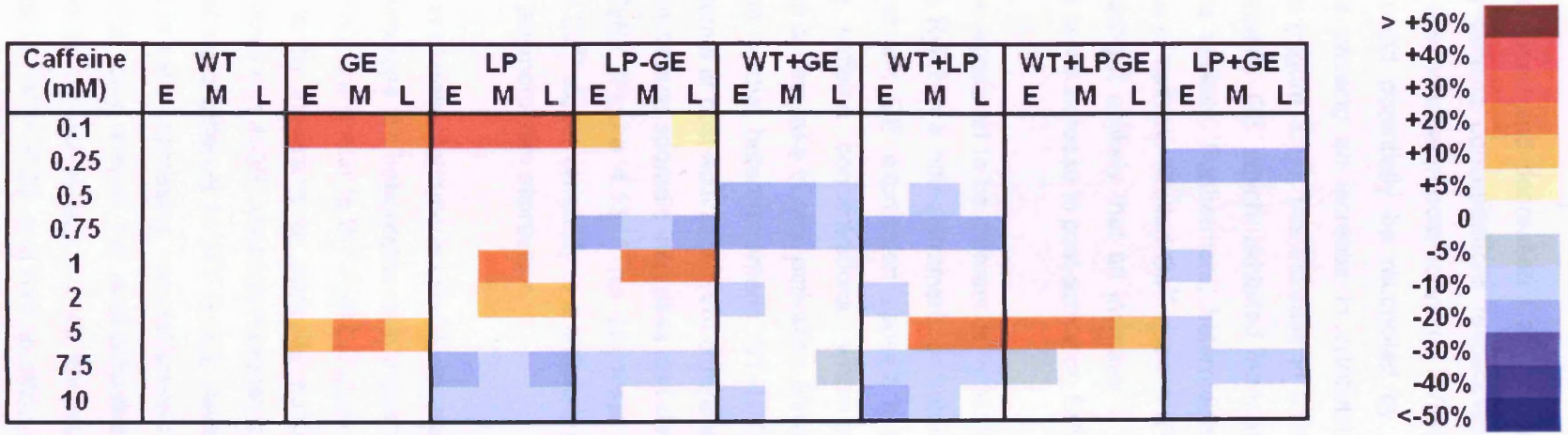

Figure 4.13. L433P and G1885E decrease the level of post-activation SVm. *SVm data was expressed as a percentage of that observed at the corresponding time point and activating caffeine concentration in HEK cells expressing WT RyR2. White-to-red transition indicates an increase in SVm whereas white-to-blue transition indicates a decrease in SVm compared to WT. Post-activation data was divided into early (E, 0-30s), middle (30-60s) and late (L, 60-90s) periods. Only data that exhibited a significant difference to WT RyR2 ($p < 0.05$) is highlighted. White cells indicated that there was no significant difference compared to WT RyR2. Raw data and the results of statistical comparison used to generate heat maps are presented in appendix II, Table 1.*

to the increased and decreased Ca^{2+} release magnitude observed at low and high activating caffeine concentrations respectively compared to WT RyR2 (Figure 3.17). Although the increase in post-activation SVm of L433P following activation with 0.1mM caffeine could potentially be reconciled by the observed increase in Ca^{2+} release magnitude causing an increase in cytoplasmic Ca^{2+} flux under these experimental conditions (Figure 3.17), this increase in SVm was also observed in cells expressing homotetrameric GE which exhibited normal Ca^{2+} release magnitude, making this hypothesis unlikely. Furthermore, heterotetrameric WT+LP expression increased the magnitude of caffeine-evoked Ca^{2+} release (Figure 3.18) yet decreased post-activation SVm, making it unlikely that an increase in caffeine-evoked Ca^{2+} release magnitude manifests as an increase in post-activation SVm.

There also appeared to be differences in post-activation SVm between cells expressing the same RyR2 in a homotetrameric or heterotetrameric fashion (i.e. GE vs WT+GE). Homotetrameric GE expression caused a significant increase in SVm at several activating caffeine concentrations, whereas heterotetrameric WT+GE expression resulted in a decrease in post-activation SVm. This observation was mirrored in LPGE expression, in that heterotetrameric WT+LPGE expression was largely similar to WT RyR2 in terms of post-activation SVm compared to WT RyR2, yet homotetrameric LPGE expression caused sporadic increases and decreases in post-activation SVm compared to WT RyR2 (Figure 4.13). This suggests that RyR2 substitutions can alter post-activation Ca^{2+} signal variability to a different extent, depending on the precise mode of mutation/polymorphism expression.

Expression of heterotetrameric LP+GE resulted in similar post-activation SVm levels to WT+LP, whereas the heterotetrameric expression of WT+LPGE resulted in SVm levels which were more similar to WT RyR2 (Figure 4.13), further suggesting that the whether G1885E is on the same or opposite subunit to the mutation alters its functional consequences on L433P. Although homotetrameric expression of LPGE presented SVm levels that were different to WT RyR2, there was little difference compared to those observed in cells expressing homotetrameric LP alone. Taken together, this suggests that G1885E only altered the post-activation SVm of heterotetrameric L433P when expressed on the same sub-unit as the mutation replicative of heterozygous *in cis* inheritance i.e. WT+LPGE, and had no effect on post-activation SVm of homotetrameric L433P i.e. LPGE.

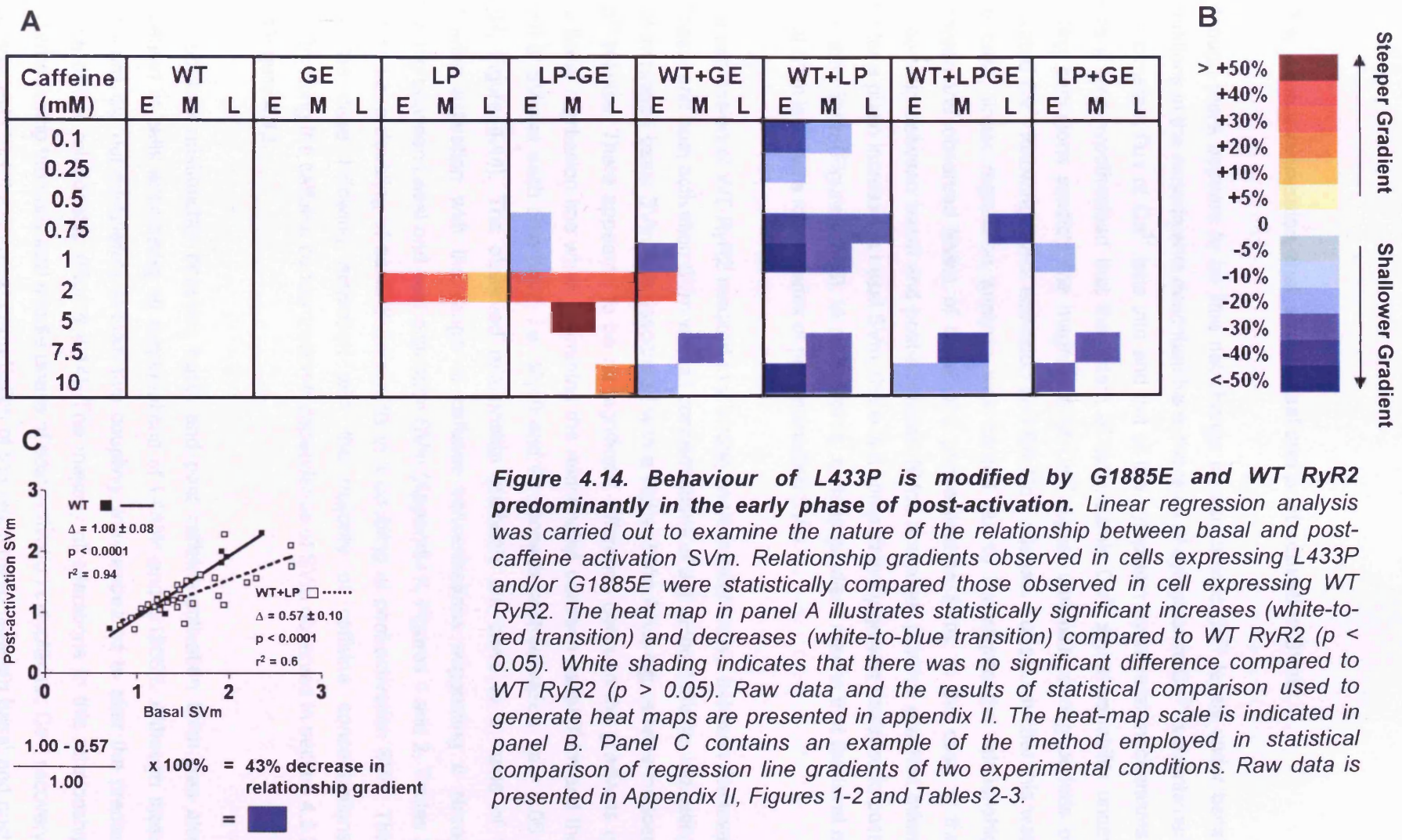

Figure 4.14. Behaviour of L433P is modified by G1885E and WT RyR2 predominantly in the early phase of post-activation. *Linear regression analysis was carried out to examine the nature of the relationship between basal and post-caffeine activation SVm. Relationship gradients observed in cells expressing L433P and/or G1885E were statistically compared those observed in cell expressing WT RyR2. The heat map in panel A illustrates statistically significant increases (white-to-red transition) and decreases (white-to-blue transition) compared to WT RyR2 ($p < 0.05$). White shading indicates that there was no significant difference compared to WT RyR2 ($p > 0.05$). Raw data and the results of statistical comparison used to generate heat maps are presented in appendix II. The heat-map scale is indicated in panel B. Panel C contains an example of the method employed in statistical comparison of regression line gradients of two experimental conditions. Raw data is presented in Appendix II, Figures 1-2 and Tables 2-3.*

4.3.4. Linear regression analysis of basal and post-activation SVm

Although there appears to be little net change in cytoplasmic Ca^{2+} levels under basal conditions in the experiments described here, the level of cytoplasmic Ca^{2+} is maintained by a constant flux of Ca^{2+} ions into and out of the cytoplasm by several mechanisms. Here it was hypothesised that the extent of cytoplasmic Ca^{2+} signal variability under resting conditions predicts the magnitude of Ca^{2+} signal variability during periods of elevated Ca^{2+} following RyR2 activation and ER Ca^{2+} release. To test whether this was the case, linear regression analysis was carried out to investigate the relationship between the observed levels of basal and post-activation SVm. In the case of the relationship between basal and post-activation SVm, a steeper positive gradient infers that for a given increase in basal SVm, there is a comparatively greater increase in post-activation SVm (Figure 4.14C). In other words, a steep gradient means that the level of basal SVm is a more robust index of post-activation SVm.

The expression of WT RyR2 resulted in a strong positive relationship between the level of basal and post-activation SVm with all concentrations of activating-caffeine, indicating that increased basal SVm was associated with a higher SVm following caffeine-induced Ca^{2+} release. There appeared to be no significant difference between the gradients of the linear regression line when examining the relationship between basal SVm and the level of SVm at each time point, i.e. 30,60 and 90 seconds post-activation ($p = 0.06$ - 0.87, Figure 4.14). The observed relationship gradients are close to a value of 1 following activation with the range of caffeine concentrations suggesting a strong coupling between basal and post activation SVm (Appendix II, Figures 1 and 2, Tables 2 and 3), i.e. a doubling of basal SVm results in a doubling of post-activation SVm. This was the case following activation with the majority of caffeine concentrations, corroborating the caffeine concentration-independence of SVm observed in section 4.3.2 and Figure 4.12.

This positive relationship between basal and post caffeine-activation SVm was also observed in cells expressing all combinations of L433P and G1885E. Although these mutations did not completely abolish this coupling, they appeared to alter the precise nature of this relationship (Figure 4.14). The majority of alterations to this relationship occurred during the early and middle phase of post-activation cytoplasmic Ca^{2+} recovery. This suggests that the greatest perturbation of the relationship between basal and post-

activation SVm occurs during the period of elevated cytoplasmic Ca^{2+} following channel activation and dissipates as cytoplasmic Ca^{2+} concentration decreases to a resting homeostatic state. This could potentially further suggest that acute dysfunctional Ca^{2+} release, as described in Chapter 3, is followed by relatively normal re-establishment of intracellular Ca^{2+} homeostasis.

Consistent with the relative levels of SVm described in section 4.3.3, the co-expression of heterotetrameric WT+LP resulted in the most significant perturbation of the relationship between basal and post activation signal variability compared to WT RyR2. This mode of expression caused significant decreases in the gradient of this relationship, particularly during the early and middle phases of intracellular Ca^{2+} recovery and suggests that in cells co-expressing WT+LP, an increase in basal SVm results in a smaller increase in post-activation SVm than that observed in cells expressing WT RyR2. Although decreases in the gradient of this relationship were observed in cells co-expressing WT+LPGE or LP+GE when compared to WT RyR2, these decreases were to a lesser extent than those observed in cells expressing WT+LP. This suggests that the co-expression of G1885E had a significant effect on restoring the coupling between basal and post-activation SVm when expressed with L433P in a heterotetrameric fashion (WT+LPGE or LP+GE)

Interestingly, homotetrameric LP expression increased the gradient of the relationship between basal and post-activation SVm at just a single activating caffeine concentration, as did homotetrameric LPGE. However, LPGE resulted in both increases and decreases in relationship gradient at several sporadic activating caffeine concentrations, reaffirming the subtle modulatory effect of G1885E observed through heterotetrameric L433P and G1885E expression.

Statistical comparison of the steepness of the linear regression line of basal and post-activation SVm revealed that homotetrameric GE expression exhibited an almost identical relationship to that observed in cells expressing WT RyR2 (Figure 4.14). Heterotetrameric WT+GE expression had more of an effect on the relationship between basal and post-activation SVm, causing both increases and decreases in the steepness of this relationship during the early phase of recovery, following activation of the channel with high concentrations of caffeine.

4.4. Discussion

4.4.1. Untransfected HEK cells exhibit a fundamentally different resting phenotype compared to those expressing RyR2

Consistent with the basal cytoplasmic Ca^{2+} quantification data detailed in section 3.3.8 and previous published data (Tong *et al.*, 1999; George *et al.*, 2003b) the expression of recombinant RyR2 caused a significant increase in the basal Ca^{2+}-dependent signal intensity compared to untransfected HEK cells (Figure 4.11A). Although the expression of each recombinant RyR2 appeared to cause a significant decrease in basal Ca^{2+} signal variability compared to untransfected HEK cells (Figure 4.11C), this is likely due to the significantly lower mean basal Ca^{2+} signal intensity and increased basal SV observed in untransfected HEK cells (Figure 4.11A-B) from which SVm is derived. As untransfected HEK cells exhibit a fundamentally different intracellular Ca^{2+} handling phenotype compared to those recombinantly expressing RyR2 (as described in section 4.3.1 and 4.3.2), untransfected HEK cells were not included in this signal variability analysis.

4.4.2. Differences in cytoplasmic Ca^{2+} SVm only manifest following RyR2 activation

The observation that expression of RyR2 containing each combination of L433P and G1885E had little effect on basal Ca^{2+} signal variability (Figure 4.11C) suggests that under basal conditions, i.e. without agonist-evoked channel activation, these substitutions have little effect on the level of cytoplasmic Ca^{2+} influx and efflux compared to WT RyR2. This infers that expression of each RyR2 results in a similar intracellular Ca^{2+} homeostatic environment at rest, which is consistent with data from a previous study investigating the effects of CPVT-linked RyR2 mutations on Ca^{2+} signal variability (George *et al.*, 2006). However, there was significantly greater heterogeneity in cytoplasmic Ca^{2+} SVm following caffeine-mediated channel activation (Figure 4.13) suggesting that alterations in cytoplasmic Ca^{2+} flux caused by L433P and G1885E only manifest following channel activation and subsequent ER Ca^{2+} release. This is in agreement with some other *in vitro* and *in vivo* studies which indicate that the physiological effects of CPVT/ARVD2 linked mutations are only evident following increased levels of channel activation, be it through agonist-evoked or β-AR activation

mechanisms (George *et al.*, 2006; Kannankeril *et al.*, 2006; Lehnart *et al.*, 2008), although there is increasing evidence that some mutations perturb basal Ca^{2+} handling (Jiang *et al.*, 2002; Fernandez-Velasco *et al.*, 2009; Uchinoumi *et al.*, 2010).

4.4.3. L433P and G1885E decrease post-activation Ca^{2+} signal variability compared to WT RyR2

A surprising observation was that the majority of the permutations of recombinant RyR2 examined here exhibited a decrease in post-activation cytoplasmic Ca^{2+} signal variability (Figure 4.13), which disagrees with findings that two C-terminal mutations (R4496C and N4104K) significantly increased the cytoplasmic Ca^{2+} signal variability following channel activation (George *et al.*, 2006). However this may be due to several differences in the experimental system or the nature of these particular mutations.

To further understand the effects of these amino acid substitutions on the level of post-activation Ca^{2+} signal variability, it would be extremely beneficial to determine the level of activity of the various cytoplasmic Ca^{2+} removal proteins, i.e. PMCA, SERCA. This would potentially provide an indication of whether alterations in cytoplasmic Ca^{2+} flux were due to altered activity of these removal proteins and whether this compensated for dysfunctional Ca^{2+} release through mutant channels.

The level of post-activation Ca^{2+} flux appeared to be independent of ER Ca^{2+} store load or Ca^{2+} release magnitude, as there was no obvious reconciliation between RyR2 mutations that altered ER Ca^{2+} load or Ca^{2+} release magnitude and those that altered post-activation SVm (Figure 3.17-3.19, 3.23 and 4.13). i.e. both WT+GE and WT+LP cause a decrease in SVm, yet WT+LP exhibits an increase in ER Ca^{2+} store whereas WT+GE exhibits an equivalent ER Ca^{2+} store to WT RyR2. Furthermore, there did not appear to be any consistent trends between the level of cytoplasmic Ca^{2+} signal variability and any of the measured Ca^{2+} handling parameters detailed in chapter 3 (Appendix 2 Figures 3-8), making it difficult to envisage a specific cause or effect of this alteration in cytoplasmic Ca^{2+} flux. The absence of any obvious dependence of signal variability on intracellular Ca^{2+} handling parameters also complicates the interpretation of why homotetrameric G1885E or L433P expression causes an increase in signal variability at some sporadic activating caffeine concentrations, yet most other

combinations of L433P or G1885E expression cause a decrease in Ca^{2+} signal variability.

Despite this, the expression of L433P and/or G1885E tends to alter post-activation signal variability predominantly during the period immediately after channel activation and to a lesser extent during the late period of cytoplasmic Ca^{2+} recovery (Figure 4.13). This suggests that as the cytoplasmic Ca^{2+} concentration approaches the pre-activation resting mean Ca^{2+} level, the level of Ca^{2+} flux also has a tendency to approach pre-activation levels. However, due to the short amount of time over which post-activation SVm was recorded (90 secs), it is unknown whether the level of cytoplasmic Ca^{2+} flux would reach the same pre-activation steady state equilibrium if post-activation data was collected over a longer time period.

4.4.4. Post-activation signal variability is dependent on the level of basal SVm and this relationship is altered by L433P

The observed relationship between basal and post-activation signal variability (summarised in Figure 4.14, raw data in Appendix II, Figures1-2 and Tables 2-3) suggests that increased basal signal variability translates to a more variable Ca^{2+} signal following caffeine-evoked channel activation. Although this relationship was observed in cells expressing each recombinant RyR2, L433P and G1885E expression did appear to alter the precise nature of this relationship. In the majority of cases, the perturbation of this relationship tended to be rather sporadic i.e. alteration at a single caffeine concentration or a single time point.

Nevertheless, unlike the absolute SVm values, the relationship between basal and post-activation Ca^{2+} signal variability appeared to be somewhat associated with Ca^{2+} release magnitude, in that WT+LP expression, which exhibited an increased ER Ca^{2+} transient amplitude (Figure 3.18), resulted in a relatively smaller increase in signal variability following channel activation (Figure 4.14). On the contrary, RyR2 mutations that caused a decrease in ER Ca^{2+} transient amplitude i.e. homotetrameric LP or LPGE (Figure 3.17) caused a relatively larger increase in post-activation Ca^{2+} signal variability (Figure 4.14). Furthermore, this positive relationship was altered predominantly during the early and middle phase of cytoplasmic Ca^{2+} recovery (Figure 4.14), reaffirming that the greatest

perturbation of signal variability occurs during the period of elevated cytoplasmic Ca^{2+} following RyR2 activation.

4.4.5. G1885E modulates post-activation SVm of cells expressing L433P

In addition to altering post-activation SVm and its dependence on the level of basal Ca^{2+} signal variability when expressed alone, G1885E was shown to modulate both the relative levels of post-activation SVm (Figure 4.13 and Appendix II, Table 1) and the relationships between basal and post-activation SVm of cells expressing L433P (Figure 4.14 and Appendix 2, Figures, 1-2 and Tables 2-3). The modulatory effects of G1885E were more pronounced when expressed with L433P in a heterotetrameric fashion (WT+LPGE or LP+GE), where the presence of G1885E partially restored post-activation SVm levels to those observed in WT RyR2. In contrast, homotetrameric LPGE expression exhibited SVm values and relationships that were very similar to those observed in cells expressing homotetrameric LP. This provides further evidence that G1885E modulates L433P channel function to varying degrees, depending on the precise mode of inheritance.

Homotetrameric GE expression resulted in identical relationships between basal and post-activation SVm compared to cells expressing WT RyR2, whereas the co-expression of WT+GE exhibited a slight, inconsistent, alteration of this relationship, providing further evidence that this polymorphism has little effect on RyR function when it is the only substitution present. However, when co-expressed with L433P (WT+LPGE or LP+GE), G1885E caused a significant reduction in the degree of perturbation of the relationship between basal and post-activation SVm. This provides further evidence that presence of G1885E causes subtle alterations in the effects of the L433P mutation, although the functional implications of the modulation of this relationship remain unknown.

4.5 Chapter Summary

Most RyR2 variants expressed here displayed similar levels of basal Ca^{2+} flux, suggesting the comparable net movement of Ca^{2+} into and out of the cytoplasm under resting conditions, indicative of similar resting Ca^{2+} homeostasis. Differences in cytoplasmic Ca^{2+} flux caused by L433P and G1885E, were only evident following channel activation and ER Ca^{2+} release which is consistent with other functional studies of RyR2 mutations.

Although the level of basal cytoplasmic Ca^{2+} flux was not a determining factor of any of the measured Ca^{2+} release parameters measured in Chapter 3, a positive relationship was observed between basal and post-activation Ca^{2+} signal variability, supporting a role of L433P and G1885E in defective post-activation Ca^{2+} handling.

Furthermore, L433P and G1885E expression appeared to mainly alter post-activation SVm levels and the relationship between basal and post-activation SVm during the early phase of cytoplasmic Ca^{2+} recovery. This novel finding suggests that the effects of RyR2 mutations on Ca^{2+} flux were most pronounced immediately following channel activation when cytoplasmic Ca^{2+} levels were at their peak, and reiterates that the defect in mutant RyR2 Ca^{2+} handling may lie in the 'inactivation' or 'recovery' phase of the Ca^{2+} transient.

Rather surprisingly, the majority of combinations of L433P and G1885E investigated here, appeared to cause a decrease in Ca^{2+} signal variability following Ca^{2+} release, although the mechanism by which this occurs and the functional consequences of this decrease in Ca^{2+} signal intensity remain unknown. Furthermore, the alterations in SVm do not provide a clear mechanistic basis for the observed differences in Ca^{2+} handling parameters detailed in Chapter 3.

In accordance with the caffeine-evoked Ca^{2+} release data in Chapter 3, G1885E had little effect on SVm when expressed alone, yet modulated the effects of L433P. Furthermore, the precise mode of G1885E co-expression with L433P had a major effect on the extent to which G1885E would alter mutant channel function, with heterotetrameric expression of G1885E exhibiting the most profound modulatory effects on L433P SVm.

As described in Chapter 3, although the majority of RyR2-expressing cells exhibited a characteristic steady basal Ca^{2+} signal prior to caffeine addition, a proportion of the transfected cells exhibited spontaneous Ca^{2+} release as Ca^{2+} oscillations, similar to the "SOICR" phenomenon described by *Jiang et al.* In light of this, the next chapter of this thesis will detail the examination of these spontaneous Ca^{2+} release events and any functional consequences L433P and G1885E expression may have on them.

Chapter 5

Characterisation of spontaneous Ca^{2+} release in HEK cells expressing L433P and G1885E

5.1. Introduction

5.1.1. The implication of spontaneous Ca^{2+} release in heart failure

It is generally accepted that HF is characterised by decreased cardiac output, reduced contractility and impaired relaxation. VT is a major cause of death in HF (Bers, 2006) and is thought to be initiated by DADs, which arise due to spontaneous Ca^{2+} release from the SR via RyR2. The elevated cytoplasmic [Ca^{2+}] resulting from spontaneous SR Ca^{2+} release is removed from the cell via the NCX in exchange for an inward depolarising Na^+ current. The result of this inward Na^+ current is a net gain in positive membrane potential during the repolarisation phase of the action potential (Schlotthauer & Bers, 2000). If the magnitude of this inward Na^+ current is sufficient, it may lead to the onset of a DAD, which can lead to the premature initiation of action potentials in neighbouring cells and potentially result in the onset of VT (Figure 5.1, Marban, 2002).

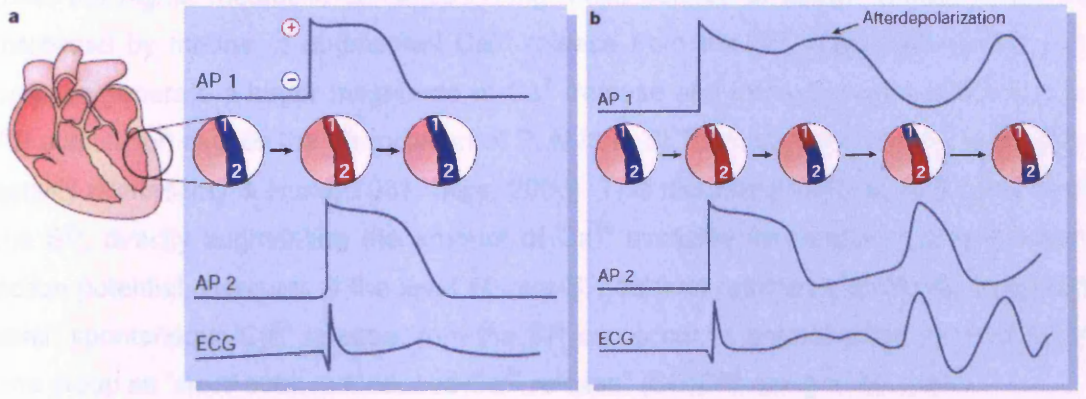

Figure 5.1. Comparison of a normal action potential and an action potential exhibiting delayed after depolarisations (DADs). *Panel a shows the representative action potentials at two neighbouring sites (1 and 2) in normal heart ventricular wall. Negatively polarised (resting) muscle is indicated in blue and depolarised tissue is indicated in red. Action potentials at both sites appear similar in duration and morphology. Panel b shows an action potential of failing heart in which DADs are occurring. During the repolarisation phase, spontaneous Ca^{2+} release occurs at site 1 and results in a DAD. This DAD causes the premature activation of an action potential at site 2 and can result in VT onset. From Marban (2002).*

Data produced from several right ventricular apical tachypacing heart failure models has demonstrated similar functional perturbation of Ca^{2+} handling in the failing heart. Both individual myocytes and intact tissue from failing canine hearts demonstrated a decrease in the amplitude of the Ca^{2+} transient released from the SR during EC-coupling

(Kubalova *et al.*, 2005; Hoeker *et al.*, 2009). This decrease in Ca^{2+} transient amplitude results in impaired contractility of the myocyte and has been attributed to increased diastolic Ca^{2+} leak and reduced Ca^{2+} sequestration in the SR. Isolated myocytes from failing hearts were also shown to exhibit a decreased level of SR Ca^{2+}, potentially caused by the observed increase in Ca^{2+} spark/wave frequency (Kubalova *et al.*, 2005; Hoeker *et al.*, 2009).

5.1.2. Spontaneous Ca^{2+} release in CPVT and ARVD2

CPVT and ARVD2 are both characterised by the onset of VT under periods of physical or emotional stress, when the level of circulating catecholamines is high and the β-AR pathway is activated (Leenhardt *et al.*, 1995; Priori *et al.*, 2002). In order for the heart to meet the higher metabolic demands during these periods of stress, cardiac output is increased by means of augmented Ca^{2+} release from the SR during EC-coupling. In order to generate a larger magnitude of Ca^{2+} release and increase contractile force, β-AR stimulation causes the dissociation of PLN from SERCA, thereby increasing SERCA activity (Periasamy & Huke, 2001; Bers, 2008). This increases Ca^{2+} sequestration in to the SR, directly augmenting the amount of Ca^{2+} available for release during the next action potential. However, if the level of intra-SR calcium reaches a particular threshold level, spontaneous Ca^{2+} release from the SR can occur, a phenomenon referred to by one group as "store-overload induced Ca^{2+} release" (SOICR, Jiang *et al.*, 2004).

5.1.3. Role of RyR2 mutations in spontaneous Ca^{2+} release

The development of CPVT/ARVD2 knock-in mouse models has made it possible to investigate the role of CPVT and ARVD2-linked RyR2 mutations in the development of DADs and triggered activity (Cerrone *et al.*, 2005; Liu *et al.*, 2006). Under non-stimulated conditions, myocytes isolated from the $R4496C^{+/-}$ knock-in mouse exhibited DADs in a small percentage of cells. β-AR stimulation caused a significant increase in the number of $R4496C^{+/-}$ myocytes that exhibited DADs (87%) and triggered activity (60%), and although β-AR stimulation also caused an increase in DADs in WT myocytes, it was to a lesser extent (11%) and no triggered activity was observed (Liu *et al.*, 2006).

A similar phenotype was observed in both the R176Q$^{+/-}$ and R2474S$^{+/-}$ knock-in mice, in that there was a higher incidence of spontaneous Ca^{2+} release in myocytes isolated from the mutant mice compared to WT myocytes, under both resting conditions and following β-AR stimulation (Kannankeril *et al.*, 2006; Lehnart *et al.*, 2008; Uchinoumi *et al.*, 2010). The fact that β-AR stimulation exacerbates the level of DADs observed under resting conditions and results in an increase in triggered activity in R176Q$^{+/-}$, R2474S$^{+/-}$ and R4497C$^{+/-}$ mice (Kannankeril *et al.*, 2006; Liu *et al.*, 2006; Lehnart *et al.*, 2008; Uchinoumi *et al.*, 2010), suggests that this is a pathogenic mechanism by which RyR2 mutations result in a CPVT-phenotype. Interestingly, the data produced from CPVT/ARVD2 knock-in mouse models corroborates data obtained from the characterisation of several disease-linked RyR2 mutations, including R4497C, in heterologous expression systems (Table 3.2).

Heterologous expression of a C-terminal CPVT-linked RyR2 mutation, V4653F, was shown to decrease the luminal Ca^{2+} threshold at which spontaneous Ca^{2+} release occurred, by increasing the sensitivity of the channel to activation by luminal Ca^{2+} (Jones *et al.*, 2008). This increased luminal Ca^{2+} sensitivity manifested as an increase in the propensity for cells to exhibit spontaneous ER Ca^{2+} release, which in the cardiac myocyte could lead to DADs. This reduced threshold for spontaneous SR Ca^{2+} release and increased luminal Ca^{2+} sensitivity was not limited to the V4653F CPVT-linked mutation and has been observed through the heterologous expression of mutations spanning the length of RyR2. Mutations from the N-terminal domain (R176Q/T2504M, L433P), central domains (S2246L, R2474) and C-terminal transmembrane domain (Q4201R, N4104K, R4496C, I4867M, N4865D) have all demonstrated increased luminal Ca^{2+} sensitivity and a decreased luminal Ca^{2+} threshold for spontaneous Ca^{2+} release (Jiang *et al.*, 2005; Jones *et al.*, 2008), which manifests as an increased propensity for cells to exhibit spontaneous Ca^{2+} release.

Chen and colleagues have proposed an attractive model for the mechanism by which CPVT/ARVD2-linked RyR2 mutations result in increased spontaneous Ca^{2+} release (Figure 5.2, Jiang *et al.*, 2004; reviewed by MacLennan & Chen, 2009). In their model they propose that under resting conditions, the level of free Ca^{2+} in the SR is below the normal threshold at which spontaneous Ca^{2+} release occurs through WT RyR2. Following β-AR stimulation, the level of free intra-SR Ca^{2+} increases, but still remains below the critical threshold for spontaneous Ca^{2+} release to occur. They propose that

arrhythmia-linked RyR2 mutations reduce the threshold of luminal Ca^{2+} at which spontaneous Ca^{2+} release occurs and at rest, the level of Ca^{2+} in the SR remains below this threshold. However, during periods where SR Ca^{2+} is elevated as a result of increased β-AR stimulation, the level of intra-SR Ca^{2+} surpasses this reduced threshold and results in spontaneous Ca^{2+} release, a phenomenon initially termed store-overload induced Ca^{2+} release or "SOICR". However, since the inception of this model, this spontaneous Ca^{2+} release has been shown to be due to an increase in RyR2 luminal Ca^{2+} sensitivity, rather than ER Ca^{2+} store overload, suggesting that "SOICR" may not be the most accurate term for this phenomenon. This spontaneous Ca^{2+} release can potentially lead to the development of DADs and arrhythmia as discussed in section 5.1.1.

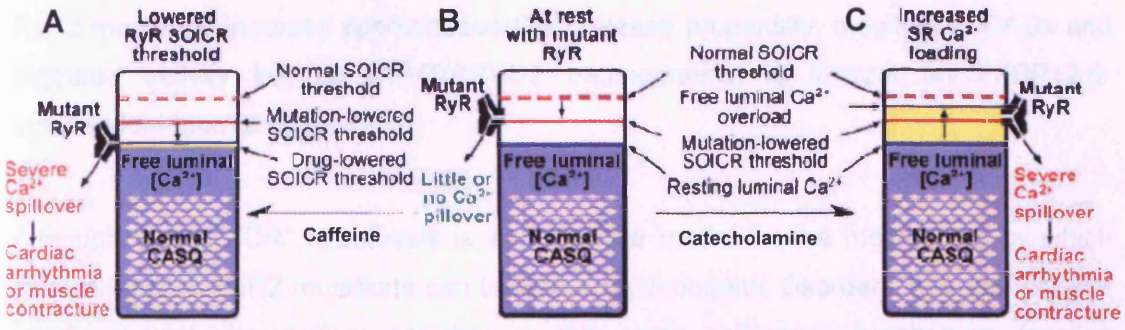

Figure 5.2. A model of the SOICR mechanism proposed for CPVT RyR2 mutations. *In myocytes expressing normal RyR2, under resting conditions, the level of free luminal Ca^{2+} (blue shading) in the SR store is below the normal threshold for spontaneous Ca^{2+} release (red dashed line), so SOICR does not occur as shown in panel B. It is proposed that CPVT-linked mutations reduce the threshold at which SOICR occurs (red solid line). β-AR stimulation increases the level of free luminal Ca^{2+} which remains below the normal SOICR threshold, so spontaneous Ca^{2+} release does not occur. The increased free luminal Ca^{2+} exceeds the mutation-lowered SOICR threshold and results in spontaneous Ca^{2+} release, as shown in panel C. Caffeine is proposed to act in a similar manner to RyR mutations by reducing the threshold at which SOICR occurs, which if below the level of free luminal Ca^{2+}, can result in SOICR as shown in panel A. From MacLennan, (2009).*

Although there remains great contention over whether the dissociation of FKBP12.6 has a role in CPVT/ARVD pathogenesis (section 1.3.4.3), there is increasing evidence that the interaction of FKBP12.6 with RyR2 has no effect on this spontaneous Ca^{2+} release propensity. Nevertheless, the investigation of the effects of CPVT/ARVD2 mutations on "SOICR" has only been described in HEK cells (Jiang *et al.*, 2002; 2004; 2005; Jones *et al.*, 2008), which do not endogenously express FKBP12.6, meaning that the role of

FKBP12.6 in regulating this process remains unresolved. Acute and chronic treatment of the R4496C$^{+/-}$ mouse with K201 (JTV519), a compound proposed to restore FKBP12.6 interaction with RyR2, did not prevent the DADs and triggered activity observed in these mice (Liu *et al.*, 2006), although it did reduce Ca^{2+} leak in an R2474S knock-in mouse model (Lehnart *et al.*, 2008). Furthermore, the RyR2:FKBP12.6 interaction in these mice was identical to that observed in WT mice, both under resting or stimulated conditions (Liu *et al.*, 2006). These observations were re-iterated through the heterologous expression of many CPVT/ARVD2-linked RyR2 mutations, which also demonstrated an equivalent FKBP12.6-RyR2 interaction in cells expressing WT or mutant RyR2, despite exhibiting an increase in spontaneous Ca^{2+} release (Jiang *et al.*, 2005; Jones *et al.*, 2008). Taken together with other experimental data (George *et al.*, 2003a; Xiao *et al.*, 2007; Zissimopoulos *et al.*, 2009), these findings suggest that the mechanism by which RyR2 mutations increase spontaneous Ca^{2+} release propensity, resulting in DADs and triggered activity key to CPVT/ARVD2 pathogenesis, is in fact an FKBP12.6-independent mechanism.

Although the "SOICR" hypothesis is an attractive model for the mechanism by which gain-of-function RyR2 mutations can lead to arrhythmogenic disorders, it is unlikely that all disease-linked mutations act through this same pathogenic mechanism (section 1.3.4). This is further highlighted by the fact that not all RyR2 mutations exhibit a similar degree of increased luminal Ca^{2+} sensitivity, with some N-terminal mutations only exhibiting altered luminal Ca^{2+} sensitivity when exposed to high luminal Ca^{2+} concentrations (i.e. >10mM, Jiang *et al.*, 2005) Furthermore, it is unlikely that mutations located in the cytoplasmic assembly alter luminal Ca^{2+} sensitivity by direct perturbation of luminal Ca^{2+} sensing, but instead may alter luminal Ca^{2+} sensitivity through channel destabilisation or altered channel inactivation properties.

5.1.4. Loss-of-function RyR2 mutations

The majority of CPVT/ARVD2 linked RyR2 mutations that have been characterised in heterologous systems have demonstrated an increased sensitivity to activation by luminal Ca^{2+}, manifesting as the increased occurrence of spontaneous basal Ca^{2+} oscillations. However, recent evidence suggests that not all disease-linked RyR2 mutations cause this gain-of-function phenotype in terms of spontaneous Ca^{2+} release

(Jiang *et al.*, 2007; Koop *et al.*, 2008). A mutation in the RyR2 pore inner helix resulting in the substitution of a glycine residue in place of an alanine residue (A4860G) was shown to completely ablate basal spontaneous Ca^{2+} release. The mutation reduced the sensitivity of the channel to activation by luminal Ca^{2+}, caused an increase in the level of Ca^{2+} in the ER store and decreased the level of basal activity as determined by [^{3}H]Ryanodine binding (Jiang *et al.*, 2007). Considering the non-polar nature of the substituted glycine residue and the position of the mutation deep within the inner-pore helix, it is unlikely that the A4860G mutation directly effects channel luminal Ca^{2+} sensing, but likely affects the gating properties of the channel.

Interestingly, as well as altering RyR2 biophysical properties, as demonstrated using single channel analysis, the common G1885E and G1886S polymorphisms have also been shown to perturb spontaneous basal Ca^{2+} release occurrence when expressed in a HEK cell system (Koop *et al.*, 2008). Expression of mouse RyR2 containing either the G1885E or G1886S polymorphism resulted in an increase in the occurrence of spontaneous basal Ca^{2+} release in the absence of altered Ca^{2+} store-load. This lead the group to hypothesise that either polymorphism sensitises the channel to activation by luminal Ca^{2+} and lowers the threshold at which spontaneous Ca^{2+} release occurs (Figure 5.3) and suggests that these two SNPs are not functionally benign when expressed as homotetramers containing either SNP. Furthermore, homotetrameric expression of both polymorphisms on the same RyR2 subunit caused near-complete ablation of spontaneous Ca^{2+} release events (Koop *et al.*, 2008). This demonstrates that the presence of both SNPs results in a very different phenotype to when either SNP is expressed alone, a similar phenomenon to that observed with SNPs in *SCN5A* and *CASQ2* and with other rare RyR2 mutations (Postma *et al.*, 2005; de la Fuente *et al.*, 2008; Medeiros-Domingo *et al.*, 2009). Coupled with the observation that cells expressing both G1885E and G1886S exhibited an increased Ca^{2+} store load, this suggests that expression of both G1885E and G1886S amino acid substitutions on every RyR2 subunit of the tetramer decreases the channel sensitivity to activation by luminal Ca^{2+} and increases the threshold at which spontaneous Ca^{2+} release occurs (Figure 5.3B). However, this mode of expression where both SNPs are present on all subunits of the tetramer (Koop *et al.*, 2008) is not representative of the composite heterozygotic mode of G1885E and G1886S co-inheritance observed in the ARVD2 patient *in vivo* (Milting *et al.*, 2006), in which a mixture of channels containing both SNPs in varying stoichiometry would be expressed. Whether the mode of inheritance observed

in vivo results in a similar loss-of-function remains to be determined, but highlights the importance of characterising SNPs and mutations when expressed in a manner replicative of the observed mode of disease-linked inheritance.

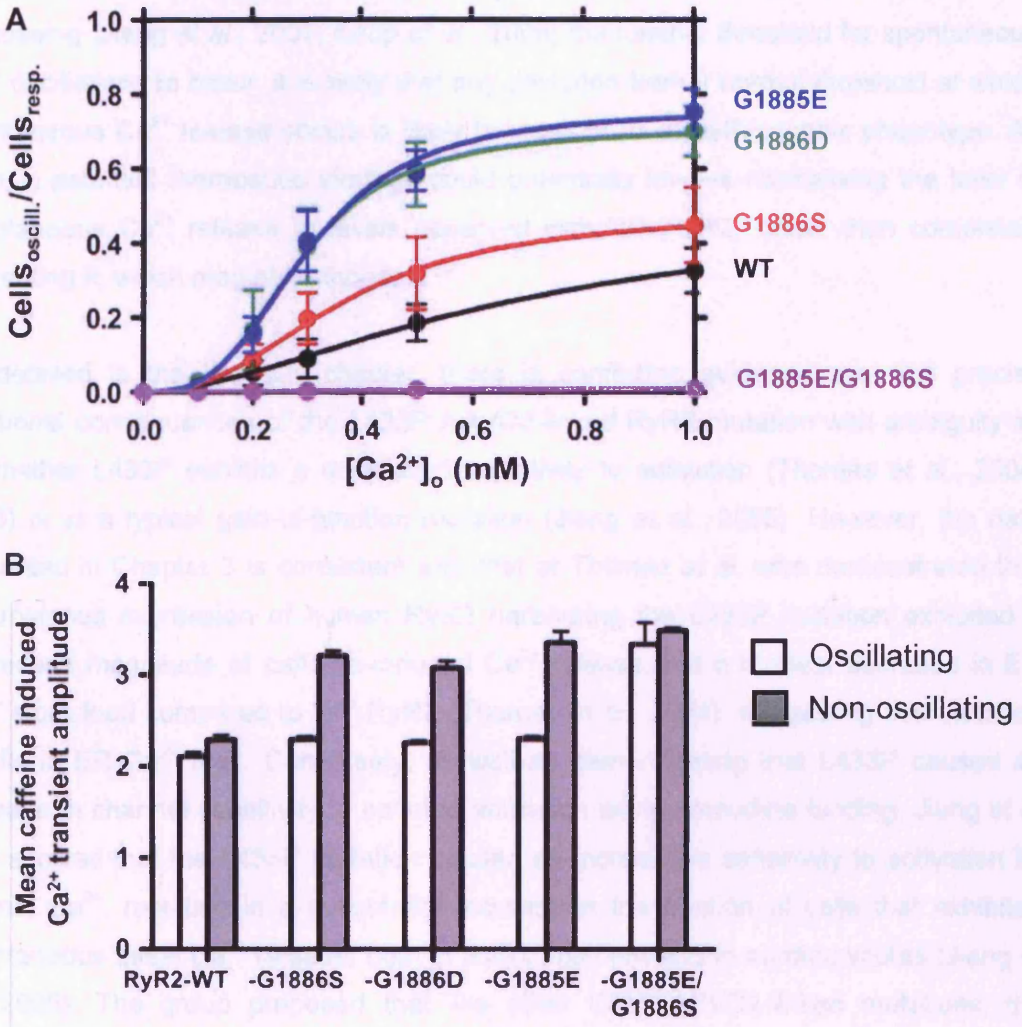

Figure 5.3. G1885E and G1886S alter spontaneous Ca^{2+} release propensity. *Cells expressing G1885E, G1886S or G1886D (mimicking constitutive phosphorylation at G1886S) exhibited increased propensity for spontaneous Ca^{2+} release at all extracellular Ca^{2+} concentrations ($[Ca^{2+}]_o$). Homotetrameric expression of G1885E/G1886S on the same subunits caused complete ablation of spontaneous Ca^{2+} release as shown in panel A. Substitutions which caused an increase in spontaneous oscillation propensity exhibited a decreased ER Ca^{2+} level in oscillating cells compared to non-oscillating cells, whereas G1885E/G1886S exhibited an increase in ER Ca^{2+} load as shown in panel B. Adapted from Koop (2008).*

The G1886S substitution forms a putative PKC phosphorylation site in RyR2 (Milting *et al.*, 2006), but this serine residue was not phosphorylated by PKA, PKC, PKG or CamKII, indicating that the functional consequences of this amino acid substitution are independent of RyR2 phosphorylation status. Given that disease-linked RyR2 mutations are responsible for both increasing (Jiang *et al.*, 2005; Jones *et al.*, 2008) and decreasing (Jiang *et al.*, 2007; Koop *et al.*, 2008) the luminal threshold for spontaneous Ca^{2+} oscillations to occur, it is likely that any deviation from a normal threshold at which spontaneous Ca^{2+} release occurs is likely to result in an arrhythmogenic phenotype. As such, a potential therapeutic strategy could potentially involve normalising the level of spontaneous Ca^{2+} release to levels observed with WT RyR2, rather than completely preventing it, which may be pathogenic.

As detailed in the previous chapter, there is conflicting evidence over the precise functional consequences of the L433P ARVD2-linked RyR2 mutation with ambiguity as to whether L433P exhibits a decreased sensitivity to activation (Thomas *et al.*, 2004; 2005) or is a typical gain-of-function mutation (Jiang *et al.*, 2005). However, the data presented in Chapter 3 is consistent with that of *Thomas et al*, who demonstrated that heterologous expression of human RyR2 harbouring the L433P mutation exhibited a decreased magnitude of caffeine-induced Ca^{2+} release and a modest decrease in ER Ca^{2+} store load compared to WT RyR2 (Thomas *et al.*, 2004), suggesting this mutation results in ER Ca^{2+} leak. Conversely, as well as demonstrating that L433P caused an increase in channel sensitivity to caffeine activation using ryanodine binding, Jiang *et al* also showed that the L433P mutation caused an increase in sensitivity to activation by luminal Ca^{2+}, resulting in a substantial increase in the fraction of cells that exhibited spontaneous basal Ca^{2+} release, both in RyR2 null cells and in cardiomycotes (Jiang *et al.*, 2005). The group proposed that like other CPVT/ARVD2-linked mutations, the increase in luminal Ca^{2+} sensitivity caused by the L433P mutation reduced the threshold at which spontaneous Ca^{2+} release occurred, thus enhancing the propensity for DADs and triggered arrhythmias. There could be reconciliation between the data presented here and that of *Jiang et al*, in that the observed reduction in caffeine-evoked Ca^{2+} release magnitude resulting from a decreased ER Ca^{2+} load (Figure 3.23) could be attributed to an increased luminal Ca^{2+} sensitivity or lower luminal threshold for spontaneous Ca^{2+} release.

5.1.5. Chapter aims

In Chapter 3, L433P was shown to decrease the caffeine sensitivity of channel activation and did not result in a typical gain-of-function intracellular Ca^{2+} handling phenotype. Gain-of-function RyR2 mutations, which increase channel sensitivity to activation, also increase the propensity for cells to exhibit spontaneous ER Ca^{2+} release (Jiang *et al.*, 2005). G1885E has been shown to alter the spontaneous Ca^{2+} release incidence of HEK cells expressing another RyR2 SNP (Koop *et al.*, 2008), G1886S. These spontaneous Ca^{2+} release events occur as Ca^{2+} 'oscillations' in the absence of RyR2 agonists e.g. caffeine, apart from Ca^{2+} in the external media. In Chapter 4, L433P and G1885E were shown to alter underlying Ca^{2+} cycling following caffeine-evoked Ca^{2+} release.

It is hypothesised that:

- Consistent with previous investigation of L433P and other CPVT/ARVD2-linked RyR2 mutations, L433P alters the incidence of spontaneous ER Ca^{2+} release and is modulated by G1885E co-expression.

- L433P perturbs intracellular Ca^{2+} handling of basal spontaneous Ca^{2+} release events in a comparable manner to that of caffeine-evoked Ca^{2+} release and is modulated by G1885E to varying degrees, depending on the mode of co-expression.

- Analysis of spontaneous Ca^{2+} release events may reveal further mechanisms of L433P Ca^{2+} handling dysfunction arising from differences in channel activation/inactivation mechanisms between spontaneous and caffeine-evoked Ca^{2+} release (Gaburjakova & Gaburjakova, 2006).

- Compensatory relationships between spontaneous Ca^{2+} release and subsequent Ca^{2+} extrusion exist in the absence of caffeine and such relationships are altered by L433P and G1885E expression.

In this chapter, the functional consequences of L433P and G1885E expression on spontaneous Ca^{2+} oscillation propensity, intracellular Ca^{2+} handling parameters of spontaneous Ca^{2+} release and the relationships between such parameters will be examined.

5.2. Methods

Single-cell Ca^{2+} imaging experiments using confocal microscopy were carried out as detailed in section 2.2.2.3. Despite being collected in the same experiments described in Chapter 3 of this thesis, data acquired from cells that exhibited spontaneous basal Ca^{2+} oscillations were omitted from the analysis detailed in Chapters 3 and 4. The omission of such data was deemed necessary due to differences in the nature of the basal Ca^{2+} signal, which is critical in determining several Ca^{2+} release parameters e.g. Ca^{2+} release magnitude. Instead data from cells exhibiting spontaneous basal Ca^{2+} oscillations in the absence of caffeine were analysed as a distinct data set, which will be the main focus of this chapter.

An example of a Ca^{2+}-imaging trace of a cell exhibiting spontaneous Ca^{2+} oscillations is shown in Figures 5.4 and 5.6. Spontaneous Ca^{2+} oscillations were defined as the rhythmic increase and decrease in cytoplasmic Ca^{2+} levels prior to agonist-evoked channel activation. In spontaneously oscillating cells, Ca^{2+} oscillation morphology was highly comparable between that of sequential Ca^{2+} oscillations within the same cell, but exhibited a different morphology to caffeine-evoked Ca^{2+} release transients (Figure 5.6).

5.2.1. Propensity for spontaneous basal Ca^{2+} release as Ca^{2+} oscillations

The relative propensity for cells transfected with each RyR2 cDNA to exhibit spontaneous Ca^{2+} release in the form of basal Ca^{2+} oscillations was determined. The number of cells, both oscillating and non-oscillating, that exhibited an increase in cytosolic Ca^{2+} immediately following caffeine addition (0.1-10mM) was recorded in a similar manner. The number of cells exhibiting spontaneous Ca^{2+} oscillations or sensitivity to caffeine activation was expressed as a percentage of the total number of cells in the field of view. Transfection efficiency was determined as shown in Figure 3.10. The number of cells per field of view that exhibited caffeine sensitivity was expressed as a percentage of the total number of cells in that field of view. The percentage of oscillating, caffeine-sensitive cells per coverslip was calculated for cells transfected with each RyR2 cDNA to determine if L433P or G1885E altered spontaneous Ca^{2+} release propensity.

5.2.2. Measurement of spontaneous Ca^{2+} release parameters

Semi-automated oscillation analysis software; SALVO (Synchrony – Amplitude – Length – Variability of Oscillation, Silvester *et al.*, 2009) was used to measure several Ca^{2+} handling parameters from single-cell Ca^{2+} imaging data (Figure 5.4). Raw Ca^{2+} imaging data was exported from Leica LAS AF software to a Microsoft Excel compatible format. Data was imported into SALVO and the beginning and the end of the Ca^{2+} oscillation ('valleys') and the highest point of the Ca^{2+} oscillation ('peak') were manually input into SALVO. Parameters that were determined by SALVO analysis and the method employed in calculating parameter values are detailed below:

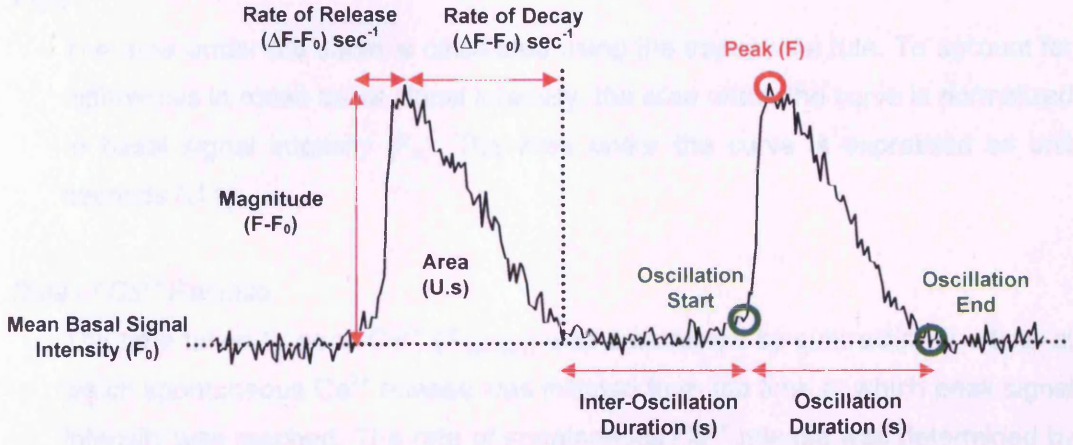

Figure 5.4. Measurement of spontaneous Ca^{2+} oscillation parameters using SALVO. *Synchrony – Amplitude – Length – Variability of Oscillations (SALVO) software was used to measure several parameters of spontaneous Ca^{2+} oscillation parameters. SALVO is semi-automated and requires the start and the end of each oscillation to be indicated by the user.*

Basal Signal Intensity

Basal signal intensity (F_0) was measured by taking a mean average of the signal intensity at each time point that occurred between spontaneous Ca^{2+} oscillations. This is not to be confused with the mean signal intensity, which is the mean signal intensity over the entire time course, including that of Ca^{2+} oscillations.

Height and Magnitude

Oscillation height was determined by measuring the oscillation peak signal intensity (F) and subtracting the average inter-oscillation basal signal (F_0) from

this value, to obtain the magnitude of Ca^{2+} release ($F-F_0$). To account for differences in basal signal intensity between cells, peak magnitude was normalised to the average basal signal intensity ($F-F_0 / F_0$).

Duration

The duration of the Ca^{2+} oscillation was determined by subtracting the time at which spontaneous Ca^{2+} release was initiated from the time at which signal intensity returned to F_0. The duration of the spontaneous Ca^{2+} oscillation was expressed in seconds (s).

Area

The area under the curve is calculated using the trapezoidal rule. To account for differences in mean basal signal intensity, the area under the curve is normalized to basal signal intensity (F_0). The area under the curve is expressed as unit seconds (U s).

Rate of Ca^{2+} Release

The time taken to peak Ca^{2+} ($T_{Release}$) was determined by subtracting the time at which spontaneous Ca^{2+} release was initiated from the time at which peak signal intensity was reached. The rate of spontaneous Ca^{2+} release was determined by dividing peak magnitude ($F-F_0 / F_0$) by the time taken to reach peak signal intensity ($[F-F_0 / F_0] / T_{Release}$) and is expressed as the change in signal intensity over time i.e dF / dt.

Rate of Ca^{2+} Removal

The time taken for signal intensity to return to basal levels ($T_{Removal}$) was determined by subtracting the time of peak signal intensity from the time at which signal intensity decreased to F_0. To determine the rate of Ca^{2+} removal from the cytosol, peak magnitude ($F-F_0 / F_0$) was divided by the time taken for signal intensity to decline back to that of the baseline $[(F-F_0 / F_0) / T_{Removal}]$

Due to the relatively short time period over which Ca^{2+} imaging data was collected prior to caffeine addition i.e. 60 seconds, it was not possible to carry out an accurate comparison of oscillation frequency between cells expressing each recombinant RyR2. Approximately 70% of oscillating cells exhibited 1 or 2 Ca^{2+} oscillations in the 60 second

period prior to caffeine activation and approximately 90% exhibited 3 Ca^{2+} oscillations in this same period. The low number of Ca^{2+} oscillations observed could lead to artefactual conclusions being made with regards to oscillation frequency and was not included in the analysis detailed in this chapter.

5.2.3. Linear regression analysis of Ca^{2+} release parameters

Linear regression analysis was used to identify whether any relationships existed between oscillation parameters. To examine this, Ca^{2+} oscillation parameters were measured using SALVO as detailed in section 5.2.2. and parameter data from cells expressing each recombinant RyR2 were collated. Linear regression analysis was carried out between pairs of spontaneous Ca^{2+} oscillation parameters as detailed in section 2.2.5, and was also used to identify whether there were any relationships between spontaneous Ca^{2+} oscillation parameters and those of the subsequent caffeine-induced Ca^{2+} release transient (Figure 5.5).

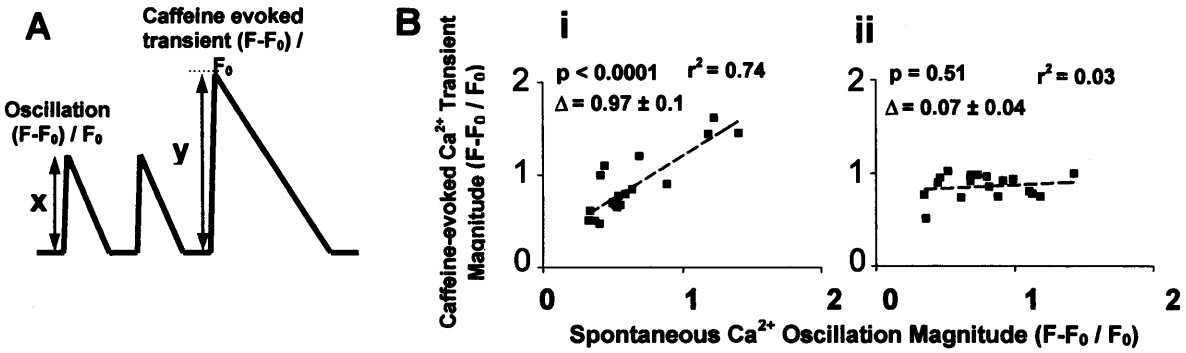

Figure 5.5. Linear regression analysis of spontaneous and caffeine-evoked Ca^{2+} release parameters. *The mean value of a particular spontaneous Ca^{2+} release parameter i.e. Ca^{2+} release magnitude, was calculated from the basal Ca^{2+} oscillations (panel A, x) and the same parameter was measured in the subsequent caffeine-evoked Ca^{2+} release transient (panel A, y) in the same cell. Examples to illustrate the presence and absence of a significant relationship are presented in panel B. Data was presented as scatter-plots and linear regression analysis descriptive statistics were determined to ascertain whether relationships existed (I or did not exist (ii) between the same Ca^{2+} handling parameter in spontaneous or caffeine-evoked Ca^{2+} release.*

However, caffeine applications were often made during periods of elevated cytoplasmic Ca^{2+} resulting from prior spontaneous Ca^{2+} release, meaning that those caffeine-evoked responses couldn't always be accurately measured from a resting baseline (Figure 5.6).

To negate this issue, only cells in which the caffeine response was observed when intracellular Ca^{2+} was at basal levels (Figure 5.6A), and not those where the response was observed partway through a Ca^{2+} oscillation (Figure 5.6B-C), were used in linear regression analysis of spontaneous and caffeine-evoked Ca^{2+} release parameters.

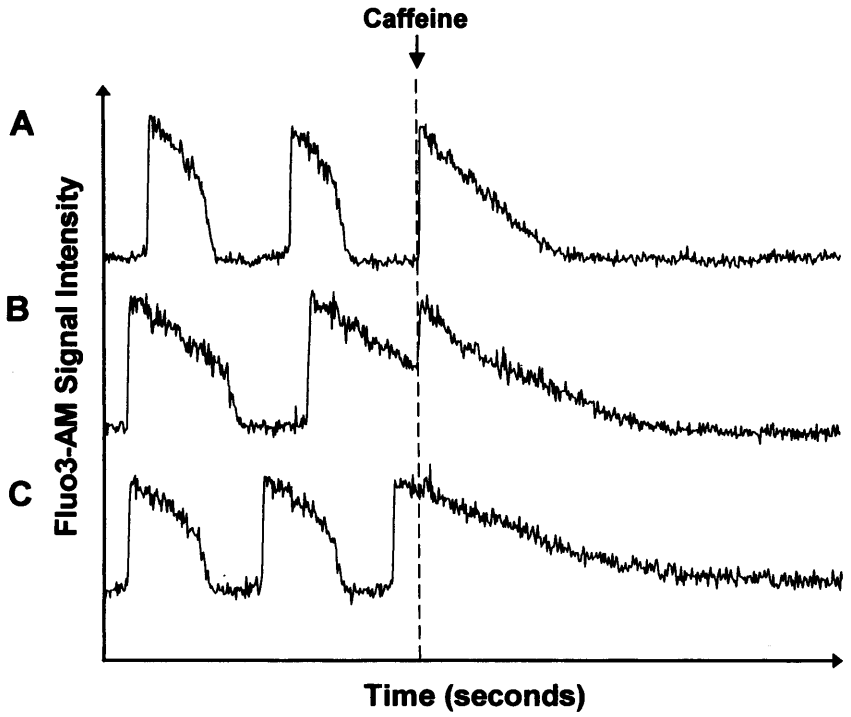

Figure 5.6. Caffeine causes further Ca^{2+} release from the ER, even if applied during a spontaneous Ca^{2+} oscillation. *A proportion of HEK cells expressing each recombinant RyR2 exhibited spontaneous basal Ca^{2+} oscillations prior to caffeine addition. Following activation of RyR2 with caffeine (dotted red line 0.1-10mM), no further Ca^{2+} oscillations were observed and the Ca^{2+}-dependent Fluo3 signal decreased to a resting level, as shown in panels A-C. Even if caffeine was added when intracellular Ca^{2+} levels were partially declined (but still significantly greater than basal levels), further Ca^{2+} was released from the ER store, as indicated in panel B. Similarly, when caffeine was added only a few seconds after the initiation of a spontaneous Ca^{2+} release event, the caffeine evoked Ca^{2+} release was much less obvious, as shown in panel C.*

Due to the inherent variability of HEK cells, goodness-of-fit (r^2) values tended to be relatively low and as such, a low arbitrary r^2 threshold value of 0.3 was adopted to infer a weak relationship between two Ca^{2+} oscillation parameters, data with a moderate fit to the regression model were characterised by r^2 values between 0.5 and 0.7, and r^2 values greater than 0.7 inferred a strong linear relationship between two given parameters. The relatively high number of oscillating cells expressing each construct (between 79-425 cells) allowed the generation of stringent significance values (*p-values*) in terms of determining increasing/decreasing trends in the data.

5.3. Results

5.3.1. RyR2 mutations and polymorphisms alter spontaneous Ca^{2+} release propensity

As described in section 3.3.2, there was no significant difference between the average transfection efficiencies of cells transfected with each RyR2 cDNA, either alone or co-expressed with WT RyR2 (Figure 3.10, $p > 0.05$, ANOVA). Chapter 3 also provides evidence that the transfection efficiency of each RyR2 cDNA was comparable to that of WT RyR2 (Students t-test, $p = 0.88$, Figure 3.10).

Only HEK cells expressing functional RyR2 channels exhibit transient Ca^{2+} release following exposure to caffeine (0.1-10mM). The percentage of cells responding to caffeine, which is indicative of functional RyR2 expression, was determined in HEK cells expressing each combination of WT RyR2, L433P and G1885E, both as homotetramers and heterotetramers (Figure 5.7A). In most cases, an equivalent number of cells expressing each combination of RyR2s containing combinations of L433P and G1885E substitutions, both alone and with WT RyR2, demonstrated a similar propensity to exhibit caffeine sensitivity compared to WT, although the heterotetrameric expression of WT+LP resulted in an increased number of caffeine-sensitive cells ($p < 0.001$, Figure 5.7A).

Surprisingly, the observed transfection efficiency, as determined by fluorescence microscopy, was approximately 5-10% lower than the percentage of cells responding to caffeine. This discrepancy was observed for cells transfected with each RyR2 cDNA and could possibly be attributable to cells expressing low levels of eGFP-tagged RyR2 not exhibiting sufficient eGFP fluorescence to allow detection using fluorescence microscopy, despite sufficient RyR2 being expressed to elicit caffeine-induced Ca^{2+} release readily detectable by confocal Ca^{2+} imaging.

Single-cell Ca^{2+} imaging experiments demonstrated that a significant percentage of cells expressing each recombinant RyR2 exhibited spontaneous basal Ca^{2+} oscillations under resting conditions, prior to agonist exposure (13-39%, Figure 5.7B). Despite the majority of recombinant RyR2s exhibiting similar numbers of caffeine-sensitive cells, there was greater variation in the propensity for cells expressing each RyR2 to exhibit spontaneous basal Ca^{2+} oscillations (Figure 5.7B). In these experiments, the propensity of

spontaneous Ca^{2+} release refers to the percentage of cells exhibiting spontaneous Ca^{2+} oscillations, and should not be confused with the frequency of oscillations in a given cell.

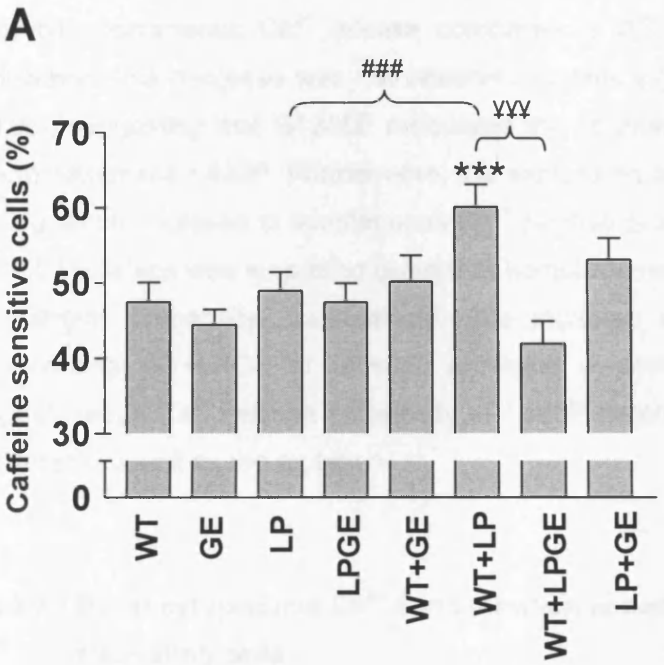

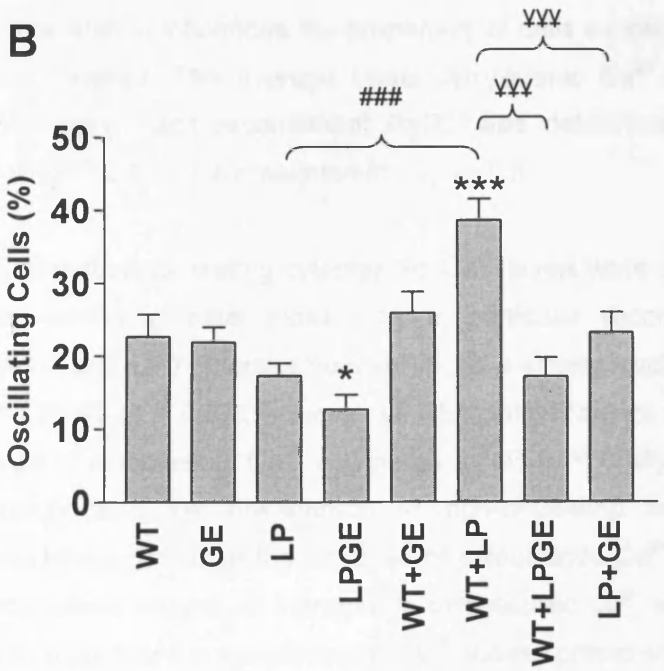

Figure 5.7. HEK cells expressing L433P and G1885E exhibit heterogeneity between spontaneous Ca^{2+} release propensity. *The percentage of all cells that exhibited caffeine sensitivity are indicated in panel A. The percentage of all cells that exhibited spontaneous basal Ca^{2+} oscillations prior to caffeine-evoked Ca^{2+} release is indicated in panel B. Data is plotted as the mean percentage ± S.E.M. The results of statistical comparison are indicated on the graphs according to the key in panel C. (brackets, $p < 0.05$, ANOVA). Caffeine sensitivity and oscillation propensity data was collected from between 39 and 75 individual coverslips from between 7 and 17 separate transfections.*

* *indicates a statistically significant difference compared to WT RyR2.*

*indicates a statistically significant difference compared to the homotetrameric counterpart of heterotetrameric substitution i.e. WT+GE vs GE or WT+LP vs LP or WT+LPGE vs LP.*

¥ *indicates a statistically significant difference compared to the respective recombinant RyR2 without G1885E co-expression. i.e. LP-GE vs LP or WT+LPGE vs WT+LP or LP+GE vs WT+LP*

G1885E expression did not alter the propensity of cells to exhibit spontaneous basal Ca^{2+} oscillations compared to WT RyR2, irrespective of whether it was expressed alone (GE, $p = 0.83$) or co-expressed with WT RyR2 (WT+GE, $p = 0.46$). The homotetrameric expression of LPGE resulted in a significant decrease in the propensity for cells to exhibit spontaneous Ca^{2+} release compared to WT RyR2 (Figure 5.7B, $p < 0.05$). However, this decrease was not observed in cells expressing homotetrameric LP ($p < 0.05$), suggesting that G1885E modulates the spontaneous Ca^{2+} release propensity of homotetrameric L433P. Furthermore, the expression of WT+LP heterotetramers caused a significant increase in spontaneous Ca^{2+} release propensity compared to WT RyR2 ($p < 0.001$), which was surprising given that homotetrameric L433P had little effect on Ca^{2+} oscillation propensity. Interestingly, this increase was not observed in cells co-expressing WT+LPGE or LP+GE, providing evidence that G1885E also alters the spontaneous Ca^{2+} release propensity of L433P heterotetramers when on the same or different subunit as the mutation.

5.3.2. Basal cytoplasmic Ca^{2+} concentration is comparable in oscillating and non-oscillating cells

Basal cytoplasmic Ca^{2+} was measured to determine whether cytoplasmic Ca^{2+} concentration influenced the propensity of cells expressing RyR2 to exhibit spontaneous Ca^{2+} release. The average basal cytoplasmic Ca^{2+} concentration of oscillating cells expressing each recombinant RyR2 was determined using the method detailed in section 3.2.6 and is presented in Figure 5.8.

In all instances, resting cytoplasmic Ca^{2+} levels were equivalent between oscillating and non-oscillating cells expressing a particular recombinant RyR2. Oscillating cells expressing LP homotetramers exhibited a similar level of cytoplasmic Ca^{2+} compared to WT RyR2 ($p = 0.67$), however LPGE homotetramers exhibited a significantly increased level of cytoplasmic Ca^{2+} compared to LP ($p < 0.05$) and WT RyR2 ($p < 0.001$). This corroborates the observation in non-oscillating cells that homotetrameric LPGE expression results in the increase of cytoplasmic Ca^{2+}. Although homotetrameric LPGE expression caused an increase in cytoplasmic Ca^{2+} concentration (Figure 5.8) coupled with a decrease in spontaneous Ca^{2+} release propensity (Figure 5.7B), a similar coupling was not observed as a result of the expression of other RyR2s that also altered Ca^{2+}

oscillation propensity, i.e. WT+LP. This data suggests that the variation in propensity for cells expressing recombinant RyR2 to exhibit spontaneous Ca^{2+} release is independent of basal cytoplasmic Ca^{2+} concentration.

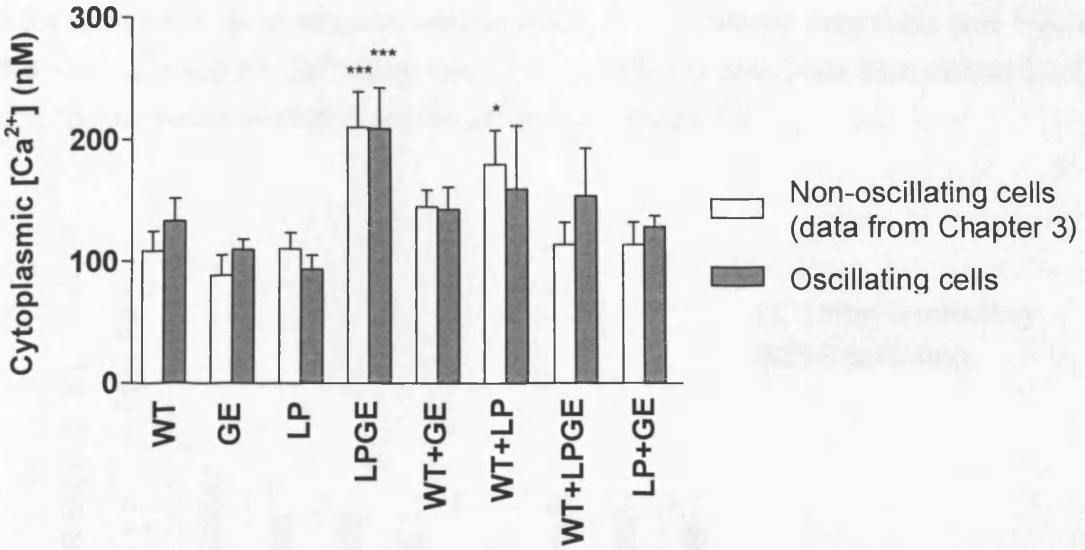

Figure 5.8. Basal cytoplasmic Ca^{2+} levels are similar in oscillating and non-oscillating cells, but vary between RyR2s. *Data presented is the mean ± S.E.M. basal cytoplasmic Ca^{2+} concentration, as determined by ionomycin and EGTA calibration described in section 3.2.6. Data was collected from between 8 and 74 transfected HEK cells and from 284 untransfected HEK cells from between 3 and 9 separate experiments. Asterisked data indicates a significant difference to WT RyR2 ($p<0.05$).*

5.3.3. Oscillating cells exhibit equal or decreased ER Ca^{2+} store content compared to non-oscillating cells

Jiang et al proposed that CPVT/ARVD2-linked RyR2 mutations, including L433P and G1885E, increase the propensity for spontaneous Ca^{2+} release due to an increase in luminal Ca^{2+} sensitivity, which consequently results in decreased ER Ca^{2+} levels (Jiang *et al.*, 2005; Koop *et al.*, 2008). Thus, the ER Ca^{2+} levels of cells exhibiting spontaneous Ca^{2+} release were determined to see whether alterations in Ca^{2+} store load reconciled with the observed alterations in spontaneous Ca^{2+} release propensity.

ER Ca^{2+} levels of RyR2-expressing HEK-293 cells exhibiting spontaneous Ca^{2+} oscillations were determined as described in section 3.2.5. Untransfected HEK, cells did not exhibit spontaneous Ca^{2+} oscillations, and as such, only cells expressing RyR2

exhibited these spontaneous Ca^{2+} release events. However, caffeine (0.5mM) was added to the cells prior to the administration of thapsigargin to allow direct comparison of the ER Ca^{2+} levels between oscillating and non-oscillating cells, as caffeine was used to identify RyR2-expressing, non-oscillating cells (section 3.2.5). If the caffeine or thapsigargin-evoked response occurred during a Ca^{2+} oscillation, this cell was excluded from analysis to allow accurate determination of Ca^{2+} release magnitude (see Figure 5.6). The average ER Ca^{2+} store load of non-oscillating cells (data from section 3.3.7) and spontaneously oscillating cells is presented in Figure 5.9.

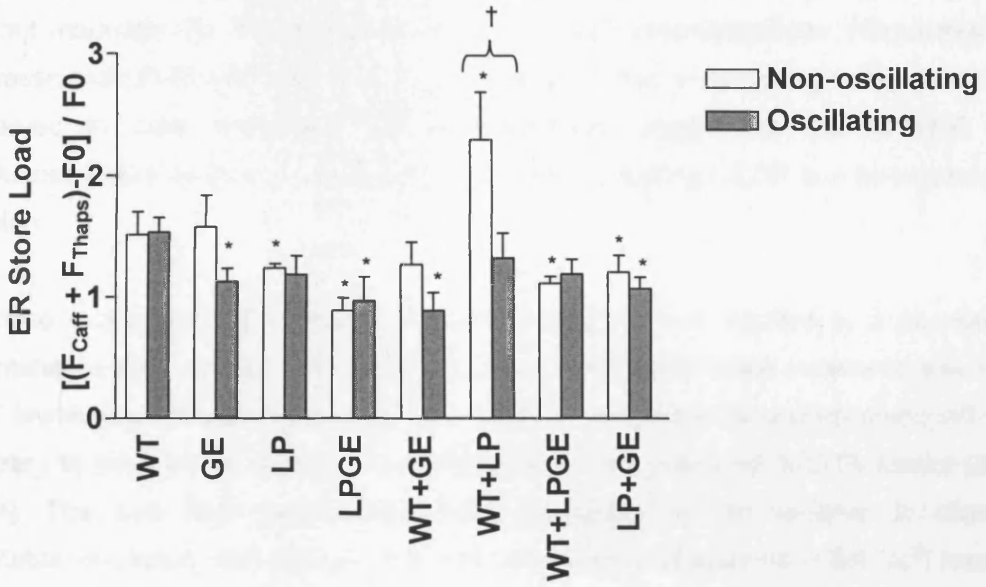

Figure 5.9. Oscillating cells expressing WT+LP exhibit altered ER Ca^{2+} load. *Data presented is the combined mean ± S.E.M. change in fluo3-AM signal intensity following addition of caffeine (0.5mM) immediately followed by thapsigargin (10μM). White bars represent the ER Ca^{2+} levels of non-oscillating cells. Grey bars represent the ER Ca^{2+} levels of spontaneously oscillating RyR2-expressing HEK-293 cells. Data was collected from between 12 and 69 transfected HEK cells and 284 untransfected HEK cells from between 3 and 9 separate experiments. † denotes a significant difference between oscillating and non-oscillating cells transfected with the same RyR ($p<0.05$). Asterisked data indicates a significant difference to WT RyR2 ($p<0.05$)*

Consistent with previous work, cells expressing WT RyR2 exhibited a similar ER Ca^{2+} store load in both oscillating and non-oscillating cells (Jiang *et al.*, 2005; Koop *et al.*, 2008). Comparable ER Ca^{2+} levels in oscillating and non-oscillating cells were also observed in cells expressing each RyR2, although the expression of heterotetrameric

WT+LP resulted in a significantly decreased level of ER Ca^{2+} in oscillating cells compared to non-oscillating cells ($p < 0.05$). Although L433P or G1885E-containing RyR2s resulted in decreased ER Ca^{2+} levels in oscillating cells compared to WT RyR2, there were no significant differences between ER Ca^{2+} levels of oscillating cells expressing each RyR2 mutation/polymorphism.

The Ca^{2+} store load of oscillating cells expressing heterotetrameric WT+LP was significantly decreased when compared to non-oscillating cells expressing WT+LP ($p < 0.05$). The expression of heterotetrameric WT+LPGE or LP+GE resulted in an equivalent level of ER Ca^{2+} compared to that of cells expressing WT+LP, indicating that G1885E did not modulate the ER store load of cells WT+LP heterotetramers. Homotetrameric expression of LPGE exhibited a decrease in ER Ca^{2+} load in oscillating cells that was not observed in cells expressing LP homotetramers, suggesting that G1885E only modulates the store load of oscillating HEK cells expressing L433P in a homotetrameric fashion.

In these experiments, expression of RyR2 mutants which resulted in a decrease in spontaneous Ca^{2+} oscillation propensity did not necessarily result in an increase in ER Ca^{2+} levels (e.g. homotetrameric LPGE), and *vice versa* (e.g. heterotetrameric WT+LP), contrary to what would be expected according to the proposed SOICR model (Jiang, 2004). The data from these experiments suggests that the variation in observed oscillation propensity can not be completely attributed to alterations in ER Ca^{2+} load and that other contributory factors are likely involved i.e. Ca^{2+} sensitivity, RyR2 stability etc.

5.3.4. Heterogeneity in basal spontaneous Ca^{2+} oscillation parameters

To determine whether L433P and G1885E altered the Ca^{2+} handling dynamics in the absence of agonist-evoked channel activation, several parameters of the spontaneous Ca^{2+} oscillation were measured. This allowed comparison of intracellular Ca^{2+} handling characteristics of cells that were undergoing basal Ca^{2+}-cycling, with RyR2 switching between the open and closed states during CICR and subsequent store refilling. Single-cell calcium imaging data was collected as described in section 2.2.2.3 and analysed using SALVO software as described in section 5.2.2.

5.3.4.1. Oscillation parameters: magnitude, duration and area

There appeared to be significant variation between several parameters of spontaneous basal Ca^{2+} oscillations between cells expressing each RyR2 (Figure 5.10 and 5.11). Alteration of these parameters is indicative of altered intracellular Ca^{2+} handling following spontaneous Ca^{2+} release, which could lead to the sustained elevation of cytoplasmic Ca^{2+} concentration leading to premature inward Na^{+} current and DAD onset in a cardiac setting.

Expression of GE homotetramers or WT+GE heterotetramers had little effect on the spatial parameters of intracellular Ca^{2+} handling, although co-expression of WT+GE caused a small, but significant increase in Ca^{2+} oscillation area compared to that of WT RyR2 ($p < 0.05$), an effect that was not evident when G1885E was expressed alone (Figure 5.10C). This is likely a cumulative effect of the observed marginal increase in oscillation magnitude (Figure 5.10A) and duration (Figure 5.10B) in cells expressing WT+GE heterotetramers.

Cells expressing homotetrameric LP or LPGE exhibited Ca^{2+} oscillations with a similar magnitude (Figure 5.10A, $p=0.53$ and $p=0.28$ respectively), but significantly increased duration and area, compared to those observed in cells expressing WT RyR2 (Figure 5.10B and C, $p < 0.05$). Oscillation magnitude, duration and area were similar between cells expressing homotetrameric LP or LPGE, indicating that G1885E has no effect on spontaneous Ca^{2+} oscillation magnitude, duration or area when found with L433P on every subunit of the tetramer.

Expression of heterotetrameric WT+LP resulted in a significant increase in Ca^{2+} oscillation magnitude compared to WT RyR2, a similar observation to that following caffeine-evoked Ca^{2+} release (section 3.3.5). This increase in oscillation magnitude culminated in an increase in oscillation area, despite similar oscillation duration compared to WT. Despite both homotetrameric LP and heterotetrameric WT+LP expression altering magnitude and duration of oscillations in a different manner, both modes of L433P expression resulted in a similar increase in oscillation area, indicative of sustained elevated cytoplasmic Ca^{2+} concentration following CICR, consistent with previous findings (Thomas *et al.*, 2004; 2005). Similar observations were made through the expression of homotetrameric LPGE and heterotetrameric WT+LPGE compared to

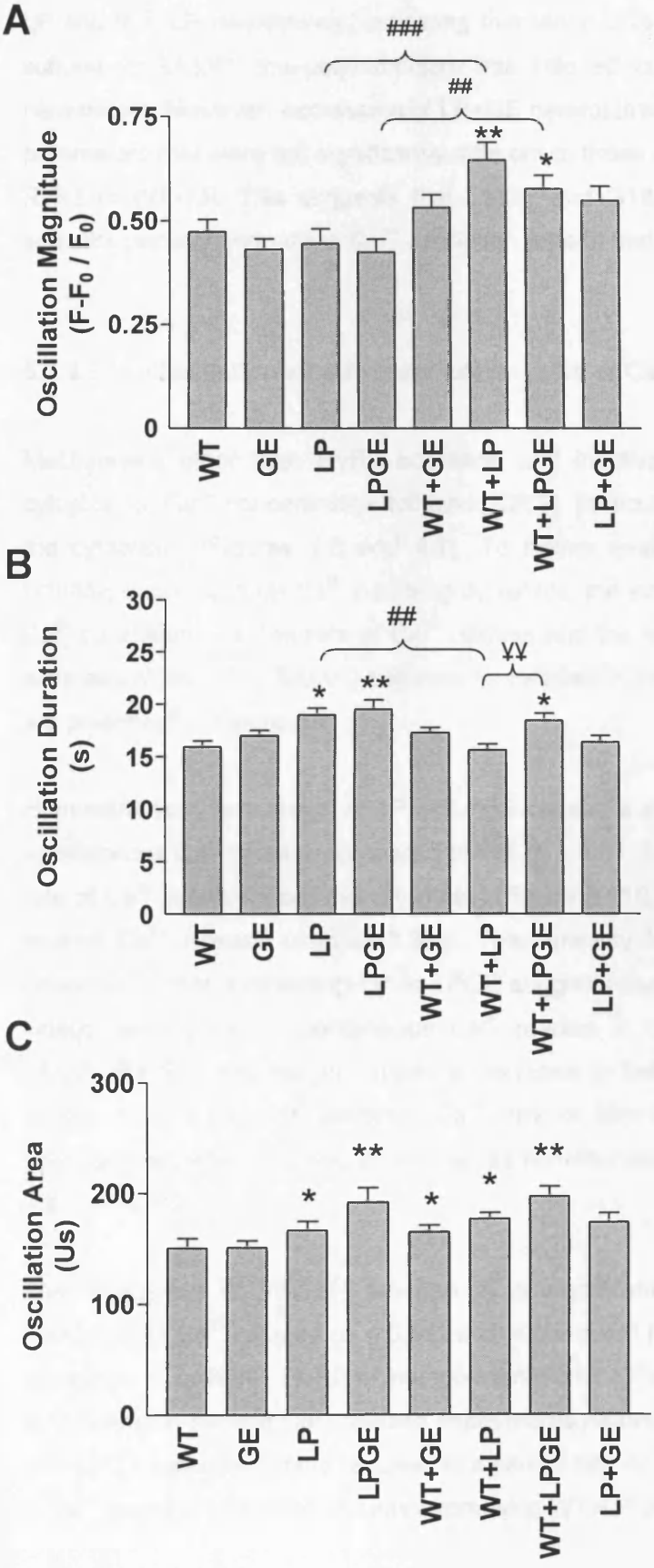

Figure 5.10. Homotetrameric and heterotetrameric expression of LP or LPGE increase oscillation area. *SALVO analytical software was used to measure spatial parameters of spontaneous basal Ca^{2+} oscillations. There was heterogeneity in Ca^{2+} oscillation magnitude (panel A), duration (panel B) and the area under the oscillation trace (panel C). The results of statistical comparisons are indicated on the graphs according to the key above. Data was collected from between 77 and 327 oscillating HEK cells expressing recombinant RyR2.*

** indicates a statistically significant difference compared to WT RyR2.*

 # indicates a statistically significant difference compared to the homotetrameric counterpart of heterotetrameric substitution
i.e. WT+GE vs GE or WT+LP vs LP or WT+LPGE vs LP.

¥ indicates a statistically significant difference compared to the respective recombinant RyR2 without G1885E co-expression.
i.e. LP-GE vs LP or WT+LPGE vs WT+LP or LP+GE vs WT+LP

LP and WT+LP respectively, indicating that when G1885E co-expressed on the same subunit as L433P, the polymorphism has little effect on spontaneous Ca^{2+} release parameters. However, expression of LP+GE heterotetramers resulted in oscillations with parameters that were not significantly different to those observed in cells expressing WT RyR2 or WT+LP. This suggests that L433P and G1885E co-expression on separate subunits partially normalises Ca^{2+} oscillation area to that observed in WT RyR2.

5.3.4.2. Oscillation kinetic parameters: rates of Ca^{2+} release and removal

Mechanisms other than RyR2 activation and inactivation are involved in regulating cytoplasmic Ca^{2+} concentration following CICR, particularly in the removal of Ca^{2+} from the cytoplasm (Figures 1.3 and 4.1). To further examine the effects of L433P and G1885E expression on Ca^{2+} handling dynamics, the kinetic parameters of spontaneous Ca^{2+} oscillations i.e. the rate of Ca^{2+} release and the rate of subsequent Ca^{2+} removal, were examined using SALVO software as detailed in section 5.2.2., the results of which are presented in Figure 5.11.

Homotetrameric expression of LP or LPGE caused a significant decrease in the rate of spontaneous Ca^{2+} release compared to WT ($p < 0.01$, Figure 5.11A) but did not alter the rate of Ca^{2+} removal from the cytoplasm (Figure 5.11B), consistent with that of caffeine evoked Ca^{2+} release (section 3.3.6). The similarity between the kinetic parameters observed in cells expressing LP or LPGE suggests that G1885E has little effect on the kinetic parameters of spontaneous Ca^{2+} release in cells expressing homotetrameric L433P. G1885E expression caused a decrease in both the rate of spontaneous Ca^{2+} release and the rate of subsequent Ca^{2+} removal from the cytoplasm, although this was only observed when GE was expressed as homotetramers, and not when co-expressed with WT RyR2.

The expression of WT+LP resulted in a significant increase in both the rate of spontaneous Ca^{2+} release ($p < 0.01$) and subsequent rate of Ca^{2+} removal ($p < 0.001$), compared to both WT RyR2 or homotetrameric LP. This finding parallels that observed in the caffeine-evoked Ca^{2+} release experiments detailed in section 3.3.6. Expression of WT+LPGE heterotetramers resulted in a similar rate of Ca^{2+} release, but decreased rate of Ca^{2+} removal compared to cells expressing WT+LP (Figure 5.11), suggesting G1885E

has a greater modulatory effect on Ca^{2+} removal processes than spontaneous Ca^{2+} release. The co-expression of LP+GE on separate subunits produced kinetic parameters that were similar to those observed in cells expressing WT+LP, indicating that G1885E had little effect on kinetic parameters of spontaneous Ca^{2+} release when not on the same subunit as L433P.

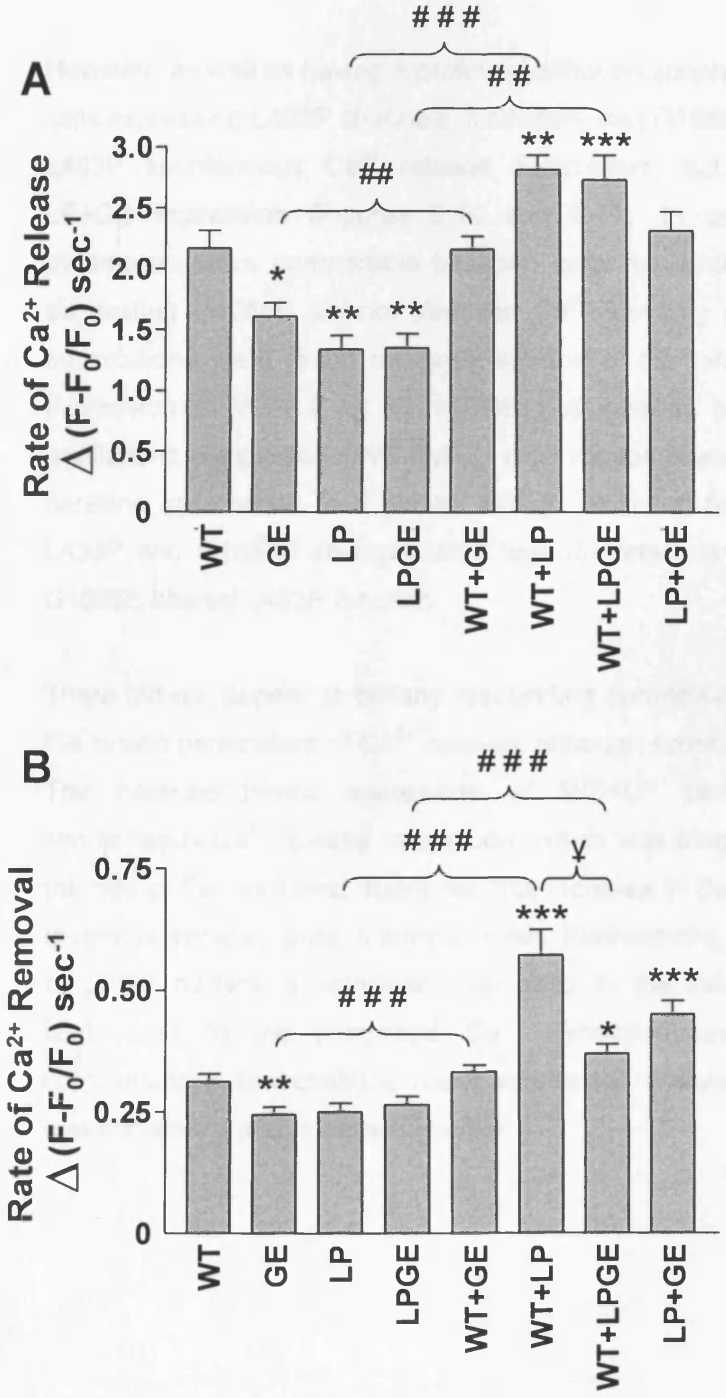

Figure 5.11. L433P and G1885E alter kinetic parameters of spontaneous Ca^{2+} release. *SALVO analytical software was used to measure kinetic parameters of spontaneous basal Ca^{2+} oscillations. There was heterogeneity in the rate of spontaneous Ca^{2+} release (panel A) and the rate of subsequent Ca^{2+} removal from the cytoplasm (panel B). The results of statistical comparisons are indicated on the graphs according to the key above. Data was collected from between 77 and 327 oscillating HEK cells expressing recombinant RyR2.*

** indicates a statistically significant difference compared to WT RyR2.*

 # indicates a statistically significant difference compared to the homotetrameric counterpart of heterotetrameric substitution i.e. WT+GE vs GE or WT+LP vs LP or WT+LPGE vs LP.

¥ indicates a statistically significant difference compared to the respective recombinant RyR2 without G1885E co-expression. i.e. LP-GE vs LP or WT+LPGE vs WT+LP or LP+GE vs WT+LP

Table 5.1 summarises the measured Ca^{2+} oscillation parameters, as well as the results of statistical comparison between the mutant/polymorphism RyR2 and WT RyR2. In accordance with the agonist-evoked Ca^{2+} release experiments detailed in Chapter 3, and the Ca^{2+} flux analysis detailed in Chapter 4, the greatest perturbation of intracellular Ca^{2+} handling parameters were observed following homotetrameric expression of LP or LPGE or the heterotetrameric expression of WT+LP.

However, as well as having a profound effect on spontaneous Ca^{2+} release propensity in cells expressing L433P channels, it appears that G1885E exhibits a modulatory effect on L433P spontaneous Ca^{2+} release parameters, but only following heterotetrameric LP+GE expression (Figures 5.10 and 5.11). In contrast, all measured oscillation parameters were comparable between cells expressing LP or LPGE homotetramers, suggesting G1885E did not alter the Ca^{2+} handling parameters of L433P when both substitutions were found on every subunit of the tetramer. Although heterotetrameric expression of WT+LP or WT+LPGE both altered parameters of spontaneous Ca^{2+} oscillations compared to WT RyR2, both modes of expression tended to augment Ca^{2+} handling parameters to a similar extent, providing further evidence that the mode of L433P and G1885E co-expression was important in determining the extent to which G1885E altered L433P function.

There did not appear to be any resounding reconciliation between oscillation area and the kinetic parameters of Ca^{2+} release, although some general observations were made. The heterotetrameric expression of WT+LP caused a significant increase in spontaneous Ca^{2+} release magnitude, which was coupled with a significant increase in the rate of Ca^{2+} removal. However, this increase in Ca^{2+} removal rate was not sufficient to restore transient area to normal levels. Furthermore, homotetrameric expression of LP or LPGE caused a significant decrease in the rate of Ca^{2+} removal, which likely contributed to the increased Ca^{2+} oscillation area. To further examine these compensatory relationships, linear regression analysis on key oscillation parameters was carried out and is detailed below.

RyR2	Oscillation Propensity (% ± S.E.M)	Ca^{2+} Store Load $(F-F_0)/F_0$		Basal Cytoplasmic $[Ca^{2+}]$ (nM)		Oscillation Parameter Measurements				
		Non Osc	Osc	Non Osc	Osc	Magnitude $(F-F_0)/F_0$	Duration (s)	Area (Us)	Rate of Ca^{2+} Release $\Delta F-F_0-F_0/s$	Rate of Ca^{2+} Removal $\Delta F-F_0-F_0/s$
Wild Type	22.7 ± 3.0	1.51 ± 0.19	1.53 ± 0.12	108.7 ± 16.2	133.5 ± 18.3	0.47 ± 0.03	15.9 ± 0.56	150.6 ± 8.7	2.17 ± 0.15	0.31 ± 0.016
G1885E	21.9 ± 2.1	1.57 ± 0.26	**1.12 ± 0.11 ***	88.5 ± 16.8	109.8 ± 8.6	0.43 ± 0.03	17.0 ± 0.49	151.2 ± 6.0	**1.61 ± 0.11 ***	**0.25 ± 0.015 ***
L433P	17.3 ± 1.7	**1.24 ± 0.04 ***	1.19 ± 0.15	110.7 ± 13.2	94.0 ± 11.4	0.44 ± 0.04	**19.0 ± 0.67 ***	**166.9 ± 7.8**	**1.34 ± 0.12 ***	0.25 ± 0.018
L433P-G1885E	**12.8 ± 2.0 ***	**0.89 ± 0.11 ***	**0.97 ± 0.2 ***	**210.3 ± 29.1 ***	**209.3 ± 33.5 ***	0.42 ± 0.03	**19.5 ± 0.91 ***	**192 ± 13.2 ***	**1.36 ± 0.11 ***	0.27 ± 0.017
WT + G1885E	26.0 ± 2.9	1.27 ± 0.18	**0.89 ± 0.15 ***	145.1 ± 14.0	143.1 ± 18.4	0.53 ± 0.03	17.3 ± 0.5	**165 ± 6.1 ***	2.16 ± 0.11	0.33 ± 0.013
WT + L433P	**38.6 ± 2.9 ***	**2.29 ± 0.39 ***	1.32 ± 0.21	**180.0 ± 28.0 ***	159.9 ± 52.3	**0.65 ± 0.04 ***	15.6 ± 0.57	**176.9 ± 5.3 ***	**2.82 ± 0.12 ***	**0.57 ± 0.053 ***
WT + L433P-G1885E	17.2 ± 2.6	**1.11 ± 0.06 ***	1.19 ± 0.12	114.2 ± 18.0	154 ± 39.0	**0.58 ± 0.03 ***	**18.5 ± 0.67 ***	**197.0 ± 8.9 ***	**2.74 ± 0.21 ***	**0.37 ± 0.019 ***
L433P+G1885E	23.3 ± 2.7	**1.21 ± 0.14 ***	**1.07 ± 0.09 ***	114.2 ± 18.5	128.7 ± 9.1	0.55 ± 0.03	16.4 ± 0.64	181 ± 8.9	2.32 ± 0.16	**0.45 ± 0.028 ***

Table 5.1. A summary of the spontaneous Ca^{2+} oscillation parameters observed in cells expressing each recombinant RyR2. *Asterisked data indicates a significant difference to WT RyR2 ($p<0.05$). Red values indicate a significant increase and blue values indicate a significant decrease compared to WT RyR2.*

5.3.5. Examination of the functional relationships between Ca^{2+} oscillation parameters

Altered systolic Ca^{2+} transient amplitude has been implicated in HF and an increase in agonist-evoked ER Ca^{2+} release magnitude is well documented phenotypic manifestation of RyR2 CPVT-linked mutations examined in heterologous systems (George *et al.*, 2003a; Thomas *et al.*, 2004; Jiang *et al.*, 2005). Due to the vast network of Ca^{2+} signalling proteins involved in intracellular Ca^{2+} handling, compensatory mechanisms may come into effect to negate the detrimental effects of sustained elevated cytoplasmic Ca^{2+} concentrations following ER Ca^{2+} release, observed through the heterologous expression of RyR2 mutations. Given that L433P has been shown here to alter the magnitude of Ca^{2+} release, particularly when co-expressed with WT RyR2 (Figures 3.17-3.19 and 5.10), linear regression analysis was employed to determine whether the magnitude of Ca^{2+} release influences other intracellular Ca^{2+} handling parameters following spontaneous Ca^{2+} release. For example, does increased spontaneous Ca^{2+} release magnitude lead to a longer lasting period of elevated cytoplasmic Ca^{2+}, does increased Ca^{2+} release result in a higher rate of Ca^{2+} removal from the cytoplasm etc. Subsequently, results of the linear regression analysis were used to determine if expression of the L433P mutation and/or the G1885E polymorphism perturbed any of these functional relationships.

5.3.5.1. Factors other than spontaneous Ca^{2+} oscillation magnitude and duration determine Ca^{2+} oscillation area

Although a positive linear relationship between spontaneous Ca^{2+} oscillation magnitude and duration was observed in cells expressing each recombinant RyR2 ($p < 0.05$, apart from L433P $p = 0.06$, Figure 5.12A), data did not tend to fit the regression model very well ($r^2 = 0.04 - 0.18$), indicating a lack of relationship between these two parameters. Unsurprisingly, this suggests that factors other than Ca^{2+} release magnitude, likely to be Ca^{2+} sequestration mechanisms, are major determinants of the duration of spontaneous Ca^{2+} oscillations. However, expression of homotetrameric LPGE resulted in a moderate positive relationship between oscillation magnitude and duration ($p < 0.0001$, $r^2 = 0.37$, Δ

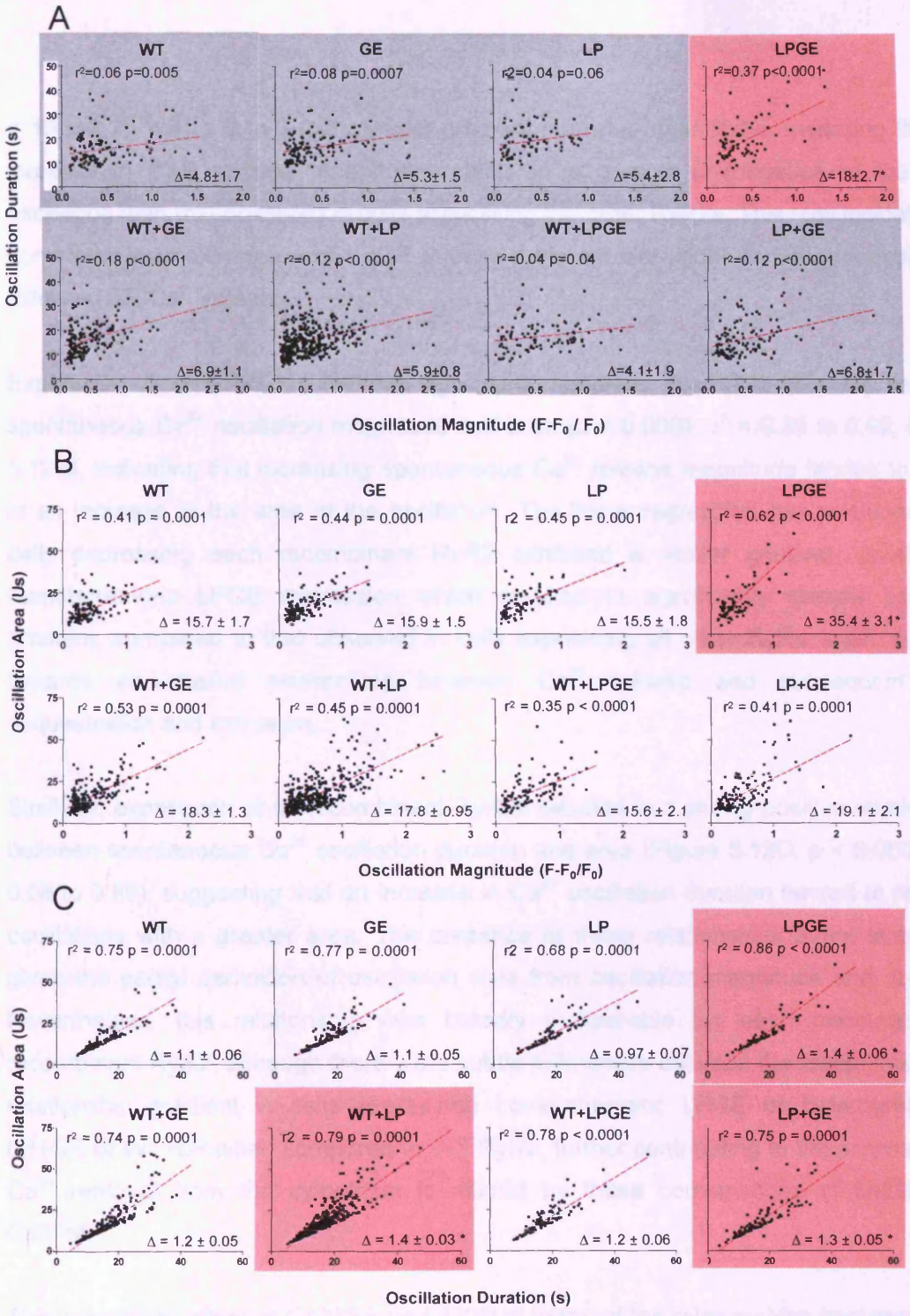

Figure 5.12. Spontaneous Ca^{2+} release magnitude does not determine oscillation duration. *Linear regression analysis was carried out to determine whether there were any relationships between the spatial parameters of spontaneous Ca^{2+} oscillations. Linear regression analysis was used to determine whether there were relationships between oscillation magnitude and duration (A), oscillation magnitude and area (B) or oscillation duration and area (C). Significance values (p) < 0.05 indicated that a significant relationship between two parameters existed. Plots highlighted in red indicate a significantly steeper gradient compared to WT whereas those highlighted in grey indicate no relationship was observed. An r^2 threshold value of 0.3 was employed to determine fitting data.*

= 18 ± 2.7), with a 2 to 3-fold steeper gradient than the other RyRs, indicating that an increase in Ca^{2+} release magnitude results in a greater prolongation of the Ca^{2+} oscillation than that observed in cells expressing the other RyR2s. This may indicate that homotetrameric expression of LPGE causes profound alterations in Ca^{2+} sequestration following ER Ca^{2+} release.

Expression of all RyR2s resulted in a significant, moderate, positive relationship between spontaneous Ca^{2+} oscillation magnitude and area ($p < 0.0001$, $r^2 = 0.35$ to 0.62, Figure 5.12B), indicating that increasing spontaneous Ca^{2+} release magnitude tended to result in an increase in the area of the oscillation. The linear regression line produced from cells expressing each recombinant RyR2 exhibited a similar gradient, apart from homotetrameric LPGE expression which resulted in significantly steeper (~2-fold) gradient, compared to that observed in cells expressing all other RyRs, again pointing towards an altered relationship between Ca^{2+} release and subsequent Ca^{2+} sequestration and extrusion.

Similarly, expression of all recombinant RyR2s resulted in a strong positive relationship between spontaneous Ca^{2+} oscillation duration and area (Figure 5.12C, $p < 0.0001$, $r^2 =$ 0.68 to 0.86), suggesting that an increase in Ca^{2+} oscillation duration tended to result in oscillations with a greater area. The presence of these relationships is not surprising, given the partial derivation of oscillation area from oscillation magnitude and duration. Nevertheless, this relationship was broadly comparable for each permutation of recombinant RyR2, although there were subtle differences between the steepness of the relationship gradient in cells expressing homotetrameric LPGE or heterotetrameric LP+GE or WT+LP when compared to WT RyR2, further contributing to the proposal that Ca^{2+} removal from the cytoplasm is altered by these combinations of L433P and G1885E.

The modulatory effect of G1885E on L433P in terms of the relationships between these parameters was most pronounced when both substitutions were co-expressed in a homotetrameric fashion (LPGE). However, G1885E also modulated L433P function when the two substitutions were co-expressed as heterotetramers (WT+LPGE and LP+GE), although only the relationship between oscillation duration and area was altered.

Although Ca^{2+} oscillation area was, rather unsurprisingly, demonstrated to be dependent on both oscillation magnitude and duration, there was no apparent relationship between these two parameters. This suggests that factors other than oscillation magnitude are involved in determining the duration of the Ca^{2+} oscillation, which is likely the rates of Ca^{2+} release and subsequent removal.

5.3.5.2. L433P and G1885E expression alter the relationships between the magnitude and kinetic parameters of spontaneous Ca^{2+} release

Linear regression analysis was used to determine whether perturbation of Ca^{2+} release magnitude, as shown in Figure 5.10, was coupled with a compensatory alteration in the kinetic parameters of intracellular Ca^{2+} handling and subsequently, whether any such relationships were altered by L433P and/or G1885E expression (Figure 5.13). Linear regression analysis demonstrated that in RyR2-expressing cells, there were significant positive relationships between the magnitude and rate of spontaneous Ca^{2+} release, suggesting that an increase in Ca^{2+} release magnitude results in a higher rate of Ca^{2+} release i.e. a steeper Ca^{2+} transient (Figure 5.13A, $p < 0.001$, $r^2 = 0.29$ to 0.58).

Similarly, a positive relationship was observed between the magnitude of Ca^{2+} release and the rate of subsequent Ca^{2+} removal from the cytoplasm (Figure 5.13B), suggesting that as the magnitude of Ca^{2+} release increases, so too does the rate at which it is removed from the cytoplasm. This is likely due to a greater increase in cytoplasmic Ca^{2+} concentration having a consequential effect of increasing the Ca^{2+}-dependent activity of Ca^{2+} extrusion mechanisms e.g. SERCA, PMCA.

Furthermore, in cells expressing each recombinant RyR2 there appeared to be a weak positive relationship between the rate of spontaneous Ca^{2+} release and the rate of subsequent Ca^{2+} removal from the cytoplasm ($p<0.05$, $r^2 = 0.18$ to 0.48, Figure 5.13C), suggesting that an increase in the rate of Ca^{2+} release results in a faster rate of Ca^{2+} removal. The existence of this relationship could be somewhat consequential, in that a higher rate of Ca^{2+} release tends to result from a greater magnitude of Ca^{2+} release (Figure 5.13A) and similarly a higher magnitude of Ca^{2+} release results in a higher rate of Ca^{2+} removal (Figure 5.13B).

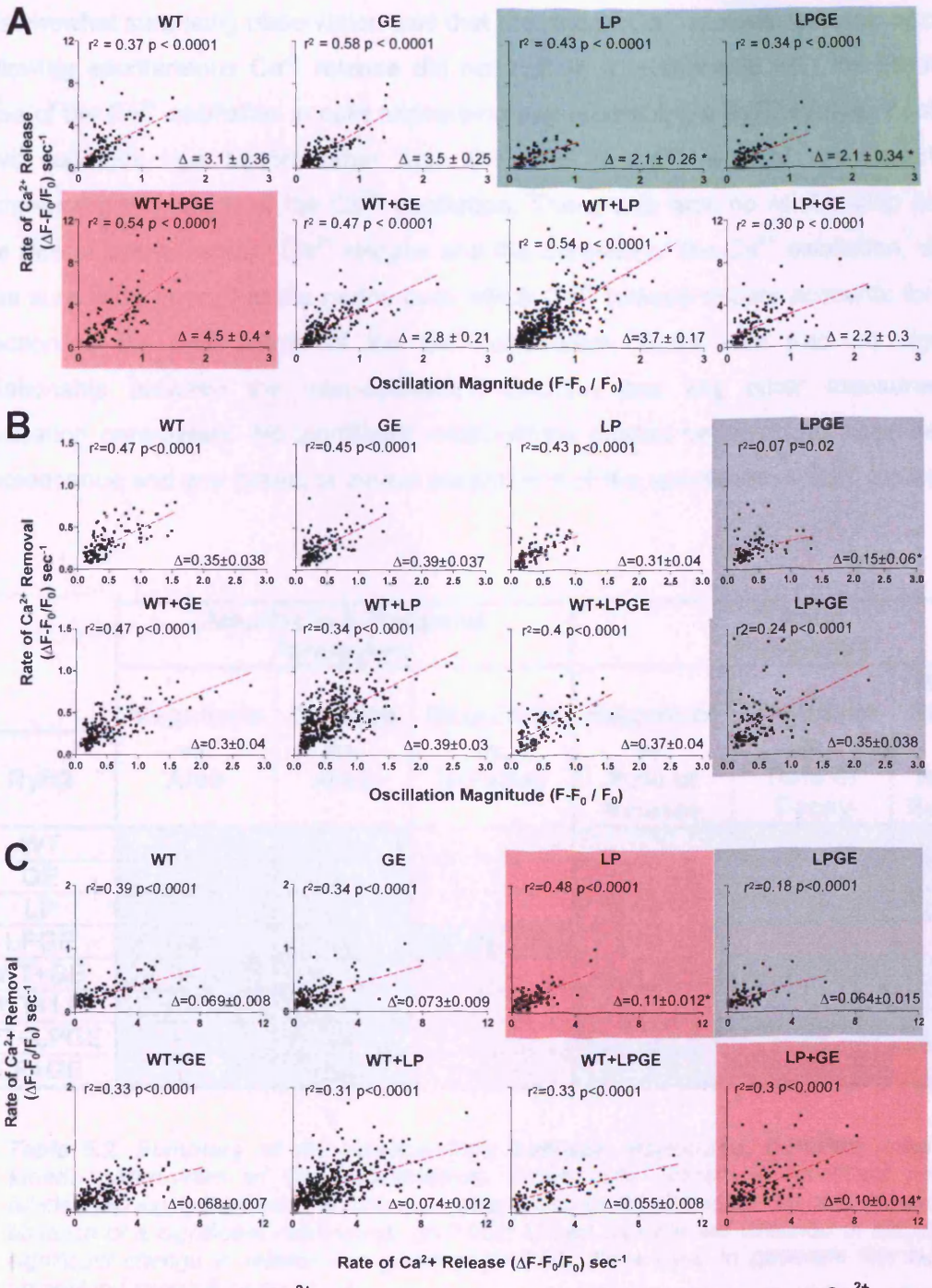

Figure 5.13. Spontaneous Ca^{2+} release magnitude is related to the rate of Ca^{2+} release and subsequent removal. *Linear regression analysis was carried out to determine whether there was a relationship between the magnitude and rate of spontaneous Ca^{2+} release as shown in panel A or the magnitude of Ca^{2+} release and rate of subsequent Ca^{2+} removal as shown in panel B. Similar analysis was carried out to determine whether the rate of Ca^{2+} release was directly related to the rate of Ca^{2+} removal as shown in panel C. Significance values (p) < 0.05 indicated that a significant relationship between two parameters existed. Plots highlighted in red indicate a significantly steeper gradient whereas those highlighted in green indicate a significantly shallower gradient compared to WT RyR2. Those highlighted in grey suggest no relationship was observed. An arbitrary r^2 threshold value >0.3 was deemed to signify acceptable linkage. Asterisked gradients indicate those that are significantly different to WT.*

A somewhat surprising observation was that the rate of Ca^{2+} removal from the cytoplasm following spontaneous Ca^{2+} release did not exhibit a relationship with the duration or area of the Ca^{2+} oscillation in cells expressing any recombinant RyR2s (data not shown). This suggests that factors other than the rate of Ca^{2+} removal are important in determining the length of the Ca^{2+} oscillation. There was also no relationship between the rate of spontaneous Ca^{2+} release and the duration of the Ca^{2+} oscillation, which is less surprising given that the period over which Ca^{2+} release occurs accounts for only a fraction of the total length of the Ca^{2+} oscillation. There was also no significant relationship between the inter-oscillation duration and any other measured Ca^{2+} oscillation parameters. No significant relationships existed between the baseline Fluo3 fluorescence and any spatial or kinetic parameters of the spontaneous Ca^{2+} oscillation.

	Amplitude & Temporal Parameters			Kinetic Parameters		
RyR2	Magnitude vs. Area	Duration vs. Area	Magnitude vs. Duration	Magnitude vs. Rate of Release	Magnitude vs. Rate of Decay	Rate of Release vs. Rate of Removal
WT						
GE						
LP				▼		▲
LPGE	▲	▲	▲	▼		
WT+GE						
WT+LP						
WT+LPGE		▲		▲		
LP+GE		▲		▼		

Table 5.2. Summary of the relationships between magnitude, duration, area and kinetic parameters of Ca^{2+} oscillations. *Green cells indicate a significant positive relationship exists between the indicated parameters ($p<0.5$) whereas red cells indicate the absence of a significant relationship ($p>0.05$). Arrows indicate the direction of statistically significant change in relationship gradient ($p<0.05$). Data used to generate this table is present in Figures 5.12 and 5.13.*

The expression of L433P alone or in various combinations with G1885E only caused subtle alterations in relationships between oscillation magnitude, duration, area and kinetic parameters described above (summarised in Table 5.2). These alterations were most prevalent in cells expressing homotetrameric LPGE which abolished the relationship between Ca^{2+} release magnitude and the rate of subsequent Ca^{2+} removal

and altered relationships between oscillation magnitude, duration and area. Homotetrameric expression of either LP or LPGE exhibited comparable decreases in the gradient of the relationship between the magnitude and rate of spontaneous Ca^{2+} release, which may be attributable to the observed decrease in ER Ca^{2+} levels (Figure 5.9) in cells expressing these RyR2s. Despite severely augmenting the Ca^{2+} release parameters (section 5.3.4), heterotetrameric WT+LP expression produced comparable relationships between Ca^{2+} oscillation parameters compared to WT, which underwent subtle alterations in the gradient of the relationship following G1885E co-expression i.e WT+LPGE or LP+GE.

5.3.6. Linear regression analysis of spontaneous and caffeine-evoked Ca^{2+} release parameters.

Linear regression analysis was also carried out to determine whether cells expressing each recombinant RyR2 exhibited any functional coupling between spontaneous Ca^{2+} release parameters and those of caffeine-evoked Ca^{2+} release. Data was grouped into caffeine dose ranges that induced sub-maximal activation (0.1-0.75mM), activation on the exponential phase of the dose response curve (1-2mM) and maximal activation (5-10mM), according to caffeine activation curves presented in Figure 3.17 and 3.18. This grouping of data was necessary due to a combination of factors:

- Certain recombinant RyR2s, particularly homotetrameric LP and LPGE, resulted in significantly fewer cells exhibiting basal Ca^{2+} oscillations.
- Caffeine-activation of RyR2 often unavoidably occurred part-way through a Ca^{2+} oscillation and these traces were excluded from subsequent analysis (Figure 5.6B-C).

Thus, in some instances (e.g. LP: 0.1-0.75mM, n=10 cells and LPGE: 1-2mM, n=9 cells), sample number was very low and this adversely affected the rigour of linear regression analysis as shown in the data in Appendix II, Figures 9-13 and summarised in Figure 5.14.

5.3.6.1. L433P and G1885E have little effect on relationships between magnitude, duration and area of spontaneous and caffeine-evoked Ca^{2+} release

Linear regression analysis demonstrated that there was a strong, positive relationship between the magnitude of spontaneous Ca^{2+} release and the magnitude of subsequent caffeine-evoked Ca^{2+} release in oscillating HEK cells expressing each recombinant RyR2 (Figure 5.14). This is likely due to the apparent dependence of both modes of Ca^{2+} release on the level of ER Ca^{2+} store load. Furthermore, this relationship was observed in cells expressing each recombinant RyR2, despite an observed heterogeneity between the magnitude of spontaneous and caffeine-evoked Ca^{2+} release between cells expressing different RyR2s (Figures 3.17-3.19 and 5.10). Although homotetrameric expression of LPGE appears to result in the ablation of the relationship between spontaneous and caffeine-evoked Ca^{2+} release magnitude following activation with 1-2mM caffeine, this may be an artefact of the relatively low number of data points for this experimental condition (n=9). This is likely as a positive relationship was observed following activating with high and low activating caffeine concentrations.

There did not appear to be a relationship between the duration of the spontaneous Ca^{2+} oscillation and the subsequent caffeine-evoked Ca^{2+} release transient, which may be attributable to differences in the nature of Ca^{2+} extrusion following spontaneous or caffeine-evoked Ca^{2+} release. The continual presence of caffeine may alter RyR2 gating and consequentially ER store refilling compared to when intracellular Ca^{2+} is undergoing spontaneous basal cycling.

There are obvious differences between the shapes of Fluo3-signal intensity traces representing spontaneous Ca^{2+} oscillations and caffeine-evoked Ca^{2+} transients and there was observed heterogeneity of Ca^{2+} oscillation area in cells expressing each recombinant RyR2 (Figure 5.10). Despite this, expression of each recombinant RyR2 resulted in a positive relationship between spontaneous Ca^{2+} oscillation and caffeine-evoked Ca^{2+} transient area to varying degrees, indicating that an increase in spontaneous Ca^{2+} oscillation area was associated with an increase in the area of the subsequent caffeine-evoked Ca^{2+} release transient. Although this relationship was observed in cells expressing each RyR2, there was a tendency for this relationship to be abolished following activation with maximal concentrations of caffeine in the majority of cases.

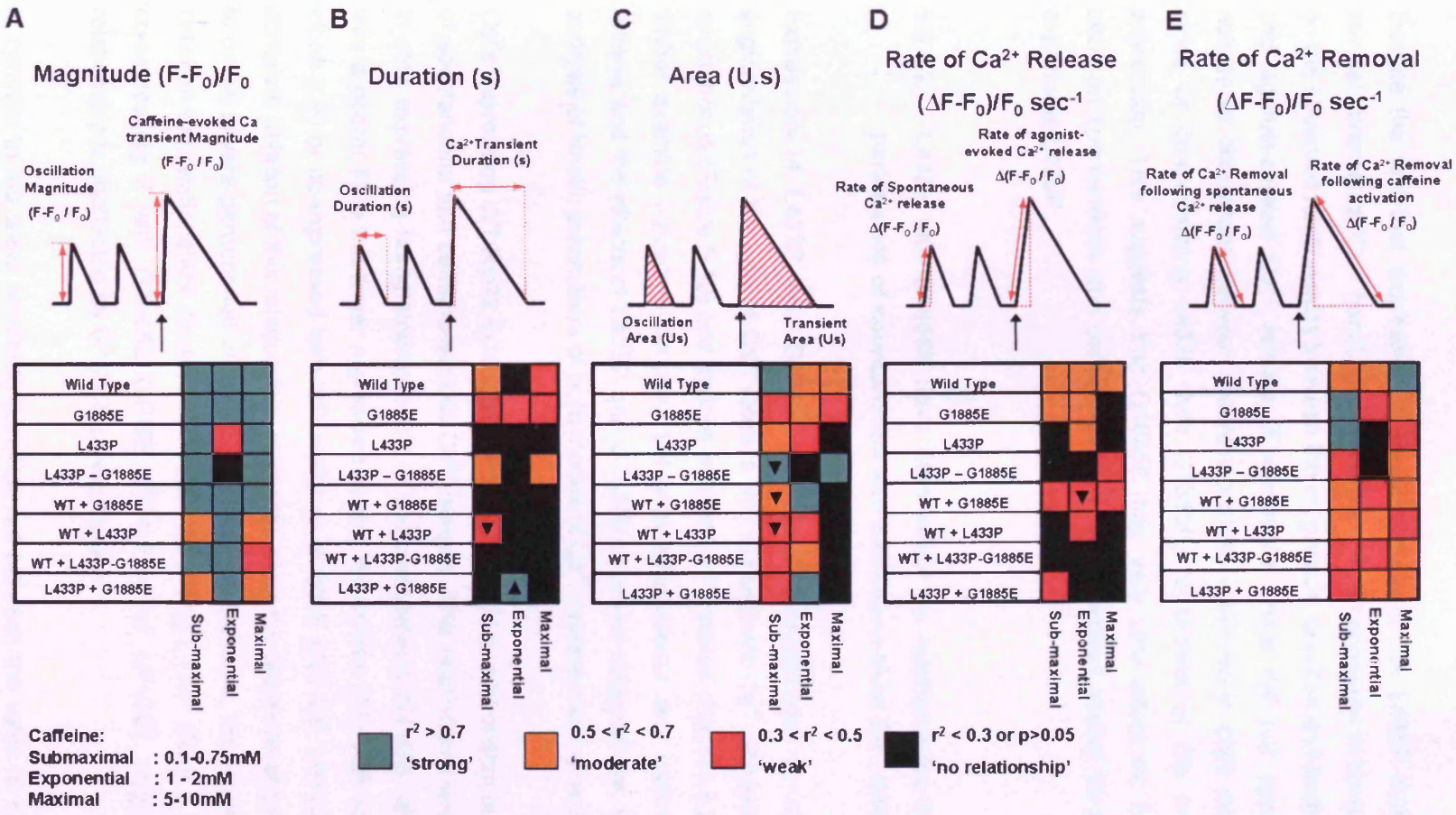

Figure 5.14. Functional coupling between spontaneous and agonist evoked Ca^{2+} release parameters. *Linear regression analysis was carried out on like-parameters of spontaneous and caffeine-evoked Ca^{2+} release. The mean parameter of spontaneous Ca^{2+} release was compared against the same parameter of the caffeine evoked Ca^{2+} transient in the same cells. Caffeine concentrations that evoked sub-maximal (0.1-0.75mM), exponential (1-2mM) or maximal (5-10mM) were applied to cells to activate RyR2, indicated by the arrow in each example trace. The gradient and robustness of observed relationships between spontaneous and caffeine evoked Ca^{2+} release was summarised as matrix diagrams here and the raw data is presented in Appendix II, Figure 9. The goodness of fit of the data (r^2) is indicated by the colour of the tabular cell (green > 0.7, orange 0.5 - 0.7m and red 0.3 - 0.5). Black squares indicate non-fitting data (p>0.05) or the absence of a significant relationship. Arrows indicate a significant increase (▲) or significant decrease (▼) in relationship gradient compared to WT RYR2 ($p < 0.05$).*

Despite the fact that expression of RyR2 containing the L433P mutation perturbed several intracellular Ca^{2+} handling parameters, L433P appeared to have very little effect on the observed relationships between the magnitude, duration and area of spontaneous and agonist-evoked Ca^{2+} release. Furthermore, there did not appear to be any noticeable differences between the relationships observed in cells expressing L433P alone or co-expressing L433P with G1885E, regardless of the precise mode of expression. This suggests that G1885E has very little effect on the relationships between spontaneous and caffeine-evoked Ca^{2+} transient spatial parameters in cells expressing L433P.

5.3.6.2. L433P and G1885E have little effect on relationships between kinetic parameters of spontaneous and caffeine-evoked Ca^{2+} release

Expression of L433P and G1885E has been demonstrated to cause significant augmentation of the rate of Ca^{2+} release and subsequent Ca^{2+} removal, following both spontaneous (Figure 5.10) and agonist-evoked Ca^{2+} release (Figures 3.20 and 3.22). To further examine functional coupling between spontaneous and caffeine-evoked Ca^{2+} release and the effects of L433P and G1885E on these relationships, linear regression analysis of kinetic parameters of both modes of Ca^{2+} release was carried out.

Cells expressing WT RyR2 exhibited a moderate positive relationship between the rates of spontaneous and caffeine-evoked Ca^{2+} release. This relationship was also observed in cells expressing homotetrameric GE or heterotetrameric WT+GE, although the data was a poorer fit to the linear regression model. All modes of L433P expression, either alone (LP) or co-expressed with WT RyR2 or G1885E (WT+LP, LP+GE), caused near complete ablation of this relationship, suggesting that the presence of L433P is sufficient to cause severe perturbation of this relationship. Furthermore, there was little difference between the relationships observed in cells expressing L433P alone (LP or WT+LP) or co-expressing it with G1885E (LPGE, WT+LPGE or LP+GE), suggesting that this relationship is unaffected by G1885E co-expression.

In contrast to the weak relationships observed between the rates of spontaneous and caffeine-evoked Ca^{2+} release only being observed in cells expressing WT RyR2 or G1885E, there appeared to be a moderate relationship between the rates of cytosolic

Ca^{2+} removal in cells expressing all recombinant RyR2s (Figure 5.14). This suggests that a higher rate of Ca^{2+} removal following spontaneous Ca^{2+} release tends to result in higher rate of Ca^{2+} removal following caffeine-evoked channel activation. Interestingly, the gradient of the regression line of this relationship is relatively low in all cases (0.24 – 0.31), indicating that an increase in rate of Ca^{2+} removal following spontaneous Ca^{2+} release only results in a comparably small increase in rate of removal following caffeine-evoked channel activation. This observation is possibly attributable to the fact that caffeine added as a bolus may alter post-activation gating, store refilling and cytoplasmic Ca^{2+} removal. The only exception to the observation of this relationship was in cells expressing homotetrameric LP or LPGE following RyR2 activation with 1-2mM caffeine, although a positive relationship was observed following minimal and maximal caffeine exposure.

Taken together, this data suggests that L433P expression only has subtle effects on the functional coupling between spontaneous and agonist-evoked Ca^{2+} release parameters, despite causing significant perturbation of the absolute values of these parameters. Cells expressing G1885E, exhibited similar relationships between spontaneous and caffeine-evoked Ca^{2+} release parameters compared to WT RyR2 in all cases. This provides further evidence that G1885E does not result in gross alteration of RyR2 function. Furthermore, co-expression of G1885E with L433P tended to exhibit similar relationships between spontaneous and caffeine-evoked Ca^{2+} release parameters to when L433P was expressed in the absence of G1885E. Taken together, these observations suggest that G1885E does not modulate the relationships between magnitude, duration, area and kinetic parameters of spontaneous and caffeine evoked Ca^{2+} release in cells expressing WT RyR2 or L433P.

5.4. Discussion

5.4.1. G1885E modulates the propensity for spontaneous Ca^{2+} release from L433P RyR2.

Spontaneous Ca^{2+} release from the ER is proposed to be causative of DADs which can lead to arrhythmia and SCD, characteristic of CPVT/ARVD2 (Liu *et al.*, 2006). Here, it was observed that heterologous expression of RyR2 containing the L433P mutation and G1885E polymorphism, both on the same subunits (representative of *in cis* inheritance) and separate RyR2 subunits (representative of *in trans* inheritance), altered the propensity for cells to exhibit spontaneous Ca^{2+} release, similar to the SOICR mechanism described by Chen and colleagues (Jiang *et al.*, 2004; MacLennan & Chen, 2009).

In disagreement with the findings of *Jiang et al,* the homotetrameric expression of L433P did not produce a significant increase in spontaneous Ca^{2+} release propensity, and a similar ER Ca^{2+} level was observed in oscillating and non-oscillating cells expressing L433P. The reasons for these discrepancies are unknown but could be attributable to differences in experimental protocol (Jiang *et al.*, 2005). The data produced here confirms that L433P does not exhibit the typical characteristics of a gain-of-function RyR2 mutation. Furthermore, the homotetrameric expression of LPGE exhibited a more severe phenotype than LP alone in terms of spontaneous Ca^{2+} release propensity, providing further evidence that despite appearing functionally benign when expressed alone, G1885E modulates the severity of L433P dysfunction. This also adds strength to the argument that L433P and L433P-G1885E are not typical gain-of-function mutations, as other arrhythmogenic loss-of-function RyR2 mutations have been shown to result in a decrease (G1885E/G1886S, Koop *et al.*, 2008) or complete ablation (A4860G, Jiang *et al.*, 2007) of spontaneous Ca^{2+} release. However, due to the autosomal dominant nature of RyR2 mutations (Tiso *et al.*, 2001; Priori *et al.*, 2002), homotetrameric expression of these substitutions is not the most physiologically accurate reflection of L433P/G1885E pathophysiology.

Co-expression of L433P with WT RyR2, which better reflects the autosomal dominant nature of CPVT/ARVD-linked RyR2 mutations, presented an extremely different phenotype to when L433P was expressed as homotetramers.This further highlights the functional importance of the precise mode of RyR2 mutation expression and the need to

characterise disease-linked RyR2 mutations in a manner representative of the observed mode of inheritance *in vivo*. The observed increase in propensity for WT+LP expressing cells to exhibit spontaneous Ca^{2+} release was more characteristic of gain-of-function mutations associated with CPVT/ARVD2 (Jiang *et al.*, 2005).

The modulatory effect of G1885E was also evident when co-expressed with L433P in a manner representative of heterozygous inheritance (WT+LPGE or LP+GE), restoring the propensity for spontaneous Ca^{2+} release to normal levels, suggesting that these modes of G1885E expression offer a protective effect with regards to normalising spontaneous Ca^{2+} release propensity. However, WT+LPGE co-expression best represents the mode of L433P and G1885E inheritance in ARVD2-patients in which these substitutions were first identified (Tiso *et al.*, 2001), yet results in similar spontaneous Ca^{2+} release propensity to cells expressing WT RyR2. This makes it unlikely that altering spontaneous Ca^{2+} release propensity is the mechanism by which heterotetrameric L433P-G1885E expression results in ARVD2 pathogenesis. However, whether similar findings are made when L433P and G1885E are expressed in a cardiac environment expressing the full complement of RyR2 accessory proteins remains to be determined.

Although when expressed alone, G1885E appears functionally benign in terms of spontaneous Ca^{2+} release, it undoubtedly alters the propensity for cells expressing L433P to exhibit spontaneous Ca^{2+} release and as such, modulates L433P channel activity in terms of one of the proposed pathogenic mechanisms of RyR2 mutations.

5.4.2. The role of ER Ca^{2+} store load in spontaneous Ca^{2+} release

The vast majority of functionally characterised CPVT mutations, display increased spontaneous Ca^{2+} release coupled with decreased Ca^{2+} in the ER/SR store of cells exhibiting spontaneous Ca^{2+} oscillations (Jiang *et al.*, 2004; Jiang *et al.*, 2005), which is proposed to result from an increased sensitivity to channel activation by luminal Ca^{2+} and a decreased threshold for spontaneous Ca^{2+} release. Conversely, RyR2 mutations which display a decreased propensity to exhibit basal Ca^{2+} oscillations, have been shown to exhibit increased ER Ca^{2+} as a result of decreased luminal Ca^{2+} sensitivity and an increase in the luminal threshold for spontaneous Ca^{2+} release (Jiang *et al.*, 2007; Koop *et al.*, 2008).

In the present experiments there was no evidence that basal cytoplasmic Ca^{2+} concentration influenced the propensity for cells to exhibit spontaneous Ca^{2+} release, as basal Ca^{2+} levels were equivalent between oscillating and non-oscillating cells. Similarly, there was little evidence that spontaneous Ca^{2+} release propensity was solely dependent on ER Ca^{2+} store load, although several notable observations were made. Firstly, ER Ca^{2+} levels were consistently lower in oscillating cells compared to non-oscillating cells expressing the same recombinant RyR2, which is consistent with previous data (Jiang *et al.*, 2007; Koop *et al.*, 2008) and supports the hypothesis that there is a luminal Ca^{2+} threshold, above which spontaneous Ca^{2+} release occurs. Secondly, there was significant heterogeneity between the ER Ca^{2+} levels of cells expressing each recombinant RyR2, with the majority exhibiting a decrease in ER Ca^{2+} compared to cells expressing WT RyR2. Finally, the level of ER Ca^{2+} did not completely reconcile the heterogeneity in spontaneous Ca^{2+} release propensity observed in cells expressing the different RyR2s, nor did it reconcile with any of the measured Ca^{2+} oscillation parameters.

Unlike the majority of characterised CPVT-linked mutations which exhibit a decrease in ER Ca^{2+} load and an increase in spontaneous Ca^{2+} release (Jiang *et al.*, 2005), here homotetrameric LPGE exhibited a decrease in ER Ca^{2+} load coupled with a decrease in spontaneous Ca^{2+} release propensity. If homotetrameric LPGE expression had simply lowered the luminal Ca^{2+} threshold for spontaneous Ca^{2+} release, an observed increase in spontaneous Ca^{2+} release propensity would have been expected, although this was not the case. This could imply that expression of L433P-G1885E may cause a small, sustained Ca^{2+} leak which is sufficient to cause ER Ca^{2+} store depletion, yet not result in spontaneous Ca^{2+} release through complete RyR2 activation. The existence of a underlying Ca^{2+} leak that does not manifest as a transient Ca^{2+} release event has recently been described (Santiago *et al.*, 2010), adding plausibility to this hypothesis. Conversely, the significant increase in spontaneous Ca^{2+} release propensity in cells expressing heterotetrameric WT+LP was coupled with a similar ER Ca^{2+} load to WT RyR2 in oscillating cells, yet according to the model proposed by *Chen et al*, an increase in spontaneous Ca^{2+} release propensity would be expected to be associated with a decreased ER Ca^{2+} load. This suggests that although there are similarities with the findings presented here and that of *Jiang et al*, but the SOICR model doesn't reconcile completely with the intracellular Ca^{2+} handling dysfunction resulting from L433P expression.

Potentially, this may suggest that WT+LP co-expression has little effect on the luminal Ca^{2+} threshold for spontaneous Ca^{2+} release, but somehow results in increased ER Ca^{2+} store refilling, accounting for the increase in ER Ca^{2+} in non-oscillating cells and consequential increase in spontaneous Ca^{2+} release propensity. However, it must be stressed that without measuring the activity of other proteins involved in ER Ca^{2+} regulation, it is impossible to determine whether the altered ER Ca^{2+} load is a direct result of RyR2 dysfunction or due to compensatory intracellular Ca^{2+} handling by other proteins e.g. SERCA, PMCA.

5.4.3. Investigation of spontaneous Ca^{2+} oscillation parameters reveals a possible mechanism of heterozygous WT+LPGE pathogenesis

In HEK cells expressing recombinant RyR2, spontaneous Ca^{2+} release events manifest as basal Ca^{2+} oscillations with a significantly different morphology to caffeine-induced Ca^{2+} transients (Jiang *et al.*, 2005; Jiang *et al.*, 2007; Jones *et al.*, 2008; Koop *et al.*, 2008). Consistent with published data, caffeine-induced Ca^{2+} transients took longer to decrease to basal Ca^{2+} levels compared to spontaneous Ca^{2+} oscillations (Koop *et al.*, 2008). Similarly, the magnitude of spontaneous Ca^{2+} release tended to be slightly lower than that observed following caffeine-evoked Ca^{2+} release. Both of these observations are likely due to RyR2 inactivation due to decreased luminal Ca^{2+} content and increased cytoplasmic Ca^{2+} concentration following spontaneous Ca^{2+} release, whereas RyR2 activated by caffeine may alter processes of channel inactivation, cytoplasmic Ca^{2+} removal and ER store refilling. Given that spontaneous Ca^{2+} release events undergo basal Ca^{2+} cycling that is not observed following caffeine-evoked activation of RyR2, the parameters of spontaneous Ca^{2+} release were examined to identify whether they provided further indications of the mechanisms by which L433P and G1885E alter intracellular Ca^{2+} handling properties.

In accordance with the caffeine-evoked Ca^{2+} release data (Chapter 3), homotetrameric expression of LP or LPGE or the heterotetrameric expression of WT+LP caused the most significant perturbation of intracellular Ca^{2+} handling dynamics following spontaneous Ca^{2+} release. However, in contrast to the caffeine-evoked Ca^{2+} release data, the heterotetrameric expression of WT+LPGE also resulted in significant alteration

of several Ca^{2+} handling parameters of spontaneous Ca^{2+} release, that were not observed following caffeine activation.

Increased magnitude of ER/SR Ca^{2+} release is a phenomenon commonly associated with arrhythmia-linked RyR2 mutations examined in heterologous systems (George *et al.*, 2003a; Thomas *et al.*, 2004; Jiang *et al.*, 2005) and is proposed to result in a sustained elevation of cytoplasmic Ca^{2+} levels which can contribute to DAD initiation and action potential prolongation. Interestingly, several modes of L433P/G1885E expression altered the magnitude and duration of spontaneous Ca^{2+} release to varying degrees (LP, LPGE, WT+LP and WT+LPGE), but all of these culminated in a significantly increased oscillation area, which can be interpreted as a sustained elevation of cytoplasmic Ca^{2+} concentration following ER Ca^{2+} release.

Although, expression of WT+LP or WT+LPGE heterotetramers also results in an increased rate of Ca^{2+} removal from the cell following spontaneous Ca^{2+} release, this increase in rate of Ca^{2+} removal was not sufficient to restore the oscillation area to normal levels. This suggests that heterozygous inheritance of either L433P or L433P-G1885E may lead to sustained elevated cytoplasmic Ca^{2+} and DAD's following RyR2 activation. Given that WT+LPGE expression is most representative of the observed genotype *in vivo* (Tiso *et al.*, 2001), this sustained elevation of cytoplasmic Ca^{2+} caused by an increase in oscillation magnitude, duration and area could contribute to the pathogenesis of heterozygously inherited L433P-G1885E. Although heterotetrameric WT+LP and WT+LPGE expression also increased the rate of spontaneous Ca^{2+} release, this only constitutes a small fraction of the Ca^{2+} oscillation and has little impact on oscillation duration or area.

The measurement of spontaneous Ca^{2+} oscillation parameters provides a possible mechanism by which WT+LPGE expression results in an arrhythmogenic phenotype, through the prolongation of cytoplasmic Ca^{2+} elevation during spontaneous basal Ca^{2+} cycling.

5.4.4. G1885E preferentially modulates cytoplasmic Ca^{2+} removal parameters of spontaneous Ca^{2+} oscillations through WT+L433P channels

The measurement of spontaneous Ca^{2+} release parameters provides further evidence that G1885E modulates L433P mutant channel function, both when co-expressed as homotetramers (LPGE) or in a heterotetrameric fashion (WT+LPGE, LP+GE). G1885E appeared to exacerbate the increase in Ca^{2+} oscillation area when expressed with L433P in a homotetrameric (LPGE) or heterotetrameric (WT+LPGE) manner, which could potentially further increase the likelihood of DAD occurrence *in vivo*. In contrast, the expression of LP+GE heterotetramers resulted in similar Ca^{2+} oscillation magnitude, duration and area compared to WT, suggesting that G1885E restored Ca^{2+} oscillation area to normal levels when expressed in this composite heterotetrameric fashion. This could potentially indicate that inheritance of L433P and G1885E on distinct alleles may offer protection against prolongation of the Ca^{2+} transient and DAD onset observed in WT+LP and WT+LPGE expression, although this would need to be investigated further in a cardiac cellular environment. Furthermore, this corroborates the finding that heterotetrameric LP+GE expression had little effect on caffeine-evoked Ca^{2+} release parameters (section 3.3.5 and 3.3.6) and emphasises the importance of the precise mode of G1885E co-expression on the extent to which it modulates L433P function.

Although G1885E had little effect on the rate of Ca^{2+} release through L433P channels, the expression of WT+LPGE or LP+GE heterotetramers partially restored the increased rate of cytoplasmic Ca^{2+} removal caused by WT+LP expression to normal levels. This suggests that G1885E preferentially modulates L433P intracellular Ca^{2+} handling during the period of cytoplasmic Ca^{2+} removal, rather than the actual Ca^{2+} release event itself. Given that G1885E is located within a region containing a low affinity cytoplasmic Ca^{2+} binding site involved in RyR inactivation (Laver, 2007), the polymorphism may alter channel activation/inactivation properties, although this would need to be confirmed using single channel analysis.

In contrast, although expression of homotetrameric LPGE increased Ca^{2+} oscillation area compared to homotetrameric LP, LP and LPGE exhibited similar rates of spontaneous Ca^{2+} release and subsequent Ca^{2+} removal, suggesting that G1885E has no modulatory effect on the kinetic Ca^{2+} handling parameters of homotetrameric L433P. Similar to observations made through the characterisation of the effects of *SCN5A* SNPs

on mutations in the same gene (Viswanathan *et al.*, 2003; Poelzing *et al.*, 2006), the precise mode of L433P and G1885E co-inheritance determines the extent to which the SNP modifies mutant channel function.

5.4.5. L433P and G1885E perturb functional coupling relationships between intra-oscillation Ca^{2+} handling parameters

Functional relationships were observed between several intracellular Ca^{2+} handling parameters following spontaneous Ca^{2+} release. As one would expect, both the magnitude of Ca^{2+} release and the duration of the basal Ca^{2+} oscillation were integral in determining the area of the spontaneous Ca^{2+} oscillation. Conversely, the magnitude of spontaneous Ca^{2+} release had little bearing on the duration of the Ca^{2+} oscillation, suggesting that there were other determining factors involved. However, oscillation duration was not significantly associated with any of the other measured parameters, including the rate of Ca^{2+} removal, suggesting that one factor alone does not determine the duration of the spontaneous Ca^{2+} oscillation.

The magnitude of spontaneous Ca^{2+} release was also a determining factor in the rate at which Ca^{2+} was released from the ER and the rate at which it was subsequently removed from the cytosol, which is consistent with published data from a canine myocyte model (Hoeker *et al.*, 2009). These observations are most likely due to an increased magnitude of Ca^{2+} release creating a steeper luminal-to-cytosolic Ca^{2+} gradient, increasing the rate of Ca^{2+} release, whereas, a greater increase in cytoplasmic Ca^{2+} concentration is likely to increase the Ca^{2+}-dependent activity of Ca^{2+} extrusion proteins, consequently increasing the rate at which Ca^{2+} is removed from the cytoplasm. The observed co-dependence of both the rate of Ca^{2+} release and subsequent removal on the magnitude of Ca^{2+} release is likely to be attributable for the observed relationship between these two kinetic parameters. Taken together, this data suggests that in cells expressing the majority of RyR2s, a functional coupling exists between Ca^{2+} release and Ca^{2+} extrusion mechanisms during basal Ca^{2+} cycling, as alterations in the magnitude of spontaneous Ca^{2+} release appear to be compensated for by the activity of other intracellular Ca^{2+} handing pathways. Furthermore, this coupling appears to be altered by L433P expression, and further modulated by the co-expression of G1885E.

Expression of homotetrameric LPGE caused the greatest level of perturbation of intra-oscillation parameter relationships, causing complete ablation of the relationship between the magnitude of Ca^{2+} release and its subsequent removal. Furthermore, homotetrameric LPGE expression altered the relationships between oscillation parameters that could contribute to transients with an increased area, suggesting that this mode of L433P and G1885E expression causes gross perturbation of intracellular Ca^{2+} handling functional coupling, particularly of that involved with cytoplasmic Ca^{2+} removal. The alteration of these intra-oscillation parameter relationships was less pronounced in cells expressing homotetrameric LP, suggesting that they are modulated by the presence of G1885E.

Despite the heterotetrameric expression of WT+LP causing severe alteration in Ca^{2+} handling parameters, it did not disrupt the functional coupling between these parameters, suggesting an element of compensation in cytoplasmic Ca^{2+} removal. However, the heterotetrameric expression of WT+LPGE or LP+GE altered the precise nature of these relationships compared to both WT or WT+LP, providing further evidence that G1885E has a role in modulating the functional coupling exhibited by L433P channels. Homotetrameric or heterotetrameric G1885E expression (GE or WT+GE) had no effect on any of the measured relationships between oscillation parameters, demonstrating that when expressed alone the polymorphism does not perturb the functional coupling of intracellular Ca^{2+} handling, but modulates L433P function when co-expressed with the mutation.

5.4.6. L433P and G1885E co-expression alters the relationships between spontaneous and caffeine-evoked Ca^{2+} release

Regression analysis was also used to determine whether there was any observable functional coupling between the like-parameters of spontaneous Ca^{2+} release events and those of subsequent caffeine-evoked Ca^{2+} release in the same cells. Given that caffeine is believed to sensitise the channel to activation by luminal or cytosolic Ca^{2+} (Sitsapesan & Williams, 1990; Kong *et al.*, 2008), one would expect the Ca^{2+} handling parameters of these two modes of ER Ca^{2+} release to be closely related. However, single channel analysis has revealed that caffeine and Ca^{2+} are very different in their mechanisms of RyR2 activation, with caffeine increasing channel P_o by prolonging the

duration of channel openings, whereas Ca^{2+} increases channel P_o by increasing the frequency of channel openings (Gaburjakova & Gaburjakova, 2006). Despite these differences in RyR2 activation mechanisms, the results of linear regression analysis confirmed that several parameters of spontaneous and caffeine-evoked Ca^{2+} release exhibited positive relationships e.g. magnitude, rate of Ca^{2+} removal, and that these relationships were not grossly altered by L433P and/or G1885E expression. Conversely, some parameters exhibited little or no relationship between those of spontaneous and caffeine-evoked Ca^{2+} release e.g. rate of Ca^{2+} release , duration, which may or not be due to differences in caffeine and Ca^{2+} activation properties.

Furthermore, L433P and G1885E appeared to have little effect on the relationships between spontaneous and caffeine-evoked Ca^{2+} release parameters. This could potentially be due to the greater level of systemic variation existing between the mechanisms of these two modes of Ca^{2+} release and subsequent Ca^{2+} removal masking any subtle alterations in coupling caused by RyR2 mutations.

5.4.7. Chapter summary

The data presented here further demonstrates that the most substantial deviation from a "normal" intracellular Ca^{2+} handling phenotype was observed following the homotetrameric expression of LP or LPGE, or the heterotetrameric expression of WT+L433P or WT+L433P-G1885E. These modes of expression altered spontaneous Ca^{2+} release propensity and perturbed the magnitude, duration, area and kinetic Ca^{2+} handling parameters of spontaneous Ca^{2+} release and disrupted functional relationships between intra-oscillation Ca^{2+} handling parameters

It also provides further evidence that alone, G1885E is predominantly functionally benign, yet it can modulate L433P channel function to different extents, depending on whether it is located on the same or different RyR2 subunits as the mutation. Furthermore, the extent to which G1885E altered L433P channel function depended on whether it was expressed as homotetramers i.e. decreased rate of Ca^{2+} release, or as heterotetramers i.e. increased rate of Ca^{2+} release. Interestingly, it appeared that G1885E tended to exhibit no-effect or an exacerbatory effect on L433P function when expressed in a homotetrameric fashion (LPGE), yet tended to have either no effect or a "normalising" effect on mutant channel function when expressed with L433P in a heterotetrameric manner (WT+LPGE or LP+GE).

Co-expression of L433P-G1885E with WT RyR2 (WT+LPGE), most representative of the ARVD2 genotype *in* vivo did not alter the propensity for spontaneous Ca^{2+} release. However, this mode of L433P-G1885E expression altered intracellular Ca^{2+} handling parameters in such a way that may result in a sustained elevation of cytoplasmic Ca^{2+} following spontaneous Ca^{2+} release, providing a potential mechanistic basis for WT+LPGE pathogenesis.

The investigation of intra-oscillation Ca^{2+} handling parameter relationships revealed that expression of RyR2 containing L433P, with and without G1885E caused alterations in compensatory mechanisms of intracellular Ca^{2+} handling, particularly through homotetrameric LPGE expression. Furthermore, G1885E exerted a subtle modulatory effect on the coupling observed with L433P, particularly of parameters involved in the 'recovery' phase of the Ca^{2+} oscillation, further indicating G1885E exerts its modulatory effects during the inactivation of RyR2.

Although the examination of relationships between identical parameters of spontaneous and caffeine-evoked Ca^{2+} release revealed that there was a degree of functional coupling between the two types of Ca^{2+} release, these relationships were not greatly altered by L433P and/or G1885E expression.

Comparing the spontaneous Ca^{2+} release data presented in this chapter with that of the caffeine-evoked Ca^{2+} release experiments in chapter 3, demonstrates that although the majority of findings are reconciled between the two data sets, there are also some differences. These are likely to be a product of differences in activation and inactivation mechanisms following caffeine-mediated or spontaneous RyR2 activation. Importantly, this data in this chapter and the rest of this thesis demonstrates the modulatory effect of a relatively common RyR2 SNP on an ARVD2-linked mutation.

Chapter 6

General Discussion

6.1. General Discussion

6.1.1. Precise mode of mutation expression is critical in determining the resulting Ca^{2+} handling phenotype

This thesis supports the concept that L433P channels underpin very different phenotypes depending on whether they were expressed as homotetramers or heterotetramers consisting of both WT and L433P subunits. Homotetrameric L433P appeared to cause a decrease in channel sensitivity to activation, consistent with the findings of *Thomas et al* (2004), whereas heterotetrameric L433P (in combination with WT subunits) exhibited a gain-of-function Ca^{2+} handling phenotype more typical of other CPVT/ARVD2 mutations (Chapters 3, 5). This observation is in contrast to the previous characterisation of heterotetrameric mutant RyR1 (Tong *et al.*, 1999) and RyR2 (Wehrens *et al.*, 2003; Lehnart *et al.*, 2008) in heterologous systems, which exhibited a 'diluted' phenotype when co-expressed with WT RyR2, although the scope of these characterisations was limited.

The observation that L433P mutant co-expression with WT RyR2 results in a complex phenotype, that could not have been predicted from the analysis of either channel separately, highlights the inherent limitations in characterising mutant channels in a homotetrameric form. This is particularly pertinent with so-called 'loss-of-function' mutations e.g. A4860G, which exhibits a complete loss of luminal Ca^{2+} sensitivity (Jiang *et al.*, 2007), which would presumably result in an extremely lethal phenotype *in vivo*. However, unlike the experimental studies of Jiang and colleagues, only a proportion of RyR2 channels would be A4860G homotetramers given the autosomal dominant nature of such mutations, with heterotetrameric and WT channels also being expressed. This is further highlighted by the disparity in the results of biophysical characterisation of homotetrameric G1885E-G1886S channels, which abolished luminal Ca^{2+} sensitivity (Koop *et al.*, 2008) compared to composite heterotetrameric G1885E+G1886S channels (Milting *et al.*, 2006) which resulted in channels exhibiting several sub-conductance states.

Taken together with the data presented here, this re-emphasises the need to characterise RyR2 mutations in a variety of experimental systems that allow investigation of the mutation in a manner representative of the heterozygous inheritance

pattern observed *in vivo* i.e. knock-in mouse models (Cerrone *et al.*, 2005; Kannankeril *et al.*, 2006; Goddard *et al.*, 2008; Lehnart *et al.*, 2008; Fernandez-Velasco *et al.*, 2009) or HL-1 cells (George *et al.*, 2003a; 2006; 2007). Recombinant expression of mutant RyR2 in immortalised cardiomyocytes (HL-1) provides the means to examine the effects of heterotetramerisation on mutant channel function in a cardiac setting. However, the presence of endogenous RyR2 in such cells makes it likely there will be disparity between the relative expression levels of each RyR2 subunit type following recombinant RyR2 expression. The generation of heterozygous knock-in mouse models further alleviates this problem, allowing the investigation of heterotetramers in a mammalian cardiac system. However, considerations need to be made for species differences i.e. heart rate, cardiac output, arrhythmia susceptibility, variation in relative Ca^{2+} homeostasis mechanisms e.g. SERCA, NCX (Cook *et al.*, 2009). Furthermore, the genetic background of transgenic mice harbouring RyR2 mutations has been proposed to influence the resulting phenotype, with discrepancies between different mouse models carrying the same mutation being reported (Lehnart *et al.*, 2008; Uchinoumi *et al.*, 2010).

6.1.2. G1885E channels appear functionally normal yet G1885E exhibits a profound modulatory effect on L433P channel dysfunction

The majority of intracellular Ca^{2+} handling parameters remained unaffected by G1885E expression (Chapters 3, 4 and 5), irrespective of whether it was expressed exclusively as G1885E homotetramers or as heterotetramers consisting of WT and G1885E subunits. This is entirely consistent with the view that G1885E is a SNP rather than a disease linked mutation, a notion which is reinforced by the prevalence of G1885E in the healthy population (Milting *et al.*, 2006; Medeiros-Domingo *et al.*, 2009). However, the data presented here shows that G1885E modulated nearly all of the examined Ca^{2+} handling parameters of L433P channels, providing the first compelling evidence that a common RyR2 SNP can modulate the effects of an ARVD2-linked RyR2 mutation, similar to the phenomenon observed in cardiac Na^{+} channelopathies (Viswanathan *et al.*, 2003; Ye *et al.*, 2003; Poelzing *et al.*, 2006; Nof *et al.*, 2010). This suggests that G1885E is a modifier of mutant channel function, rather than a dominant disease-causing mutation. Also consistent with the emergence of the role of SNPs in other cardiac channelopathies, was the observation that the precise mode of L433P and G1885E co-expression was critical in determining the extent to which G1885E altered

L433P channel function, which is further highlighted by the disparity in findings by *Koop et al* and *Milting et al.*

6.1.3. Mutant dysfunction is most prominent in the decay phase of the Ca^{2+} transient

A recurrent theme was the link between intracellular Ca^{2+} handling dysfunction and alterations in the decay phase of the Ca^{2+} transient (Chapters 3,4 and 5). RyR2 containing the L433P mutation, in the presence and absence of G1885E, perturbed intracellular Ca^{2+} parameters in such a way that could lead to prolongation of elevated cytoplasmic Ca^{2+} levels (Chapter 5). This is entirely consistent with a previous characterisation of L433P, which demonstrated L433P reduced Ca^{2+}-dependent inactivation (Thomas *et al.*, 2005). This phenomenon has been associated with increased DAD occurrence and corroborates data generated in mutant RyR2 mouse models (Liu *et al.*, 2006; Fernandez-Velasco *et al.*, 2009), providing a potential mechanism for LP, LPGE, WT+LP and WT+LPGE pathogenesis. Although composite heterotetrameric expression of LP+GE perturbed several Ca^{2+} release parameters, this appeared to be compensated for by altered Ca^{2+} extrusion mechanism activity (Chapter 5), resulting in the observation of a 'normal' post-activation cytoplasmic Ca^{2+} profile, although further investigation is required to determine the exact nature of these extrusion and sequestration mechanisms.

6.1.4. The mode of G1885E and L433P co-expression determines the functionality of the resultant channels

The degree of modulation afforded by G1885E on L433P dysfunction depended heavily on the precise mode of co-expression, in a similar manner to that observed with SNPs and mutations in *SCN5A* (Viswanathan *et al.*, 2003; Ye *et al.*, 2003; Poelzing *et al.*, 2006). RyR2 homotetramers formed from subunits containing both substitutions (representative of '*homozygous in cis*' inheritance) exhibited augmented dysfunction compared to homotetrameric L433P channels. Conversely, RyR2 heterotetrameric channels comprising of L433P and G1885E subunits (representative of '*heterozygous in*

trans' inheritance) or WT and L433P-G1885E subunits (representative of '*heterozygous in cis'* inheritance) displayed a marked attenuation of L433P linked channel dysfunction.

Although both modes of heterotetrameric L433P and G1885E co-expression (WT+LPGE and LP+GE) appeared to exhibit a normalising effect on perturbed L433P Ca^{2+} handling, the extent of this also varied between the modes of heterotetrameric co-expression, with LP+GE expression exhibiting the most significant degree of modulation. Although a molecular basis for this observation remains unknown, a recent study examining intra-molecular RyR2 interactions has provided a potential insight into these observed differences. The interaction between the N-terminal and central mutation domains in the RyR2 structure has been shown to be an intra-subunit interaction, as opposed to an interaction of these two domains of the same RyR2 subunit (Liu *et al.*, 2005; Liu *et al.*, 2010). Given the relatively close proximity of DR3, which encompasses G1885E (Zhang *et al.*, 2003), to the N-terminal mutation domain, which contains L433P (Wang *et al.*, 2007), it is plausible to speculate that there may be a certain degree of physical or allosteric interaction between the regions containing G1885E and L433P on separate subunits (LP+GE) compared to when they are expressed on the same subunits (WT+LPGE). However, whether DR3 interacts with the N-terminal domain to elicit channel modulation remains unknown.

Given that DR3 is proposed to contain a low-affinity Ca^{2+} binding site involved in channel inactivation (Hayek *et al.*, 1999; Zhang *et al.*, 2003), the insertion of a glycine for a negatively charged glutamate residue in this region may alter the inactivation properties of the mutant channel, which is consistent with a much of the data presented here suggesting that dysfunction arises during the recovery phase of the Ca^{2+} transient. However, the absence of dysfunctional Ca^{2+} removal in cells expressing G1885E alone, suggests that any alterations to Ca^{2+}-dependent 'inactivation' caused by G1885E only manifest when L433P is also expressed. The examination of L433P and G1885E function in single channel bilayer studies would provide a valuable insight into the effects that these substitutions have on channel gating and conductance characteristics.

6.1.5. Towards therapeutic benefit

Recently, it has been reported that the gene transfer of SERCA2a into a rat ischemic HF model offered significant long-term protection against HF onset and increased survival rates (Niwano, 2008), providing evidence of the potential benefits of gene therapy in treating cardiomyopathies. In the context of gene therapy and from a practical perspective, the transfer of an additional copy of a down-regulated gene i.e. SERCA2a or S100A1 (Hajjar, 2005) in HF, or a "rescuing" copy of a dysfunctional gene, is more feasible than attempting to modify a dysfunctional allele that is present in the patient i.e. *in cis* modification. The finding that G1885E co-expressed in '*in trans*' partly ameliorated the dysfunction of the autosomal-dominant L433P mutation (Chapter 3 and 5), provides the impetus for investigating this mode of complementation in the treatment of inherited RyR2-linked arrhythmias.

However, the modulatory effects of this SNP have only been described for two RyR2 substitutions, L433P and G1886S (Chapter 3-5, Milting, 2006, Koop, 2008), and whether this SNP exerts a similar modulatory function on other RyR2 mutations, particularly those that are not found in close physical proximity, remains unknown. Furthermore, before the translational use of a 'therapeutic' polymorphism-based strategy could be considered, there would need to be a greater understanding of the mechanism of L433P (and RyR2 mutations in general) and how it is modulated by a common SNP (G1885E). The generation and characterisation of transgenic mice heterozygous for L433P or composite heterozygous for L433P and G1885E, could potentially elucidate whether this SNP afforded protective benefits on mutant RyR2 function in an intact mammalian system. This could provide an indication as to whether common RyR2 SNPs present a potential therapeutic tool for the treatment of genetic RyR2 dysfunction.

Another limiting factor is the rarity of individual mutations, with some particular mutations only being identified in a single family, making the development of "tailor-made" gene therapies unfeasible at present. However, if subsequent investigation of the effects of the more common RyR2 SNPs e.g. Q2958R (allelic frequency of between 26-34%) on RyR2 mutant channel function reveals that a single SNP can exert beneficial modulation of many different RyR2 mutations, development of such therapies may become more plausible.

6.1.6. Further Work

In order to gain a better understanding of the mechanisms by which these substitutions result in an arrhythmia-linked phenotype and how G1885E can modulate dysfunctional L433P Ca^{2+} handling, further work in other experimental systems is necessary. However, it has been suggested that the abundance of different investigative techniques used to examine RyR2 function, may contribute to the disparity in findings relating to the consequences of RyR2 mutations (George, 2008). This is likely further exacerbated by variation in the experimental tools used between research groups i.e antibody efficiency (Huke & Bers, 2008), transgenic mouse background (Lehnart *et al.*, 2008; Uchinoumi *et al.*, 2010), mode of recombinant expression (Thomas *et al.*, 2004; Jiang *et al.*, 2005), assay used etc. However, until comprehensive, standardised techniques become available to characterise the effects of RyR2 mutations on intracellular Ca^{2+} handling dynamics, the complementary use of several of these experimental systems is the best means of mutant investigation.

Single channel analysis of RyR2 containing these substitutions would provide an insight into the effects of these substitutions on channel gating and conductance parameters. However, careful consideration would need to be given to the examination of heterotetrameric channels in these experiments due to the unknown stoichiometry of single RyR2 channels isolated from cells co-transfected with two distinct RyR2 cDNAs i.e. WT and L433P.

Although the use of an RyR-null HEK cell model provides more control over relative expression levels of distinct RyR2 subunits compared to other cell models which endogenously express RyR2, HEK cells lack many cardiac specific Ca^{2+} handling and RyR2 accessory proteins. Given that the activity of these accessory proteins may or may not alter or be altered by the presence of L433P and G1885E, it would be beneficial to further examine the effects of these substitutions in a cellular environment more closely mimicking the scenario in vivo i.e. HL-1 cells, knock-in mouse models. Given the location of G1885E being in close proximity to the FKBP12.6, binding site, it would be of particular interest to determine if this SNP has any effect on FKBP12.6 binding affinity or activity, both in cell based experiments or single channel studies. It would also be extremely useful to determine the rates of the individual Ca^{2+} extrusion mechanisms in

cells expressing each recombinant RyR2, to confirm the existence and nature of compensatory Ca^{2+} extrusion following dysfunctional Ca^{2+} release.

Although the results presented here demonstrate that G1885E modulates L433P, the co-inheritance of these substitutions has only been observed in a single family (Claycomb *et al.*, 1998; Tiso *et al.*, 2001; Bauce *et al.*, 2002) suggesting that it is an extremely rare genotype. However, L433P has not been identified in a CPVT/ARVD patient in the absence of G1885E, suggesting that this like all other CPVT mutations, this is an extremely rare genotype. Given the increasing documentation of the co-inheritance of common SNPs with CPVT/ARVD2-linked RyR2 mutations (Medeiros Domingo, 2009), it would be interesting to determine whether any other SNPs exhibit similar functional modulation on co-inherited mutations or whether this phenomenon was unique to the combination of SNP/mutation examined here.

Appendix I

Cloning

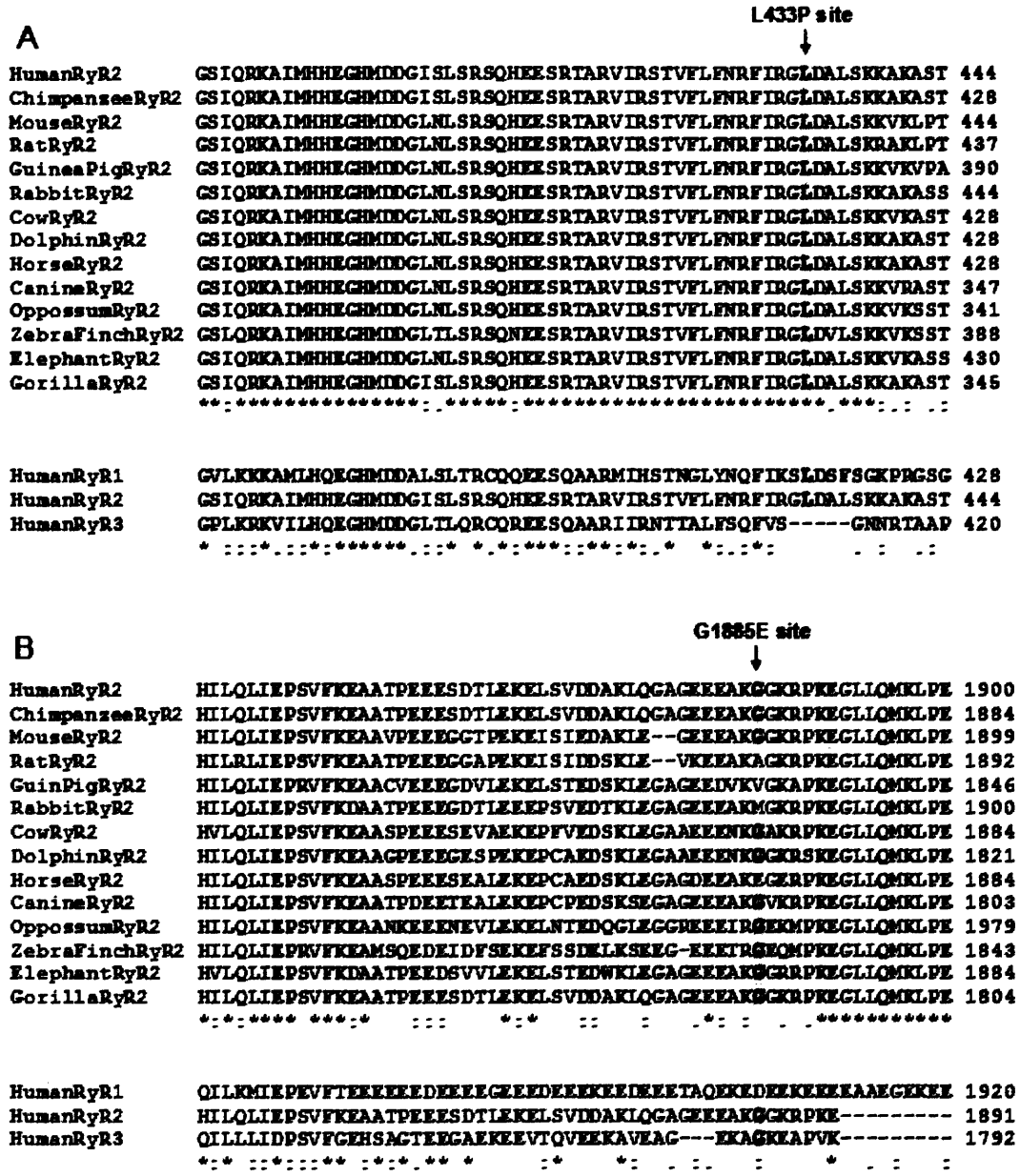

Figure 1. L433 and G1885 are conserved among species and isoforms *RyR primary sequences were obtained from the ENSMBL database and underwent multiple sequence alignment using CLUSTALW as shown in panel A. Alignments of RyR2 sequence from multiple species confirmed that the Leucine at residue 433 was highly conserved across all species (upper panel) and was conserved between human RyR1 and RyR2 (lower panel) as shown in panel B. Sequence alignment demonstrated the glycine at residue 1885 was relatively conserved among mammals and occurred in a region of high sequence variability (DR3, upper panel). The glycine residue at 1885 was conserved between human RyR2 and RyR3 and occurs in a region of high variability between human RyR isoforms.*

Abbreviation	Construct	Description
WT RyR2	pcDNA3-eGFP-hRyR2	The pcDNA3 mammalian expression vector containing the cDNA encoding human RyR2 fused to eGFP at the N-terminus
SK1	pSL1180-SK1	The intermediate expression vector containing the *SanDI / Kpn1* RyR2 mutagenesis cassette.
n/a	pSL1180-SK1-G1885E	The intermediate expression vector, pSL1180, containing the *SanDI / KpnI* RyR2 mutagenesis cassette harbouring the G1885E-encoding nucleotide substitution
n/a	SK1-G1885E	The isolated *SanDI / KpnI* mutagenesis cassette containing the G1885E-encoding nucleotide substitution.
G1885E or GE	pcDNA3-eGFP-hRyR2-G1885E	The pcDNA3 expression vector containing the cDNA encoding GFP-tagged, full length, human RyR2 containing the G1885E-encoding nucleotide substitution
L433P or LP	pcDNA3-eGFP-hRyR2-L433P	The pcDNA3 expression vector containing the cDNA encoding GFP-tagged, full length, human RyR2 containing the L433P-encoding nucleotide substitution
L433P-G1885E or LPGE	pcDNA3-eGFP-hRyR2-L433P-G1885E	The pcDNA3 expression vector containing the cDNA encoding GFP-tagged, full length, human RyR2 containing both the L433P and G1885E-encoding nucleotide substitutions.

Table 1. RyR2 cDNA nomenclature. *A summary of the nomenclature of the various cDNA constructs used in the generation of full length eGFP-tagged, human RyR2 harbouring the L433P mutation and G1885E polymorphism.*

Figure 2. Schematic representation of cDNA constructs produced from the cloning of RyR2 containing L433P and/or G1885E. *Schematic representations of the various cDNA plasmids produced during the generation of full length RyR2 plasmid cDNA containing combinations of L433P and G1885E encoding nucleotide substitutions. Thin black bars represent the vector sequence, red bars represent RyR2 encoding sequence and green arrows represent the eGFP coding sequence. The yellow rectangle represents the location of the point mutation encoding the indicated amino acid substitution.*

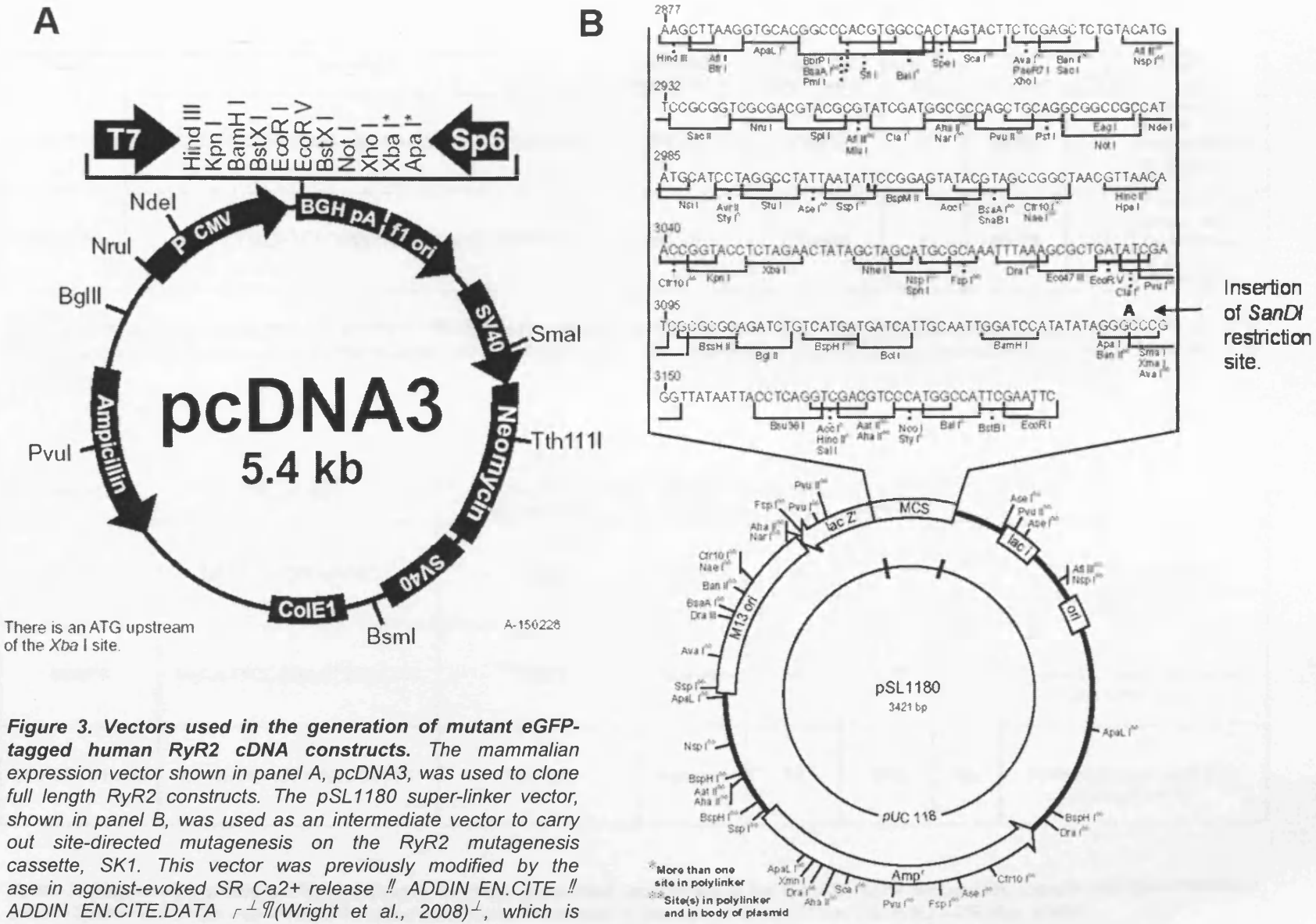

Figure 3. Vectors used in the generation of mutant eGFP-tagged human RyR2 cDNA constructs. *The mammalian expression vector shown in panel A, pcDNA3, was used to clone full length RyR2 constructs. The pSL1180 super-linker vector, shown in panel B, was used as an intermediate vector to carry out site-directed mutagenesis on the RyR2 mutagenesis cassette, SK1. This vector was previously modified by the ase in agonist-evoked SR Ca2+ release ‼ ADDIN EN.CITE ‼ ADDIN EN.CITE.DATA ⌐⊥¶(Wright et al., 2008)⊥, which is*

Name	Sequence	Nucleotide substitution	Amino Acid Substitution	Length (bp)	GC content	T_m (°C)	Notes
G1885E For	GAACCCGGCGAACGGGAGGAACCGAAGAAGGAG	G5454A	G1885E	33	63.6%	71	Forward primer for the mutagenesis of hRyR2 (G1885E)
G1885E Rev	CTCCTTCTTCGGTTCCTCCCGTTCGCCGGGTTC	C5454T	G1885E	33	63.6%	71	Reverse primer for the mutagenesis of hRyR2 (G1885E)

Table 2. Site-directed mutagenesis primers. *Mutagenesis primers used in the insertion of the G1885E encoding polymorphism in the SK1 RyR2 mutagenesis cassette. Shaded nucleotides indicate those undergoing substitution. Nucleotide positions are derived from the RyR2 ATG start codon.*

Name	Sequence	Primer Start Nucleotide	Primer Direction	Length (bp)	GC content	T_m (°C)	Notes
B23F4	CAGTTGATTGAGCCC	C5530	Forward	15	53.3%	46	Primer for G1885E mutagenesis verification.
B23F3	TACAGTCCAGAGTTCCCAC	T5332	Forward	19	52.6%	53	Primer for SanDI restriction site verification.
SPFOR7513-30	CAAGGCAGCCATGGTTTT	C7392	Forward	18	50%	54	Primer for KpnI restriction site verification.

Table 3. Sequencing primers. *Primers used in the direct automated sequencing of the G1885E SDM site and SK1 SanDI and KpnI restriction sites in ligated full length eGFP-hRyR2 mutant constructs. Nucleotide positions are derived from the RyR2 ATG start codon.*

Appendix II

Experimental Data

	HEK				WT				GE				LP				LP-GE			
Caffeine (mM)	Basal	Early	Middle	Late	Basal	Early	Middle	Late	Basal	Early	Middle	Late	Basal	Early	Middle	Late	Basal	Early	Middle	Late
0.1	2.20 ± 0.07 p<0.0001	2.21 ± 0.07 p<0.0001	2.17 ± 0.07 p<0.0001	1.96 ± 0.06 p<0.0001	1.35 ± 0.11	1.34 ± 0.11	1.40 ± 0.12	1.28 ± 0.12	1.94 ± 0.10 p=0.0004	1.83 ± 0.09 p=0.002	1.93 ± 0.09 p=0.001	1.65 ± 0.09 p=0.0139	1.88 ± 0.15 p=0.0127	1.85 ± 0.14 p=0.014	1.86 ± 0.13 p=0.0219	1.67 ± 0.11 p=0.0278	1.61 ± 0.09 p=0.0907	1.48 ± 0.09 p=0.3799	1.54 ± 0.10 p=0.4131	1.36 ± 0.09 p=0.5970
0.25	1.87 ± 0.06 p=0.065	1.93 ± 0.06 p=0.0237	1.93 ± 0.07 p=0.0156	1.66 ± 0.05 p=0.0102	1.44 ± 0.11	1.43 ± 0.11	1.46 ± 0.11	1.28 ± 0.11	1.59 ± 0.12 p=0.8464	1.57 ± 0.11 p=0.9075	1.60 ± 0.11 p= 0.7097	1.39 ± 0.1 p=0.5593	1.88 ± 0.12 p=0.5813	1.88 ± 0.14 p=0.5378	1.72 ± 0.11 p=0.385	1.54 ± 0.09 p=0.1925	1.73 ± 0.09 p=0.3874	1.60 ± 0.08 p=0.788	1.86 ± 0.08 p=0.4794	1.49 ± 0.08 p= 0.2588
0.5	1.83 ± 0.05 p = 0.5925	1.87 ± 0.04 p=0.0252	1.83 ± 0.04 p = 0.3469	1.60 ± 0.04 p=0.3222	1.78 ± 0.1	1.66 ± 0.1	1.74 ± 0.11	1.51 ± 0.09	1.49 ± 0.12 p=0.0857	1.38 ± 0.12 p=0.0823	1.43 ± 0.12 p=0.06	1.26 ± 0.1 p=0.0781	1.78 ± 0.14 p=0.9862	1.61 ± 0.11 p=0.8012	1.71 ± 0.11 p=0.8499	1.43 ± 0.1 p=0.5938	1.67 ± 0.12 p=0.5809	1.49 ± 0.1 p=0.3023	1.54 ± 0.1 p=0.1919	1.40 ± 0.09 p=0.4028
0.75	1.89 ± 0.05 p=0.4539	1.86 ± 0.05 p=0.1688	1.83 ± 0.05 p=0.4493	1.54 ± 0.04 p=0.8418	1.82 ± 0.08	1.73 ± 0.09	1.76 ± 0.09	1.56 ± 0.08	1.63 ± 0.1 p=0.1610	1.51 ± 0.09 p=0.0860	1.59 ± 0.1 p=0.2303	1.41 ± 0.1 p=0.2303	2.07 ± 0.12 p=0.3440	2.00 ± 0.16 p=0.3329	2.01 ± 0.18 p=0.3825	1.73 ± 0.19 p=0.5007	1.46 ± 0.07 p=0.0013	1.33 ± 0.06 p=0.0001	1.42 ± 0.06 p=0.0021	1.24 ± 0.06 p=0.0014
1	2.00 ± 0.03 p<0.0001	1.99 ± 0.03 p <0.0001	1.96 ± 0.03 p<0.0001	1.69 ± 0.03 p<0.0001	1.40 ± 0.09	1.30 ± 0.08	1.27 ± 0.08	1.18 ± 0.07	1.59 ± 0.1 p=0.1449	1.43 ± 0.08 p=0.2710	1.50 ± 0.09 p=0.0599	1.29 ± 0.08 p=0.2881	1.81 ± 0.1 p=0.0987	1.45 ± 0.09 p=0.2374	1.51 ± 0.09 p=0.0442	1.37 ± 0.07 p=0.0877	1.67 ± 0.1 p=0.5251	1.51 ± 0.08 p=0.7803	1.56 ± 0.09 p=0.1514	1.46 ± 0.09 p=0.4800
2	2.03 ± 0.04 p<0.0001	2.04 ± 0.04 p<0.0001	1.98 ± 0.04 p<0.0001	1.70 ± 0.04 p<0.0001	1.51 ± 0.08	1.49 ± 0.05	1.52 ± 0.05	1.36 ± 0.05	1.74 ± 0.07 p=0.0040	1.61 ± 0.07 p=0.1463	1.63 ± 0.07 p=0.2146	1.50 ± 0.06 p=0.0582	1.75 ± 0.06 p=0.0018	1.64 ± 0.07 p=0.0798	1.7 ± 0.06 p=0.0403	1.53 ± 0.05 p=0.0255	1.59 ± 0.08 p=0.2634	1.46 ± 0.08 p=0.7334	1.58 ± 0.09 p=0.5811	1.43 ± 0.08 p=0.4905
5	1.85 ± 0.04 p=0.002	1.90 ± 0.04 p<0.0001	1.83 ± 0.04 p=0.0007	1.35 ± 0.04 p=0.9341	1.60 ± 0.08	1.40 ± 0.07	1.39 ± 0.06	1.35 ± 0.07	1.77 ± 0.06 p=0.0808	1.64 ± 0.07 p=0.0218	1.69 ± 0.06 p=0.0008	1.53 ± 0.05 p=0.0421	1.52 ± 0.07 p=0.4127	1.43 ± 0.06 p=0.7721	1.53 ± 0.06 p=0.0923	1.37 ± 0.05 p=0.8545	1.72 ± 0.17 p=0.5002	1.55 ± 0.18 p=0.3822	1.64 ± 0.18 p=0.1115	1.64 ± 0.16 p=0.0899
7.5	2.04 ± 0.05 p=0.0172	2.13 ± 0.06 p=0.0786	2.01 ± 0.06 p=0.0463	1.89 ± 0.05 p=0.6358	1.83 ± 0.06	1.71 ± 0.07	1.82 ± 0.08	1.65 ± 0.06	1.81 ± 0.06 p=0.7957	1.67 ± 0.05 p<0.0001	1.79 ± 0.05 p=0.7826	1.60 ± 0.05 p=0.5131	1.46 ± 0.06 p<0.0001	1.32 ± 0.05 p=0.6214	1.46 ± 0.07 p=0.0008	1.31 ± 0.06 p=0.0001	1.60 ± 0.08 p=0.0377	1.52 ± 0.07 p<0.0001	1.57 ± 0.07 p=0.0214	1.43 ± 0.07 p=0.0248
10	2.11 ± 0.04 p<0.0001	2.16 ± 0.04 p<0.0001	2.08 ± 0.04 p=0.0003	1.77 ± 0.07 p=0.0106	1.79 ± 0.07	1.76 ± 0.08	1.79 ± 0.06	1.58 ± 0.01	1.92 ± 0.09 p=0.3256	1.81 ± 0.1 p=0.6798	1.96 ± 0.1 p=0.2135	1.71 ± 0.09 p=0.2484	1.57 ± 0.09 p=0.0618	1.44 ± 0.08 p=0.0036	1.52 ± 0.08 p=0.0133	1.37 ± 0.07 p=0.0314	1.64 ± 0.11 p=0.2743	1.51 ± 0.11 p=0.0535	1.65 ± 0.12 p=0.3063	1.52 ± 0.12 p=0.6326

Table 1. Average basal and post-activation SVm values in cells expressing homotetrameric RyR2 and results of statistical comparison with WT RyR2. *The average basal and post-activation SVm values at each experimental condition were calculated and the mean ± S.E.M SVm values are displayed. SVm values of untransfected HEK cells or cells expressing G1885E, L433P or L433P-G1885E were compared to the corresponding condition in cells expressing WT RyR2. Green shading indicates a significant difference to WT RyR ($p < 0.05$). Red shading indicates a significant difference between L433P and L433P-G1885E ($p < 0.05$). Data is represented as a heat map in Figure 4.13.*

	WT				WT + GE				WT + LP				WT + LPGE				LP + GE			
Caffeine (mM)	Basal	Early	Middle	Late	Basal	Early	Middle	Late	Basal	Early	Middle	Late	Basal	Early	Middle	Late	Basal	Early	Middle	Late
0.1	1.35 ±0.11	1.34 ±0.11	1.40 ±0.12	1.28 ±0.12	1.448 ±0.10 p=0.5191	1.37 ±0.11 p=0.8699	1.46 ±0.10 p=0.7000	1.25 ±0.09 p=0.2638	1.41 ±0.08 p=0.6615	1.22 ±0.65 p=0.3356	1.33 ±0.07 p=0.6176	1.20 ±0.07 p=0.8527	1.27 ±0.14 p=0.7002	1.25 ±0.13 p=0.8673	1.16 ±0.11 p=0.2893	1.09 ±0.11 p=0.4954	1.27 ±0.06 p=0.5419	1.26 ±0.07 p=0.5226	1.30 ±0.06 p=0.4396	1.14 ±0.07 p=0.3705
0.25	1.44 ±0.11	1.43 ±0.11	1.46 ±0.11	1.28 ±0.11	1.50 ±0.12 p=0.8540	1.39 ±0.13 p=0.0108	1.48 ±0.13 p=0.8678	1.30 ±0.11 p=0.9533	1.42 ±0.08 p=0.5321	1.28 ±0.07 p=0.5316	1.32 ±0.08 p=0.2436	1.22 ±0.07 p=0.6659	1.44 ±0.06 p=0.5390	1.40 ±0.06 p=0.1464	1.37 ±0.06 p=0.3730	1.25 ±0.05 p=0.7834	1.12 ±0.07 p=0.0191	1.10 ±0.07 p=0.0108	1.15 ±0.07 p=0.0315	1.01 ±0.06 p=0.0663
0.5	1.78 ±0.1	1.66 ±0.1	1.74 ±0.11	1.51 ±0.09	1.36 ±0.07 p=0.0033	1.32 ±0.06 p=0.0094	1.37 ±0.06 p=0.0060	1.26 ±0.07 p=0.0364	1.52 ±0.09 p=0.1019	1.40 ±0.09 p=0.0889	1.43 ±0.09 p=0.0500	1.29 ±0.09 p=0.1071	1.53 ±0.09 p=0.1188	1.54 ±0.07 p=0.4168	1.62 ±0.09 p=0.04098	1.37 ±0.09 p=0.3001	1.50 ±0.13 p=0.1510	1.69 ±0.17 p=0.8683	1.63 ±0.17 p=0.5782	1.47 ±0.14 p=0.7930
0.75	1.82 ±0.08	1.73 ±0.09	1.76 ±0.09	1.56 ±0.08	1.40 ±0.07 p=0.0028	1.32 ±0.07 p=0.0037	1.35 ±0.06 p=0.0057	1.26 ±0.07 p=0.0204	1.57 ±0.09 p=0.0516	1.29 ±0.07 p=0.0004	1.35 ±0.07 p=0.0014	1.24 ±0.07 p=0.0056	1.61 ±0.14 p=0.2776	1.72 ±0.15 p=0.9537	1.75 ±0.16 p=0.9667	1.43 ±0.08 p=0.4668	1.43 ±0.14 p=0.0674	1.50 ±0.13 p=0.0876	1.29 ±0.10 p=0.1356	1.40 ±0.07 p=0.0735
1	1.40 ±0.08	1.30 ±0.08	1.27 ±0.08	1.18 ±0.07	1.40 ±0.04 p=0.9581	1.31 ±0.04 p=0.9315	1.36 ±0.04 p=0.2799	1.26 ±0.04 p=0.2680	1.47 ±0.07 p=0.5204	1.26 ±0.05 p=0.6790	1.29 ±0.05 p=0.8392	1.19 ±0.05 p=0.9283	1.42 ±0.09 p=0.8339	1.41 ±0.08 p=0.3957	1.39 ±0.08 p=0.2990	1.29 ±0.07 p=0.3062	1.25 ±0.05 p=0.1185	1.10 ±0.05 p=0.0310	1.13 ±0.05 p=0.1083	1.03 ±0.04 p=0.0652
2	1.51 ±0.06	1.49 ±0.05	1.52 ±0.05	1.36 ±0.05	1.44 ±0.05 p=0.7563	1.34 ±0.01 p=0.0259	1.40 ±0.04 p=0.0854	1.24 ±0.04 p=0.0544	1.53 ±0.07 p=0.5317	1.29 ±0.05 p=0.0074	1.38 ±0.06 p=0.0706	1.28 ±0.05 p=0.2299	1.63 ±0.06 p=0.0842	1.49 ±0.05 p=0.9892	1.54 ±0.06 p=0.8318	1.41 ±0.06 p=0.4755	1.52 ±0.07 p=0.5604	1.40 ±0.07 p=0.2402	1.43 ±0.06 p=0.2494	1.30 ±0.05 p=0.3933
5	1.60 ±0.06	1.40 ±0.07	1.39 ±0.06	1.35 ±0.07	1.59 ±0.07 p=0.9361	1.43 ±0.07 p=0.7791	1.53 ±0.07 p=0.1304	1.42 ±0.06 p=0.5140	1.66 ±0.07 p=0.0136	1.55 ±0.06 p=0.051	1.74 ±0.06 p=0.0002	1.62 ±0.06 p=0.0040	1.68 ±0.07 p=0.4304	1.68 ±0.07 p=0.0054	1.69 ±0.06 p=0.0013	1.59 ±0.06 p=0.0145	1.36 ±0.09 p=0.0409	1.24 ±0.08 p=0.1496	1.34 ±0.06 p=0.5634	1.23 ±0.06 p=0.1868
7.5	1.83 ±0.06	1.71 ±0.07	1.82 ±0.06	1.65 ±0.06	1.71 ±0.06 p=0.2124	1.56 ±0.05 p=0.0783	1.68 ±0.05 p=0.1364	1.50 ±0.04 p=0.0429	1.66 ±0.07 p=0.0880	1.43 ±0.05 p=0.0012	1.60 ±0.06 p=0.0232	1.44 ±0.05 p=0.0066	1.62 ±0.11 p=0.0781	1.54 ±0.09 p=0.1418	1.70 ±0.08 p=0.3097	1.59 ±0.08 p=0.5473	1.50 ±0.07 p=0.0010	1.42 ±0.06 p=0.0014	1.54 ±0.05 p=0.0031	1.43 ±0.05 p=0.0065
10	1.79 ±0.07	1.76 ±0.08	1.79 ±0.06	1.58 ±0.01	1.60 ±0.06 p=0.0443	1.46 ±0.05 p=0.0011	1.64 ±0.06 p=0.1167	1.48 ±0.05 p=0.2503	1.57 ±0.07 p=0.0415	1.28 ±0.04 p=0.0001	1.47 ±0.05 p=0.0003	1.44 ±0.05 p=0.0917	1.78 ±0.07 p=0.9563	1.61 ±0.06 p=0.1087	1.79 ±0.05 p=0.9615	1.65 ±0.06 p=0.4559	1.77 ±0.09 p=0.8567	1.50 ±0.07 p=0.0127	1.69 ±0.07 p=0.3240	1.51 ±0.07 p=0.4822

Table 2. Average basal and post-activation SVm values of cells expressing heterotetrameric RyR2 and results of statistical comparison with WT RyR2. *The average basal and post-activation SVm values at each experimental condition were calculated and the mean ± S.E.M SVm values are displayed. SVm values of untransfected HEK cells or cells expressing G1885E, L433P or L433P-G1885E were compared to the corresponding condition in cells expressing WT RyR2. Green shading indicates a significant difference to WT RyR ($p < 0.05$). Red shading indicates a significant difference between L433P and L433P-G1885E ($p < 0.05$). Data is represented as a heat map in Figure 4.13.*

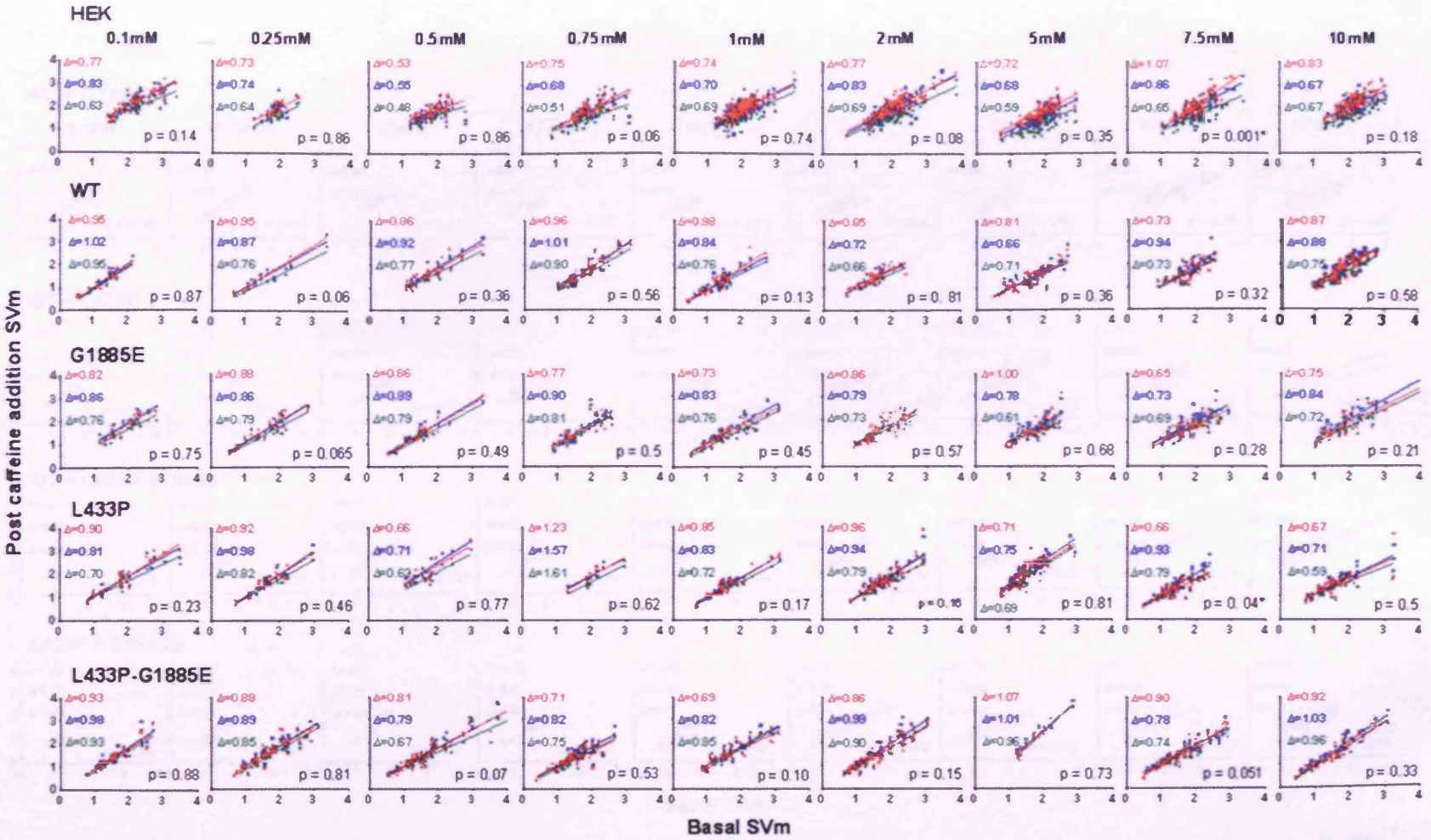

Figure 1. Linear regression analysis of basal vs. post-activation SVm values of untransfected and homotetrameric RyR2 expressing HEK cells. *Linear regression analysis examining the relationships between basal and post-activation cytoplasmic Ca^{2+} SVm was carried out. Early (0-30secs), middle (30-60 secs) and late (60-90secs) were analysed. As detailed in section 2.2.5 and 4.2.3, the regression line gradient (Δ), goodness-of-fit value (r^2) and significance value testing whether the gradient is significantly different to 0 (p) were determined and are summarised in Appendix 2, Table 2. Asterisked data indicates a significant difference between the relationship gradients at each post-activation time point ($p<0.05$).*

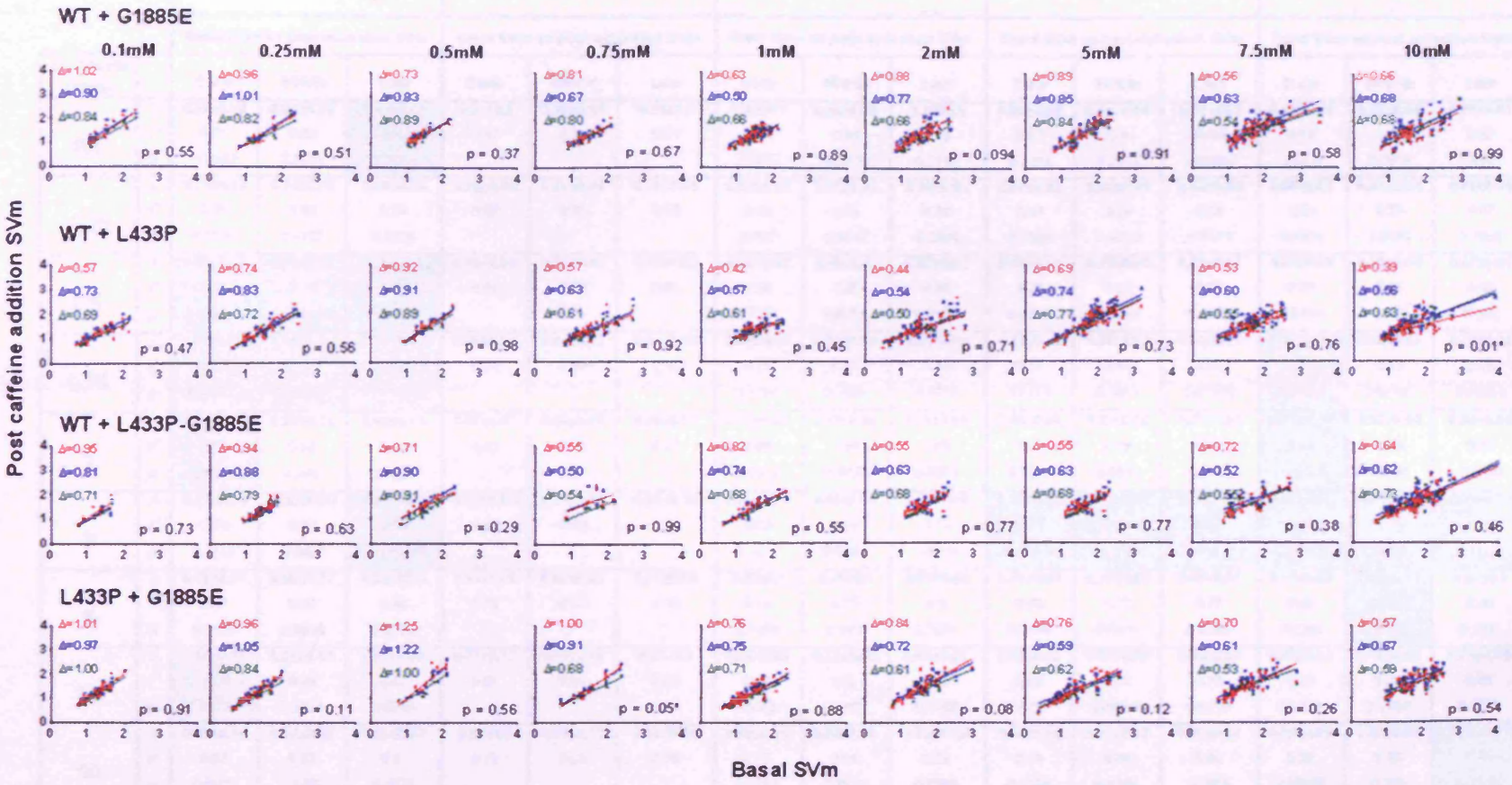

Figure 2. Linear regression analysis of basal vs. post-activation SVm values of HEK cells expressing heterotetrameric RyR2. *Linear regression analysis examining the relationships between basal and post-activation cytoplasmic Ca^{2+} SVm was carried out. Early (0-30secs), middle (30-60 secs) and late (60-90secs) were analysed. As detailed in sections 2.2.5 and 4.2.3, the regression line gradient (Δ), goodness-of-fit value (r^2) and significance value testing whether the gradient is significantly different to 0 (p) were determined and are summarised in Appendix 2, Table 3. Asterisked data indicates a significant difference between the relationship gradients at each post-activation time point ($p<0.05$).*

		HEK			WT			GE			LP			LPGE		
		Basal SVm vs post-activation SVm			Basal SVm vs post-activation SVm			Basal SVm vs post-activation SVm			Basal SVm vs post-activation SVm			Basal SVm vs post-activation SVm		
Caffeine (mM)		Early	Middle	Late	Early	Middle	Late	Early	Middle	Late	Early	Middle	Late	Early	Middle	Late
0.1	Δ	0.77±0.08	0.83±0.06	0.63±0.08	0.95±0.1	1.02±0.08	0.95±0.1	0.82±0.1	0.86±0.08	0.76±0.1	0.90±0.08	0.81±0.09	0.70±0.07	0.93±0.07	0.98±0.09	0.93±0.07
	r^2	0.71	0.82	0.62	0.87	0.92	0.86	0.78	0.86	0.76	0.87	0.8	0.83	0.88	0.82	0.87
	p	0.2593	0.1401	0.04427				0.3789	0.2078	0.2148	0.7216	0.2311	0.09257	0.8738	0.8016	0.8681
0.25	Δ	0.74±0.13	0.74±0.19	0.64±0.13	0.95±0.04	0.87±0.07	0.76±0.05	0.88±0.08	0.86±0.07	0.79±0.07	0.92±0.08	0.98±0.11	0.82±0.08	0.88±0.05	0.89±0.04	0.85±0.05
	r^2	0.59	0.41	0.54	0.98	0.93	0.96	0.89	0.89	0.87	0.89	0.84	0.86	0.85	0.59	0.87
	p	0.1135	0.5227	0.3536				0.497	0.9449	0.6999	0.7667	0.4022	0.5411	0.4878	0.8082	0.2938
0.5	Δ	0.53±0.09	0.55±0.11	0.48±0.1	0.86±0.08	0.92±0.07	0.77±0.07	0.90±0.07	0.94±0.07	0.82±0.05	0.66±0.11	0.71±0.09	0.62±0.07	0.84±0.05	0.79±0.05	0.67±0.05
	r^2	0.41	0.35	0.34	0.81	0.88	0.85	0.90	0.9	0.94	0.76	0.85	0.87	0.86	0.86	0.82
	p	0.009546	0.006415	0.01492				0.6794	0.8711	0.5128	0.1975	0.1005	0.1808	0.6494	0.195	0.282
0.75	Δ	0.75±0.06	0.68±0.08	0.51±0.07	0.96±0.07	1.01±0.08	0.90±0.05	0.79±0.09	0.92±0.08	0.81±0.09	1.23±0.46	1.57±0.13	1.61±0.16	0.71±0.07	0.82±0.07	0.75±0.06
	r^2	0.72	0.55	0.44	0.84	0.84	0.90	0.74	0.82	0.76	0.78	0.99	0.98	0.69	0.72	0.76
	p	0.02621	0.004504	0.0001509				0.1364	0.4684	0.3779	0.6215	0.3011	0.07032	0.01595	0.08387	0.06618
1	Δ	0.74±0.05	0.70±0.05	0.69±0.05	0.87±0.07	0.84±0.08	0.76±0.07	0.73±0.04	0.83±0.06	0.76±0.06	0.85±0.06	0.83±0.06	0.72±0.04	0.69±0.07	0.82±0.06	0.85±0.05
	r^2	0.61	0.53	0.56	0.83	0.78	0.77	0.89	0.84	0.83	0.88	0.89	0.91	0.76	0.86	0.89
	p	0.006984	0.147	0.4031				0.1009	0.8922	0.9879	0.1964	0.8582	0.5783	0.00525	0.806	0.3069
2	Δ	0.77±0.04	0.83±0.04	0.69±0.05	0.66±0.08	0.72±0.09	0.66±0.08	0.85±0.08	0.80±0.09	0.74±0.06	0.96±0.08	0.94±0.07	0.79±0.05	0.86±0.05	0.99±0.05	0.90±0.04
	r^2	0.74	0.77	0.62	0.63	0.63	0.64	0.68	0.63	0.75	0.74	0.80	0.82	0.86	0.86	0.91
	p	0.2157	0.2907	0.005539				0.1072	0.5554	0.4354	0.01088	0.048	0.0002969	0.03609	0.01583	0.0001
5	Δ	0.72±0.05	0.68±0.07	0.59±0.08	0.81±0.08	0.66±0.06	0.71±0.08	1.00±0.1	0.78±0.1	0.61±0.08	0.71±0.07	0.75±0.07	0.69±0.05	1.07±0.09	1.01±0.11	0.96±0.1
	r^2	0.67	0.54	0.38	0.73	0.72	0.64	0.68	0.58	0.6	0.66	0.73	0.78	0.95	0.91	0.93
	p	0.3188	0.8016	0.2735				0.1368	0.313	0.3571	0.3768	0.3211	0.8295	0.1286	0.02242	0.1921
7.5	Δ	1.07±0.07	0.86±0.08	0.65±0.08	0.73±0.12	0.94±0.12	0.73±0.1	0.65±0.06	0.73±0.08	0.69±0.07	0.66±0.07	0.93±0.08	0.79±0.07	0.90±0.04	0.78±0.05	0.74±0.05
	r^2	0.75	0.64	0.47	0.51	0.64	0.60	0.62	0.6	0.63	0.69	0.74	0.75	0.90	0.85	0.81
	p	0.01785	0.5724	0.5988				0.5356	0.1472	0.7167	0.6277	0.9334	0.6318	0.1278	0.1768	0.9271
10	Δ	0.83±0.06	0.67±0.07	0.67±0.07	0.87±0.1	0.88±0.11	0.75±0.08	0.75±0.06	0.84±0.06	0.72±0.05	0.67±0.08	0.71±0.07	0.59±0.07	0.92±0.05	1.03±0.05	0.96±0.06
	r^2	0.67	0.53	0.51	0.71	0.66	0.70	0.76	0.84	0.82	0.64	0.76	0.65	0.92	0.93	0.89
	p	0.6862	0.1067	0.5038				0.3163	0.7531	0.7262	0.1184	0.1746	0.1565	0.65682	0.185	0.04793

Table 3. Linear regression analysis of basal vs. post-activation SVm values of untransfected and homotetrameric RyR2 expressing HEK cells. *Linear regression analysis examining the relationships between basal and post-activation cytoplasmic Ca^{2+} SVm was carried out, the results of which are presented here. As detailed in section 2.2.5 and 4.2.3, the regression line gradient (Δ), goodness-of-fit value (r^2) and significance value testing whether the gradient is significantly different to 0 (p) were determined. Experimental conditions that produced a significantly different relationship gradient compared to the corresponding experimental condition in cells expressing WT RyR2 are highlighted in green ($p<0.05$) and as such are presented on the heat map in Figure 4.14.*

		WT			WT + GE			WT + LP			WT + LPGE			LP + GE		
		Basal SVm vs post-activation SVm			Basal SVm vs post-activation SVm			Basal SVm vs post-activation SVm			Basal SVm vs post-activation SVm			Basal SVm vs post-activation SVm		
Caffeine (mM)		Early	Middle	Late	Early	Middle	Late	Early	Middle	Late	Early	Middle	Late	Early	Middle	Late
0.1	Δ	0.95±0.1	1.02±0.08	0.95±0.1	1.02±0.13	0.90±0.12	0.84±0.09	0.57±0.12	0.73±0.07	0.69±0.09	0.70±0.31	0.59±0.27	0.63±0.24	1.01±0.09	0.97±0.07	1.00±0.07
	r^2	0.87	0.92	0.86	0.81	0.8	0.87	0.55	0.85	0.76	0.62	0.62	0.69	0.84	0.89	0.89
	p				0.7012	0.4529	0.4395	0.02305	0.008677	0.2784	0.3913	0.9063	0.2784	0.66	0.6518	0.6573
0.25	Δ	0.95±0.04	0.87±0.07	0.76±0.05	0.96±0.13	1.01±0.11	0.82±0.12	0.77±0.09	0.83±0.08	0.72±0.06	0.94±0.13	0.88±0.11	0.79±0.09	0.96±0.07	1.05±0.07	0.84±0.07
	r^2	0.96	0.93	0.96	0.83	0.89	0.81	0.73	0.82	0.87	0.72	0.77	0.82	0.89	0.88	0.85
	p				0.916	0.2967	0.5987	0.049	0.7241	0.6405	0.9535	0.9424	0.7758	0.8387	0.08839	0.3504
0.5	Δ	0.86±0.08	0.92±0.07	0.77±0.07	0.73±0.07	0.83±0.08	0.89±0.09	0.92±0.12	0.91±0.13	0.89±0.11	0.71±0.1	0.90±0.11	0.91±0.09	1.25±0.18	1.22±0.17	1.00±0.18
	r^2	0.81	0.88	0.85	0.83	0.84	0.83	0.82	0.79	0.83	0.79	0.83	0.88	0.84	0.84	0.78
	p				0.3808	0.4552	0.3212	0.7049	0.9568	0.4017	0.3641	0.8601	0.2953	0.05294	0.09423	0.1687
0.75	Δ	0.96±0.07	1.01±0.08	0.90±0.05	0.81±0.12	0.67±0.14	0.80±0.1	0.57±0.09	0.63±0.09	0.61±0.08	0.55±0.37	0.50±0.41	0.54±0.09	1.01±0.08	0.91±0.1	0.68±0.08
	r^2	0.84	0.84	0.90	0.76	0.62	0.81	0.58	0.64	0.69	0.27	0.2	0.85	0.94	0.89	0.87
	p				0.3757	0.07213	0.4227	0.001956	0.002362	0.002708	0.1082	0.06881	0.02066	0.7766	0.5214	0.05099
1	Δ	0.98±0.07	0.84±0.08	0.76±0.07	0.63±0.11	0.59±0.1	0.66±0.09	0.42±0.14	0.57±0.1	0.61±0.08	0.82±0.08	0.74±0.11	0.68±0.07	0.76±0.07	0.75±0.06	0.71±0.05
	r^2	0.85	0.78	0.77	0.47	0.47	0.58	0.27	0.55	0.69	0.85	0.73	0.84	0.72	0.74	0.79
	p				0.00957	0.0648	0.3993	0.0003736	0.04752	0.1973	0.1961	0.4754	0.4959	0.02599	0.3397	0.5634
2	Δ	0.65±0.08	0.72±0.09	0.66±0.08	0.88±0.06	0.77±0.08	0.66±0.07	0.44±0.09	0.54±0.09	0.50±0.07	0.55±0.11	0.63±0.14	0.68±0.13	0.84±0.08	0.72±0.07	0.61±0.07
	r^2	0.63	0.63	0.64	0.79	0.61	0.60	0.36	0.42	0.54	0.47	0.42	0.47	0.74	0.73	0.67
	p				0.02345	0.7256	0.9539	0.1051	0.2017	0.3756	0.4418	0.5619	0.1015	0.1053	0.9856	0.0758
5	Δ	0.81±0.08	0.66±0.06	0.71±0.08	0.89±0.1	0.85±0.1	0.84±0.08	0.69±0.07	0.74±0.08	0.77±0.06	0.71±0.1	0.71±0.11	0.63±0.1	0.76±0.07	0.59±0.06	0.62±0.06
	r^2	0.73	0.72	0.64	0.69	0.68	0.77	0.65	0.63	0.76	0.51	0.57	0.58	0.79	0.71	0.74
	p				0.4948	0.09286	0.2873	0.2546	0.4225	0.5999	0.4605	0.6723	0.5502	0.642	0.4147	0.3611
7.5	Δ	0.73±0.12	0.94±0.12	0.73±0.1	0.56±0.07	0.63±0.07	0.54±0.06	0.53±0.08	0.60±0.08	0.55±0.06	0.72±0.1	0.52±0.11	0.55±0.11	0.70±0.07	0.61±0.07	0.53±0.07
	r^2	0.51	0.64	0.60	0.52	0.58	0.60	0.55	0.57	0.65	0.70	0.5	0.53	0.68	0.61	0.57
	p				0.2408	0.02783	0.09774	0.1567	0.02139	0.1249	0.947	0.01189	0.2418	0.8263	0.02002	0.09816
10	Δ	0.87±0.1	0.88±0.11	0.75±0.08	0.66±0.08	0.68±0.09	0.68±0.07	0.39±0.06	0.56±0.06	0.63±0.05	0.64±0.06	0.62±0.06	0.73±0.07	0.57±0.1	0.67±0.08	0.59±0.08
	r^2	0.71	0.66	0.70	0.58	0.53	0.62	0.41	0.63	0.70	0.64 *	0.63	0.65	0.53	0.71	0.67
	p				0.04962	0.1515	0.4985	0.0001	0.0062	0.5038	0.049	0.03844	0.825	0.03358	0.123	0.1513

Table 4. Linear regression analysis of basal vs. post-caffeine-activation SVm values in HEK cells expressing heterotetrameric RyR2. *Linear regression analysis examining the relationships between basal and post-activation cytoplasmic Ca^{2+} SVm was carried out, the results of which are presented here. As detailed in section 2.2.5 and 4.2.3, the regression line gradient (Δ), goodness-of-fit value (r^2) and significance value testing whether the gradient is significantly different to 0 (p) were determined. Experimental conditions that produced a significantly different relationship gradient compared to the corresponding experimental condition in cells expressing WT RyR2 are highlighted in green ($p<0.05$) and as such are presented on the heat map in Figure 4.14.*

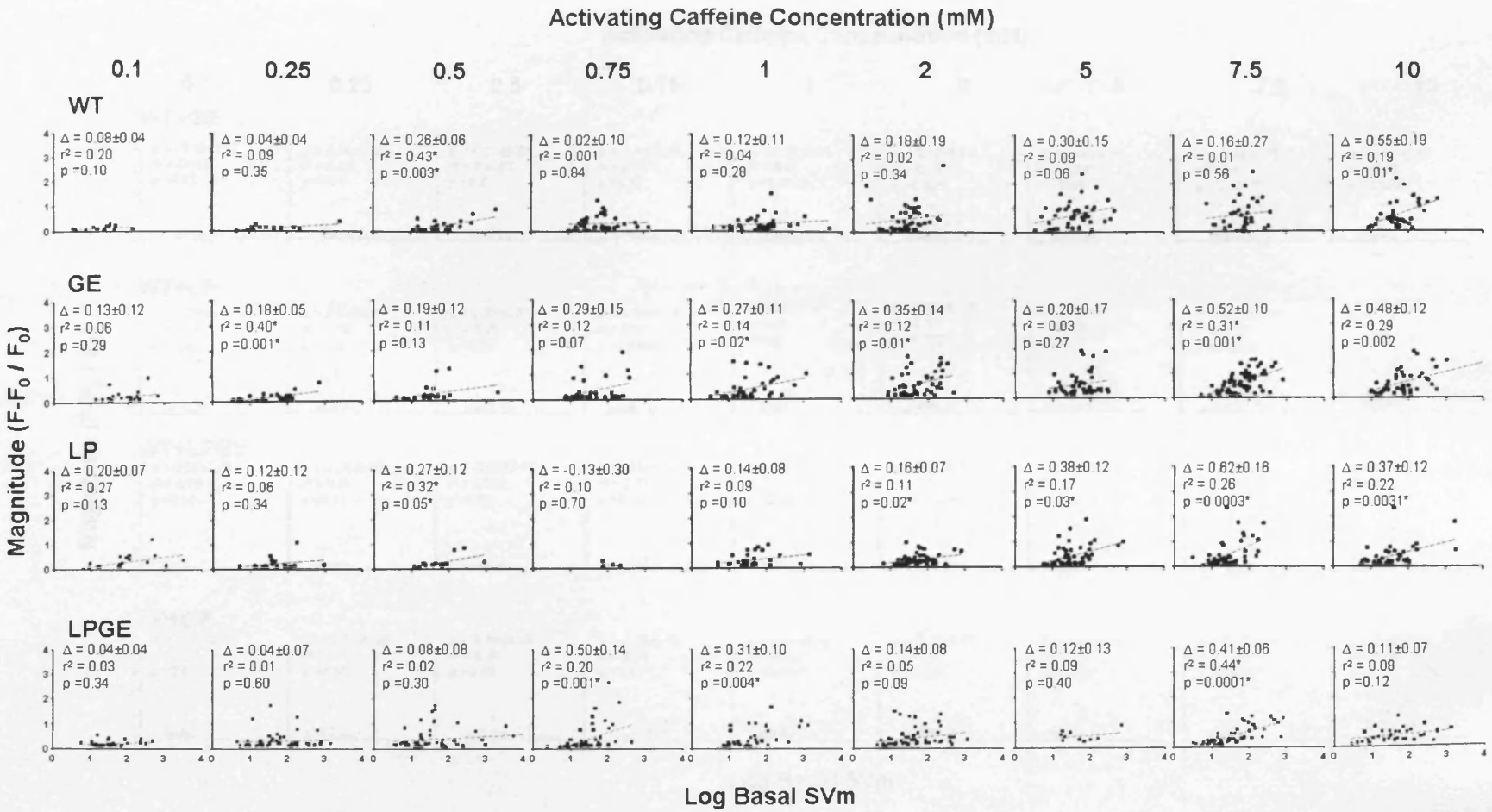

Figure 3. There is no relationship between basal SVm and magnitude of caffeine-evoked Ca^{2+} release following homotetrameric RyR2 expression. *Linear regression analysis examining the relationships between basal SVm and caffeine-evoked Ca^{2+} release magnitude was carried out. As detailed in section 2.2.5 and 4.2.3, the regression line gradient (Δ), goodness-of-fit value (r^2) and significance value testing whether the gradient is significantly different to 0 (p) were determine. Asterisked p-values indicate a linear regression line that was significantly different to 0 ($p<0.05$) whereas asterisked r^2 values indicate data which was an acceptable fit to the linear regression model ($r^2>0.3$).*

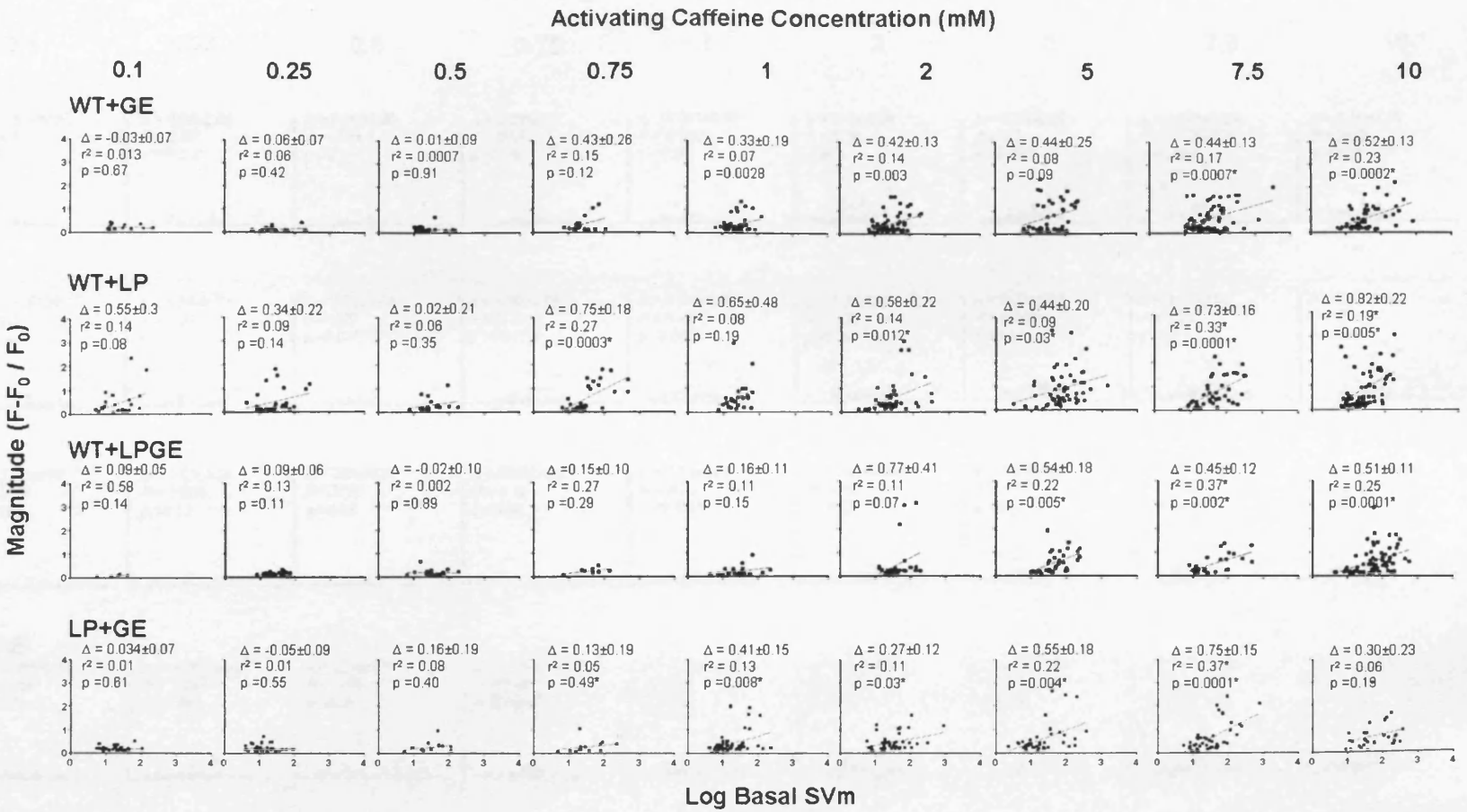

Figure 4. There is no relationship between basal SVm and magnitude of caffeine-evoked Ca^{2+} release following heterotetrameric RyR2 expression. *Linear regression analysis examining the relationships between basal SVm and caffeine-evoked Ca^{2+} release magnitude was carried out. As detailed in section 2.2.5, the regression line gradient (Δ), goodness-of-fit value (r^2) and significance value testing whether the gradient is significantly different to 0 (p) were determined. Asterisked p-values indicate a linear regression line that was significantly different to 0 ($p<0.05$) whereas asterisked r^2 values indicate data which was an acceptable fit to the linear regression model*

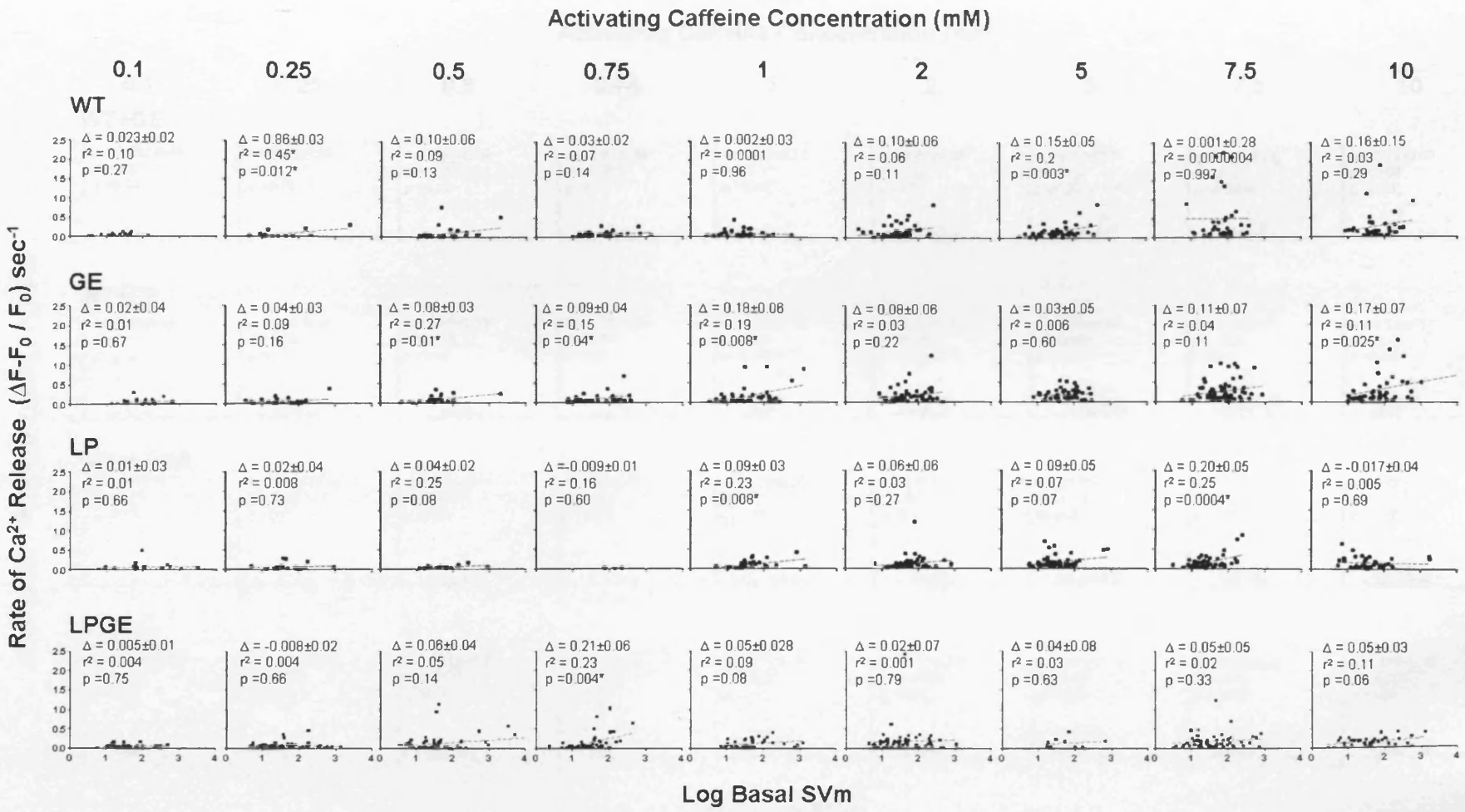

Figure 5. There is no relationship between basal SVm and rate of caffeine-evoked Ca^{2+} release following homotetrameric RyR2 expression. *Linear regression analysis examining the relationships between basal SVm and the rate of caffeine-evoked Ca^{2+} release was carried out. As detailed in section 2.2.5, the regression line gradient (Δ), goodness-of-fit value (r^2) and significance value testing whether the gradient is significantly different to 0 (p) were determined. Asterisked p-values indicate a linear regression line that was significantly different to 0 ($p<0.05$) whereas asterisked r^2 values indicate data which was an acceptable fit to the linear regression model ($r^2>0.3$).*

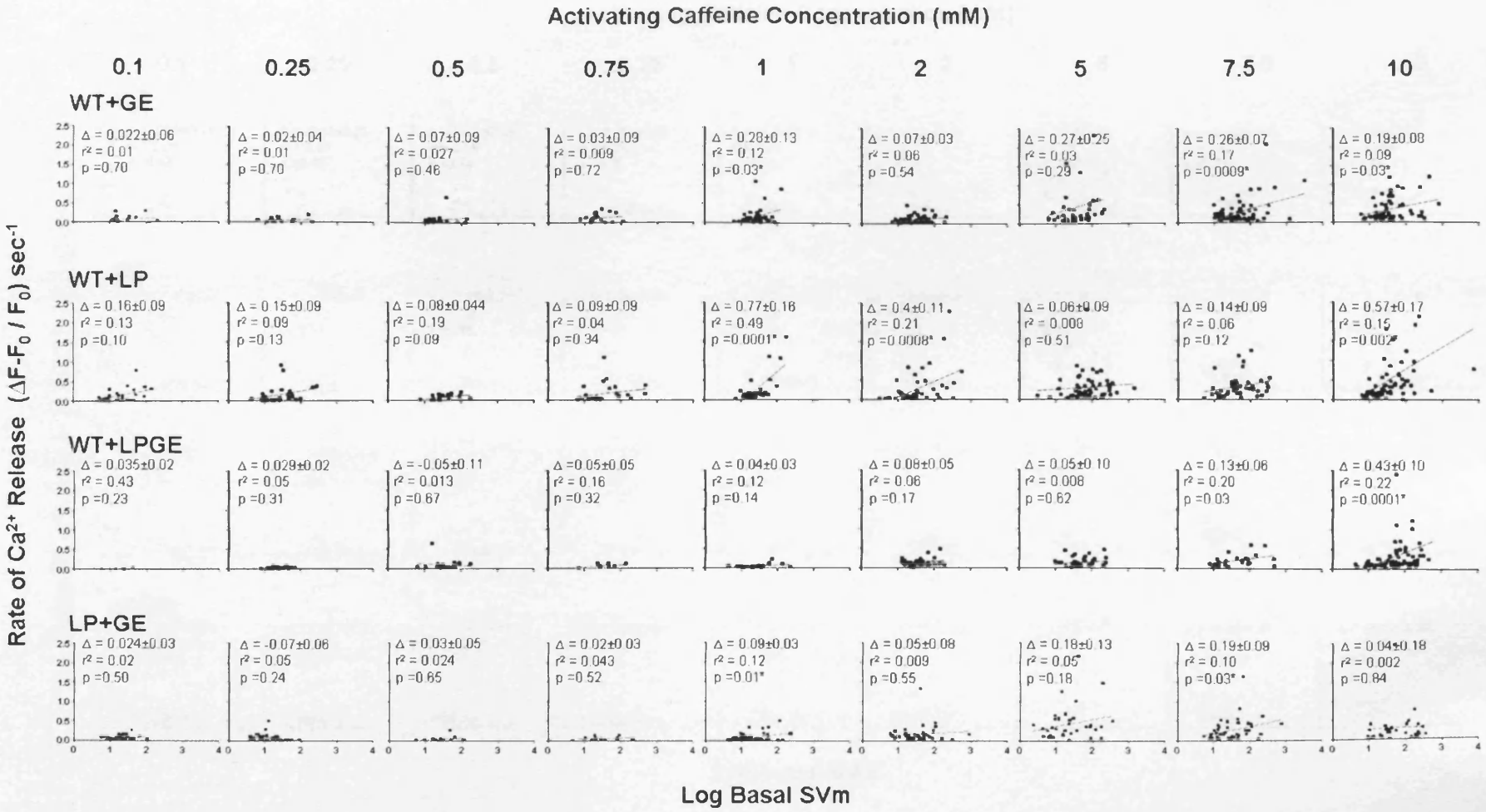

Figure 6. There is no relationship between basal SVm and rate of caffeine-evoked Ca^{2+} release following heterotetrameric RyR2 expression. *Linear regression analysis examining the relationships between basal SVm and the rate of caffeine-evoked Ca^{2+} release was carried out. As detailed in section 2.2.5, the regression line gradient (Δ), goodness-of-fit value (r^2) and significance value testing whether the gradient is significantly different to 0 (p) were determined. Asterisked p-values indicate a linear regression line that was significantly different to 0 ($p<0.05$) whereas asterisked r^2 values indicate data which was an acceptable fit to the linear regression model ($r^2>0.3$).*

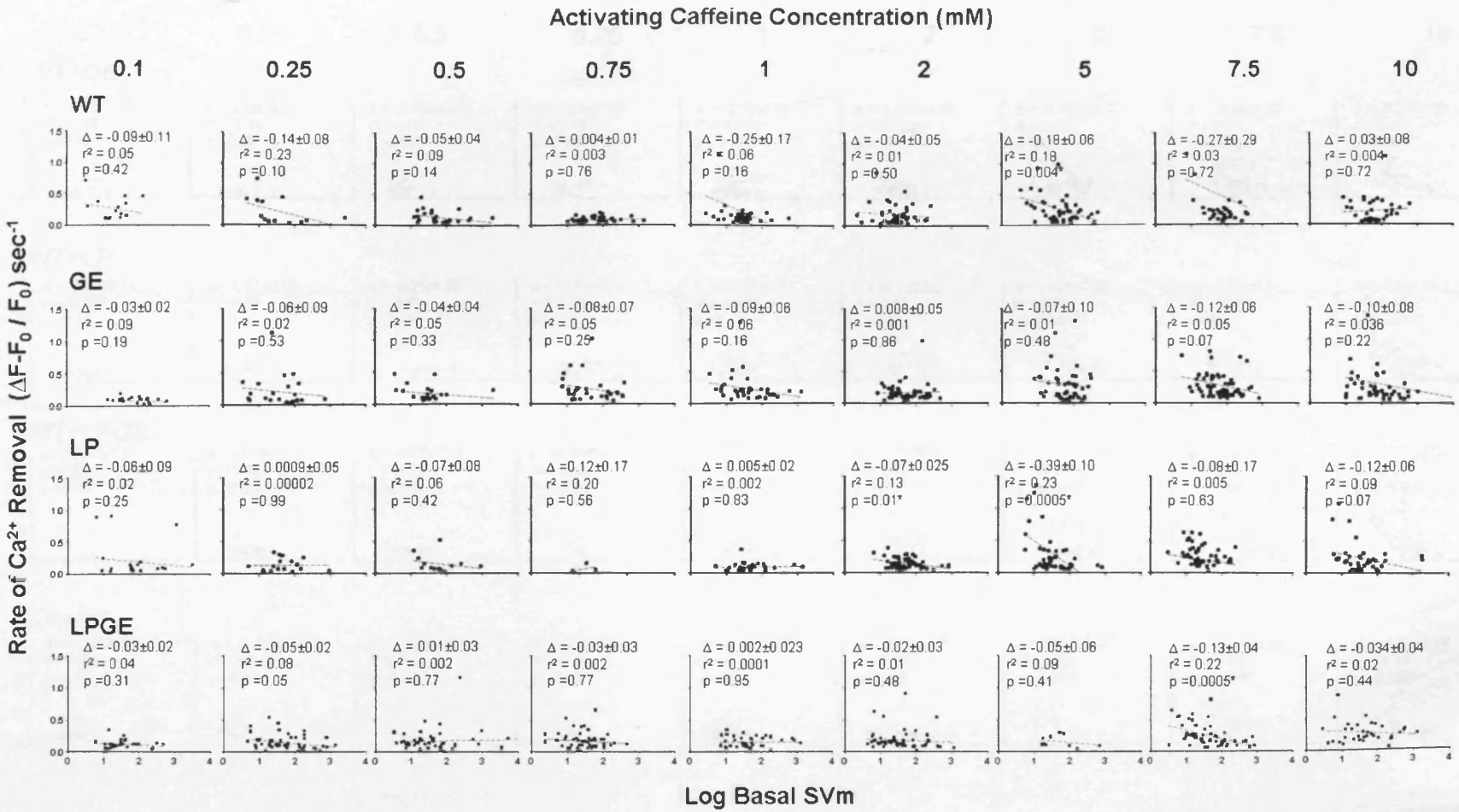

Figure 7. There is no relationship between basal SVm and rate of cytoplasmic Ca^{2+} removal following caffeine-evoked Ca^{2+} release in cells expressing homotetrameric RyR2. *Linear regression analysis examining the relationships between basal SVm and the rate of cytoplasmic Ca^{2+} removal following caffeine-evoked Ca^{2+} release was carried out. As detailed in section 2.2.5, the regression line gradient (Δ), goodness-of-fit value (r^2) and significance value testing whether the gradient is significantly different to 0 (p) were determined. Asterisked p-values indicate a linear regression line that was significantly different to 0 ($p<0.05$) whereas asterisked r^2 values indicate data which was an acceptable fit to the linear regression model ($r^2>0.3$).*

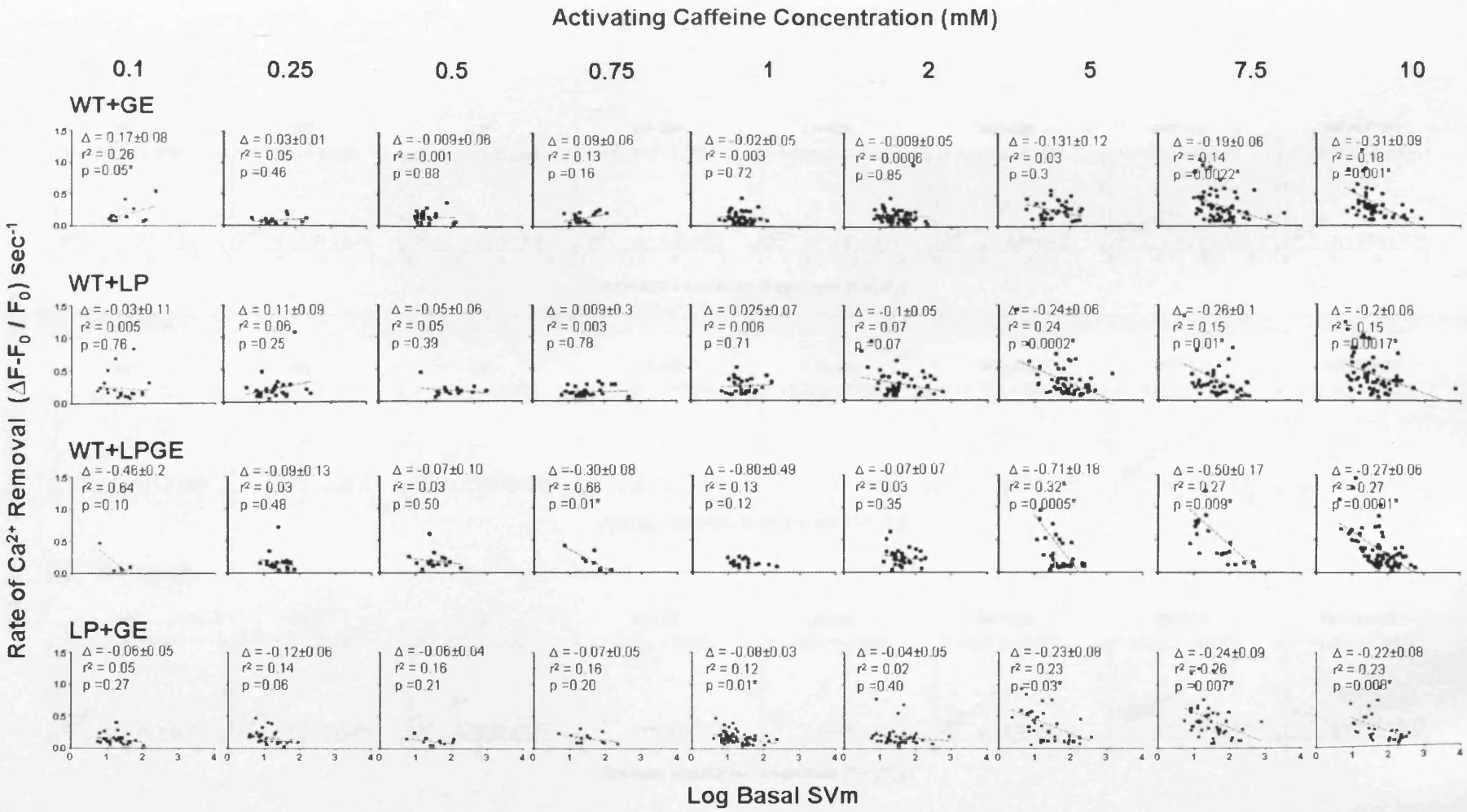

Figure 8. There is no relationship between basal SVm and rate of cytoplasmic Ca^{2+} removal following caffeine-evoked Ca^{2+} release in cells expressing heterotetrameric RyR2. *Linear regression analysis examining the relationships between basal SVm and the rate of cytoplasmic Ca^{2+} removal following caffeine-evoked Ca^{2+} release was carried out. As detailed in section 2.2.5, the regression line gradient (Δ), goodness-of-fit value (r^2) and significance value testing whether the gradient is significantly different to 0 (p) were determined. Asterisked p-values indicate a linear regression line that was significantly different to 0 ($p<0.05$) whereas asterisked r^2 values indicate data which was an acceptable fit to the linear regression model ($r^2>0.3$).*

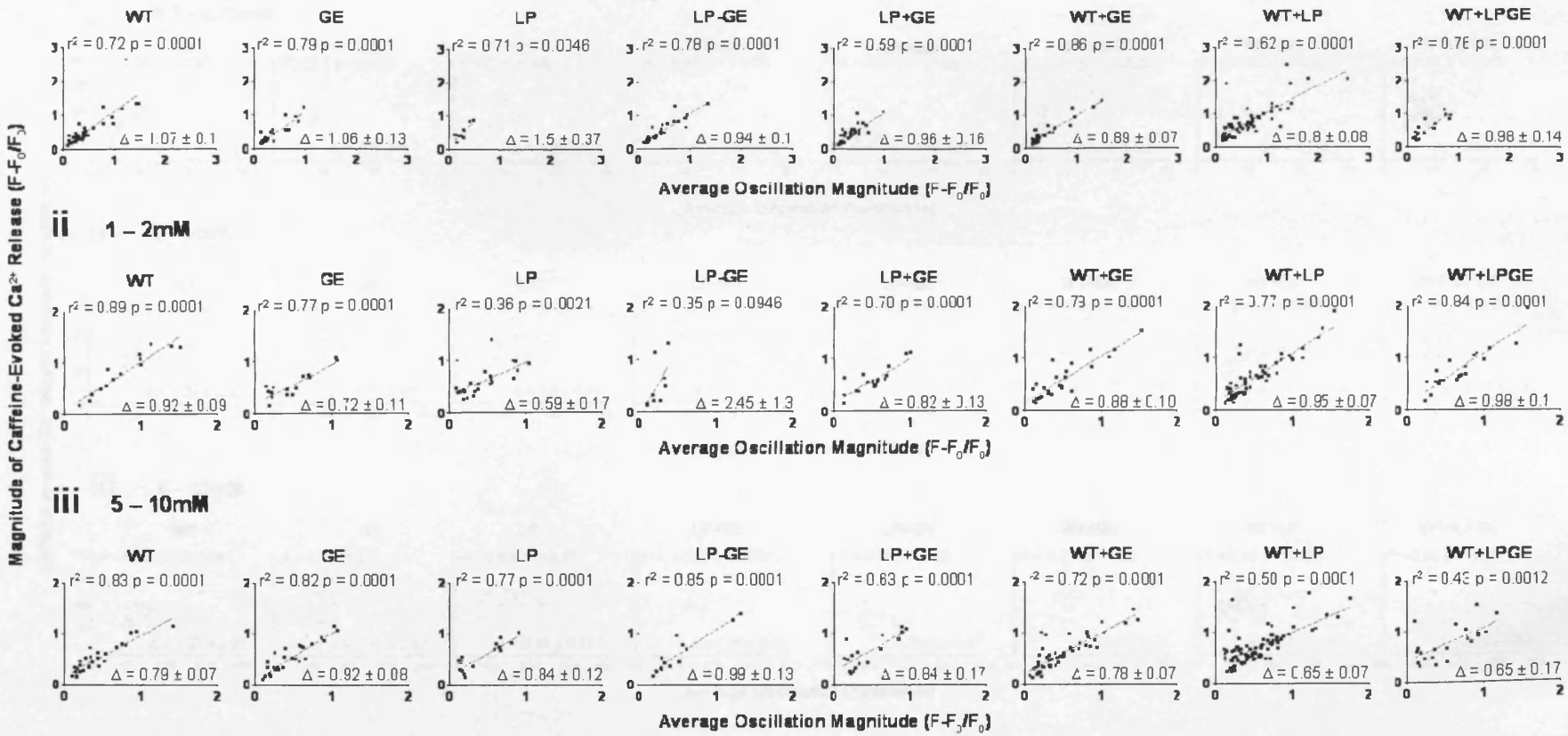

Figure 9. Linear regression analysis of spontaneous and caffeine-evoked Ca^{2+} release magnitude. *Linear regression analysis was carried out to investigate relationships between the magnitude of spontaneous and caffeine-evoked Ca^{2+} release. Data was divided into groups by activating caffeine concentration (minimal: 0.1-0.75mM, exponential: 1-2mM and maximal: 5-10mM, see section 5.3.6). Data was obtained from between 9 and 85 cells per experimental condition. As detailed in section 2.2.5, key linear regression parameters were determined including goodness-of-fit values (r^2), whether the relationship was significantly different to 0 ($p<0.05$) and the gradient of the linear regression line (Δ). Asterisked gradient values indicate a significant difference to WT RyR2. Data is summarised in Figure 5.14.*

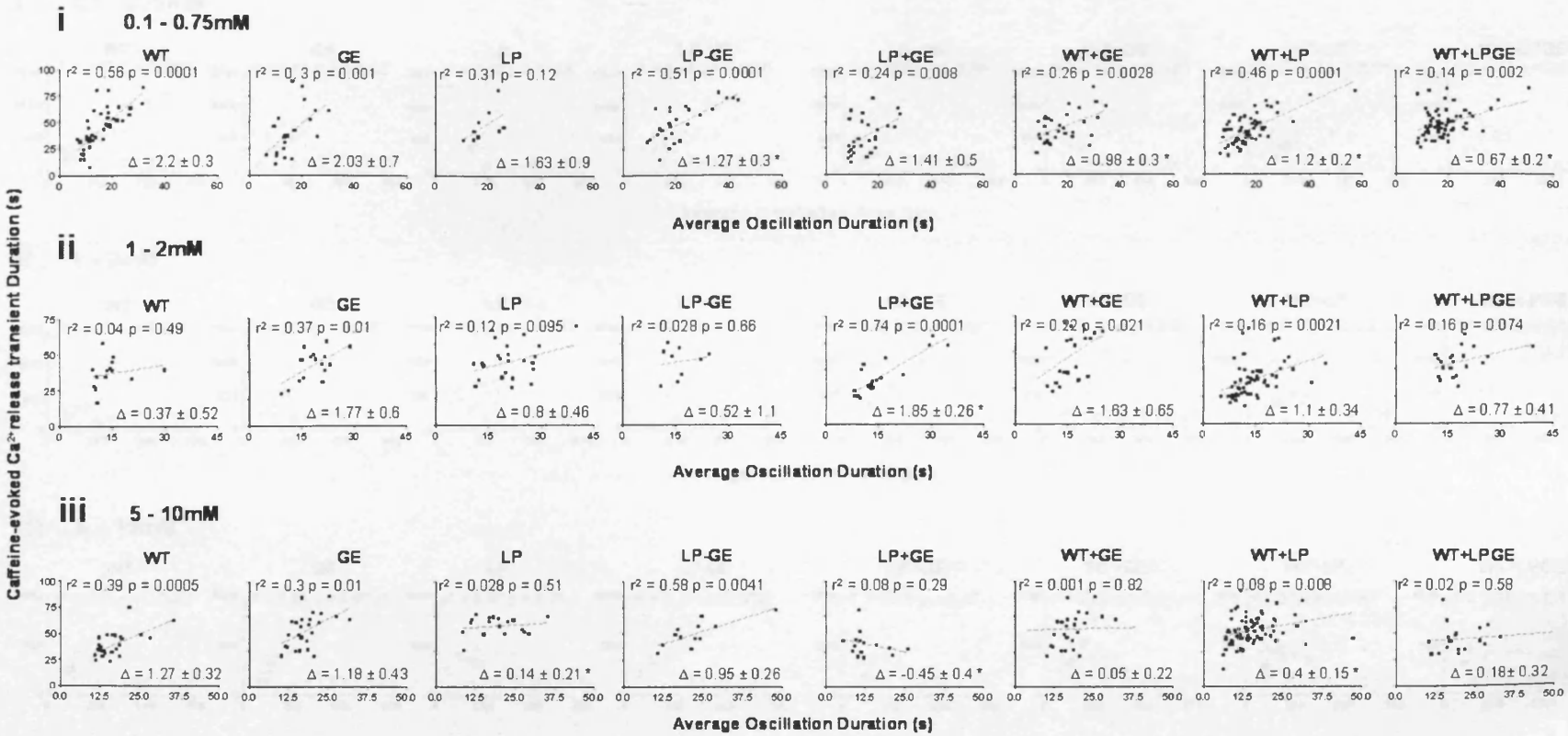

Figure 10. Linear regression analysis of spontaneous Ca^{2+} oscillation and caffeine-evoked Ca^{2+} transient duration. *Linear regression analysis was carried out to investigate relationships between the duration of spontaneous and caffeine-evoked Ca^{2+} release events. Data was divided into groups by activating caffeine concentration (minimal: 0.1-0.75mM, exponential: 1-2mM and maximal: 5-10mM, see section 5.3.6). Data was obtained from between 9 and 85 cells per experimental condition. As detailed in section 2.2.5, key linear regression parameters were determined including goodness-of-fit values (r^2), whether the relationship was significantly different to 0 ($p<0.05$) and the gradient of the linear regression line (Δ). Asterisked gradient values indicate a significant difference to WT RyR2. Data is summarised in Figure 5.14.*

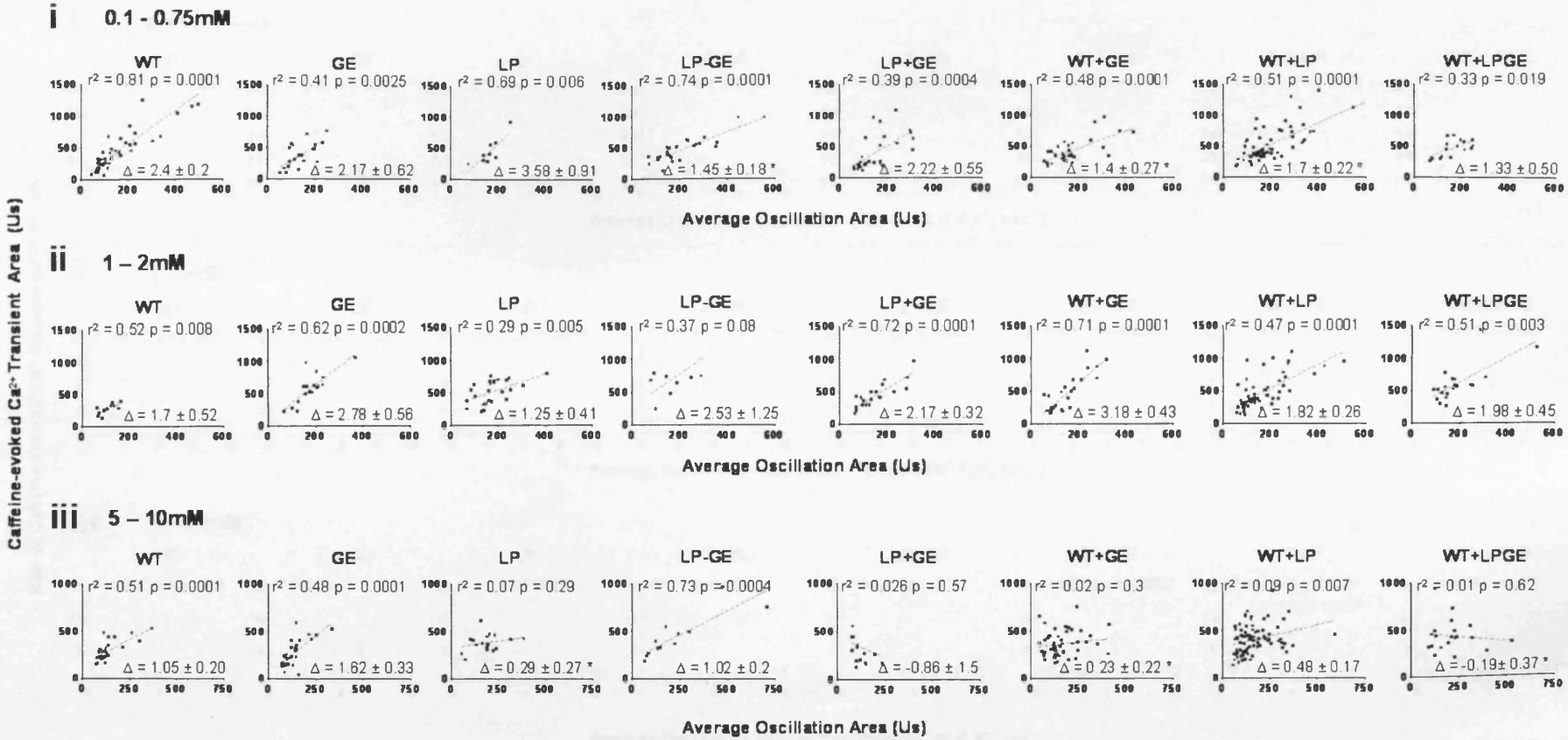

Figure 11. Linear regression analysis of spontaneous Ca^{2+} oscillation and caffeine-evoked Ca^{2+} transient area. *Linear regression analysis was carried out to investigate relationships between the area of spontaneous and caffeine-evoked Ca^{2+} release events. Data was divided into groups by activating caffeine concentration (minimal: 0.1-0.75mM, exponential: 1-2mM and maximal: 5-10mM, see section 5.3.6). Data was obtained from between 9 and 85 cells per experimental condition. As detailed in section 2.2.5, key linear regression parameters were determined including goodness-of-fit values (r^2), whether the relationship was significantly different to 0 ($p<0.05$) and the gradient of the linear regression line (Δ). Asterisked gradient values indicate a significant difference to WT RyR2. Data is summarised in Figure 5.14.*

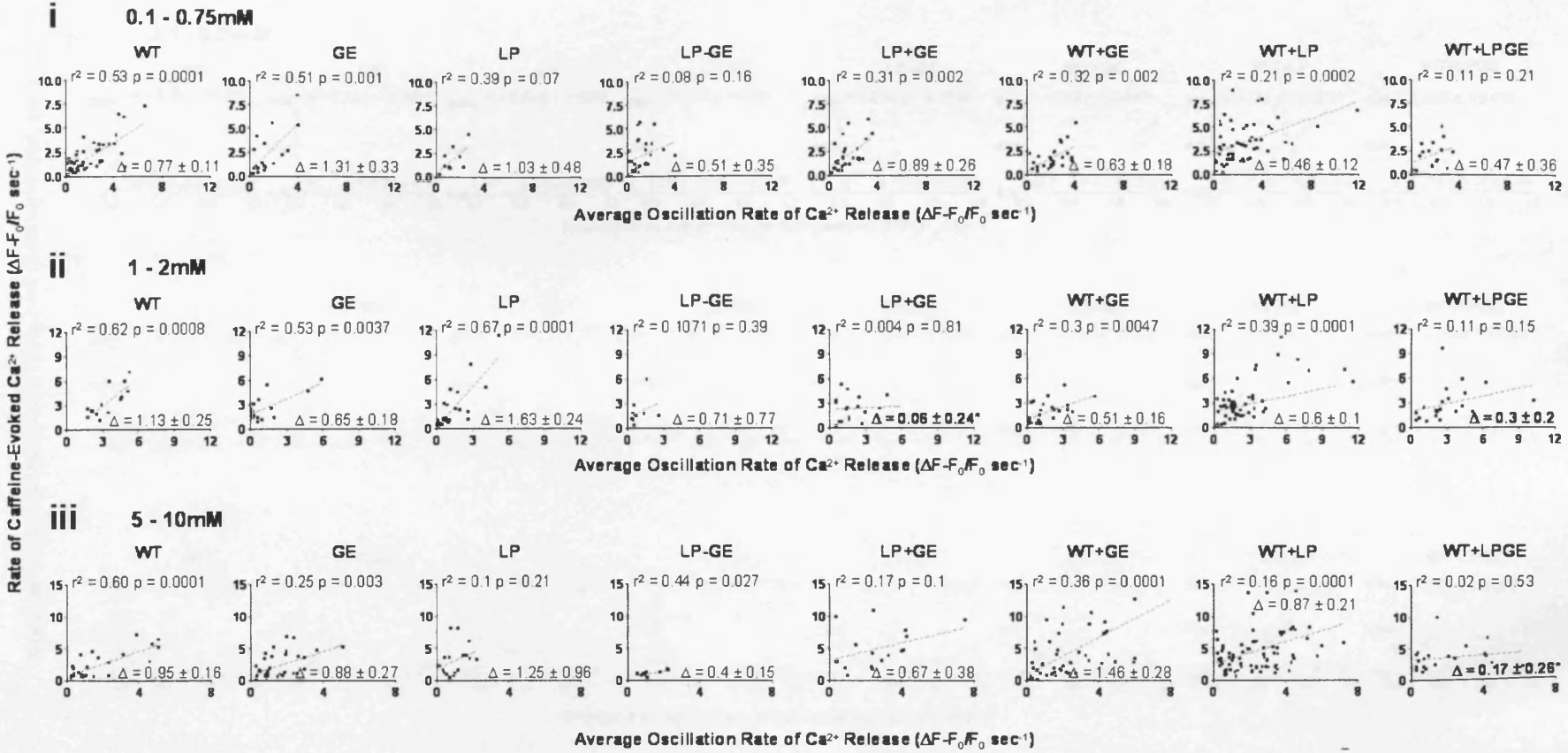

Figure 12. Linear regression analysis of the rate of spontaneous and caffeine-evoked Ca^{2+} release. *Linear regression analysis was carried out to investigate relationships between the rate of spontaneous and caffeine-evoked Ca^{2+} release. Data was divided into groups by activating caffeine concentration (minimal: 0.1-0.75mM, exponential: 1-2mM and maximal: 5-10mM, see section 5.3.6). Data was obtained from between 9 and 85 cells per experimental condition. As detailed in section 2.2.5, key linear regression parameters were determined including goodness-of-fit values (r^2), whether the relationship was significantly different to 0 ($p<0.05$) and the gradient of the linear regression line (Δ). Asterisked gradient values indicate a significant difference to WT RyR2. Data is summarised in Figure 5.14.*

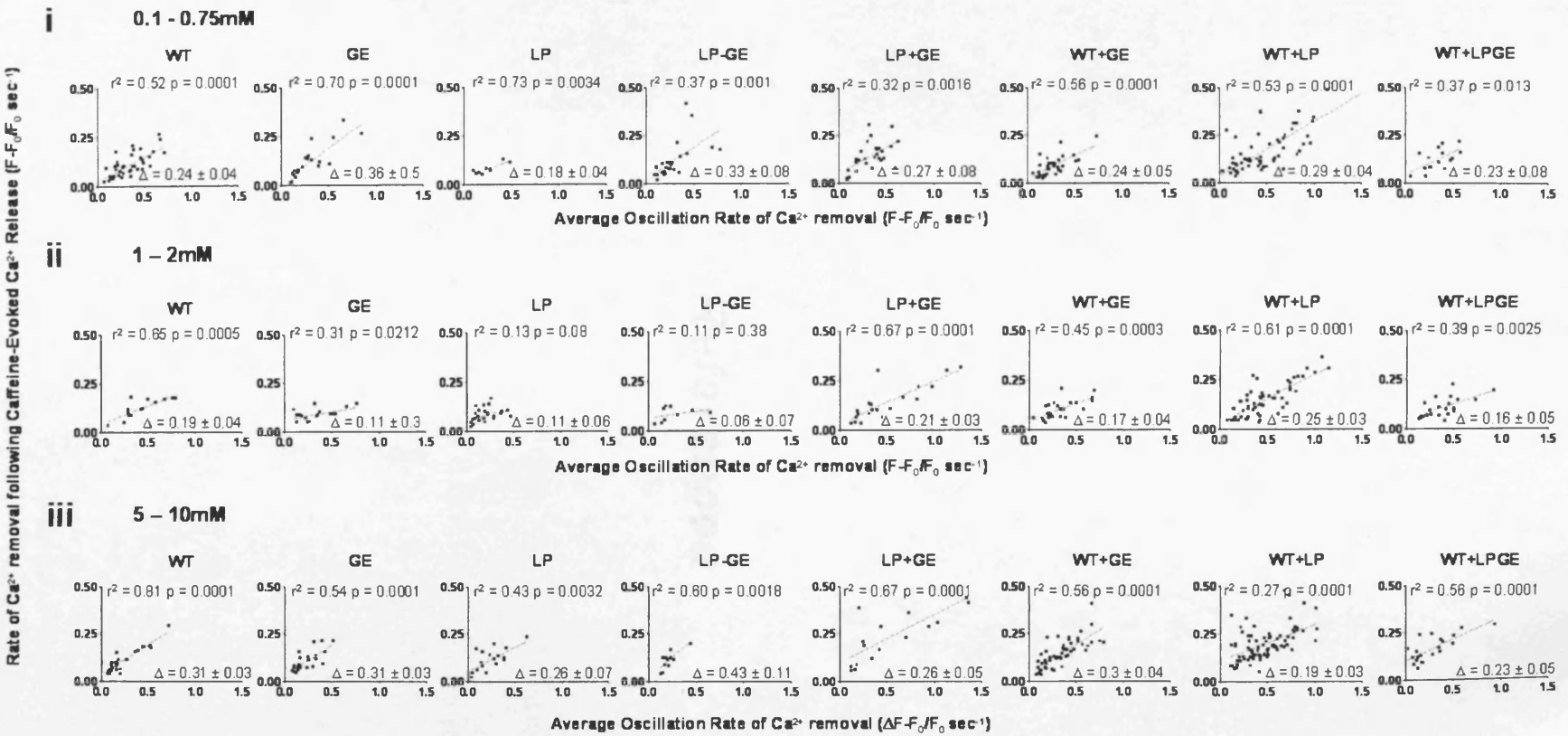

Figure 13. Linear regression analysis of the rate of cytoplasmic Ca^{2+} removal following spontaneous and caffeine-evoked Ca^{2+} release. *Linear regression analysis was carried out to investigate relationships between the rate of cytoplasmic Ca^{2+} removal following spontaneous and caffeine-evoked Ca^{2+} release. Data was divided into groups by activating caffeine concentration (minimal: 0.1-0.75mM, exponential: 1-2mM and maximal: 5-10mM, see section 5.3.6). Data was obtained from between 9 and 85 cells per experimental condition. As detailed in section 2.2.5, key linear regression parameters were determined including goodness-of-fit values (r^2), whether the relationship was significantly different to 0 ($p<0.05$) and the gradient of the linear regression line (Δ). Asterisked gradient values indicate a significant difference to WT RyR2. Data is summarised in Figure 5.14.*

References

Abriel H. (2010). Cardiac sodium channel Na(v)1.5 and interacting proteins: Physiology and pathophysiology. *J Mol Cell Cardiol* **48,** 2-11.

Balser JR. (1999). Structure and function of the cardiac sodium channels. *Cardiovasc Res* **42,** 327-338.

Baroudi G, Acharfi S, Larouche C & Chahine M. (2002). Expression and intracellular localization of an SCN5A double mutant R1232W/T1620M implicated in Brugada syndrome. *Circ Res* **90,** E11-16.

Bassani JW, Bassani RA & Bers DM. (1994). Relaxation in rabbit and rat cardiac cells: species-dependent differences in cellular mechanisms. *J Physiol* **476,** 279-293.

Benitah JP, Alvarez JL & Gomez AM. (2010). L-type Ca(2+) current in ventricular cardiomyocytes. *J Mol Cell Cardiol* **48,** 26-36.

Berridge MJ, Lipp P & Bootman MD. (2000). The versatility and universality of calcium signalling. *Nat Rev Mol Cell Biol* **1,** 11-21.

Bers DM. (2002). Cardiac excitation-contraction coupling. *Nature* **415,** 198-205.

Bers DM. (2006). Altered cardiac myocyte Ca regulation in heart failure. *Physiology (Bethesda)* **21,** 380-387.

Bers DM. (2008). Calcium cycling and signaling in cardiac myocytes. *Annu Rev Physiol* **70,** 23-49.

Bobe R, Bredoux R, Corvazier E, Andersen JP, Clausen JD, Dode L, Kovacs T & Enouf J. (2004). Identification, expression, function, and localization of a novel (sixth) isoform of the human sarco/endoplasmic reticulum Ca2+ATPase 3 gene. *J Biol Chem* **279,** 24297-24306.

Bootman MD & Berridge MJ. (1995). The elemental principles of calcium signaling. *Cell* **83,** 675-678.

Bootman MD, Collins TJ, Peppiatt CM, Prothero LS, MacKenzie L, De Smet P, Travers M, Tovey SC, Seo JT, Berridge MJ, Ciccolini F & Lipp P. (2001). Calcium signalling - an overview. *Semin Cell Dev Biol* **12,** 3-10.

Bootman MD, Higazi DR, Coombes S & Roderick HL. (2006). Calcium signalling during excitation-contraction coupling in mammalian atrial myocytes. *J Cell Sci* **119,** 3915-3925.

Cerrone M, Colombi B, Santoro M, di Barletta MR, Scelsi M, Villani L, Napolitano C & Priori SG. (2005). Bidirectional ventricular tachycardia and fibrillation elicited in a knock-in mouse model carrier of a mutation in the cardiac ryanodine receptor. *Circ Res* **96,** e77-82.

Chalfie M, Tu Y, Euskirchen G, Ward WW & Prasher DC. (1994). Green fluorescent protein as a marker for gene expression. *Science* **263,** 802-805.

Chen LY, Ballew JD, Herron KJ, Rodeheffer RJ & Olson TM. (2007). A common polymorphism in SCN5A is associated with lone atrial fibrillation. *Clin Pharmacol Ther* **81,** 35-41.

Cheng H, Lederer WJ & Cannell MB. (1993). Calcium sparks: elementary events underlying excitation-contraction coupling in heart muscle. *Science* **262,** 740-744.

Chin D & Means AR. (2000). Calmodulin: a prototypical calcium sensor. *Trends Cell Biol* **10,** 322-328.

Ching LL, Williams AJ & Sitsapesan R. (2000). Evidence for Ca(2+) activation and inactivation sites on the luminal side of the cardiac ryanodine receptor complex. *Circ Res* **87,** 201-206.

Chugun A, Sato O, Takeshima H & Ogawa Y. (2007). Mg2+ activates the ryanodine receptor type 2 (RyR2) at intermediate Ca2+ concentrations. *Am J Physiol Cell Physiol* **292,** C535-544.

Cook SA, Clerk A & Sugden PH. (2009). Are transgenic mice the 'alkahest' to understanding myocardial hypertrophy and failure? *J Mol Cell Cardiol* **46,** 118-129.

Creighton W, Virmani R, Kutys R & Burke A. (2006). Identification of novel missense mutations of cardiac ryanodine receptor gene in exercise-induced sudden death at autopsy. *J Mol Diagn* **8,** 62-67.

Cubitt AB, Heim R, Adams SR, Boyd AE, Gross LA & Tsien RY. (1995). Understanding, improving and using green fluorescent proteins. *Trends Biochem Sci* **20,** 448-455.

Davies KE & Nowak KJ. (2006). Molecular mechanisms of muscular dystrophies: old and new players. *Nat Rev Mol Cell Biol* **7,** 762-773.

de la Fuente S, Van Langen IM, Postma AV, Bikker H & Meijer A. (2008). A case of catecholaminergic polymorphic ventricular tachycardia caused by two calsequestrin 2 mutations. *Pacing Clin Electrophysiol* **31,** 916-919.

Di Leva F, Domi T, Fedrizzi L, Lim D & Carafoli E. (2008). The plasma membrane Ca2+ ATPase of animal cells: structure, function and regulation. *Arch Biochem Biophys* **476,** 65-74.

Diaz ME, Graham HK & Trafford AW. (2004). Enhanced sarcolemmal Ca2+ efflux reduces sarcoplasmic reticulum Ca2+ content and systolic Ca2+ in cardiac hypertrophy. *Cardiovasc Res* **62,** 538-547.

Dibb KM, Graham HK, Venetucci LA, Eisner DA & Trafford AW. (2007). Analysis of cellular calcium fluxes in cardiac muscle to understand calcium homeostasis in the heart. *Cell Calcium* **42,** 503-512.

Dirksen WP, Lacombe VA, Chi M, Kalyanasundaram A, Viatchenko-Karpinski S, Terentyev D, Zhou Z, Vedamoorthyrao S, Li N, Chiamvimonvat N, Carnes CA, Franzini-Armstrong C, Gyorke S & Periasamy M. (2007). A mutation in

calsequestrin, CASQ2D307H, impairs Sarcoplasmic Reticulum Ca2+ handling and causes complex ventricular arrhythmias in mice. *Cardiovasc Res* **75,** 69-78.

Du GG, Imredy JP & MacLennan DH. (1998). Characterization of recombinant rabbit cardiac and skeletal muscle Ca2+ release channels (ryanodine receptors) with a novel [3H]ryanodine binding assay. *J Biol Chem* **273,** 33259-33266.

Du GG, Khanna VK, Guo X & MacLennan DH. (2004). Central core disease mutations R4892W, I4897T and G4898E in the ryanodine receptor isoform 1 reduce the Ca2+ sensitivity and amplitude of Ca2+-dependent Ca2+ release. *Biochem J* **382,** 557-564.

Fabiato A. (1985). Effects of ryanodine in skinned cardiac cells. *Fed Proc* **44,** 2970-2976.

Fernandez-Velasco M, Rueda A, Rizzi N, Benitah JP, Colombi B, Napolitano C, Priori SG, Richard S & Gomez AM. (2009). Increased Ca2+ sensitivity of the ryanodine receptor mutant RyR2R4496C underlies catecholaminergic polymorphic ventricular tachycardia. *Circ Res* **104,** 201-209, 212p following 209.

Fill M & Copello JA. (2002). Ryanodine receptor calcium release channels. *Physiol Rev* **82,** 893-922.

Fry DL. (2008). Modulating Intracellular Ca^{2+} Signalling Using Recombinant Fragments of the Human Cardiac Ryanodine Receptor (RyR2). *PhD Thesis, Cardiff University, School of Medicine.*

Gaburjakova J & Gaburjakova M. (2006). Comparison of the effects exerted by luminal Ca2+ on the sensitivity of the cardiac ryanodine receptor to caffeine and cytosolic Ca2+. *J Membr Biol* **212,** 17-28.

Gaburjakova J & Gaburjakova M. (2008). Effect of luminal Ca2+ on the stability of coupled gating between ryanodine receptors from the rat heart. *Acta Physiol (Oxf)* **193,** 219-227.

Gee KR, Brown KA, Chen WN, Bishop-Stewart J, Gray D & Johnson I. (2000). Chemical and physiological characterization of fluo-4 Ca(2+)-indicator dyes. *Cell Calcium* **27,** 97-106.

George CH. (2008). Sarcoplasmic reticulum Ca2+ leak in heart failure: mere observation or functional relevance? *Cardiovasc Res* **77,** 302-314.

George CH, Higgs GV & Lai FA. (2003a). Ryanodine receptor mutations associated with stress-induced ventricular tachycardia mediate increased calcium release in stimulated cardiomyocytes. *Circ Res* **93,** 531-540.

George CH, Higgs GV, Mackrill JJ & Lai FA. (2003b). Dysregulated ryanodine receptors mediate cellular toxicity: restoration of normal phenotype by FKBP12.6. *J Biol Chem* **278,** 28856-28864.

George CH, Jundi H, Thomas NL, Fry DL & Lai FA. (2007a). Ryanodine receptors and ventricular arrhythmias: emerging trends in mutations, mechanisms and therapies. *J Mol Cell Cardiol* **42,** 34-50.

George CH, Jundi H, Walters N, Thomas NL, West RR & Lai FA. (2006). Arrhythmogenic mutation-linked defects in ryanodine receptor autoregulation reveal a novel mechanism of Ca2+ release channel dysfunction. *Circ Res* **98,** 88-97.

George CH, Rogers SA, Bertrand BM, Tunwell RE, Thomas NL, Steele DS, Cox EV, Pepper C, Hazeel CJ, Claycomb WC & Lai FA. (2007b). Alternative splicing of ryanodine receptors modulates cardiomyocyte Ca2+ signaling and susceptibility to apoptosis. *Circ Res* **100,** 874-883.

George CH, Sorathia R, Bertrand BM & Lai FA. (2003c). In situ modulation of the human cardiac ryanodine receptor (hRyR2) by FKBP12.6. *Biochem J* **370,** 579-589.

George CH, Yin CC & Lai FA. (2005). Toward a molecular understanding of the structure-function of ryanodine receptor Ca2+ release channels: perspectives from recombinant expression systems. *Cell Biochem Biophys* **42,** 197-222.

Ginsburg KS & Bers DM. (2005). Isoproterenol does not enhance Ca-dependent Na/Ca exchange current in intact rabbit ventricular myocytes. *J Mol Cell Cardiol* **39,** 972-981.

Goddard CA, Ghais NS, Zhang Y, Williams AJ, Colledge WH, Grace AA & Huang CL. (2008). Physiological consequences of the P2328S mutation in the ryanodine receptor (RyR2) gene in genetically modified murine hearts. *Acta Physiol (Oxf)* **194,** 123-140.

Graham FL, Smiley J, Russell WC & Nairn R. (1977). Characteristics of a human cell line transformed by DNA from human adenovirus type 5. *J Gen Virol* **36,** 59-74.

Gramolini AO, Kislinger T, Asahi M, Li W, Emili A & MacLennan DH. (2004). Sarcolipin retention in the endoplasmic reticulum depends on its C-terminal RSYQY sequence and its interaction with sarco(endo)plasmic Ca(2+)-ATPases. *Proc Natl Acad Sci U S A* **101,** 16807-16812.

Grynkiewicz G, Poenie M & Tsien RY. (1985). A new generation of Ca2+ indicators with greatly improved fluorescence properties. *J Biol Chem* **260,** 3440-3450.

Gui J, Wang T, Jones RP, Trump D, Zimmer T & Lei M. (2010a). Multiple loss-of-function mechanisms contribute to SCN5A-related familial sick sinus syndrome. *PLoS One* **5,** e10985.

Gui J, Wang T, Trump D, Zimmer T & Lei M. (2010b). Mutation-specific effects of polymorphism H558R in SCN5A-related sick sinus syndrome. *J Cardiovasc Electrophysiol* **21,** 564-573.

Gyorke S, Stevens SC & Terentyev D. (2009). Cardiac calsequestrin: quest inside the SR. *J Physiol* **587,** 3091-3094.

Hayek SM, Zhao J, Bhat M, Xu X, Nagaraj R, Pan Z, Takeshima H & Ma J. (1999). A negatively charged region of the skeletal muscle ryanodine receptor is involved in Ca(2+)-dependent regulation of the Ca(2+) release channel. *FEBS Lett* **461,** 157-164.

Hayek SM, Zhu X, Bhat MB, Zhao J, Takeshima H, Valdivia HH & Ma J. (2000). Characterization of a calcium-regulation domain of the skeletal-muscle ryanodine receptor. *Biochem J* **351,** 57-65.

Holmberg SR & Williams AJ. (1989). Single channel recordings from human cardiac sarcoplasmic reticulum. *Circ Res* **65,** 1445-1449.

Hu XF, Liang X, Chen KY, Zhu PH & Hu J. (2005). Depletion of FKBP does not affect the interaction between isolated ryanodine receptors. *Biochem Biophys Res Commun* **336,** 128-133.

Huke S & Bers DM. (2008). Ryanodine receptor phosphorylation at Serine 2030, 2808 and 2814 in rat cardiomyocytes. *Biochem Biophys Res Commun* **376,** 80-85.

Hunt DJ, Jones PP, Wang R, Chen W, Bolstad J, Chen K, Shimoni Y & Chen SR. (2007). K201 (JTV519) suppresses spontaneous Ca2+ release and [3H]ryanodine binding to RyR2 irrespective of FKBP12.6 association. *Biochem J* **404,** 431-438.

Hurtado C, Prociuk M, Maddaford TG, Dibrov E, Mesaeli N, Hryshko LV & Pierce GN. (2006). Cells expressing unique Na+/Ca2+ exchange (NCX1) splice variants exhibit different susceptibilities to Ca2+ overload. *Am J Physiol Heart Circ Physiol* **290,** H2155-2162.

Ikemoto N & Yamamoto T. (2000). Postulated role of inter-domain interaction within the ryanodine receptor in Ca(2+) channel regulation. *Trends Cardiovasc Med* **10,** 310-316.

Ikemoto N & Yamamoto T. (2002). Regulation of calcium release by interdomain interaction within ryanodine receptors. *Front Biosci* **7,** d671-683.

Inui M, Saito A & Fleischer S. (1987). Isolation of the ryanodine receptor from cardiac sarcoplasmic reticulum and identity with the feet structures. *J Biol Chem* **262,** 15637-15642.

Iwasa H, Itoh T, Nagai R, Nakamura Y & Tanaka T. (2000). Twenty single nucleotide polymorphisms (SNPs) and their allelic frequencies in four genes that are responsible for familial long QT syndrome in the Japanese population. *J Hum Genet* **45,** 182-183.

Jiang D, Chen W, Wang R, Zhang L & Chen SR. (2007). Loss of luminal Ca2+ activation in the cardiac ryanodine receptor is associated with ventricular fibrillation and sudden death. *Proc Natl Acad Sci U S A* **104,** 18309-18314.

Jiang D, Chen W, Xiao J, Wang R, Kong H, Jones PP, Zhang L, Fruen B & Chen SR. (2008). Reduced threshold for luminal Ca2+ activation of RyR1 underlies a causal mechanism of porcine malignant hyperthermia. *J Biol Chem* **283,** 20813-20820.

Jiang D, Wang R, Xiao B, Kong H, Hunt DJ, Choi P, Zhang L & Chen SR. (2005). Enhanced store overload-induced Ca2+ release and channel sensitivity to

luminal Ca2+ activation are common defects of RyR2 mutations linked to ventricular tachycardia and sudden death. *Circ Res* **97,** 1173-1181.

Jiang D, Xiao B, Yang D, Wang R, Choi P, Zhang L, Cheng H & Chen SR. (2004). RyR2 mutations linked to ventricular tachycardia and sudden death reduce the threshold for store-overload-induced Ca2+ release (SOICR). *Proc Natl Acad Sci U S A* **101,** 13062-13067.

Jiang D, Xiao B, Zhang L & Chen SR. (2002). Enhanced basal activity of a cardiac Ca2+ release channel (ryanodine receptor) mutant associated with ventricular tachycardia and sudden death. *Circ Res* **91,** 218-225.

Jones PP, Jiang D, Bolstad J, Hunt DJ, Zhang L, Demaurex N & Chen SR. (2008). Endoplasmic reticulum Ca2+ measurements reveal that the cardiac ryanodine receptor mutations linked to cardiac arrhythmia and sudden death alter the threshold for store-overload-induced Ca2+ release. *Biochem J* **412,** 171-178.

Kannankeril PJ, Mitchell BM, Goonasekera SA, Chelu MG, Zhang W, Sood S, Kearney DL, Danila CI, De Biasi M, Wehrens XH, Pautler RG, Roden DM, Taffet GE, Dirksen RT, Anderson ME & Hamilton SL. (2006). Mice with the R176Q cardiac ryanodine receptor mutation exhibit catecholamine-induced ventricular tachycardia and cardiomyopathy. *Proc Natl Acad Sci U S A* **103,** 12179-12184.

Kao JP, Harootunian AT & Tsien RY. (1989). Photochemically generated cytosolic calcium pulses and their detection by fluo-3. *J Biol Chem* **264,** 8179-8184.

Kim E, Youn B, Kemper L, Campbell C, Milting H, Varsanyi M & Kang C. (2007). Characterization of human cardiac calsequestrin and its deleterious mutants. *J Mol Biol* **373,** 1047-1057.

Kong H, Jones PP, Koop A, Zhang L, Duff HJ & Chen SR. (2008). Caffeine induces Ca2+ release by reducing the threshold for luminal Ca2+ activation of the ryanodine receptor. *Biochem J* **414,** 441-452.

Koo SH, Teo WS, Ching CK, Chan SH & Lee EJ. (2007). Mutation screening in KCNQ1, HERG, KCNE1, KCNE2 and SCN5A genes in a long QT syndrome family. *Ann Acad Med Singapore* **36,** 394-398.

Koop A, Goldmann P, Chen SR, Thieleczek R & Varsanyi M. (2008). ARVC-related mutations in divergent region 3 alter functional properties of the cardiac ryanodine receptor. *Biophys J* **94,** 4668-4677.

Lahat H, Eldar M, Levy-Nissenbaum E, Bahan T, Friedman E, Khoury A, Lorber A, Kastner DL, Goldman B & Pras E. (2001a). Autosomal recessive catecholamine-or exercise-induced polymorphic ventricular tachycardia: clinical features and assignment of the disease gene to chromosome 1p13-21. *Circulation* **103,** 2822-2827.

Lahat H, Pras E & Eldar M. (2002). Autosomal recessive catecholamine-induced polymorphic ventricular tachycardia. *Exp Clin Cardiol* **7,** 128-130.

Lahat H, Pras E, Olender T, Avidan N, Ben-Asher E, Man O, Levy-Nissenbaum E, Khoury A, Lorber A, Goldman B, Lancet D & Eldar M. (2001b). A missense

mutation in a highly conserved region of CASQ2 is associated with autosomal recessive catecholamine-induced polymorphic ventricular tachycardia in Bedouin families from Israel. *Am J Hum Genet* **69,** 1378-1384.

Laitinen PJ, Brown KM, Piippo K, Swan H, Devaney JM, Brahmbhatt B, Donarum EA, Marino M, Tiso N, Viitasalo M, Toivonen L, Stephan DA & Kontula K. (2001). Mutations of the cardiac ryanodine receptor (RyR2) gene in familial polymorphic ventricular tachycardia. *Circulation* **103,** 485-490.

Laitinen PJ, Swan H & Kontula K. (2003). Molecular genetics of exercise-induced polymorphic ventricular tachycardia: identification of three novel cardiac ryanodine receptor mutations and two common calsequestrin 2 amino-acid polymorphisms. *Eur J Hum Genet* **11,** 888-891.

Laude AJ & Simpson AW. (2009). Compartmentalized signalling: Ca2+ compartments, microdomains and the many facets of Ca2+ signalling. *FEBS J* **276,** 1800-1816.

Laver DR. (2007). Ca2+ stores regulate ryanodine receptor Ca2+ release channels via luminal and cytosolic Ca2+ sites. *Biophys J* **92,** 3541-3555.

Leenhardt A, Lucet V, Denjoy I, Grau F, Ngoc DD & Coumel P. (1995). Catecholaminergic polymorphic ventricular tachycardia in children. A 7-year follow-up of 21 patients. *Circulation* **91,** 1512-1519.

Lehnart SE, Mongillo M, Bellinger A, Lindegger N, Chen BX, Hsueh W, Reiken S, Wronska A, Drew LJ, Ward CW, Lederer WJ, Kass RS, Morley G & Marks AR. (2008). Leaky Ca2+ release channel/ryanodine receptor 2 causes seizures and sudden cardiac death in mice. *J Clin Invest* **118,** 2230-2245.

Li L, Chu G, Kranias EG & Bers DM. (1998). Cardiac myocyte calcium transport in phospholamban knockout mouse: relaxation and endogenous CaMKII effects. *Am J Physiol* **274,** H1335-1347.

Liang X, Hu XF & Hu J. (2007). Dynamic interreceptor coupling: a novel working mechanism of two-dimensional ryanodine receptor array. *Biophys J* **92,** 1215-1223.

Liu N, Colombi B, Memmi M, Zissimopoulos S, Rizzi N, Negri S, Imbriani M, Napolitano C, Lai FA & Priori SG. (2006). Arrhythmogenesis in catecholaminergic polymorphic ventricular tachycardia: insights from a RyR2 R4496C knock-in mouse model. *Circ Res* **99,** 292-298.

Liu Z, Wang R, Tian X, Zhong X, Gangopadhyay J, Cole R, Ikemoto N, Chen SR & Wagenknecht T. (2010). Dynamic, inter-subunit interactions between the N-terminal and central mutation regions of cardiac ryanodine receptor. *J Cell Sci* **123,** 1775-1784.

Liu Z, Wang R, Zhang J, Chen SR & Wagenknecht T. (2005). Localization of a disease-associated mutation site in the three-dimensional structure of the cardiac muscle ryanodine receptor. *J Biol Chem* **280,** 37941-37947.

Liu Z, Zhang J, Li P, Chen SR & Wagenknecht T. (2002). Three-dimensional reconstruction of the recombinant type 2 ryanodine receptor and localization of its divergent region 1. *J Biol Chem* **277,** 46712-46719.

Liu Z, Zhang J, Wang R, Wayne Chen SR & Wagenknecht T. (2004). Location of divergent region 2 on the three-dimensional structure of cardiac muscle ryanodine receptor/calcium release channel. *J Mol Biol* **338,** 533-545.

Lytton J, Westlin M & Hanley MR. (1991). Thapsigargin inhibits the sarcoplasmic or endoplasmic reticulum Ca-ATPase family of calcium pumps. *J Biol Chem* **266,** 17067-17071.

MacLennan DH & Chen SR. (2009). Store overload-induced Ca2+ release as a triggering mechanism for CPVT and MH episodes caused by mutations in RYR and CASQ genes. *J Physiol* **587,** 3113-3115.

Marban E. (2002). Cardiac channelopathies. *Nature* **415,** 213-218.

Marjamaa A, Laitinen-Forsblom P, Lahtinen AM, Viitasalo M, Toivonen L, Kontula K & Swan H. (2009a). Search for cardiac calcium cycling gene mutations in familial ventricular arrhythmias resembling catecholaminergic polymorphic ventricular tachycardia. *BMC Med Genet* **10,** 12.

Marjamaa A, Laitinen-Forsblom P, Wronska A, Toivonen L, Kontula K & Swan H. (2009b). Ryanodine receptor (RyR2) mutations in sudden cardiac death: Studies in extended pedigrees and phenotypic characterization in vitro. *Int J Cardiol.*

Marx SO & Marks AR. (2002). Regulation of the ryanodine receptor in heart failure. *Basic Res Cardiol* **97 Suppl 1,** I49-51.

Marx SO, Reiken S, Hisamatsu Y, Jayaraman T, Burkhoff D, Rosemblit N & Marks AR. (2000). PKA phosphorylation dissociates FKBP12.6 from the calcium release channel (ryanodine receptor): defective regulation in failing hearts. *Cell* **101,** 365-376.

Medeiros-Domingo A, Bhuiyan ZA, Tester DJ, Hofman N, Bikker H, van Tintelen JP, Mannens MM, Wilde AA & Ackerman MJ. (2009). The RYR2-encoded ryanodine receptor/calcium release channel in patients diagnosed previously with either catecholaminergic polymorphic ventricular tachycardia or genotype negative, exercise-induced long QT syndrome: a comprehensive open reading frame mutational analysis. *J Am Coll Cardiol* **54,** 2065-2074.

Meissner G. (2004). Molecular regulation of cardiac ryanodine receptor ion channel. *Cell Calcium* **35,** 621-628.

Meur G, Parker AK, Gergely FV & Taylor CW. (2007). Targeting and retention of type 1 ryanodine receptors to the endoplasmic reticulum. *J Biol Chem* **282,** 23096-23103.

Niggli E & Shirokova N. (2007). A guide to sparkology: the taxonomy of elementary cellular Ca2+ signaling events. *Cell Calcium* **42,** 379-387.

Nof E, Cordeiro JM, Perez GJ, Scornik FS, Calloe K, Love B, Burashnikov E, Caceres G, Gunsburg M & Antzelevitch C. (2010). A common single nucleotide polymorphism can exacerbate long-QT type 2 syndrome leading to sudden infant death. *Circ Cardiovasc Genet* **3,** 199-206.

Orlova EV, Serysheva, II, van Heel M, Hamilton SL & Chiu W. (1996). Two structural configurations of the skeletal muscle calcium release channel. *Nat Struct Biol* **3,** 547-552.

Periasamy M, Bhupathy P & Babu GJ. (2008). Regulation of sarcoplasmic reticulum Ca2+ ATPase pump expression and its relevance to cardiac muscle physiology and pathology. *Cardiovasc Res* **77,** 265-273.

Periasamy M & Huke S. (2001). SERCA pump level is a critical determinant of Ca(2+)homeostasis and cardiac contractility. *J Mol Cell Cardiol* **33,** 1053-1063.

Piacentino V, 3rd, Weber CR, Chen X, Weisser-Thomas J, Margulies KB, Bers DM & Houser SR. (2003). Cellular basis of abnormal calcium transients of failing human ventricular myocytes. *Circ Res* **92,** 651-658.

Pizzale S, Gollob MH, Gow R & Birnie DH. (2008). Sudden death in a young man with catecholaminergic polymorphic ventricular tachycardia and paroxysmal atrial fibrillation. *J Cardiovasc Electrophysiol* **19,** 1319-1321.

Poelzing S, Forleo C, Samodell M, Dudash L, Sorrentino S, Anaclerio M, Troccoli R, Iacoviello M, Romito R, Guida P, Chahine M, Pitzalis M & Deschenes I. (2006). SCN5A polymorphism restores trafficking of a Brugada syndrome mutation on a separate gene. *Circulation* **114,** 368-376.

Postma AV, Denjoy I, Kamblock J, Alders M, Lupoglazoff JM, Vaksmann G, Dubosq-Bidot L, Sebillon P, Mannens MM, Guicheney P & Wilde AA. (2005). Catecholaminergic polymorphic ventricular tachycardia: RYR2 mutations, bradycardia, and follow up of the patients. *J Med Genet* **42,** 863-870.

Priori SG & Napolitano C. (2005). Cardiac and skeletal muscle disorders caused by mutations in the intracellular Ca2+ release channels. *J Clin Invest* **115,** 2033-2038.

Priori SG, Napolitano C, Gasparini M, Pappone C, Della Bella P, Giordano U, Bloise R, Giustetto C, De Nardis R, Grillo M, Ronchetti E, Faggiano G & Nastoli J. (2002a). Natural history of Brugada syndrome: insights for risk stratification and management. *Circulation* **105,** 1342-1347.

Priori SG, Napolitano C, Memmi M, Colombi B, Drago F, Gasparini M, DeSimone L, Coltorti F, Bloise R, Keegan R, Cruz Filho FE, Vignati G, Benatar A & DeLogu A. (2002b). Clinical and molecular characterization of patients with catecholaminergic polymorphic ventricular tachycardia. *Circulation* **106,** 69-74.

Priori SG, Napolitano C, Tiso N, Memmi M, Vignati G, Bloise R, Sorrentino V & Danieli GA. (2001). Mutations in the cardiac ryanodine receptor gene (hRyR2) underlie catecholaminergic polymorphic ventricular tachycardia. *Circulation* **103,** 196-200.

Purves WK, Sadava D, Orians GH & Heller HC. (2003). Life: The Science of Biology, 7th Edition.

Radermacher M, Rao V, Grassucci R, Frank J, Timerman AP, Fleischer S & Wagenknecht T. (1994). Cryo-electron microscopy and three-dimensional reconstruction of the calcium release channel/ryanodine receptor from skeletal muscle. *J Cell Biol* **127,** 411-423.

Rampazzo A, Nava A, Erne P, Eberhard M, Vian E, Slomp P, Tiso N, Thiene G & Danieli GA. (1995). A new locus for arrhythmogenic right ventricular cardiomyopathy (ARVD2) maps to chromosome 1q42-q43. *Hum Mol Genet* **4,** 2151-2154.

Reppel M, Fleischmann BK, Reuter H, Pillekamp F, Schunkert H & Hescheler J. (2007). Regulation of Na+/Ca2+ exchange current in the normal and failing heart. *Ann N Y Acad Sci* **1099,** 361-372.

Reuter H, Henderson SA, Han T, Mottino GA, Frank JS, Ross RS, Goldhaber JI & Philipson KD. (2003). Cardiac excitation-contraction coupling in the absence of Na(+) - Ca2+ exchange. *Cell Calcium* **34,** 19-26.

Roses AD. (2000). Genetic susceptibility to cardiovascular diseases. *Am Heart J* **140,** S45-47.

Rousseau E & Meissner G. (1989). Single cardiac sarcoplasmic reticulum Ca2+-release channel: activation by caffeine. *Am J Physiol* **256,** H328-333.

Samso M & Wagenknecht T. (2002). Apocalmodulin and Ca2+-calmodulin bind to neighboring locations on the ryanodine receptor. *J Biol Chem* **277,** 1349-1353.

Sanguinetti MC, Curran ME, Spector PS & Keating MT. (1996). Spectrum of HERG K+-channel dysfunction in an inherited cardiac arrhythmia. *Proc Natl Acad Sci U S A* **93,** 2208-2212.

Santiago DJ, Curran JW, Bers DM, Lederer WJ, Stern MD, Rios E & Shannon TR. (2010). Ca sparks do not explain all ryanodine receptor-mediated SR Ca leak in mouse ventricular myocytes. *Biophys J* **98,** 2111-2120.

Schaub MC, Hefti MA & Zaugg M. (2006). Integration of calcium with the signaling network in cardiac myocytes. *J Mol Cell Cardiol* **41,** 183-214.

Schlotthauer K & Bers DM. (2000). Sarcoplasmic reticulum Ca(2+) release causes myocyte depolarization. Underlying mechanism and threshold for triggered action potentials. *Circ Res* **87,** 774-780.

Shimada T, Kawazato H, Yasuda A, Ono N & Sueda K. (2004). Cytoarchitecture and intercalated disks of the working myocardium and the conduction system in the mammalian heart. *Anat Rec A Discov Mol Cell Evol Biol* **280,** 940-951.

Silvester NC, Barberini-Jammaers SR, Ashton PM, Jayanthi A, Yeung WY, Jundi H, Kotecha A, Lai FA & George CH. (2009). Investigating the Ca2+-cycling basis of rhythmicity and synchronicity in coupled cardiomyocyte monolayers. *Biophysical Journal* **96,** 273a-274a.

Sitsapesan R & Williams AJ. (1990). Mechanisms of caffeine activation of single calcium-release channels of sheep cardiac sarcoplasmic reticulum. *J Physiol* **423,** 425-439.

Sitsapesan R & Williams AJ. (1994). Regulation of the gating of the sheep cardiac sarcoplasmic reticulum Ca(2+)-release channel by luminal Ca2+. *J Membr Biol* **137,** 215-226.

Song LS, Guatimosim S, Gomez-Viquez L, Sobie EA, Ziman A, Hartmann H & Lederer WJ. (2005). Calcium biology of the transverse tubules in heart. *Ann N Y Acad Sci* **1047,** 99-111.

Sorrentino V & Volpe P. (1993). Ryanodine receptors: how many, where and why? *Trends Pharmacol Sci* **14,** 98-103.

Stange M, Xu L, Balshaw D, Yamaguchi N & Meissner G. (2003). Characterization of recombinant skeletal muscle (Ser-2843) and cardiac muscle (Ser-2809) ryanodine receptor phosphorylation mutants. *J Biol Chem* **278,** 51693-51702.

Stewart R, Zissimopoulos S & Lai FA. (2003). Oligomerization of the cardiac ryanodine receptor C-terminal tail. *Biochem J* **376,** 795-799.

Takeshima H, Komazaki S, Hirose K, Nishi M, Noda T & Iino M. (1998). Embryonic lethality and abnormal cardiac myocytes in mice lacking ryanodine receptor type 2. *EMBO J* **17,** 3309-3316.

Tateishi H, Yano M, Mochizuki M, Suetomi T, Ono M, Xu X, Uchinoumi H, Okuda S, Oda T, Kobayashi S, Yamamoto T, Ikeda Y, Ohkusa T, Ikemoto N & Matsuzaki M. (2009). Defective domain-domain interactions within the ryanodine receptor as a critical cause of diastolic Ca2+ leak in failing hearts. *Cardiovasc Res* **81,** 536-545.

Tester DJ, Dura M, Carturan E, Reiken S, Wronska A, Marks AR & Ackerman MJ. (2007). A mechanism for sudden infant death syndrome (SIDS): stress-induced leak via ryanodine receptors. *Heart Rhythm* **4,** 733-739.

Tfelt-Hansen J, Winkel BG, Grunnet M & Jespersen T. (2010). Inherited cardiac diseases caused by mutations in the Nav1.5 sodium channel. *J Cardiovasc Electrophysiol* **21,** 107-115.

Thomas NL, George CH & Lai FA. (2004). Functional heterogeneity of ryanodine receptor mutations associated with sudden cardiac death. *Cardiovasc Res* **64,** 52-60.

Thomas NL, Lai FA & George CH. (2005). Differential Ca2+ sensitivity of RyR2 mutations reveals distinct mechanisms of channel dysfunction in sudden cardiac death. *Biochem Biophys Res Commun* **331,** 231-238.

Thomas NL, Maxwell C, Mukherjee S & Williams AJ. (2010). Ryanodine receptor mutations in arrhythmia: The continuing mystery of channel dysfunction. *FEBS Lett* **584,** 2153-2160.

Tiso N, Stephan DA, Nava A, Bagattin A, Devaney JM, Stanchi F, Larderet G, Brahmbhatt B, Brown K, Bauce B, Muriago M, Basso C, Thiene G, Danieli GA & Rampazzo A. (2001). Identification of mutations in the cardiac ryanodine receptor gene in families affected with arrhythmogenic right ventricular cardiomyopathy type 2 (ARVD2). *Hum Mol Genet* **10,** 189-194.

Tong J, McCarthy TV & MacLennan DH. (1999). Measurement of resting cytosolic Ca2+ concentrations and Ca2+ store size in HEK-293 cells transfected with malignant hyperthermia or central core disease mutant Ca2+ release channels. *J Biol Chem* **274,** 693-702.

Toyoshima C, Nakasako M, Nomura H & Ogawa H. (2000). Crystal structure of the calcium pump of sarcoplasmic reticulum at 2.6 A resolution. *Nature* **405,** 647-655.

Trafford AW, Diaz ME & Eisner DA. (2001). Coordinated control of cell Ca(2+) loading and triggered release from the sarcoplasmic reticulum underlies the rapid inotropic response to increased L-type Ca(2+) current. *Circ Res* **88,** 195-201.

Treinys R & Jurevicius J. (2008). L-type Ca2+ channels in the heart: structure and regulation. *Medicina (Kaunas)* **44,** 491-499.

Treves S, Pouliquin R, Moccagatta L & Zorzato F. (2002). Functional properties of EGFP-tagged skeletal muscle calcium-release channel (ryanodine receptor) expressed in COS-7 cells: sensitivity to caffeine and 4-chloro-m-cresol. *Cell Calcium* **31,** 1-12.

Uchinoumi H, Yano M, Suetomi T, Ono M, Xu X, Tateishi H, Oda T, Okuda S, Doi M, Kobayashi S, Yamamoto T, Ikeda Y, Ohkusa T, Ikemoto N & Matsuzaki M. (2010). Catecholaminergic polymorphic ventricular tachycardia is caused by mutation-linked defective conformational regulation of the ryanodine receptor. *Circ Res* **106,** 1413-1424.

Valdivia HH. (1998). Modulation of intracellular Ca2+ levels in the heart by sorcin and FKBP12, two accessory proteins of ryanodine receptors. *Trends Pharmacol Sci* **19,** 479-482.

van Noord C, Eijgelsheim M & Stricker BH. (2010). Drug- and non-drug-associated QT interval prolongation. *Br J Clin Pharmacol* **70,** 16-23.

Verboomen H, Wuytack F, De Smedt H, Himpens B & Casteels R. (1992). Functional difference between SERCA2a and SERCA2b Ca2+ pumps and their modulation by phospholamban. *Biochem J* **286 (Pt 2),** 591-595.

Viswanathan PC, Benson DW & Balser JR. (2003). A common SCN5A polymorphism modulates the biophysical effects of an SCN5A mutation. *J Clin Invest* **111,** 341-346.

Wakimoto H, Alcalai R, Song L, Arad M, Seidman CE, Seidman JG & Berul CI. (2007). Prevention of fatal arrhythmia in a catecholaminergic polymorphoc ventricular tachycardia mouse model carrying calsequestrin-2 mutation. *Circulation* **116,** 216.

Walker CA & Spinale FG. (1999). The structure and function of the cardiac myocyte: a review of fundamental concepts. *J Thorac Cardiovasc Surg* **118,** 375-382.

Wang R, Chen W, Cai S, Zhang J, Bolstad J, Wagenknecht T, Liu Z & Chen SR. (2007). Localization of an NH(2)-terminal disease-causing mutation hot spot to the "clamp" region in the three-dimensional structure of the cardiac ryanodine receptor. *J Biol Chem* **282,** 17785-17793.

Wehrens XH, Lehnart SE, Huang F, Vest JA, Reiken SR, Mohler PJ, Sun J, Guatimosim S, Song LS, Rosemblit N, D'Armiento JM, Napolitano C, Memmi M, Priori SG, Lederer WJ & Marks AR. (2003). FKBP12.6 deficiency and defective calcium release channel (ryanodine receptor) function linked to exercise-induced sudden cardiac death. *Cell* **113,** 829-840.

Wilton SB, Anderson TJ, Parboosingh J, Bridge PJ, Exner DV, Forrest D & Duff HJ. (2008). Polymorphisms in multiple genes are associated with resting heart rate in a stepwise allele-dependent manner. *Heart Rhythm* **5,** 694-700.

Xiao B, Masumiya H, Jiang D, Wang R, Sei Y, Zhang L, Murayama T, Ogawa Y, Lai FA, Wagenknecht T & Chen SR. (2002). Isoform-dependent formation of heteromeric Ca2+ release channels (ryanodine receptors). *J Biol Chem* **277,** 41778-41785.

Xu L & Meissner G. (1998). Regulation of cardiac muscle Ca2+ release channel by sarcoplasmic reticulum lumenal Ca2+. *Biophys J* **75,** 2302-2312.

Xu X, Yano M, Uchinoumi H, Hino A, Suetomi T, Ono M, Tateishi H, Oda T, Okuda S, Doi M, Kobayashi S, Yamamoto T, Ikeda Y, Ikemoto N & Matsuzaki M. (2010). Defective calmodulin binding to the cardiac ryanodine receptor plays a key role in CPVT-associated channel dysfunction. *Biochem Biophys Res Commun* **394,** 660-666.

Yang Z, Ikemoto N, Lamb GD & Steele DS. (2006). The RyR2 central domain peptide DPc10 lowers the threshold for spontaneous Ca2+ release in permeabilized cardiomyocytes. *Cardiovasc Res* **70,** 475-485.

Ye B, Valdivia CR, Ackerman MJ & Makielski JC. (2003). A common human SCN5A polymorphism modifies expression of an arrhythmia causing mutation. *Physiol Genomics* **12,** 187-193.

Yin CC, Blayney LM & Lai FA. (2005a). Physical coupling between ryanodine receptor-calcium release channels. *J Mol Biol* **349,** 538-546.

Yin CC, Han H, Wei R & Lai FA. (2005b). Two-dimensional crystallization of the ryanodine receptor Ca2+ release channel on lipid membranes. *J Struct Biol* **149,** 219-224.

Zhang G, Gurtu V & Kain SR. (1996). An enhanced green fluorescent protein allows sensitive detection of gene transfer in mammalian cells. *Biochem Biophys Res Commun* **227,** 707-711.

Zhang J, Liu Z, Masumiya H, Wang R, Jiang D, Li F, Wagenknecht T & Chen SR. (2003). Three-dimensional localization of divergent region 3 of the ryanodine

receptor to the clamp-shaped structures adjacent to the FKBP binding sites. *J Biol Chem* **278,** 14211-14218.

Zhao M, Li P, Li X, Zhang L, Winkfein RJ & Chen SR. (1999). Molecular identification of the ryanodine receptor pore-forming segment. *J Biol Chem* **274,** 25971-25974.

Zimmer M. (2009). GFP: from jellyfish to the Nobel prize and beyond. *Chem Soc Rev* **38,** 2823-2832.

Zimmer T & Surber R. (2008). SCN5A channelopathies--an update on mutations and mechanisms. *Prog Biophys Mol Biol* **98,** 120-136.

Zissimopoulos S & Lai FA. (2005). Interaction of FKBP12.6 with the cardiac ryanodine receptor C-terminal domain. *J Biol Chem* **280,** 5475-5485.

Zissimopoulos S, Thomas NL, Jamaluddin WW & Lai FA. (2009). FKBP12.6 binding of ryanodine receptors carrying mutations associated with arrhythmogenic cardiac disease. *Biochem J* **419,** 273-278.